Inaugural dissertation for obtaining the Doctoral degree

of the

Combined Faculty of Mathematics, Engineering and Natural Sciences

of the

Ruperto Carola University Heidelberg

Presented by

M.Sc. Ignacio Andrés Vergara Dal Pont

born in: Buenos Aires, Argentina

Oral examination: 06.10.2022

Establishment of an *in vitro* platform for the characterization of proteins involved in the intestinal epithelial barrier dysfunction of Inflammatory Bowel Disease, with a focus on TNFα/TNR1A/TNR1B

Referees:

Prof. Dr. Gudrun Rappold

Prof. Dr. Christian Schaaf

ABSTRACT

The gastrointestinal (GI) epithelium consists of a cellular monolayer that prevents the infiltration of pathogens and antigens into the GI mucosa and concomitantly mediates the highly selective resorption and secretion of nutrients, solutes and water. An intact monolayer of epithelial cells is achieved by two types of intercellular junctional protein complexes that seal the paracellular space: the Adherens (AJs) and the Tight Junctions (TJs). Inflammatory Bowel Disease (IBD) is a complex pathological condition originating from a disturbed homeostasis of the immune and epithelial barrier functions of the GI mucosa that results in a perturbance of the tight balance in between pro- and anti-inflammatory cytokines, and consequently in between the immune tolerance and the defensive inflammatory responses towards the microbiota and microbial antigens. The dysfunction of the GI epithelial barrier plays a major role in both the pathogenesis and the chronic manifestation of IBD. Tumor Necrosis Factor alpha (TNFα) as a key pro-inflammatory cytokine with pleiotropic functions is highly upregulated at the intestinal mucosa in IBD. The TNFα signalling cascade is initiated by two different ligands, the membrane (mTNFα) and the soluble (sTNFα) forms of TNFα, and mediated by two different membrane receptors TNR1A (*TNFRSF1A*) and TNR1B (*TNFRSF1B*). The latter are not only activated in separate ways, but can determine divergent effects in a tissue- and cell-specific manner.

In my Ph.D. work, I aimed to: **i)** establish an *in vitro* platform for the characterization of candidate genes/proteins with regards to the key mechanisms that regulate the paracellular permeability at the GI epithelium, **ii)** establish an inflammatory model to resemble the barrier dysfunction that takes place in IBD, **iii)** investigate the mechanisms of action of the key pro-inflammatory cytokines TNFα, Interferon gamma (IFNγ) and Interleukin1- beta (IL-1β), with a special focus on the dissection of the axis TNFα/TNR1A/TNR1B, in intestinal epithelial barrier function.

An *in vitro* model of the inflamed intestinal epithelium was generated by differentiating the colorectal carcinoma cell lines T84 and CACO-2 on Transwell inserts and applying the pro-inflammatory cytokines sTNFα, IFNγ and IL-1β from the basolateral side at different concentrations and combinations. To assess the consequences of these stimuli on the different permeability pathways of the paracellular route, different assays were performed: measurement of the Trans Epithelial Electrical Resistance (TEER), permeability assays with fluorescently labelled molecular species, cell viability assays and assessment of the expression and subcellular localization of key tight junctional proteins (TJPs). Once defined the optimal pro-inflammatory input to mimic the IBD condition, the barrier function impairing effects of the single cytokines sTNFα and IFNγ were investigated in detail. Fully differentiated T84 monolayers were subjected to a single cytokine induction in the presence of potent and selective blockers of both the ligands and of the respective cognate membrane receptors to confirm the validity of the model. A part from applying the key functional and cell viability assays, the cross-regulatory mechanisms taking place in between both cytokines were investigated with transcriptional expression analyses. The results of these experiments confirmed a synergism in between both cytokines based on not only a positive

regulatory loop exerted by IFNγ on *TNFRSF1A* and *TNFRSF1B*, but also on a positive regulatory loop exerted by sTNFα on *IFNGR1* and *IFNGR2*. Furthermore, a putative anti-necroptotic effect determined by IFNγ was observed to take place on these GI epithelial cells.

In the last part of my work, I applied potent and selective pharmacological modulators directed towards different levels of the TNFα signalling. The colorectal carcinoma cell line T84 was fully differentiated on Transwell inserts and different end-point experiments were run by applying combinations of sTNFα (natural agonist of TNR1A and marginal agonist of TNR1B), TROS (competitive, selective antagonist of TNR1A) and ADALIMUMAB (competitive, global antagonist of the sTNFα signalling). The consequences of these modulations were analyzed with the different aforementioned functional assays, and a detailed image of the cellular pathways differentially regulated was obtained by a transcriptomic expression analysis. The results of these experiments demonstrated that TNR1A mediates most of the barrier function impairment determined by sTNFα. The complete dissection of the signalling, by future investigation of the role of TNR1B in this specific context, could provide the basis for the initiation of the work towards the modification of the actual pharmacological therapies for IBD that are dominated by global TNFα inhibitors. A receptor-specific therapy could lead to a better outcome rather than the neutralization of the whole signalling pathway.

ZUSAMMENFASSUNG

Das Epithel des Magen-Darm-Trakts besteht aus einer Einzelzellschicht, die das Eindringen von Krankheitserregern und Antigenen in die Magen-Darm-Schleimhaut verhindert und gleichzeitig die hochselektive Resorption und Sekretion von Nährstoffen, gelösten Stoffen und Wasser vermittelt. Eine intakte Epithelzellschicht wird durch zwei Arten von interzellulären Proteinkomplexen erreicht, die den parazellulären Raum abdichten: die Adhärens (AJs) und die Tight Junctions (TJs). Die chronisch-entzündliche Darmerkrankung (IBD) ist eine komplexe Erkrankung, die auf eine gestörte Homöostase der Immun- und Epithelbarrierefunktion der Magen-Darm-Schleimhaut zurückzuführen ist und zu einer Störung des Gleichgewichts zwischen pro- und anti-inflammatorischen Zytokinen und folglich zwischen Immuntoleranz und defensiven Entzündungsreaktionen gegenüber Mikrobiota und mikrobiellen Antigenen führt. Die Störung der Epithelbarriere des Magen-Darm-Trakts spielt sowohl bei der Pathogenese als auch bei der chronischen Manifestation von IBD eine wichtige Rolle. Tumor-Nekrose-Faktor alpha (TNFα), ein wichtiges proinflammatorisches Zytokin mit pleiotropen Funktionen, ist bei IBD an der Darmschleimhaut stark hochreguliert. Die TNFα-Signalkaskade wird durch zwei verschiedene Liganden, die membranständige (mTNFα) und die lösliche (sTNFα) Form von TNFα, initiiert und durch zwei Membranrezeptoren TNR1A (*TNFRSF1A*) und TNR1B (*TNFRSF1B*) vermittelt. Letztere werden nicht nur auf unterschiedliche Weise aktiviert, sondern können auch gewebe- und zellspezifisch unterschiedliche Wirkungen entfalten.

In meiner Doktorarbeit hatte ich zum Ziel: **i)** eine *in vitro*-Plattform zur Charakterisierung von Kandidatengenen/-proteinen im Hinblick auf die Schlüsselmechanismen, die die parazelluläre Permeabilität des GI-Epithels regulieren, zu etablieren, **ii)** ein Entzündungsmodell zu etablieren, das der bei IBD auftretenden Barrieredysfunktion ähnelt, **iii)** die Wirkmechanismen der wichtigsten proinflammatorischen Zytokine TNFα, Interferon gamma (IFNγ) und Interleukin-1 beta (IL1β) zu untersuchen, mit besonderem Augenmerk bezüglich der Achse TNFα/TNR1A/TNR1B in der Barrierefunktion des Darmepithels.

Ein *in vitro* Modell für entzündliches Darmepithel wurde durch Differenzierung der kolorektalen Karzinom-Zelllinien T84 und CACO-2 auf Transwell-Inserts und Verwendung der pro-inflammatorischen Zytokine sTNFα, IFNγ und IL-1β von der basolateralen Seite in unterschiedlichen Konzentrationen und Kombinationen generiert. Um die Konsequenzen dieser Stimuli auf die verschiedenen Permeabilitätswege der parazellulären Route zu bewerten, wurden verschiedene Assays durchgeführt: Messung des elektrischen Trans-Epithelial-Widerstands (TEER), Permeabilitätsassays mit fluoreszenzmarkierten molekularen Substanzen, Zellviabilitätsassays und Bewertung der Expression und subzellulären Lokalisierung wichtiger Tight-Junctional-Proteine (TJPs). Nach der Festlegung des optimalen proinflammatorischen Inputs zur Nachahmung der IBD-Bedingungen wurden die die Barrierefunktion beeinträchtigenden Auswirkungen der einzelnen Zytokine sTNFα und IFNγ im Detail untersucht. Vollständig ausdifferenzierte T84-Monolayer wurden in Gegenwart potenter und selektiver

Blocker sowohl der Liganden als auch der jeweiligen Membranrezeptoren einer einzigen Zytokininduktion unterzogen, um die Gültigkeit des Modells zu bestätigen. Neben der Anwendung der wichtigsten Funktions- und Zellviabilitätstests wurden die zwischen den beiden Zytokinen ablaufenden kreuzregulatorischen Mechanismen mit Transkriptionsexpressionsanalysen untersucht. Die Ergebnisse dieser Experimente bestätigten einen Synergismus zwischen beiden Zytokinen, der nicht nur auf einem positiven Regelkreis von IFNγ auf *TNFRSF1A* und *TNFRSF1B* beruht, sondern auch auf einem positiven Regelkreis von sTNFα auf *IFNGR1* und *IFNGR2*. Darüber hinaus wurde auf diesen gastrointestinalen Epithelzellen eine mögliche anti-nekrototische Wirkung von IFNγ beobachtet.

Im letzten Teil meiner Arbeit habe ich wirksame und selektive pharmakologische Modulatoren eingesetzt, die auf verschiedene Ebenen des TNFα-Signalwegs ausgerichtet sind. Die Kolorektalkarzinom-Zelllinie T84 wurde auf Transwell-Inserts vollständig differenziert, und es wurden verschiedene Endpunktexperimente mit Kombinationen von sTNFα (natürlicher Agonist von TNR1A und marginaler Agonist von TNR1B), TROS (kompetitiver und selektiver Antagonist von TNR1A) und ADALIMUMAB (kompetitiver und globaler Antagonist des sTNFα-Signalwegs) durchgeführt. Die Folgen dieser Modulationen wurden mit den verschiedenen oben erwähnten funktionellen Assays analysiert, und ein detailliertes Bild der unterschiedlich regulierten zellulären Signalwege durch eine transkriptomische Expressionsanalyse gewonnen. Die Ergebnisse dieser Experimente zeigten, dass TNR1A den größten Teil der durch sTNFα verursachten Beeinträchtigung der Barrierefunktion vermittelt. Die vollständige Aufklärung der Signalübertragung durch zukünftige Untersuchungen der Rolle von TNR1B in diesem spezifischen Kontext könnte Grundlage für weitere Arbeiten und möglicherweise Änderung der derzeitigen pharmakologischen Therapien für IBD bilden, die derzeit von globalen TNFα-Inhibitoren dominiert werden. Eine rezeptorspezifische Therapie könnte zu einem besseren Ergebnis führen als die Neutralisierung des gesamten Signalweges.

GRAPHICAL ABSTRACT

Aims of the Ph.D. work

- Establishment of an *in vitro* platform for the complete characterization of genes/proteins involved in intestinal epithelial barrier function
- Establishment of an inflammatory model for the study of cytokines signallings implicated in the barrier dysfunction taking place in IBD
- Dissection of the TNFα signalling with regards to all the mechanisms underlying barrier function

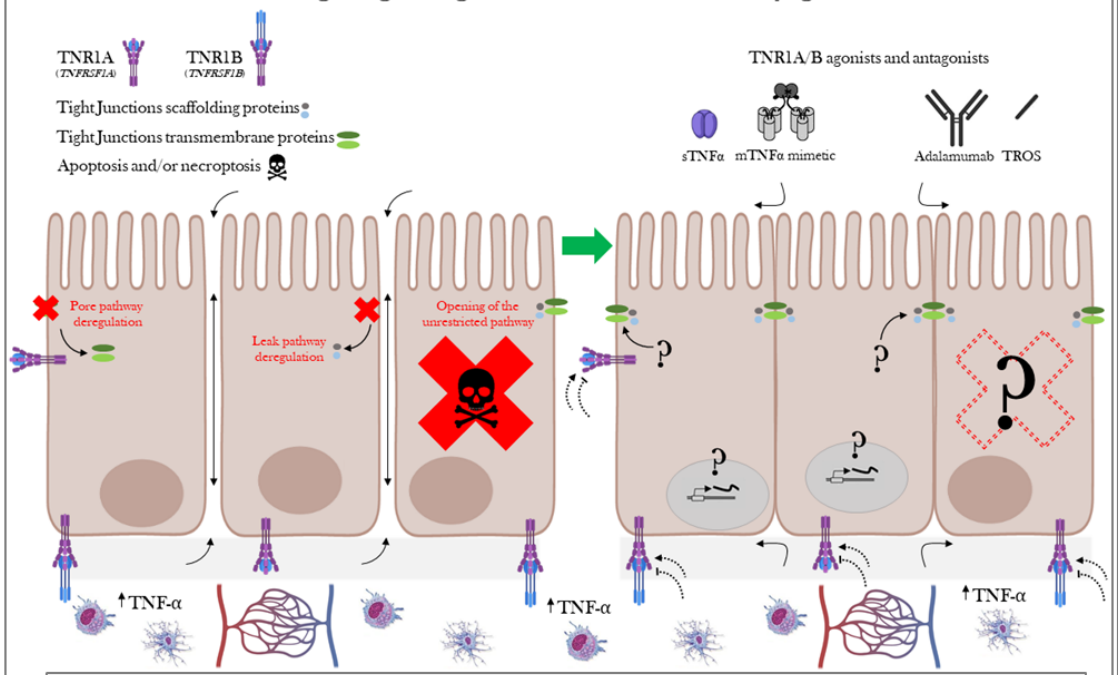

TRANSLATIONAL AIMS

- Refinement and improvement of the actual anti-TNFα therapeutical strategies in IBD
- Improvement and complementation of the therapeutical strategies for IBD by targeting the GI epithelial barrier dysfunction.

Methodological approach

Pharmacological interference approach in an *in vitro* model of the intestinal epithelium

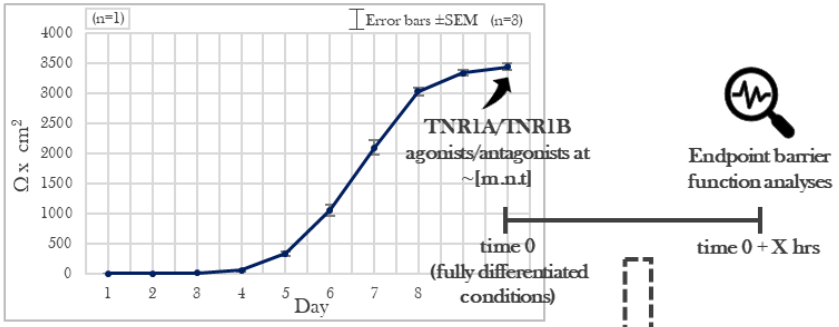

Time 0 hrs	Time 0 hrs	Time 0 hrs
sTNFα antagonist ~[m.n.t]	TNR1A antagonist ~[m.n.t]	TNR1B agonist ~[m.n.t]
↓	↓	↓
Time +12 hrs	Time +12 hrs	Time +12 hrs
sTNFα 100 ng/mL	sTNFα 100 ng/mL	alone / sTNFα 100 ng/mL
↓	↓	↓ ↓

Endpoint barrier function analyses: time +24 hrs

- **Trans Epithelial Electrical Resistance** (TEER) (pore, leak and unrestricted pathways)
- **FITC-Dextran 4 kDa** permeability assay (leak and unrestricted pathways)
- **LDH assay** to assess necrosis and necroptosis (unrestricted pathway)

Novel biological data generated

- **TNR1A mediates most of the barrier function-impairing effects determined by sTNFα**. TNR1A induces barrier function impairment by deregulating the leak and the unrestricted paracellular permeability pathways (increase of necroptosis, at least).
- **IFNγ determines an anti-necroptotic effect in intestinal epithelial cells**. Further experiments are necessary to confirm it.
- Transcriptional expression analyses by RT-qPCR confirm a **positive regulatory loop exerted by IFNγ on *TNFRSF1A* and *TNFRSF1B***, at the basis of the synergism in between sTNFα and IFNγ described by others.
- RNAseq data show: **i)** a novel **positive regulatory loop exerted by sTNFα on *IFNGR1* and *IFNGR2*** that contributes to the synergism in between sTNFα and IFNγ, **ii)** a significant **downregulation of *MYLK*** determined by sTNFα (master regulator of the leak permeability pathway found upregulated by sTNFα in other cell lines, in works published by others).

PRESENTATIONS AND PUBLICATIONS

Data generated in my Ph.D. project were already presented at the following conference:

- 32nd Annual Meeting of the German Society for Human Genetics (GfH); 16.03.2022 – 18.03.2022, Würzburg (Germany); poster/talk

The following publication will result from some of the data exposed in my Ph.D. thesis:

- *In vitro platform for the characterization of proteins involved in intestinal epithelial barrier function employing an endpoint pharmacological interference approach.*

At least the following publications will result from some of the data exposed in my Ph.D. thesis and additional work that I will carry out:

- *In vitro dissection of the TNFα/TNR1A/TNR1B signalling axis in intestinal epithelial barrier function employing an endpoint pharmacological interference approach and a colorectal carcinoma cell line.*
- *Anti-necroptotic effects of IFNγ at the level of the intestinal epithelium.*
- *In vitro dissection of the serotonergic system in intestinal epithelial barrier function employing an endpoint pharmacological interference approach and a colorectal carcinoma cell line.*

LIST OF CONTENTS

GLOSSARY

AJs	Adherens Junctions
aPKC	Atypical Protein Kinase C
ATP	Adenosine triphosphate
BMP	Bone Morphogenetic Proteins
BrdU	5-Bromo-2´-deoxy-uridine
BSA	Bovine Serum Albumin
BVES	Blood vessel epicardial substance
CAR	Coxsackievirus and Adenovirus Receptor
CBCCs	Crypt Base Columnar Cells
CD	Crohn's disease
CD^+	Cluster of differentiation positive
cIAPs	cellular Inhibitor of Apoptosis Proteins
CNS	Central Nervous System
CRDs	Cysteine-rich domains
DAPI	4′,6-Diamidino-2-phenylindole·2HCl
DCLK1	Doublecortin like kinase 1
DD	Death Domain
DMEM	Dulbecco's modified eagle medium
EC	Enteroendocrine cells
ECM	Extracellular Matrix
EDTA	Ethylenediaminetetraacetic acid
EGF	Epidermal Growth Factor
ENS	Enteric Nervous System
ERK	Extracellular signal-regulated kinases
EtOH	Ethanol
FADD	Fas-associated death domain
FAE	Follicle Associated Epithelium
FBS	Fetal bovine serum
FD4	Fluorescein isothiocyanate-Dextran 4 kDa
FD70	Fluorescein isothiocyanate-Dextran 70 kDa
FHC	Human fetal colonic normal epithelial cell line
FITC	Fluorescein isothiocyanate
5-HT	5-hydroxytryptamine (Serotonin)
5-HTRs	5-HT receptors
GALT	Gut-associated lymphoid tissue
gDNA	Genomic DNA
GI	Gastro intestinal

HBSS	Hanks' Balanced Salt Solution
HEK	Human embryonic kidney
HIFs	Hypoxia-Inducible Factors
IBD	Inflammatory Bowel Disease
ICC	Interstitial Cells of Cajal
IECs	Intestinal Epithelial Cells
IF	Immunofluorescence
IFNγ	Interferon γ
IgA	Immunoglobulin A
IL	Interleukin
ILFs	Intestinal Lymphoid Follicles
IPTG	Isopropyl β-D-1-thiogalactopyranoside
JAK-STAT	Janus Kinases-Signal Transducer and Activator of Transcription pathway
JAMs	Junctional Adhesion Molecules
JNK	c-Jun N-terminal kinase
LDH	Lactate dehydrogenase
LGR5	Leucine-rich repeat-containing G-protein coupled receptor 5
LTα	Lymphotoxin-α
M cells	Membranous or Microfold cells
MAGI	Membrane-associated guanylate kinase inverted
MAGI	Membrane-Associated Guanylate Kinase Inverted
MAPK	Mitogen-activated protein kinase
MARVEL	MAL and related proteins for vesicle trafficking and membrane link
MLCK	Myosin light chain kinase
MLKL	Mixed linked kinase-like protein
mTNFα	Membrane TNFα
MUPP1	Multi-PDZ domain protein 1
NAD	Nicotinamide adenine dinucleotide
Nbs	Nanobodies
NFkB	Nuclear Factor kappa-light-chain-enhancer of activated B cells
NK	Natural Killer
NLRs	NOD-like receptors
NOD	Nucleotide Oligomerization Domain
NSAIDs	Non-steroidal anti-inflammatory drugs
PALS1	Protein Associated with Lin-1 1
PAMPs	Pathogen Associated Molecular Patterns
PAR	Partitioning Defective
PATJ	PALS1-associated tight junction
PBS	Dulbecco’s phosphate buffered Saline

PFA	Paraformaldehyde
PI3K/PKB/Akt	Phosphatidylinositol 3-kinases/protein kinase B
PRRs	Pattern Recognition Receptors
RACE	Rapid Amplification of cDNA Ends
RFU	Relative Fluorescent Unit
RIPK	Receptor Interacting Protein Kinase
RLU	Relative Luminescence Unit
ROS	Reactive Oxygen Species
RT°C	Room Temperature
SCFAs	Short-chain fatty acids
sTNFα	Soluble TNFα
TACE/ADAM17	Matrix metalloprotease TNF converting enzyme
TEER	Trans Epithelial Electrical Resistance
TGF-β	Transforming Growth Factor beta
T_H	Helper T cells
THD	TNF homology domain
TJB	Tight Junctional Belt
TJD	Tight Junctional Density
TJPs	Tight Junctional Proteins
TJs	Tight Junctions
TLRs	Toll Like Receptors
TNFRSF	TNF receptor superfamily
TNFSF	TNF superfamily of ligands
TNFα	Tumor necrosis factor alpha
TNR1A	Tumor necrosis factor receptor superfamily member 1A or TNFR1
TNR1B	Tumor necrosis factor receptor superfamily member 1B or TNFR2
TRADD	TNR1A-associated death domain
TRAF2	TNF receptor associated factor 2
T_{reg}	Regulatory T cells
TROS	TNF Receptor-One Silencer
TUNEL	Terminal deoxynucelotidyl transferase-mediated dUTP nick end labeling
TW	Transwell
UC	Ulcerative colitis
Wnt	Wingless-related integration site
ZBP1	Z-DNA-binding protein 1
ZO	Zonula Occludens
ZONAB	ZO1-associated nucleic acid binding protein

1. INTRODUCTION

1.1. The human gastrointestinal (GI) tract and the GI wall

1.1.1. General notions about the GI tract

During the process of organogenesis, the GI tract or digestive tube develops from the combination and integration of components derived from all three endodermal, mesodermal and ectodermal embryonic germ layers. Its final configuration consists of functional units connected in series one after the other that, together with accessory organs (tongue, salivary glands, liver, gallbladder and pancreas), give rise to the digestive system.

In the adult individual the GI tract spans approximately 5 meters in length and presents an epithelial surface area of approximately 32 m^2 [1]. The anterior-most portion of the GI tract comprises the mouth and pharynx, which are shared in common with the respiratory tube. In mammals, the teeth, major salivary glands and anterior taste buds are of ectodermal origin, while the posterior taste buds, salivary and mucous glands derive from the endoderm[2]. Moving towards the posterior direction, the tube becomes narrower to form the esophagus, which is followed by the stomach, small intestine (duodenum, jejunum, ileum) and large intestine (caecum, colon, rectum, anus). In this whole region comprised in between the esophagus and the anus the three embryonic germ layers take part in the formation of the most important components of the GI tract: the endoderm generates the epithelium that separates the interior of the body from the GI lumen and mediates the absorption of nutrients; the splanchnic portion of the lateral plate mesoderm provides the smooth muscle layers for the peristalsis and the gut-associated lymphoid tissue (GALT) that, together with immune cells scattered throughout the mucosa and the GI epithelium itself, give rise to the GI mucosal immune system; and the neural crest cells from the vagal and sacral regions generate the sensory, sympathetic and parasympathetic ganglia of both plexuses of the enteric nervous system (ENS) that orchestrates the intrinsic functions of the GI tract[2,3]. The three accessory organs liver, pancreas and gallbladder develop immediately caudal to the stomach out of endodermal progenitor cells and have the role of producing and secreting enzymes and other molecules essentials for the digestion and absorption processes (see below)[2].

The completion of the human GI tract is achieved with the colonization of the GI lumen during early embryonic developmental stages *in utero* (from the placenta), but mainly during the birth process, by a complex community of symbiotic microbes derived from the mother[4]. This collection of microbial organisms is composed of bacteria, fungi, protozoans and viruses, and constitutes what is generally known as the microbiota[5]. The stomach and the upper part of the small intestine are inhabited by a low number of microbes and few microbial species, but this is gradually reverted from the jejunum to the posterior-most portion of the GI tract[5]. The colon indeed hosts the vast majority of the GI microbiota and presents the highest cell densities

recorded for any microbial habitat, 10^{11}-10^{12} cells/mL[6]. At first glance, the significance of this community can be apprehended by considering that the overall number of microbial cells residing in the adult human body has been estimated to be 100 trillion (tenfold the number of host's cells) and the collective microbiota genome, termed microbiome, contains approximately 100 times more unique genes than the human genome[7]. In fact, the human species has coevolved together with the microbiota in order to establish a lifelong symbiotic interaction which is often referred as commensalism, even though the relationship with the same microbe can span from mutualism to commensalism and even parasitism in accordance to the genetic landscape, nutritional status, or co-infection of its host[2,8]. In this complex symbiotic relationship the microbiota gets benefits from the warm, nutrient-rich environment of the GI lumen and at the same time plays several crucial beneficial roles for the host's physiology: it supplies primary energy sources (short-chain fatty acids, SCFAs) and indispensable amino acids and vitamins (K_2 and B vitamins) to the host[7]; it calibrates all the aspects of the host's innate and adaptive immune systems ranging from their development and maturation to their fine tuning within the GI mucosa[8]; it prevents the invasion of the GI mucosa by pathogenic microbes exerting an ecological competition, producing antimicrobial peptides and degrading toxins[5,9]; it plays important roles in the development of the GI epithelium and capillary system; it influences the development and the post-natal maturation of the ENS and even of the central nervous system (CNS) in different ways as by producing neurotransmitters and hormones[2,4,9]; and it plays a role in the metabolism of bile salts, estrogens, androgens, lipids, carbohydrates, various nitrogenous substances and drugs[9]. A disadvantageous alteration of the species composition and the function of the GI microbiota is termed dysbiosis and can impact on any of the aforementioned physiological processes depending on the host-microbiota interactions[5]. These alterations can be determined directly by the host's genetics and also by diet, personal hygiene, environmental pollution, antibiotics and other drugs[9].

As a key part of the digestive system, the GI tract with its organs and all their histological and microbial components accomplishes the paramount functions of motility, secretion, digestion and absorption. The digestion of the nutrients starts already in the mouth by mechanical action (chewing) and by the chemical action of the α-amylase (secreted in the saliva) which catalyzes the hydrolysis of certain polysaccharides. In the stomach some water-soluble and lipid-soluble substances are absorbed (e.g. medium-chain fatty acids, alcohol and some drugs), but the main function of this organ is the secretion of proteolytic enzymes and strong acids that initiate the digestion of proteins and fat preparing the small intestine for the completion of the digestion process and for the uptake of nutrients. In the small intestine different biochemicals and enzymes produced by the liver and the exocrine pancreas completely break down carbohydrates, proteins and fats into monosaccharides, amino acids and fatty acids that the epithelium selectively takes up for the conveyance into the portal circulation or the lymphatic system. In the colon there is

no more digestion carried out by human enzymes and the main processes that take place are the absorption of water, minerals and vitamins[10,11]. The characteristics of the colon (slow transit, anaerobic conditions and highest microbiota cell densities) make of it the optimal site for the fermentation of the dietary fibers resistant to the host's digestion (lignin, non-starch polysaccharides, resistant starch and oligosaccharides). Bacteria members of the phyla Bacteroidetes and Firmicutes encode genes which allow them to digest those fibers and release SCFAs (formate, acetate, propionate, butyrate, valerate, isovalerate and hexanoate), organic acids and alcohols. The microbiota of the colon is also responsible for the digestion of undigested proteins via extracellular bacterial proteases and peptidases, releasing peptides, amino acids and other metabolites[12].

Recently a huge interest over another pivotal role of the GI tract has emerged and is nowadays under intense study by the scientific community. Apart from fulfilling the aforementioned tasks, the GI tract senses and responds to the vast array of intrinsic, extrinsic and environmental cues with which it continuously interacts[1]. Being at the interface in between the external hostile environment and the interior of the organism, the GI tract has the difficult task of balancing its inherent functionalities with the needs for a physical barrier and a continuous immune surveillance. Across the GI epithelium (see section 1.2.) an intricated homeostatic communication takes place in between the dietary factors, the commensal microbiota, the mucosal immune system and the ENS[1]. The outcomes of this communication go far beyond the digestive system and can easily reach and affect other districts of the organism via the bloodstream and via the direct and bidirectional communication in between the ENS and the CNS. Due to the multiple players and the inherent complexity, different aspects of these interconnected pathways at this critical interface are still poorly understood.

1.1.2. Histological ultrastructure of the GI wall and segment-specific features

The different cellular components of the GI wall are organized in a series of concentric histological structures (figure 1): serosa or adventitia, muscularis, submucosa and mucosa.

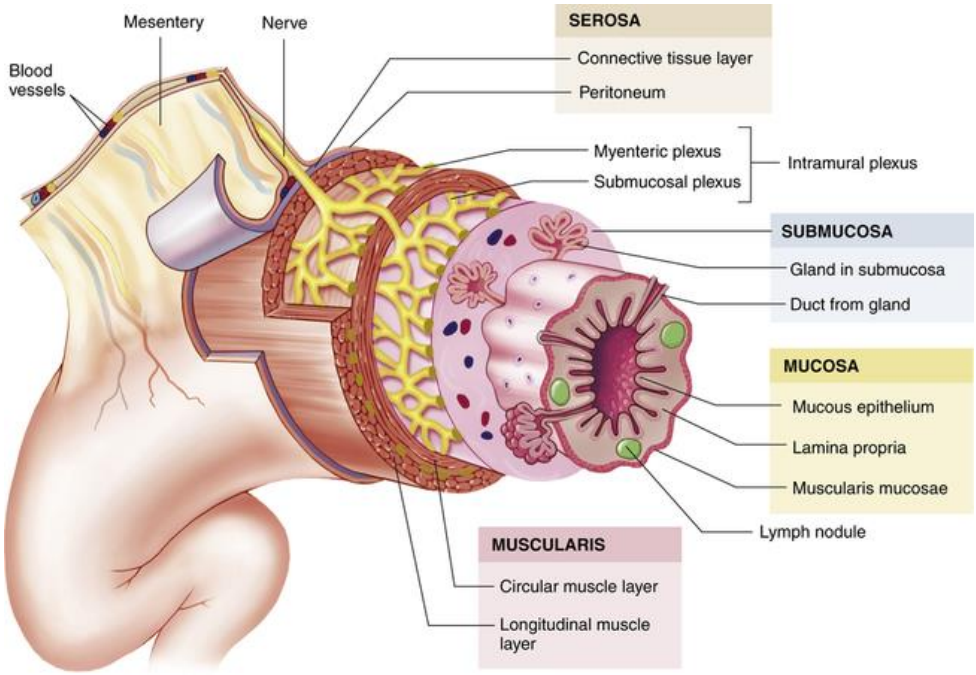

Figure 1: Histological components of the GI wall. The scheme represents a section of the intestines (from Patton KT, Thibodeau GA: Anatomy & physiology, ed 8, St Louis, 2013, Mosby).

The serosa or adventitia is the outermost layer of the GI wall (farthest from the lumen), it encapsulates and lubricates the GI tract so that peristaltic contractions are uninhibited. This layer takes the name of adventitia if it is composed of connective tissue attached to surrounding tissue, and of serosa if it is composed of connective tissue covered by a mesothelium of simple squamous epithelial cells (peritoneum) that are in direct contact with the peritoneal cavity. The segments of the GI tract surrounded by a serosa are connected to the posterior abdominal wall by the mesentery that supports blood and lymphatic vessels and nerves[11].

Moving towards the lumen the following region is called muscularis and consists of an outer longitudinal and an inner circular muscular layers that, being orthogonal to each other, provide stretch and shear flexibility. In between the two layers is located the myenteric or Auerbach's plexus of the ENS that coordinates the contractions that result in the peristaltic process. The frequency of the contractions is dictated by a syncytial network of pacemaker cells called Interstitial Cells of Cajal (ICC) that also function as stretch receptors. The whole muscularis is scattered with resident immune cells[1,9,11].

Adjacent to the muscularis is located the submucosa, a connective tissue layer that lies outside of and supports the mucosa. It contains an extensive blood and lymphatic vasculature, immune structures such as Payer's patches and lymphoid follicles that extend into the mucosa, submucosal glands, and the Meissner's or submucosal plexus of the ENS. The latter is a network of neuronal and glial cells that controls local blood flow, mucosal transport and secretions, and modulates immune and endocrine functions[1,11,13].

The mucosa is the innermost region of the GI wall, and presents three different sublayers: the muscularis mucosa adjacent to the submucosa, the lamina propria and the GI epithelium directly in contact with the lumen. The muscularis mucosa is a thin layer of smooth muscle that presumably exerts important influences on the absorptive and secretory functions of epithelium[14]. ICC lie between peripheral nerve endings and smooth muscle cells[11]. The lamina propria consists of a connective tissue layer rich of blood and lymphatic vessels and of neuronal and glial processes that extend across. The vessels provide nutritional support to the GI epithelium and concomitantly deliver into the body circulation the hormones secreted by the endocrine epithelium and the digested nutrients absorbed from the lumen. The intrinsic neuronal and glial processes of the myenteric and submucosal plexuses, as well as the extrinsic processes originating in the CNS, signal directly to the GI epithelium, sense the GI lumen and are responsible for the GI neuroimmuno-modulation. The lamina propria harbors in fact a high density of innate and adaptive immune cells[1,11]. The innermost sublayer of the mucosa is the GI epithelium that faces the GI lumen. It protects the organism against microbial infections being a physical barrier and a key component of the innate immune system, it mediates the highly selective absorption of nutrients, it secretes mucus to protect the mucosa itself and it also behaves as an (entero-) endocrine tissue by releasing neuroendocrine molecules that control aspects of feeding but that can also have many other systemic effects.

The aforementioned histological ultrastructure of the GI wall acquires some changes in a segment-specific fashion, and so do the specific cell components of the different tissues.

The upper segments of the GI tract, comprising the mouth, pharynx and esophagus, present at least three main differences with respect to the middle and lower segments. All three regions are characterized by a protective mucosal epithelium composed of stratified squamous epithelial cells and not of a simple columnar epithelium. In the mouth, pharynx and upper esophagus the muscularis is composed of striated muscle directly innervated by skeletal motor neurons that control the swallowing process and not of smooth muscle. In the esophagus, the outermost layer is called adventitia and is composed of connective tissue attached to surrounding tissue and not suspended in the abdominal cavity as the serosa[11].

Given its important role in mixing the food with the digestive juices and propelling the partially digested food, the stomach wall (figure 2) is characterized by three layers of smooth muscle: an outer, longitudinal layer; a middle, circular layer; and an inner, oblique layer (the most prominent). The gastric mucosa contains specialized cells that produce mucus, hydrochloric acid, pepsinogen, gastric lipase, hormones, intrinsic factor (necessary for the intestinal absorption of vitamin B_{12}) and gastroferrin (that facilitates small intestine absorption of iron). The mucus, epithelial tight and adherent junctions, bicarbonate secretion, submucosal acid sensors, and a rich mucosal blood flow protect the gastric mucosa against the hydrochloric acid

and proteolytic enzymes. The gastric epithelium is characterized by depressions called gastric pits where the gastric glands empty their secretions[9].

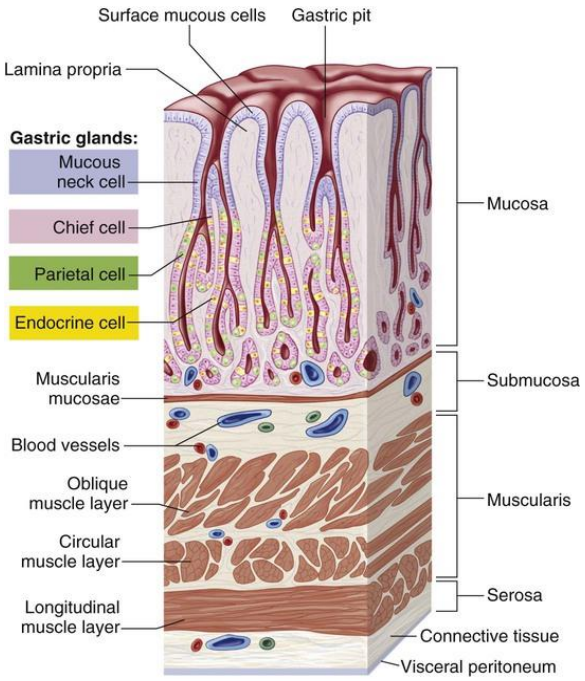

Figure 2: The stomach wall (from Patton KT *et al*: Essentials of anatomy & physiology, St Louis, 2012, Mosby).

In the small intestine (figure 3) the *muscularis* is composed of two smooth muscle layers. The mucosa is characterized by circular folds (or *plicae circulares*) that slow the passage of food (favoring digestion and absorption) and by absorptive functional units called *villi*. Each *villus* represents a protrusion of the small intestinal mucosa into the lumen that increases the surface area available for absorption. It is surrounded by a monolayer of absorptive columnar cells and other cell types (see section 1.2.1.) tightly associated by means of intercellular junctional complexes and protected by a mucous layer. The luminal plasma membrane surface of these cells presents tiny projections called microvilli that further increase the absorptive area. The lamina propria underneath the epithelium contains arterioles that ascend within each *villus* and branch into a capillary array that extends around the base of the absorptive cells and cascades down to the venules that convey the absorbed substances into the hepatic portal circulation[9]. The opposing ascending and descending blood flows provide a countercurrent exchange system for absorbed substances and blood gases. An important consequence of this is an oxygen gradient along the base to tip *villus* axis with an oxygen partial pressure (pO_2) of 60-85 mm Hg at the base and a pO_2 of less than 10 mm Hg at the tip (similar the one of the lumen)[15]. A central lymphatic capillary is also contained within each *villus*. In between the bases of different *villi* locate the crypts of Lieberkühn that extend towards the submucosal layer and contain actively dividing intestinal epithelial stem cells (see section 1.2.2.). The post-mitotic daughter cells move

towards the tip of the villus, gradually differentiate and after functioning for a few days are shed into the GI lumen and digested[9].

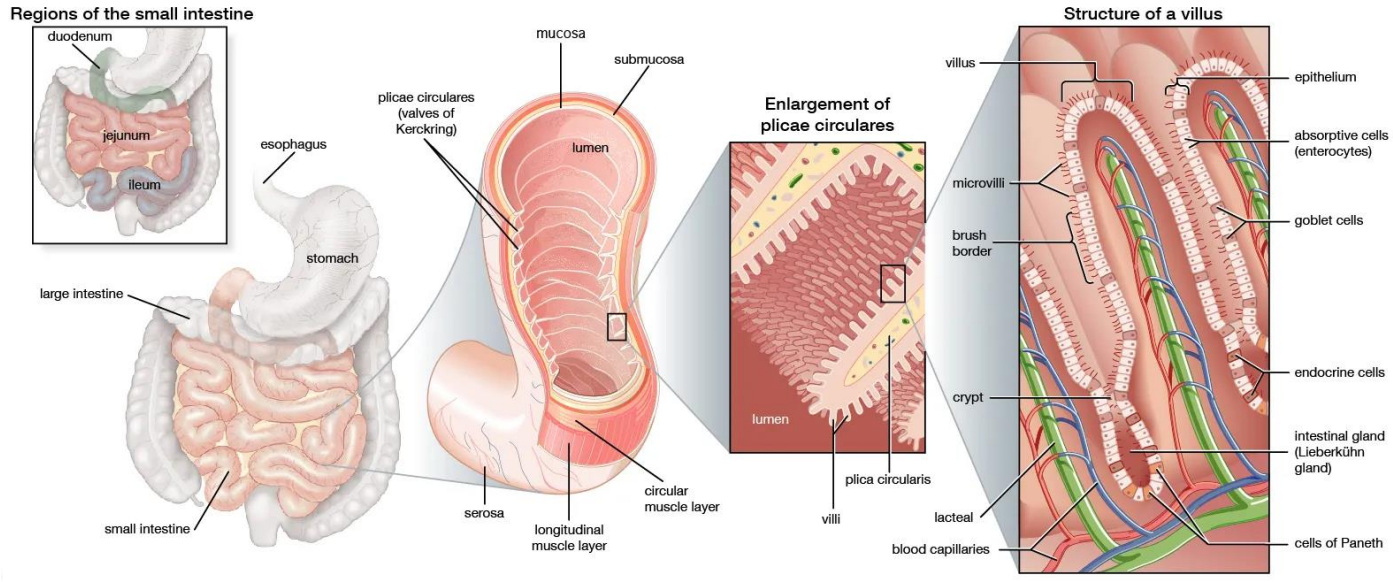

Figure 3: The small intestine wall (from https://www.britannica.com, Encyclopædia Britannica, Inc., 2014).

The large intestine wall (figure 4) also contains two smooth muscle layers but they are assembled in a special configuration: the longitudinal muscle layer consists of three longitudinal bands called *teniae coli* that give to the colon the gathered appearance, and the circular muscles separate the gathers into outpouchings called *haustra coli*. The large intestinal mucosa presents folds called *rugae* mainly located in between the *haustra*, it presents Lieberkühn crypts but no *villi* and is covered by a single layer of columnar epithelial absorptive cells and by mucous secreting cells among other cell types (see section 1.2.1.)[9].

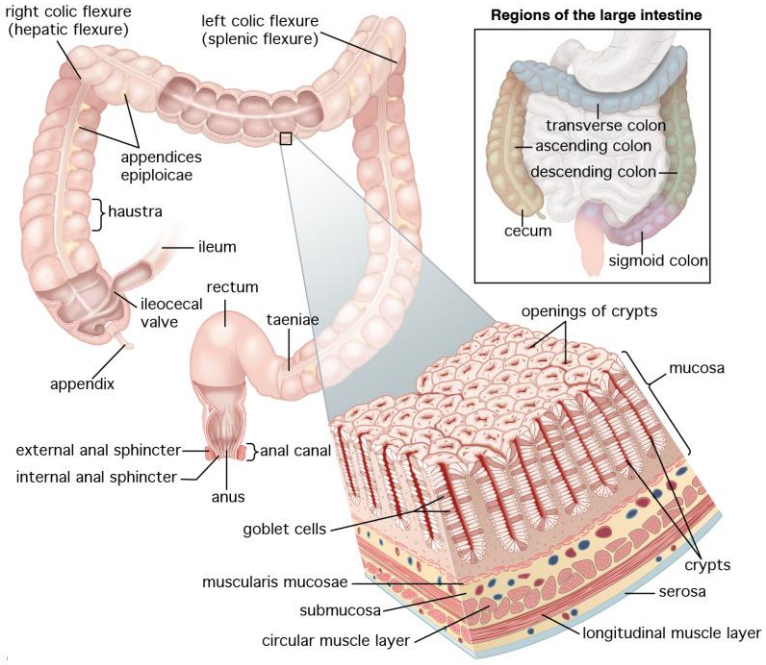

Figure 4: The large intestine wall (from https://www.britannica.com, Encyclopædia Britannica, Inc., 2013).

The anal canal mucosa has only a protective role so is covered by a stratified squamous epithelium as the upper segments of the GI tract.

1.2. The intestinal epithelium and the epithelial barrier function

The GI epithelium is the first layer of defense against pathogenic microbes, pathogenic antigens and noxious luminal contents (as gastric acid and harmful components eventually present in the food) along the entire GI tract. From the stomach to the sigmoid colon two key specific structural configurations consent a tightly regulated compromise in between the protective function and the mediation of a highly selective resorption and secretion of nutrients, solutes and water: on one side the transition from a stratified to a simple epithelium, and on the other the acquisition of a functional cellular polarization determined by the formation of a specific set of intercellular junctional complexes that are the basis of the barrier function (see 1.2.3. and 1.2.4.).

1.2.1. Intestinal epithelial cell (IEC) types

Several cell types compose the intestinal epithelium and regional differences in this composition account for the regional functional specializations as well as for barrier function (see 1.2.4.) differences across the length of the intestine. The number and proportion of each of the intestinal epithelial cell types that characterize the different segments of the intestine (and of the whole GI tract) is defined by the mucosal immune environment as each cell type expresses receptors for immune mediators that can directly affect their viability[16].

During the developmental process the first cell type that emerges in the mature intestinal epithelium is the progenitor stem cell. These cells anchor to the site of nascent crypts initiating the process of crypt development that is regulated by the Wingless-related integration site (Wnt) and Bone Morphogenetic Proteins (BMP) signallings. Post mitotic differentiated cells in the intestine derive from stem cells that reside at the base of the crypts and can be classified into absorptive and secretory based not only on their distinct functions but also on their genetic differentiation programs. The small intestinal epithelium is composed of one type of absorptive cell (enterocyte) and four types of secretory cells (Goblet, Paneth, Enteroendocrine and Tuft cells). In the large intestine Paneth cells are absent and the absorptive cells are termed colonocytes. Two additional cell types, Cup cells and Membranous or Microfold (M) cells, could not yet be assigned to the absorptive or to the secretory groups[17].

Enterocytes and colonocytes are the most abundant cell types in both small and large intestines. Their primary role is the absorption of nutrients at the apical side (characterized by the presence of microvilli) and the release of them at the basolateral one into the interstitial space, and so into the bloodstream[17]. Alkaline phosphatase expression is considered a marker for enterocyte

differentiation. All Enterocytes and Colonocytes express Pattern Recognition Receptors (PRRs) that recognize enteric pathogens and pathogenic antigens allowing the initiation of an innate immune response[16].

Goblet cells are the most abundant secretory lineage of the intestinal epithelium. Their role is to produce and secrete mucus in order to protect the epithelium against noxious luminal contents. Different mucins (*MUC1*, *MUC2*, *MUC3*, *MUC17*) and Trefoil Factor Peptides are produced and secreted by Goblet cells, and an impairment in these secretory processes is associated with a reduced host defense and an increase in barrier permeability. That is why the proportion of Goblet cells among all the other epithelial cell types increases aborally from the duodenum to the distal colon, following the increase in the microbial load[16]. This cell type represents an important population of the intestinal epithelium, 10–15% of the small intestinal epithelium and up to 50% of the colonic epithelium[17].

Paneth cells are located only in the crypts of the small intestine and are characterized by distinct granules. They produce and secrete antimicrobial peptides (α-defensins and RegIIIγ) into the lumen in response to the activation of their PRRs as Nucleotide Oligomerization Domain 2 (NOD2)[16]. Paneth cells produce also ligands for Wnt, Notch, and Epidermal Growth Factor (EGF) receptors, suggesting that they regulate the activity of adjacent intestinal stem cells[17].

Tuft cells or brush cells are located in or near crypts, they express the marker Doublecortin Like Kinase 1 (*DCLK1*) and present a characteristic shape including long and thick microvilli[16,17]. The role of these cells is very probably the chemical sensation of luminal contents and the secretion of opioids as well as Interleukin-25 (IL-25)[16].

Enteroendocrine cells (EC) represent only 1% of the small and large intestinal epithelium, they are scattered throughout the whole mucosa as individual cells and play an important role in the sensing of both physiological and pathophysiological luminal stimuli, to which they respond releasing more than 20 different peptide hormones[16,17]. ECs coordinate gastric, biliary and pancreatic secretions and peristalsis, vasodilatation, growth and turnover of GI epithelial cells, hunger, appetite, satiety and emesis. Furthermore, ECs fulfill immune functions given the fact that produce and secrete more than 90% of the total serotonin (5-HT) of the body (that can activate the cognate receptors expressed by all immune cells)[18,19], and can function as innate immune sensors expressing Toll Like Receptors (TLRs), responding to microbes and microbial components and communicating the message to the immune cells of the lamina propria[16].

M cells are located in intestinal Payer's Patches and Intestinal Lymphoid Follicles (ILFs) (particularly in the Ileum), constituting 10% of all epithelial cells in the Follicle Associated Epithelium (FAE)[16]. These cells lack microvilli and contain unusual basolateral membrane structures which facilitate the presentation of microbes and microbial antigens to underlying lymphocytes, macrophages and dendritic cells[16,17]. Interestingly, M cells arise by a unique

differentiation program from intestinal stem cells, or by transdifferentation of mature enterocytes[17].

Cup cells have been poorly studied and their roles are still not defined. These cells have glycocalyces that are more extensive than those of absorptive cells and some studies suggest that these cells may represent preferential sites for attachment of some strains of bacilli[20].

1.2.2. Clonal renewal at the crypt and cell differentiation

In the developmental process, the Wnt/β-catenin pathway plays a crucial role in the establishment of the stem cell niches at the intervilli zones. Then, the BMP signalling will contribute to the development and formation of the mature crypts of Lieberkühn[17].

Intestinal stem cells or Crypt Base Columnar Cells (CBCCs) are located at the very base of the crypts and express the stem cell marker Leucine-rich repeat-containing G-protein coupled receptor 5 (*LGR5*). These cells are strictly associated with differentiated Paneth cells located also at the base of the crypts, they continuously self-renew throughout life and generate all the differentiated cells of the intestinal epithelium. In a continuous process CBCCs undergo symmetrical division giving rise to one daughter cell that will remain adjacent to a Paneth cell and another that will be displaced away from the base towards the tip of the *villus* (figure 5). In this transit amplifying fate, CBCCs will become initially progenitor cells that will further divide and then will progressively differentiate into the many epithelial cell types[2]. The differentiation process is regulated by opposing gradients of Wnt2b and Bmp4 (that promote stemness and differentiation respectively)[2], and also by an oxygen gradient. The oxygen level, in fact, decreases significantly along the *villus* crypt-to-tip axis, as oxygen-rich vessels release most of it at the base of the crypt (pO_2 of 60 to 85 mm Hg) and reach the tip of the *villus* with a lower oxygen partial pressure (pO_2 below 10 mm Hg)[15]. Different regulatory mechanisms modulated by the oxygen level as hypoxia-inducible factors (HIFs) and reactive oxygen species (ROS) produced by mitochondria can play important roles in the Intestinal Epithelial Cells (IECs) differentiation process[15,21].

Homeostatic cell death of differentiated IECs occurs at the tip of the *villus* in a process of programmed cell death called anoikis. Anoikis is initiated via unligated integrins that signal the loss of cell-to-cell and cell-to-matrix contacts in dying IECs and involves an organized zipper-like closure of the AJs and TJs of neighbouring cells that proceeds in a basolateral to apical direction. Neighboring cells extend cytoplasmic processes underneath the shedding cell as it leaves the monolayer to reform TJs and AJs ensuring the removal of the dying apical cells maintaining epithelial contiguity without compromising the barrier function[22,23].

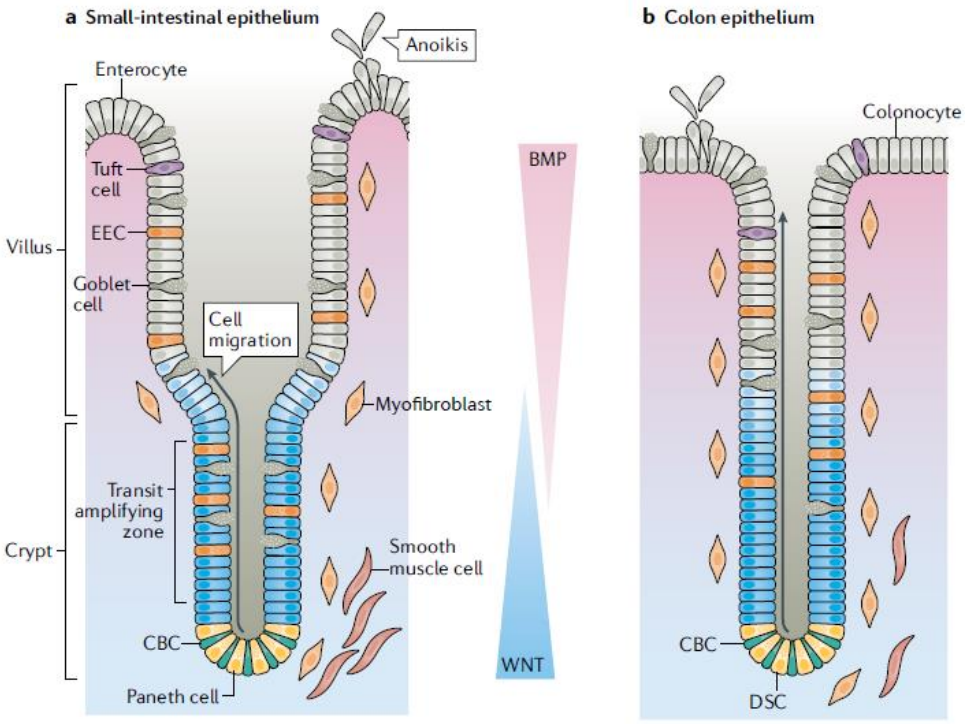

Figure 5: Clonal renewal at the crypt and cell differentiation in both small and large intestines (from Beuemer and Clevers, 2021).

The complete renewal of the functional *villus* epithelium is very rapid, occurring every 2 to 6 days in most adult mammals[23]. As the intestinal epithelium is the most rapid and continuously proliferating tissue in the human body[16], the rate of cell proliferation in the stem and transit amplifying compartments at the crypt base needs to be tightly balanced with the rate of removal of dying cells by anoikis at the tip of the *villus*. Increased rates of proliferation and IEC migration increase the rate of IEC removal at the tip of the *villus* where proliferation pressure induces mechanical extrusion, expulsion and finally anoikis[22].

In IBD different cell death mechanisms are triggered and overregulated, shifting the aforementioned tight balance towards cell death. This leads to drastic physiological outcomes that promote the progression of the disease (see section 1.4).

1.2.3. Cell-to-matrix and cell-to-cell interactions at the basis of IECs differentiation

The differentiated intestinal epithelium consists on an intact and sealed monolayer of cells that fulfills two main physiological roles: i) it behaves as a physical barrier that represents the first layer of defense against pathogenic microbes and antigens in the intestinal tract, and at the same time ii) behaves as a selective sieve that mediates the resorption of nutrients, solutes and water by both passive and active transport mechanisms. These two functions, that at first glance seem to be incompatible, are achieved by three crucial structural characteristics of the intestinal epithelium that have as a common denominator the intercellular junctional complexes: i) strong cell-to-cell interactions that keep the structure of the monolayer and complement the cell-to-

matrix interactions that anchor it to the Extracellular Matrix (ECM), ii) the complete blockage of the space in between adjacent epithelial cells (the paracellular space) and iii) the establishment of a well-defined cell polarity.

The basement membrane constitutes the substrate to which the intestinal epithelial monolayer is associated from the basolateral side. It consists on a thin layer (100 nm) of ECM that provides support and separates the intestinal epithelium from the lamina propria. Its composition is given by glycoproteins such as laminins and nidogen, collagens (predominantly type IV), proteoglycans, and calcium binding proteins such as fibulin[24,25]. Intestinal epithelial cells interact with the different molecular components of the basement membrane via integrin receptors heterodimers forming two kinds of multiprotein complexes: Hemidesmosomes and Focal Adhesions (figure 6). Hemidesmosomes are at the basis of the firm anchorage of the intestinal epithelial monolayer to the basement membrane. These interactions are mediated by the α6β4 integrin that interconnects the laminin-332 to the intermediate keratin filaments through the cytoplasmic-linker protein plectin[26,27]. Focal adhesions are very similar to Hemidesmosomes but are implicated in signal transduction processes and interact mainly with the microfilaments of the cytoskeleton. Once bound to certain components of the ECM, the intracellular domain of the integrin heterodimer transduces those signals by recruiting an array of cytoskeletal adaptors, signalling proteins and enzymes that altogether form the focal adhesion complexes. These complexes modulate then the cytoskeletal organization and initiate a cascade of events that lead to cell survival, proliferation, polarization and complete differentiation. An adequate molecular composition of the ECM of the basement membrane is indeed crucial for the homeostatic regulation of those cellular processes[24,28].

Intestinal epithelial cells polarization is a key pre-requisite for the completion of the cellular differentiation process. The term polarization indicates the process of acquisition of clear differences in ultrastructure, protein composition and cellular functions in between the two apical and basolateral poles of each cell. The resulting apical pole of polarized cells is prepared to face the intestinal lumen, so the external environment, and the basolateral one to interact with the basement membrane and the interstitial space, so the inside of the organism. The identity (structural and functional polarization) of the two apical and basolateral plasma membranes is maintained by key intercellular junctional complexes that will impede the lateral diffusion of integral membrane proteins in between these two domains. The process of polarization occurs through integrin-mediated signals coming from the basement membrane which trigger directional membrane trafficking as early as the first cell division. The process starts with the formation of the apical membrane initiation site and is followed by the formation of a pre-apical patch, demarcated by intercellular junctions that will then block any protein diffusion within the plasmamembrane[28]. β1 integrins have a central role in the establishment of the cell polarity

controlling both the basement membrane deposition by the epithelial cells themselves and the intracellular apical-basal orientation[24].

A set of intercellular junctions mediates the cell-to-cell interactions at the level of the intestinal epithelium (figure 6). These can be grouped into two categories: the apical junctional complex and the communicating GAP junctions.

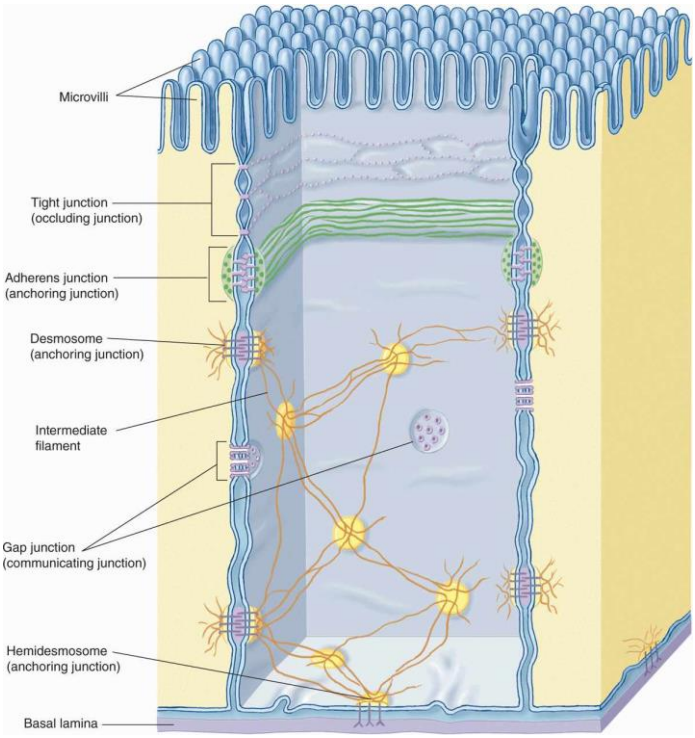

Figure 6: All cell-to-cell and cell-matrix interactions established by intestinal epithelial cells (Focal Adhesions are missing) (from www.basicmedicalkey.com).

Although less studied in this context, GAP junctions can play a key role in the regulation of epithelial function by determining a direct cytosolic connection of adjacent epithelial cells and allowing the free passage of ions and low molecular weight metabolites (less than 2 kDa)[29]. On the other side, the apical junctional complex (figure 7) located at the latero-apical plasma membrane of adjacent intestinal epithelial cells is crucial for the establishment of an integer monolayer of cells, for the tight occlusion of the paracellular space and for the definition and maintenance of the cell polarity at the level of the plasma membrane. From an apical to basal direction, this complex is constituted by the TJs, the AJs and the Desmosomes. The apical junctional complex as a whole is associated with a dense network of microfilaments of actin and myosin (perijunctional actomyosin ring) and with intermediate filaments of keratin. The perijunctional actomyosin ring encircles the apical aspect of each cell and is tightly associated with the cortical actin web that supports the microvilli brush border[30].

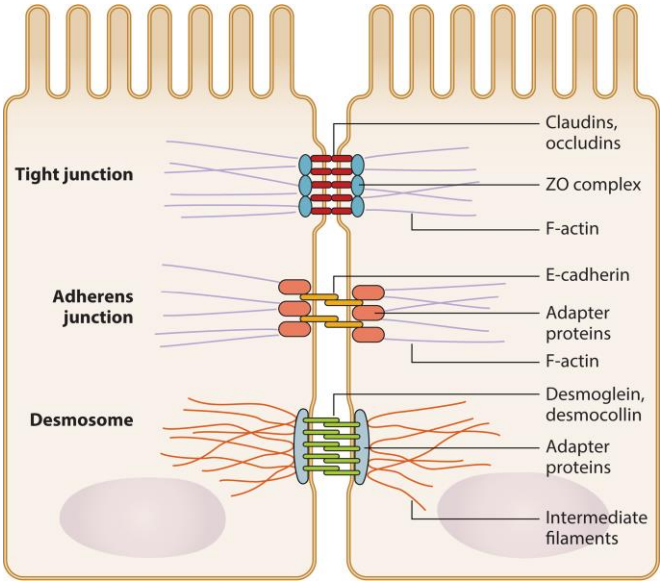

Figure 7: The apical junctional complex including TJs, AJs and Desmosomes. Each of these intercellular junctions is composed of transmembrane proteins, anchored to the micro or to the intermediate filaments of the cytoskeleton by means of adapter proteins (from Hudson *et al.* 2017 [31]).

TJs are the most apical intercellular junctional complex in intestinal epithelial cells. They constitute the intercellular physical barrier that represent the rate-limiting step for the paracellular transport of small molecules and ions (gate function) and the diffusion barrier that restrict the intermixing of apical and basolateral lipids and transmembrane proteins (fence function) within each epithelial cell. Most TJs are formed in between two neighbouring cells, but tricellular junctions can also be formed. These multi-protein complexes are composed of intercellular transmembrane proteins that associate adjacent epithelial plasma membranes, of scaffolding proteins that anchor the first ones to the perijunctional actomyosin cytoskeleton of each cell and of regulatory proteins (figure 8). The transmembrane proteins are the direct responsibles of both the gate and fence functions of the TJs and are associated with cholesterol-rich, raft-like microdomains of the plasma membrane[32]. Among the transmembrane proteins we find the tetraspan proteins of the Claudin family (27 members in humans), the three junctional "MAL and related proteins for vesicle trafficking and membrane link" (MARVEL) domain proteins Occludin, Tricellulin and MARVELD3, the trispan protein blood vessel epicardial substance (BVES), and by a large group of single-span adhesion proteins with two immunoglobulin-like domains that comprises Junctional Adhesion Molecules (JAMs), Coxsackievirus and Adenovirus Receptor (CAR) and Angulins. The scaffolding proteins form the so-called junctional plaque and work as connectors in between the cytoplasmic domains of the aforementioned transmembrane proteins and the F-actin of the perijunctional actomyosin cytoskeleton. This group includes the Zonula Occludens 1, 2 and 3 (ZO-1, ZO-2 and ZO-3), cingulin (that binds to microtubules), Paracingulin, the Multi-PDZ Domain Protein 1 (MUPP1),

Membrane-Associated Guanylate Kinase Inverted (MAGI), Partitioning Defective 3 and 6 (PAR3 and PAR6), Protein Associated with Lin-1 1 (PALS1) and PALS1-associated tight junction (PATJ). The last group of proteins that take part in the TJ complexes are the signalling or regulatory proteins that interact with either the transmembrane or the scaffolding proteins, and include: protein kinases (as the Atypical Protein Kinase C or aPKC), phosphatases, monomeric and trimeric GTP-binding proteins and transcriptional (as the transcriptional regulator ZO1-associated nucleic acid binding protein (ZONAB)) and post-transcriptional regulators. The diverse functional properties of the many Claudins with regards to the sealing of the paracellular space provides an explanation for the high number of transmembrane proteins recruited to the TJ density, but this is not the case for the numerous adaptor proteins. Knockouts and knockdowns of single adaptor proteins showed that many of them have redundant functions[33]. The complexity of the TJD as a whole entity is anyway the reason for its multi-functionality, as TJs fulfill another key role a part from the aforementioned ones. They behave as platforms that transduce signals to the interior of the cell in response to cell density and also to cellular stressors determining modifications in the structure of the cytoskeleton and regulating cell proliferation and differentiation. Different TJPs as ZONAB and ZO-2 have a dual localization at both the TJ density and the nucleus where they can interact with different transcription factors and regulate gene expression. TJs can also signal to the cell interior through various classical pathways such as the JUN N-terminal kinase (JNK) MAPK (Mitogen-activated protein kinase) and ERK (Extracellular signal-regulated kinases)[33].

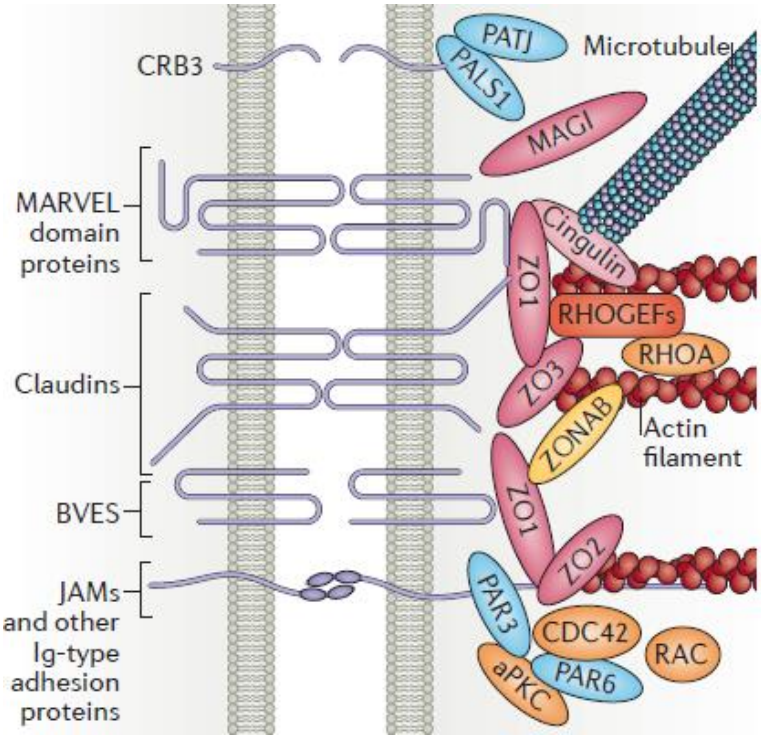

Figure 8: The components of the TJs (from Zihni *et al.* 2016[33]).

AJs and Desmosomes locate basolaterally to the TJs and their primary role is to provide adhesive forces to the cell-to-cell interactions. They are not involved in the gate and fence functions fulfilled by the TJs but they support the establishment of the last ones. AJs are composed of cadherins, single spanning transmembrane proteins that interact homotypically with the extracellular portion of cadherins on adjacent cells. On the cytoplasmic side, cadherins interact directly with p120 catenin and β-catenin, which in turn interact with α-catenin which interacts with the actomyosin cytoskeleton (figure 9). AJs regulate the perijunctional actin assembly providing further strength to this structure, are necessary for the efficient assembly of TJs and also are involved in intracellular signalling and transcriptional regulation[30,34].

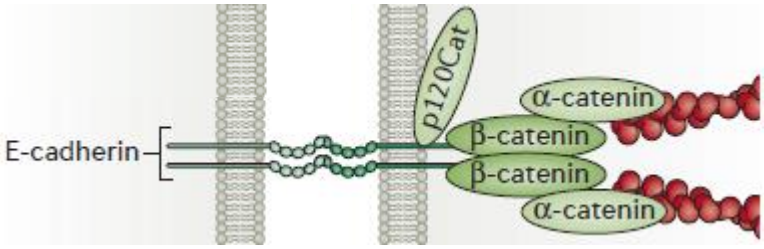

Figure 9: The components of the AJs (from Zihni *et al.* 2016[33]).

At the bottom of the apical junctional complex are located the Desmosomes (figure 10) which are adhesive structures composed of the desmosomal cadherins Desmocollin and Desmogelin that are anchored to the intermediate filaments by Desmoplakin[30].

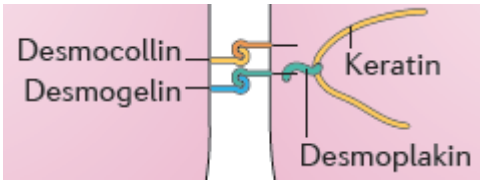

Figure 10: The components of the Desmosomes (from Odenwald *et al.* 2016[30]).

1.2.4. Intestinal epithelial barrier function and transepithelial transport

The term epithelial barrier function refers to all the mechanisms leading to the homeostatic regulation of a certain epithelium whose role can be either to delimit different compartments of the body or to line the surfaces of the body in direct contact with the external environment. In the context of the intestinal epithelium a broad definition of barrier function is used to refer to all the extrinsic and intrinsic factors involved in the maintenance of its integrity and homeostasis as part of the intestinal mucosa (generally denoted as mucosal barrier), and a more specific one refers only to the intrinsic characteristics of the intestinal epithelial cells monolayer that allow it to restrict the free exchange of single ions, water, macromolecules and complete microorganisms between the intestinal lumen and the interstitial space. The object of this thesis is focused on the second definition of barrier function, but both concepts will be briefly described as follows.

The intestinal epithelial barrier is composed mainly by the plasma membranes of the single epithelial cells, which are of very high resistance and impermeable to hydrophilic solutes unless specific membrane transporters are present. As a free passive diffusion of hydrophilic solutes can take place only across the space in between adjacent epithelial cells, the paracellular space, the term barrier function refers specifically to the level of permeability across it. As explained before, TJs are the primary determinants of the paracellular permeability, so their functional localization and integrity (supported also by the AJs and the Desmosomes) constitute the main intrinsic factor underlying the intestinal epithelial barrier function. The other intrinsic factors are the mechanisms of epithelial repair and restitution that allow the maintenance of the contiguity of the epithelial monolayer and of the TJBs avoiding the formation of wide empty spaces generated by the basal homeostatic rate of cell death and particularly by an abnormal increase of cell death that can take place under pathological conditions.

The extrinsic factors that contribute to the barrier function of the intestinal epithelium as part of a mucosal barrier, act at the GI lumen and at different levels of the intestinal mucosa. In the GI lumen, biliary juices and gastric and pancreatic acids can directly degrade microorganisms and microbial antigens that could potentially generate a breach across the intestinal epithelium. Furthermore, the intestinal microbiota can inhibit the colonization of pathogenic microorganisms that are able to reach this site[16]. The following series of extrinsic factors act on the outer side of the intestinal mucosa and consist on the different components of the mucus layer (uninterruptedly present along the whole digestive tube). This is a hydrated gel composed of mucins secreted by goblet cells that prevents large particles and microorganisms from coming into direct contact with the underlying epithelium. In addition, the mucus layer consists of bicarbonate, of Immunoglobulin A (IgA) (one of the most abundant antibodies in mucosal secretions) and of antimicrobial peptides produced by Paneth cells[30,35]. The final series of factors that contribute to the barrier function of the epithelium and of the whole mucosa act underneath the intestinal epithelium itself and consist of the innate and adaptive immune cells that continuously patrol the lamina propria and that can even sense the intestinal lumen (acting even before a pathogenic microorganism can generate a breach across the epithelium).

The intestinal epithelial barrier function (level of permeability across the paracellular space from now on) increases longitudinally and radially along the intestinal tract[16]. Longitudinally in the sense that from the beginning of the small intestine to the colon the resistance of the intestinal epithelium increases. This is explained by the fact that the main role of both the small and large intestines is the absorption of electrolytes, nutrients and fluids and the barrier function is essential for these processes to take place in a selective fashion. Furthermore, at the level of the colon the density of microbial organisms belonging to the microbiota increases drastically so, notwithstanding being commensal, is important for the host that they do not overpass the epithelium. The radial increase of barrier function refers to the fact that it increases along the

crypt-to-tip of the *villus* axis. This is explained by the fact that the cells at the tip of the *villi* are the differentiated ones, a process that is accompanied by the increase in barrier function.

As mentioned before, the selective transport of ions and molecules across the intestinal epithelium (quintessential for the homeostasis of the organism) demands an increased level of barrier function. The transport of a certain solute across the intestinal epithelium can take place in principle via two possible transepithelial pathways (figure 11): the paracellular (in between cells) and the transcellular (across the apical and basolateral membranes of polarized epithelial cells) pathways.

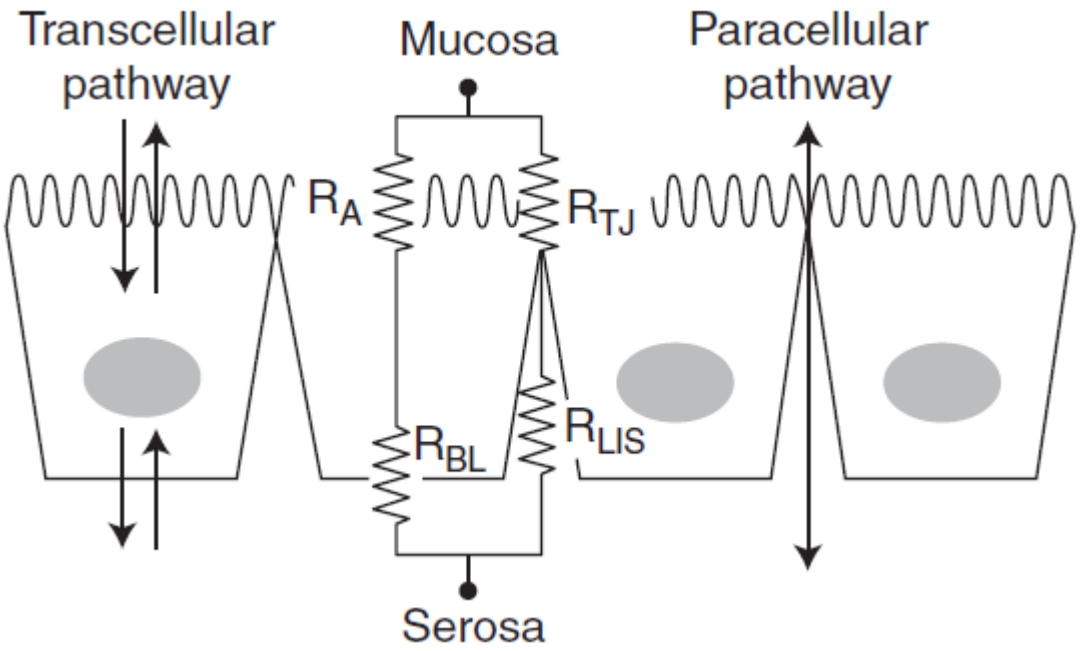

Figure 11: The transcellular and paracellular transepithelial transport pathways (from Anderson and Itallie, 2009). The resistive elements (towards ionic currents) of a polarized epithelium are evidenced. The resistance across the transcellular pathway is the sum of the apical membrane (R_A) and basolateral membrane (R_{BL}) resistances, that are in series. These two are in parallel with the resistors of the paracellular pathway: the resistance of the TJs (R_{TJ}) and the resistance of the lateral intercellular space (R_{LIS}), that are in series. The R_{LIS} is in general neglectable.

In a differentiated epithelium, the high level of barrier function forces the transport of ions and hydrophilic molecules (that cannot diffuse passively across the plasma membranes) via the transcellular route. Even though a selective transport of these species can take place via the paracellular space (see below), most of it takes place via the array of membrane pumps, carriers and ion channels that constitute the transcellular pathway. The main characteristics of the transcellular transport of ions and hydrophilic small molecules, that distinguish it from the paracellular one, are that it is rectifying, active and highly regulated by physiological stimuli. The rectifying transport (directed either to the interstitial space or to the lumen) is determined by the polarized distribution of the different transporters to either the apical or the basolateral

plasma membrane domains. The primary transcellular transport is by definition active, so powered by the hydrolysis of ATP, and it moves specific ions against their electrochemical gradients. These gradients are then exploited by a secondary active transport carrier to couple energetically unfavorable uphill movements of nutrients, such as glucose or aminoacids, to the downhill movement of a specific ion. The physiological regulation of the transcellular transport is in principle more sophisticated than the one of the TJ gate, including both short and long term hormonal modulations[16].

While the primary and secondary transcellular transport mechanisms work for ions and small to medium size hydrophilic molecules, large molecules, like proteins and bacterial products, that cannot traverse the cell membrane or the paracellular space, can be transported through the transcellular route via a series of different mechanisms grouped under the terms of endocytosis and transcytosis. Following endocytosis, the engulfed substances are actively transported through the cytoplasm by transcytosis and released from the other pole of the epithelial cell. Endocytosis and transcytosis mediate the uptake of foreign antigens against which the organism can initiate an immune response and are also pathways hijacked by pathogenic microorganisms to initiate and infection process[35].

As mentioned before, water, ions and small hydrophilic molecules are not totally excluded from the paracellular route because the integer TJ gate behaves as a selective semipermeable rather than an impenetrable diffusion barrier. The transepithelial paracellular transport pathway is also highly selective (being able to discriminate in between water and solutes on the basis of size and charge), but passive (not requiring the hydrolysis of ATP), non-rectifying (the different ions and molecular species will always move downhill their electrochemical gradient upon an increase of paracellular permeability) and likely less regulated than the transcellular one. Across the paracellular route three different permeability pathways (figure 12) have been identified on the basis of their size-selectivity, charge-selectivity, conductance (the ability to pass ionic currents) and capacity (quantity of ions and small uncharged solutes that can permeate). The pore pathway is a high-conductance, high-capacity route that is charge-selective and extremely size-selective, with an upper limit of 6 to 8 Å in diameter. On the contrary, the leak pathway is a low-conductance, low-capacity route that does not discriminate between solutes on the basis of charge and allows limited flux of large hydrophilic molecules with an upper size limit of 100 Å in diameter[32,36]. The unrestricted permeability pathway is the third possible paracellular route which manifest no size nor charge selectivity and a high conductance and capacity.

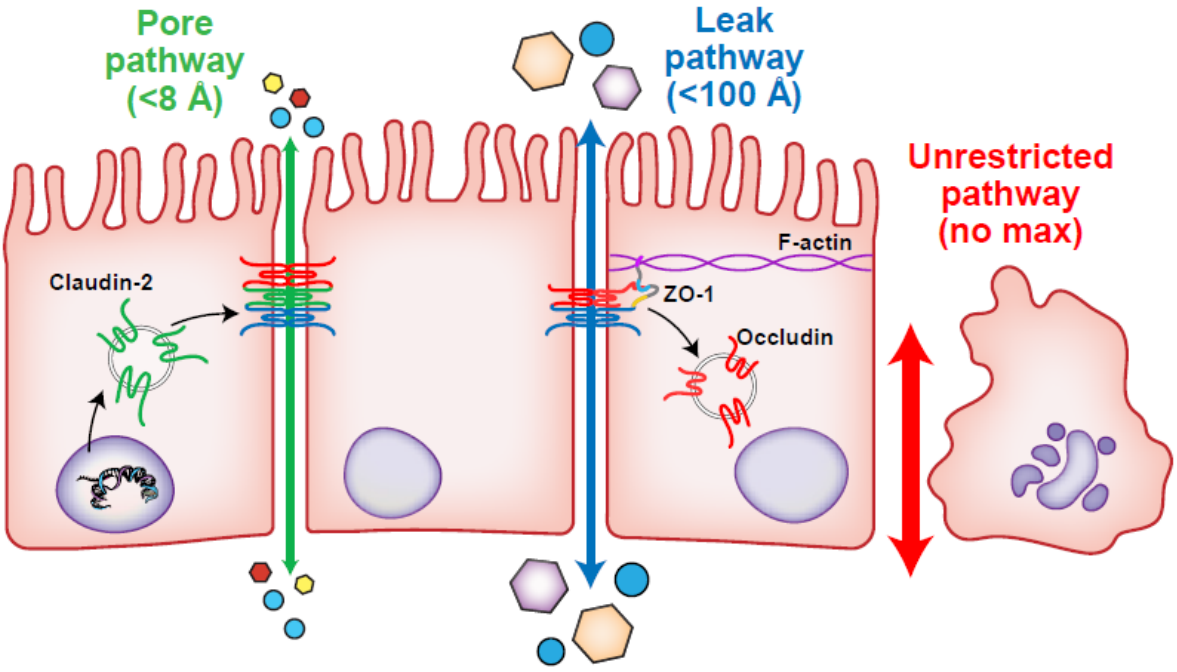

Figure 12: The three permeability pathways of the paracellular route (from Zuo *el al.*, 2020).

The mechanisms at the basis of the different permeability pathways can be explained by the ultrastructure of the TJD. The actual knowledge indicates that the TJ paracellular gate consists of strands (anastomosing network of transmembrane particles observed by freeze-fracture electron microscopy) that are absolute barriers punctuated by pores that can be open or closed. The resistance of each strand is a function of the open probability of the pores[32]. These pores are known to consist on Claudin complexes that behave as ion channels with a specific gating and ion-selectivity. The pore permeability pathway is indeed represented by the integer TJ gate in which the size- and charge-selectivity towards ions and small molecules is dictated by its Claudins composition. Alternative splicing of the 27 Claudin genes gives rise to an even greater number of Claudin proteins which can be divided into pore-forming cation-selective (as Claudin-2, 10b, 15 and 16), pore-forming anion-selective (as Claudin-10a and 17) and barrier-forming (as Claudin-1, 3, 5, 11 and 19)[33,36,37]. The possible combinations of all these proteins at the TJD regulates the pore permeability pathway. The mechanisms underlying the leak pathway are less well understood but it is certain that ZO-1 and Occludin down-regulation and removal from the TJD are implicated in its regulation. A possible model (figure 13) involves dynamic properties of the TJ strands, such as remodeling of the branches or even dissociation and reformation of strand sections, leading to transient openings of the paracellular space to allow the stepwise diffusion across the junction of molecules of more than 8 Å in diameter[33]. The remodeling of the TJ strands is controlled by cytoskeletal dynamics (microfilament depolarization) and myosin light chain kinase (MLCK) activity (which correlates with Occludin internalization via a specific type of lipid raft called caveolae and with the alteration of ZO-1 protein dynamics[32,38]).

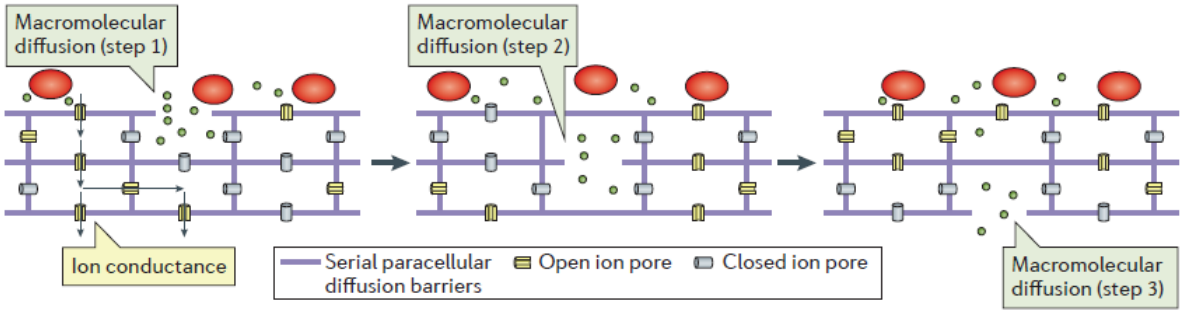

Figure 13: Mechanistical explanation of the pore and leak permeability pathways of the paracellular route (from Zihni *et al*., 2016). The green particles indicate hydrophilic molecules of less than 100 Å in diameter; red particles indicate larger hydrophilic molecules that can only traverse the paracellular route via the unrestricted permeability pathway or the transcellular route via endocytosis followed by transcytosis; the serial blue lines, which sequentially open and close, indicate the TJ strands seen in freeze-fracture electron microscopy.

Important to mention is that an increase of permeability across the leak pathway, determined by certain cellular physiological conditions, does not necessarily affect the pore permeability pathway[39], whereas the opening of the unrestricted pathway inevitably affects both pore and leak pathways and determines the most drastic effect on the overall epithelial barrier function. The unrestricted permeability pathway is independent on the TJ gate's integrity as it consists on wide, empty spaces along the epithelial monolayer that correspond to sites of consummated Apoptosis or Necroptosis or sites of a failed restitution following the physiological process of Anoikis at the tip of the *villi*.

1.3. The GI immune system

Being in direct contact with the external environment, the GI mucosa is under the continuous threat of pathogens and pathogenic antigens. The necessity for a semipermeable epithelial barrier, capable of selectively translocating solutes in both directions, is accomplished by an intrinsically fragile monolayer of cells, which represents one of the predilected routes for pathogens to initiate an infectious process. The GI immune system has evolved for the protection of this exposed surface and is composed by an innate component, consisting on the epithelium itself, antimicrobial peptides and cells bearing invariant pathogen-recognition receptors (that detect common microbial structures or the damage caused by them), and by an adaptive component, given by immune cells bearing antigen receptors that are specific to individual pathogens (and confer sensitivity, specificity and immunological memory to the response).

The GI innate immune system represents the first line of defense against any possible pathogenic threat, and is characterized by the rapidity of the reaction. Its main component is the GI mucosal barrier, constituted by the tightly sealed epithelial monolayer, its protective layer of mucous on the luminal side and the non-pathogenic microbes of the commensal microbiota. The sealing of the paracellular spaces at the GI epithelium, forces any possible microbe translocation through

the highly selective transcellular route. The mucous layer together with the gut peristalsis, prevent microbes from adhering to the GI epithelium. Commensal microbes not only contribute to the development and maturation of the GI immune system, they also keep pathogens away by ecological competition, by producing certain antimicrobial substances and by inducing the GI epithelium to produce them[3,16].

Antimicrobial peptides represent another important component of the GI innate immune system, that supplements the action of the antimicrobial chemicals of the upper GI tract. Paneth cells of the GI epithelium produce and secrete: the glycosidase Lysozyme that digest the peptidoglycan component of the bacterial cell wall, Phospholipase A_2 that can hydrolyze phospholipids of the bacterial cell membranes, as many as 21 different Defensins that disrupt the bacterial cell membranes and the membranes of some enveloped viruses, Cathelicidins that also determine bacterial cell membranes lysis, and C-type Lectins that form pores in the bacterial membranes[3].

If a breach at the GI mucosal barrier allows the translocation of pathogenic microbes, the next mechanism of innate immune defense that takes action is the Complement system. Complement proteins are more than thirty, are produced mainly by the liver and are constantly present in the bloodstream and in interstitial fluids, in an inactive form. In the presence of a pathogen or of an antibody-bound pathogen, the Complement system gets activated and contributes to the elimination of the threat by triggering an inflammatory process, the phagocytosis of the pathogen or the lysis of its plasma membrane[3].

The aforementioned GI innate immune mechanisms are characterized by being ready at any moment, in order to take immediate action. If the pathogenic entity is able to overpass them, the so-called induced innate immune response will get activated and give rise to an inflammatory process that will be kept for several days. The main actors of the induced innate immune response are the phagocytic and sensor cells that stably reside at the lamina propria, patrolling the whole GI mucosa (even sensing the luminal side of the GI epithelium) in normal homeostatic conditions. The first cell type of this category, that most pathogens will encounter after traversing the GI epithelium, is represented by Macrophages. They derive from circulating Monocytes of the bloodstream and represent the most abundant phagocytic sensor cells at both the lamina propria and submucosal layers. Neutrophils, and at lower extent other granulocytes, are important phagocytic sensor cells at the GI mucosa but they stably reside in the bloodstream and are rapidly recruited to this site upon an infection takes place. The last important cell type of this category is constituted by Dendritic cells, which stably reside at the GI mucosa and at peripheral lymphoid organs, and fulfill the important roles of phagocyting and digesting microbes and presenting their antigens to T-cells for inducing an adaptive immune response. The common characteristic shared by these three cell types is the presence of innate sensor proteins at their plasma membranes, which not only activate the cell's individual effector function, but which are also responsible for the induction of the inflammatory process. These

sensor proteins are called PRRs and recognize simple molecules or conserved molecular patterns of pathogenic (and in many cases also non-pathogenic) microorganisms that are known as Pathogen Associated Molecular Patterns (PAMPs). PRRs include the transmembrane proteins TLRs and the cytoplasmic proteins NOD-like receptors (NLRs), among others[3]. Upon the engagement of PAMPs, PRRs activate the sensor phagocytic cells to produce an array of inflammatory mediators called cytokines and chemokines. Cytokines are small proteins (± 25 kDa) secreted by many different cell types of the body, that convey signals to target cells expressing specific cognate receptors. The transfer of the signal carried by each cytokine can take place in an autocrine, a paracrine or an endocrine manner and it affects the target cells, of one or more types, in accordance to the pattern of specific receptors expressed by them. There are more than 60 different cytokines that determine a multiplicity of cellular physiological effects and they are grouped into families, as well as their receptors, in accordance to their structure[3]. Chemokines also constitute a numerous group of small proteins secreted at the early stages of an infection process, but specialized in the induction of a directed chemotaxis of monocytes, neutrophils and lymphocytes from the bloodstream to the site of infection.

The inflammatory process takes place within hours after the establishment of the infection process and is initiated by Macrophages that, upon engagement of PAMPs, release pro-inflammatory cytokines, such as TNFα, and chemokines. The whole inflammatory process is orchestrated by the multiple effects of the cytokines and chemokines, and contributes to the elimination of the pathogenic threat by inducing four changes in the local blood vessels of the site of infection. The first two (in a temporal sequence) are: **i)** an enlargement of the vascular diameter that increases the local blood flow (in order to convey effector immune molecules and cells to the site of infection) but reduces its velocity, and **ii)** the induction of endothelial cells of the blood vessels to express cell-adhesion molecules. The reduction of the blood flow velocity and the expression of the cell-adhesion molecules consent to the leukocytes of the bloodstream to extravasate into the tissues of the site of infection. The first ones that reach these tissues are the Neutrophils, then the Monocytes (which can differentiate as Macrophages and Dendritic cells), and finally the Eosinophils and the Lymphocytes. The other two changes that the local blood vessels undergo, under the effect of the cytokines, are: **iii)** an increase of the endothelial permeability that determines an exit of fluid and effector molecules from the blood to the surrounding tissues (giving rise to the edema) and **iv)** the induction of local blood clotting that blocks the spread of the infectious agent from the site of infection to other districts, and promotes the reparation of the injured tissue[3]. The drastic changes that the inflammatory process induces in the surrounding tissues of the site of infection can block the completion of this process and its spread into other districts of the body, but also determines side effects that should ideally be confined to that site. These side effects are a direct consequence of the nature of the numerous pro- and anti-inflammatory cytokines, which fulfill pleiotropic roles by engaging multiple

cognate receptors (which not always lead to the same cellular response). The inflammatory process evolved as double-edged sword that can lead to disastrous effects if kept chronically active (determining to chronic inflammatory diseases) or if translated and amplified at the systemic level (generating the so-called cytokines storms that, through the bloodstream, can reach other districts of the body). The tight control of the balance in between pro- and anti-inflammatory cytokines is quintessential for the spatial and temporal confinement of the inflammatory process.

Disregarding of the ability of the sole inflammatory process in neutralizing the infectious threat, the recruitment of Dendritic cells to the site of infection activates by default the adaptive immune response, that will confer specificity and memory to the immunological response. Interestingly, comparative studies suggest that the GI immune system was the first component of the Vertebrate's immune system to evolve an adaptive immunity, and this was very probably linked to the necessity of keeping under control the Microbiota that co-evolved with Vertebrates[3]. This underlines once again the importance of the Microbiota, that is not only necessary for the correct embryonic development of the immune system of the single individual, but that was also at the basis and shaped the evolution of the most sophisticated branch of the immune system. GALTs, that include the tonsils, the adenoids, the appendix, the isolated ILFs of both small and large intestines and the Peyer's patches of the small intestine, are secondary lymphoid tissues specialized for the collection of pathogens and pathogenic antigens at GI tract and for the subsequent initiation of an adaptive immune response. Peyer's patches are the most important GALTs and consist of a central large follicle of B lymphocytes surrounded by a reduced number of T lymphocytes. Specialized epithelial M cells collect the antigens at the GI epithelium, deliver them to Dendritic cells which in turn present them to the T lymphocytes of the Peyer's patches. Activated T lymphocytes, via Peyer's patches or via the sole action of Dendritic cells presenting antigens in other GALTs, travel through the lymphatic system into the bloodstream and are then conveyed back to the GI mucosa as effector cells. The effector T cells that reach the GI mucosa can deal with the ongoing infection in three ways: can directly kill infected cells (Cytotoxic T cells), can produce pro-inflammatory cytokines and activate B cells for producing, mainly, IgA antibodies (Helper T cells, or T_H) or can suppress the activity of other lymphocytes and keep the immune response under control (Regulatory T cells, or T_{reg})[3]. Interestingly, many effector and memory T cells locate stably not only at the lamina propria but also at the GI epithelium. The presence at the GI epithelium of intraepithelial lymphocytes (IELs) (one of the largest populations of lymphocytes of the body), of Dendritic cells and Macrophages, and the capacity of this tissue not only to respond to basolateral cytokine signals but also to secrete cytokines by itself, make of it an active component of both innate and an adaptive GI immune system, rather than a simple physical barrier.

The production of anti-inflammatory cytokines as Transforming Growth Factor beta (TGF-β) and Interleukin 10 (IL-10) by T_{reg} cells is at the basis of the homeostatic regulation of the GI immune responses and of the immune tolerance of the GI immune system to the nutrients and the Microbiota. The proved bi-directional communication in between the CNS and the ENS, and in between the last one and the GI immune system, could contribute to the regulation of both the immune responses at the GI mucosa and to the GI immune tolerance. However, the mechanisms by which the ENS circuits integrate with the microbe-mediated GI immune responses are poorly understood so far[1].

All the components of the GI innate and adaptive immune system are illustrated in Figure 14.

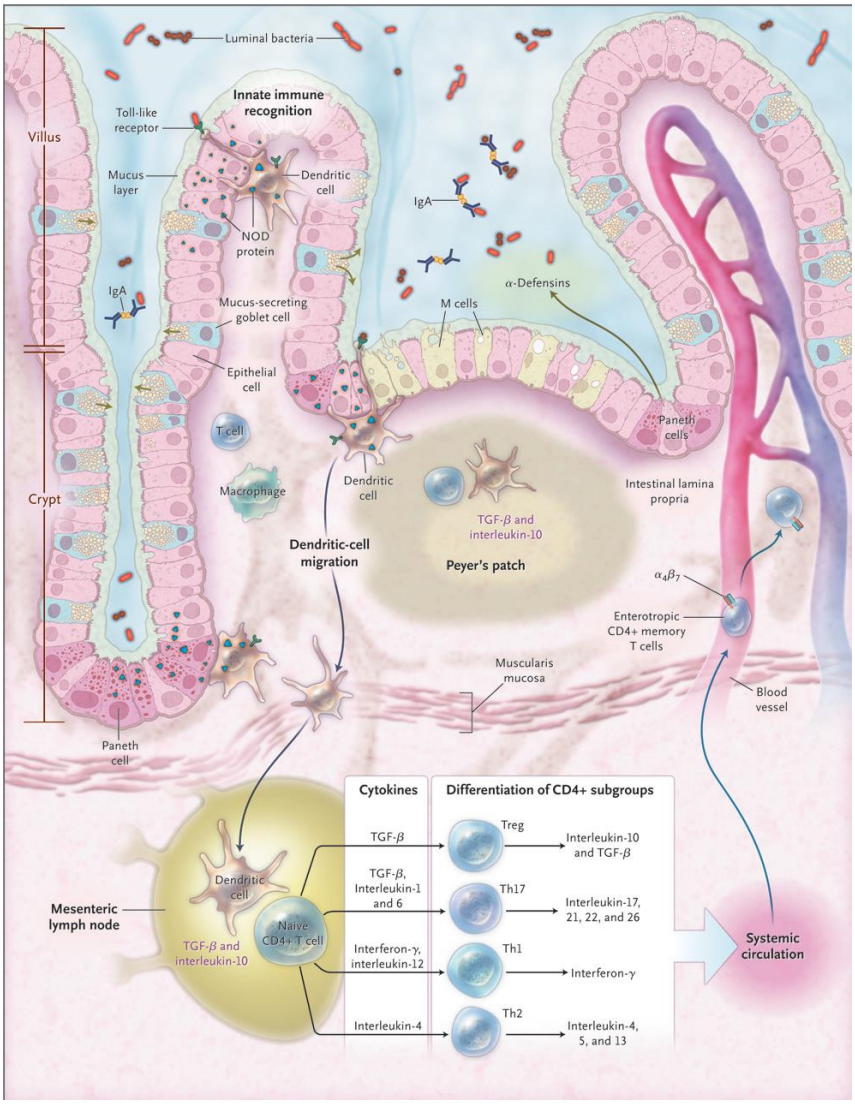

Figure 14: Components of the intestinal innate and adaptive immune system (from Abraham and Cho, 2009).

1.4. Inflammatory Bowel Disease (IBD)

IBD is a complex pathological condition originating from a disturbed homeostasis of the GI immune system that results in a perturbance of the tight balance in between the immune tolerance

and the defensive inflammatory responses towards the Microbiota. IBD presents many features of an autoimmune disease, even though the aberrant immune response that characterizes it is not primarily directed towards self-antigens. The failure of the regulatory mechanisms that confer an immune tolerance towards the commensal microbes that stably reside at the GI lumen, and their microbial antigens, gives rise to an unrestricted and uncontrolled immune response with destructive side effects, primarily confined to the GI tract. IBD encompasses two main clinical entities in accordance to the spatial circumscription of their inflammatory processes: a manifestation of solely mucosal inflammation more limited to the colon named ulcerative colitis (UC), and a condition of transmural inflammation of any part of the GI tract denominated Crohn's disease (CD)[40].

Being IBD a complex genetic disease, the interaction and combination of both genetic and environmental factors are the basis of the disruption of the homeostatic state at the GI wall, that bring both innate and adaptive branches of the GI immune systems to mount the exaggerated immune responses towards the Microbiota. More than 200 independent genetic risk loci have been identified in the pathogenesis and in the progression of IBD including genes associated with the recognition of microbial antigens by the innate immune system, with the coordination and regulation of both innate and adaptive immune responses, with the epithelial barrier function and repair and with the apoptotic and necroptotic pathways[40-42]. Among the key environmental factors that contribute to the pathogenesis of IBD are worth to be mentioned: dysbiosis (originating from changes in the diet and with the exaggerated consumption of wide-spectrum antibiotics), recurrent infections, stress, consumption of Non-steroidal anti-inflammatory drugs (NSAIDs) and smoking[43].

The pathogenesis and pathomechanisms of IBD are simplistically summarized in Figure 15. In genetically susceptible individuals, environmental stresses or an acute GI infection initiate the process by impairing the epithelial barrier function. An initial uncontrolled influx of microbes and microbial antigens activates Dendritic cells to translocate into and present antigens at the mesenteric lymph nodes, where they promote the differentiation of naive T cells. The cytokine milieu, secreted in part by Dendritic cells at both lymph nodes and GI mucosa, is the responsible for skewing the differentiation of naive $CD4^+$ T cells into T_H1-, T_H2-, T_H17- or T_{reg}-cell subsets. This process, tightly regulated in homeostatic conditions, in IBD is biased towards the production of cytokines, as IL-12 and IL-23, that determine the differentiation into T_H1- and T_H17-effector cells. Either the differentiation bias of naive T cells or a failure of T_{reg}-cells to suppress T_H1- and T_H17-cells, can be the reasons for the disruption of the tight equilibrium in between effector and regulatory signals. As a consequence of this, a massive production of pro-inflammatory cytokines (e.g. TNFα, IFNγ and IL1β) and a downregulation of anti-inflammatory ones (e.g. TGFβ and IL-10)[3,43] unleashes exaggerated innate and adaptive immune responses at the GI mucosa or at the whole GI wall. As mentioned above, an initial impairment of the GI

barrier function triggers the whole process, either as a result of an environmental insult and/or because of congenital defects in the epithelial cells proliferation, polarization and differentiation processes, in the consequent establishment of barrier function, in the epithelial cell-matrix adhesion capacities and in the epithelial restitution processes after injury. A part from this, a further and more pronounced GI epithelial barrier disruption is always the consequence of the inflammatory process itself. In fact, it is the imbalance in between pro- and anti-inflammatory cytokines that directly modulates the activity of specific receptors at the basolateral surfaces of GI epithelial cells, determining drastic modifications in the TJ and AJ complexes and an increase of the cell death rate (by Apoptosis and Necroptosis). The further increase of the epithelium's permeability determines a continuous infiltration into the lamina propria of microbes and antigens and a continuous recall of innate and adaptive immune cells from the bloodstream into the GI mucosa that amplify the response. This positive feedback loop, generated by the cytokine-mediated impairment of the epithelial barrier function, gives rise to the chronic manifestation of the exaggerated inflammatory condition, that in the long term leads to complications such as development of fibrosis, stenosis, fistulas, colorectal cancer and even extra intestinal complications due to the passage of the cytokines to the blood circulation[40,43].

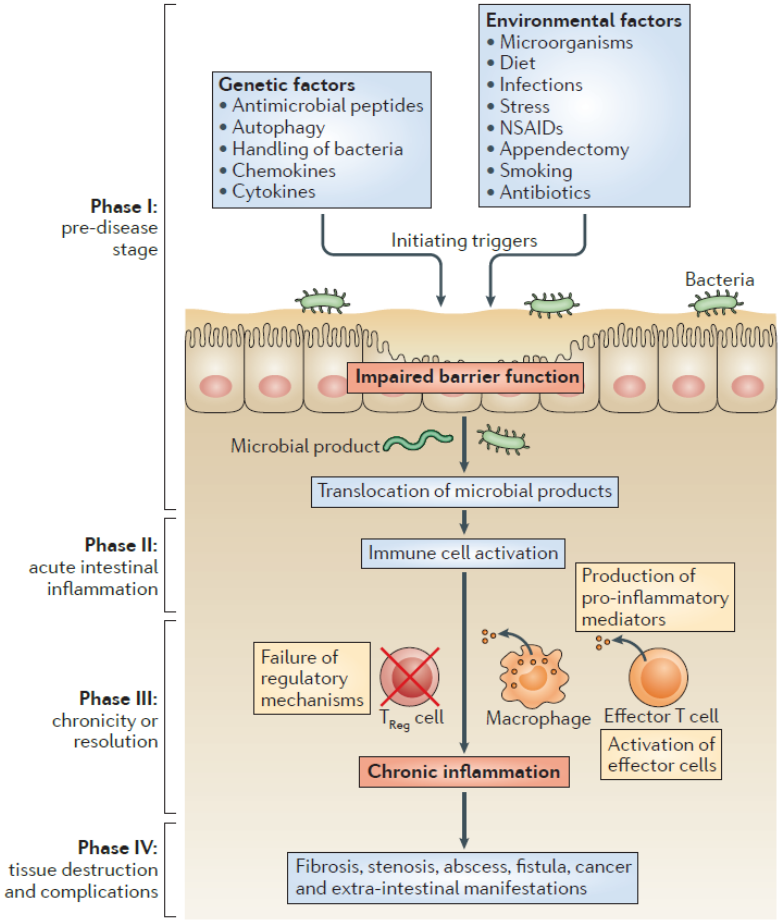

Figure 15: Overview of the pathogenesis and of the pathomechanisms of IBD (from Neurath, 2014).

The effects that the imbalance in between pro- and anti-inflammatory cytokines determines on the GI epithelial barrier function are multiple and not yet fully understood. The complexity of the mechanisms at the basis of the regulation of the paracellular permeability, added to the intrinsic complexity of the cytokines signallings, suggest that for both pro- and anti-inflammatory single cytokines, a combination of even opposite and contradictory physiological effects could act on the barrier function. It will be the overall sum of the single barrier-disruptive and barrier-protective effects (affecting the three paracellular permeability pathways) of the multiple cytokines taking action, to determine the final level of paracellular permeability. Pro-inflammatory cytokines as TNFα and IFNγ have been shown to alter the TJs integrity and to induce cell death, whereas cytokines as IL-22 (which determines both pro- and anti-inflammatory effects) induce cell survival and proliferation[43]. In summary, the pro- and anti-inflammatory cytokines stimuli on epithelial barrier function can alter: **i)** the pore permeability pathway by differentially affecting the expression and functional latero-apical subcellular localization of both pore-forming and sealing Claudin proteins, **ii)** the leak permeability pathway by affecting the expression and functional latero-apical subcellular localization of Occludin and/or ZO-1, **iii)** the unrestricted permeability pathway by affecting the balance in between cell proliferation and programmed cell death. By allowing the transcellular translocation of even entire microbes, the unrestricted permeability pathway is the most relevant one in the context of IBD. The three mechanisms of programmed cell death that affect the unrestricted paracellular permeability pathway in IBD are Apoptosis, Necroptosis and Pyroptosis. Apoptosis is a programme of cell death triggered by cellular challenges that activate either receptor-driven (extrinsic) or mitochondria-driven (intrinsic) pathways, that culminate in the activation of the executioner Caspases 3 and 7, via the initiator Caspase 8 (for the extrinsic pathway) or Caspase 9 (for the intrinsic pathway). The formation of apoptotic bodies prevents the release of cytosolic content into the surrounding microenvironment, that would fuel the inflammatory response. The other two modes of programmed cell death are instead pro-inflammatory, as characterized by a plasma membrane lysis that consent the leak of cytosolic material. Necroptosis is a process of programmed cell death caspase-independent, and it even requires the inhibition of effector caspases. The engagement of death receptors as TNR1A, TLRs and Z-DNA-binding protein 1 (ZBP1) by external stimuli, culminates in the phosphorylation (mediated by Receptor Interacting Protein Kinase 3 or RIPK3), oligomerization, membrane translocation and pore formation of the mixed linked kinase-like protein (MLKL). Pyroptosis is a pathogen-induced programmed cell death triggered by PAMPs that determine the activation of PRRs of the NLRs family. Different activated PRRs can oligomerize and transfer the death signal to Caspase 1, via adaptor proteins, forming the so-called Inflamasome that execute the pyroptotic cell death via plasma membrane lysis[22].

The actual pharmacological therapies approved for IBD work on the general down-regulation of the immune system by targeting key pro-inflammatory cytokines, master regulators of the inflammatory processes. Anti-cytokine therapies (such as antibodies specific for TNFα, IFNγ, IL-12 or IL-23) and cytokine signalling blockers (such as inhibitors of the Janus Kinases-Signal Transducer and Activator of Transcription proteins pathway, or JAK-STAT) seem to have beneficial clinical effects only in certain subgroups of patients and, being highly immunosuppressive, result in an increased risk of infection or reactivation of infections[40,43]. On the other side, anti-proliferative therapies that aim to target the innate and adaptive immune cells of the lamina propria, determine drastic side effects on the GI epithelial barrier.

The actually approved therapies were designed for acting on the immune cells of the lamina propria and submucosal layers, but not for protecting the GI epithelial barrier dysfunction that is at the basis of the chronicity of IBD. Promising pharmacological strategies for protecting the GI barrier dysfunction could be: the blocking of the expression of the pore-forming Claudin 2, the antagonism of the MLCK (which determines the endocytosis of Occludin and the opening of the leak pathway), the stimulation of cell proliferation with the mitogens EGF and R-spondin-1[30] and the employment of PANoptotic inhibitors to counteract the increase of programmed cell death (taking into consideration potential tumorigenic side effects). A combination of more refined immunosuppressive therapies (that could reduce their side-effects) with barrier-protective ones would highly improve the outcome of the treatment, considering that is the high epithelial paracellular permeability that determines the fueling of the hyper-reactive immune system with microbes and microbial antigens.

1.5. The TNFα signalling

TNFα is an extraordinarily pleiotropic cytokine with major roles in both physiological homeostatic and pathological processes. Being part of the TNF superfamily of ligands (TNFSF), TNFα is best known as a master regulator of the innate and adaptive immune responses, playing crucial roles in the initiation and orchestration of inflammation and in the recruitment and activation of innate and adaptive immune cells. Two opposite behaviors of TNFα with regards to tissue homeostasis and immune response are clearly evidenced. When produced at low levels, in a controlled manner, TNFα has beneficial tissue homeostatic functions (e.g. regulating the cell turnover and cell differentiation, mediating the resolution of inflammatory processes and promoting tissue repair) and takes part in key defense mechanisms against infections (in particular the ones determined by intracellular fungi, bacteria and viruses). On the contrary, when produced at high concentrations and in a non-regulated manner, TNFα becomes deleterious by promoting chronic inflammation and extensive tissue damage[44].

The TNFα signalling cascade is initiated by two different ligands, the membrane (mTNFα) and the soluble (sTNFα) forms of TNFα. The 26 kDa monomeric type II transmembrane protein (mTNFα) is initially expressed by a certain cell and can be cleaved, or not, by the matrix metalloprotease TNF converting enzyme (TACE/ADAM17), to release the 17 kDa monomeric soluble protein (sTNFα). Finally, both mTNFα and sTNFα acquire a functional quaternary structure by assembling as homotrimers[44-46]. TNFα is produced by both immune cell types, such as monocytes and macrophages, T cells, natural killer (NK) cells, neutrophils, and microglia as well as by non-immune cells such as fibroblasts, astrocytes, neuronal cells, keratinocytes and also GI epithelial cells (which, as explained in section 1.3, are essential cells of the GI innate immunity)[44,47]. The rapid expression of TNFα at any given moment is made possible by the high cellular steady state levels of its mRNA, which is kept unstable by rapid post-transcriptional degradation. Upon an inflammatory stimulus, the mRNA is stabilized as a result of the MAPK ERK/MK2 signalling cascade, leading to its rapid translation into the TNFα protein[47].

Almost all cells of the human body show at least some responsiveness to TNFα, in one or both of its ligand forms. The signal transduction is mediated by the two homotrimeric membrane receptors TNR1A (*TNFRSF1A*) and TNR1B (*TNFRSF1B*) which, as happens for other cytokines, present important differences that contribute to the pleiotropic effects of TNFα. These two receptors are characterized indeed by being expressed in different cell types, by being activated in separate ways and by giving rise to divergent effects in a tissue- and cell-specific manners. Whereas TNR1A is constitutively expressed on almost all nucleated cells, the expression of TNR1B is more restricted to the immune system, the vasculature, muscle and brain tissues including myeloid cells, certain T- and B-cell subsets, glial cells, some endothelial cell types, fibroblasts and also epithelial cells[46,48]. While mTNFα activates both TNR1A and TNR1B signalling pathways with high efficacy, binding of sTNFα results in the strong activation of TNR1A but not of TNR1B[48]. Finally, once activated, these two receptors can determine divergent and often opposing cellular and tissue effects. In general, the s/mTNFα/TNR1A signalling mediates pro-apoptotic and inflammatory responses, and the mTNFα/TNR1B signalling contributes to immune regulation, tissue regeneration and neuroprotection. TNR1B can elicit proinflammatory effects too, but numerous works also show that it determines strong anti-inflammatory and protective effects on oligodendrocytes, cardiomyocytes, and keratinocytes[45,49-52].

Interestingly, other factors can contribute to the complexity of the whole signalling and should be taken into consideration when the biological effects of the two receptors are analyzed, especially *in vivo*. The ligand mTNFα can also act as a receptor because mTNFα-bearing cells show biological activity via reverse signalling when activated by mainly TNR1B[44]. On the other side, there is a second homotrimeric ligand called lymphotoxin-α (LTα) which can interact with TNR1A and TNR1B in a very similar manner as sTNFα[49]. Finally, both receptors can be

processed into their soluble forms, sTNR1A and sTNR1B, determining the establishment of a negative feedback system. The soluble receptors can behave as "molecular sponges" by binding their ligands in circulation and reducing their availability to provoke a biological effect. Furthermore, shedding of the receptors lowers the amount of competent receptors that can initiate a signalling at the cells membranes[47].

The TNF receptor superfamily (TNFRSF) consists of more than twenty members, are defined by having at least one extracellular cysteine-rich domains (CRDs), and can bind the different TNFSF ligands, characterized by having the TNF homology domain (THD)[49]. With the exception of some members such as Fas receptor and TNR1A, specialized to induce cell death, the majority of the TNF receptors activate both the non-canonical Nuclear Factor kappa-light-chain-enhancer of activated B cells (non-canonical NFkB) and the Phosphatidylinositol 3-kinases/protein kinase B (PI3K/PKB/Akt) pathways. The fact that these two pathways induce cell survival, and the PI3K/PKB/Akt also cell proliferation[3], recapitulates the key differences in between the TNR1A and TNR1B signallings (figure 16).

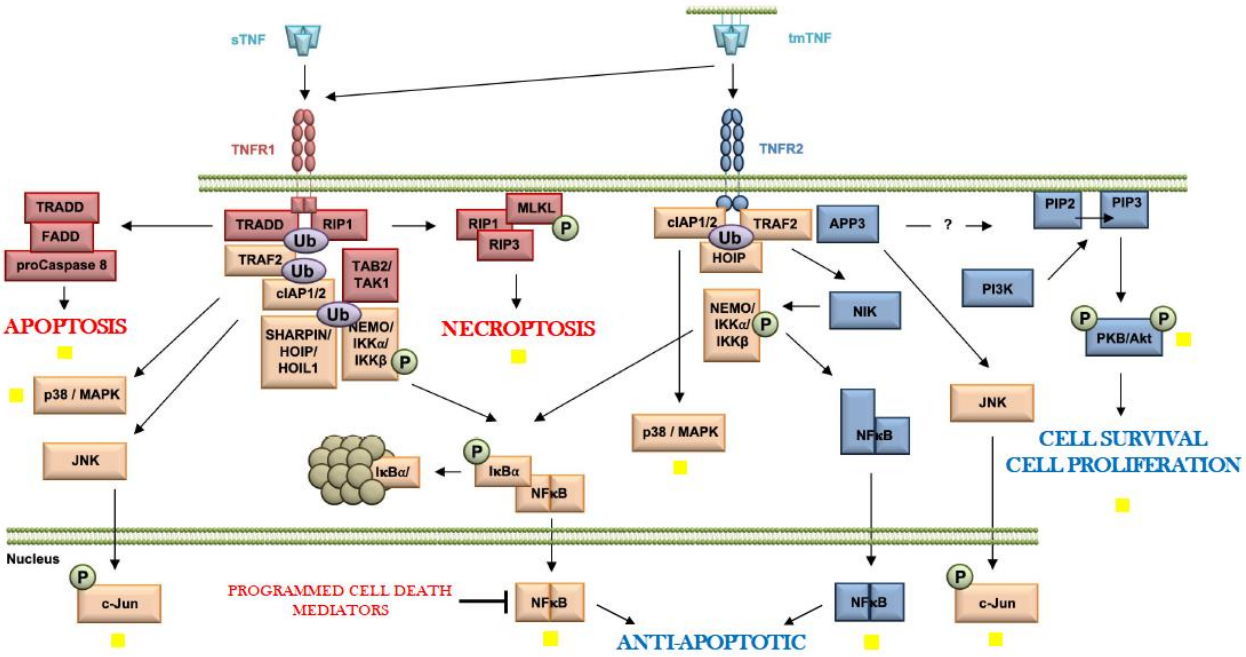

Figure 16: Overview of the signalling pathways of TNR1A (TNFR1) and TNR1B (TNFR2). In red the the exclusive signalling mediated by TNR1A, in blu the exclusive signalling mediated by TNR1B, in orange the signalling shared by both receptors, and in yellow the signalling pathways with a proved direct impact on epithelial barrier function (adapted from Fischer *et al.*, 2020).

TNR1A and TNR1B belong to two distinct subgroups of the TNFRSF. They share only a 28% of sequence homology concentrated at the extracellular domains of the two receptors, where they have in common four CRDs, but their intracellular regions are mostly unrelated[45]. TNR1A has a death domain (DD) in its cytoplasmic part that interacts with two DD-containing proteins, TNR1A-associated death domain (TRADD) protein and Fas-associated death domain (FADD)

protein, determining the strong activation of proinflammatory pathways and of Apoptosis via Caspase 8. When Caspase 8 is absent or inactivated, the RIPK1 recruits and activates RIPK3, resulting in the induction of Necroptosis. The activation of TNR1A determines also the recruitment of TNF receptor associated factor 2 (TRAF2) and of the cellular Inhibitor of Apoptosis Proteins (cIAPs) 1 and 2, which determine the activation of the p38/MAPK, JNK/c-Jun and the canonical NFκB pathways[46]. In contrast, TNR1B lacks a cytoplasmic DD so recruits only TRAF2 and cIAPs1/2 and, as TNR1A, activates the p38/MAPK and JNK/c-Jun pathways. But, unlike TNR1A, it also activates the non-canonical NFκB pathway and the PI3K/PKB/Akt pathways[45,46]. Very importantly, TNR1A-induced canonical NFκB and cell death signalling pathways are reciprocally inhibitory to each other, making TNR1B the only of these two receptors capable of activating the NFκB pathway[49].

The production of both sTNFα and mTNFα by lamina propria Macrophages, Fibroblasts and T cells is markedly augmented in patients with IBD. TNFα signalling in IBD drives pleiotropic pro-inflammatory effects, including augmented angiogenesis, the induction of Paneth cell death via Necroptosis, the production of matrix metalloproteinases by myofibroblasts, the activation of macrophages and effector T cells, and the direct impairment of the GI epithelial barrier function[43]. By now, the two cellular mechanisms considered to be the main responsibles for the TNFα-mediated increase of GI epithelial permeability are: an increase of expression of Claudin-2 (pore-forming Claudin, regulator of the pore pathway) and an increase of expression and activity of the MLCK (which, by disrupting the TJ scaffold, regulates the leak pathway)[30,38,43,53]. The role of MLCK has been studied more in detail by different groups, which concluded that this enzyme mediates the increase of permeability across the leak pathway by determining the endocytosis of Occludin and by alterating the ZO-1 dynamics[53,54]. It has been also defined that the (s)TNF-α induced increase in MLCK gene expression and protein activity is preceded by the activation of NF-κB[53,55] and that TNR1B, but not TNR1A, mediates this[30,56]. Despite contradictory results obtained in both *in vivo* and *in vitro* conditions, the fact that TNR1B activates the non-canonical NF-κB pathway would confirm this, and a crucial role of MLCK in the regulation of the leak pathway seems to be out of discussion. But the important point to consider when evaluating the single contributions of TNR1A and TNR1B to these mechanisms is that the aforementioned research works employed sTNFα in their experiments, without considering that, even though it has affinity for both receptors, it is efficacious in activating only TNR1A. Furthermore, the definition of TNR1B as the only mediator of the MLCK/NF-κB-dependent barrier disruption was done in the presence of both sTNFα and IFNγ and completely opposite effects have been observed in the NF-κB involvement in the sTNFα or in the sTNFα/IFNγ combination induced barrier function impairments[16]. On the other side, a clear definition of the specific roles of both receptors with regards to the regulation of the unrestricted

permeability pathway (which could account for up to 50% of the GI barrier impairing effects determined by TNFα[55]) is still missing.

The actual pharmacological strategies for modulating the TNFα signalling in IBD are dominated by global inhibitors, which determine a complete shut down by indiscriminately antagonizing both sTNFα and mTNFα. Taking into consideration the complexity of the TNFα signalling, is very plausible that a clear differential role of both receptors takes place in the regulatory mechanisms that define the overall GI barrier function (see figure 16). All possible pharmacological strategies for modulating the TNFα are summarized in figure 17.

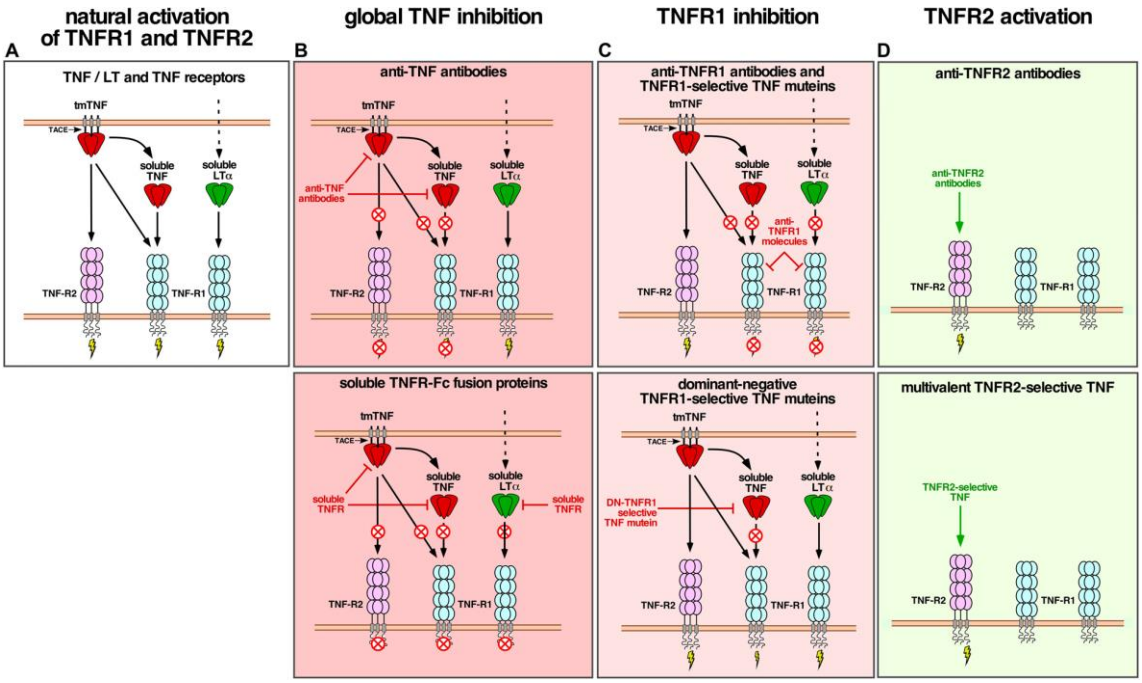

Figure 17: Overview of the possible pharmacological strategies for modulating the TNFα signalling (from Fischer *et al.*, 2020).

These pharmacological modulations represent, first and foremost, valuable tools for disentangling the specific roles of both receptors in both *in vitro* and *in vivo* models. A refinement of the pharmacological therapeutical strategies by differentially modulating the two receptors (eventually keeping a basal activation TNR1B or enhancing it, to take advantage of its possible beneficial effects) is a very promising option that, considering the high complexity of the TNFα and other cytokines signallings at the GI mucosa, should be first thoroughly studied at each cellular and tissue level.

2. AIM OF THE PROJECT

So far more than 200 independent genetic risk loci have been found implicated in the pathogenesis and in the progression of IBD, including not only genes associated with the regulation of the innate and adaptive immune responses, but also with the regulation of the different permeability pathways at the basis of the GI epithelial barrier function. Even though the attenuation of the general immune activity with strong immuno-modulatory therapies (targeting key inflammatory pathways) appears to be crucial for treating the IBD condition, it is necessary to consider that the current therapies (e.g. global α-TNFα and α-p40 antibodies) increase the risk of developing or reactivating infections, and that forty per cent or more of all IBD patients are intolerant to them[57].

The GI epithelial barrier constitutes a key tissue structure that consents the maintenance of the organism's homeostasis, by working as a tightly regulated molecular sieve and by concomitantly constituting a hardly penetrable physical barrier that protects the individual's interior from continuous threats. The multiple physiological roles of this formidable tissue structure, added to its close interaction with similarly complex entities as the microbiota and the immune and neuronal networks of the GI mucosa and submucosa, suggest a high complexity in the mechanisms that regulate its normal function.

My Ph.D. project focused *in primis* on the establishment of an *in vitro* platform for the comprehensive and detailed investigation of the roles of candidate genes/proteins in the regulation of the key mechanisms underlying the intestinal epithelial paracellular permeability. Given the aforementioned intrinsic complexity of the GI wall, my aim was the definition of the *in vitro* conditions for the exclusive characterization of the mechanisms underlying the paracellular permeability (and not the transcellular one, having a lesser relevance in IBD), avoiding the interference of other cell types different than the intestinal epithelial ones. The differentiation of transformed epithelial cell lines was established *in vitro* by optimizing key parameters related with the growth substrate, atmospheric gas composition and cell confluency. Furthermore, the characterization of a normal epithelial stem cell line has been done as a starting point for the future establishment of its differentiation *in vitro*. The optimal inflammatory input, for mimicking the pathological conditions of IBD at the GI epithelium, has been established by testing different cytokine combinations, concentrations and times of application at sub and fully differentiated conditions. A pharmacological interference methodological approach, with associated key functional and molecular biological assays, was established and validated in my *in vitro* model, constituting a platform for the characterization of candidate genes/proteins in this context.

Given the importance of the GI epithelial barrier integrity in the pathogenesis and in the chronic manifestation of IBD, my Ph.D. work proceeded with the characterization of the pro-inflammatory cytokines sTNFα, IFNγ and IL-1β in this context. My aim was to contribute not only to the understanding of their biology, but also to the elucidation of novel molecular mechanisms which could account for the restoration of this epithelial barrier under the aforementioned pathological conditions. The mechanisms dictating the synergistic interaction in between sTNFα and IFNγ were elucidated with transcriptional

analyses. The role of these cytokines with regards to key programmed cell death mechanisms has been evidenced.

Taking into consideration the already described opposed roles of TNR1A and TNR1B with regards to inflammatory processes, in the last part of my Ph.D. I worked on the full characterization of the mode of action of these two receptors mediating the TNFα cytokine signalling, in GI epithelial cells. A selective pharmacological interference approach was followed for the precise characterization of the role of TNR1A in intestinal epithelial barrier function. To complete the study, I will carry out the selective agonism of TNR1B alone and in the presence of sTNFα, to understand if the activation of this receptor impairs or eventually protects the intestinal epithelial barrier function. Gaining knowledge about the specific role of each of the receptors in this specific context could provide the basis for the initiation of work towards the modification of the actual pharmacological therapies that are dominated by global TNFα inhibitors (that fully neutralize both sTNFα and mTNFα). A selective targeting of each of the receptors (antagonism or agonism) could lead to a better therapeutical outcome rather than the complete neutralization of the whole signalling by targeting the ligands.

Finally, as a side project of my Ph.D., I started the characterization of the 5-HT signalling in this context, that I will complete with the systematic characterization of the 5-HTRs having a potential role in the regulation of the intestinal epithelial barrier function. This could open the way to the definition of new potential pharmacological targets, less immunosuppressive but still effective, for counteracting the epithelial barrier dysfunction in IBD.

3. MATERIALS AND METHODS

3.1. Materials

3.1.1. Bacterial strains

Chemocompetent NovaBlue Singles Competent Cells *endA1 hsdR17 (rK12– mK12+) supE44 thi-1 recA1 gyrA96 relA1 lac F'[proA+B+ lacIqZΔM15::Tn10*] (TetR)	Merck Millipore

3.1.2. Reagents for bacterial culture

Ampicillin	Roth
Bacto-Agar	Becton Dickinson
Bacto-Tryptone	Becton Dickinson
Glucose	Merck (Sigma-Aldrich)
Isopropyl β-D-1-thiogalactopyranoside (IPTG)/ X-Gal	Usb Corporation
Kanamycin	Roth
Magnesium chloride (MgCl2)	Merck (Sigma-Aldrich)
Magnesium sulfate (MgSO4)	Merck (Sigma-Aldrich)
Potassium chloride (KCl)	Merck (Sigma-Aldrich)
Sodium chloride (NaCl)	Merck (Sigma-Aldrich)
Yeast extract	Becton Dickinson

3.1.3. Media for bacterial culture

- **LB-Agar (ampicillin/kanamycin)**

LB medium + 1.5 % Bacto-Agar + 50 µg/mL ampicillin or 30 µg/ml kanamycin

- **LB-Agar (ampicillin/kanamycin and IPTG/ X-Gal)**

LB medium + 1.5 % Bacto-Agar + 50 µg/mL ampicillin or 30 µg/ml kanamycin + 40 µg/mL IPTG/X-Gal

- **LB-medium (ampicillin/kanamycin)**

1% Bacto-Tryptone + 0.5 % Yeast extract + 1% sodium chloride + 50 µg/mL ampicillin or 30 µg/ml kanamycin

- **SOB-medium**

10 mM sodium chloride + 10 mM magnesium chloride + 0.5 mM potassium chloride + 10 mM magnesium sulfate + 2 % Bacto-Tryptone + 0.5% Yeast extract

- **SOC-medium**

1 L SOB-medium + 20 mL glucose (20%)

3.1.4. Human cell lines

Human colorectal adenocarcinoma epithelial cell line (Caco-2)	ATCC® HTB-37™
Human colorectal carcinoma epithelial cell line derived from a lung metastasis (T84)	ATCC® CCL-248™
Human fetal colonic normal epithelial cell line (FHC)	ATCC® CRL-1831™

3.1.5. Reagents and pre-made solutions for human cell culture

Acetic Acid 99.8 % - 100%	Chemikalienlager UKHD (Bernd Kraft)
apo-Transferrin human	Merck (Sigma-Aldrich)
Cholera Toxin from Vibrio cholera	Merck (Sigma-Aldrich)
Collagen from rat tail Type I	Merck (Sigma-Aldrich)
Distilled water	Gibco™ (Thermo Fisher Scientific)
Dulbecco's Modified Eagle Medium:Nutrient Mixture F-12 (DMEM/F-12) high glucose	Gibco™ (Thermo Fisher Scientific)
Dulbecco's Modified Eagle Medium:Nutrient Mixture F-12 (DMEM/F-12) high glucose, GlutaMAX™ Supplement	Gibco™ (Thermo Fisher Scientific)
Ethanol absolute	VWR Chemicals
Fetal bovine serum (FBS) heat inactivated	Gibco™ (Thermo Fisher Scientific)
HEPES	Gibco™ (Thermo Fisher Scientific)
Hydrocortisone	Merck (Sigma-Aldrich)
Insulin solution from bovine pancreas	Merck (Sigma-Aldrich)
Matrigel® Basement Membrane Matrix Growth Factor Reduced Phenol Red Free	Corning®
1X Dulbecco's phosphate buffered Saline (PBS)	Gibco™ (Thermo Fisher Scientific)
Penicillin/Streptomycin (Pen/Strep)	Gibco™ (Thermo Fisher Scientific)
Trypsin-EDTA (0.25%), phenol red	Gibco™ (Thermo Fisher Scientific)

3.1.6. Media and buffers for human cell culture

All culture media were filtered with a 0.22 µm sieve after preparation.

- **Caco-2 and T84 culture medium**

DMEM/F12 high glucose + 10% FBS + 1% Pen/Strep

- **Collagen Type I stock and working solutions**

100X stocks were prepared by reconstitution in 0.1 M Acetic Acid to a final concentration of 1 mg/mL and incubation for 3 hrs at RT°C (mixing).
The 1X solution was prepared by diluting the 100X in 60% EtOH.

- **FHC culture medium**

DMEM/F-12 high glucose, GlutaMAX™ Supplement + 10% FBS heat inactivated + 1% Pen/Strep + 25 mM HEPES + 10 ng/mL Cholera Toxin + 5 µg/mL Insulin + 5 µg/mL apo-Transferrin human + 100 ng/mL Hydrocortisone

3.1.7. Plates and inserts for *in vitro* human epithelial tissue culture model

Corning® Transwell® cell culture inserts, TC-treated, with 0.4 and 3.0 µm pore polycarbonate membrane of 6.5 mm (Ø) and 0.33 cm^2 (cell growth area)	Merck (Sigma-Aldrich)
Costar® 24-well plate, TC-treated, with lid	Merck (Sigma-Aldrich)

3.1.8. Reagents and pre-made solutions for cell and molecular biological analyses

Acetic acid (CH_3COOH)	Merck (Sigma-Aldrich)
Aqua Poly/Mount mounting medium for IF	Polysciences
Bovine Serum Albumin (BSA) – Fraction V, pH 7.0	Serva Electrophoresis
Chloroform ($CHCl_3$)	Merck (Sigma-Aldrich)
4′,6-Diamidino-2-phenylindole·2HCl (DAPI)	SERVA Electrophoresis GmbH
Disodium hydrogenphosphate (Na_2HPO_4)	VWR Chemicals
Ethylenediaminetetraacetic acid (EDTA)	Merck (Sigma-Aldrich)
Fluorescein isothiocyanate (FITC) – dextran average molecular weight 4 and 70 kDa	Merck (Sigma-Aldrich)
Glycerol ($C_3H_8O_3$)	Merck (Sigma-Aldrich)
Hanks' Balanced Salt Solution (HBSS), calcium, magnesium, no phenol red	GibcoTM (Thermo Fisher Scientific)
Hoechst 33342 trihydrochloride, trihydrate	Thermo Fisher Scientific
Isopropanol ($(CH_3)_2CHOH$)	Merck (Sigma-Aldrich)
Midori Green DNA stain	Nippon Genetics
Paraformaldehyde (PFA)	Merck (Sigma-Aldrich)
1X Dulbecco's phosphate buffered Saline (PBS)	GibcoTM (Thermo Fisher Scientific)
Potassium chloride (KCl)	Merck (Sigma-Aldrich)
Potassium dihydrogen phosphate (KH_2PO_4)	Ferak Berlin GmbH
Recombinant Human IFN-γ	PeproTech
Recombinant Human IL-1β	PeproTech
Recombinant Human TNF-α	PeproTech
Sodium chloride (NaCl)	Merck (Sigma-Aldrich)
Sodium citrate ($Na_3C_6H_5O_7$)	AppliChem

Sodium hypochlorite (NaClO) solution (6–14 % active chlorine)	ChemSolute
TRIS (Tris-(hydroxymethyl)-aminomethan)	Carl Roth
Triton X-100	Merck (Sigma-Aldrich)
TRIzol™ Reagent	Thermo Fisher Scientific
Tween-20	Carl Roth
Vectashield antifade mounting medium for IF	Vector Laboratories

3.1.9. Buffers for cell and molecular biological analyses

- **10X LDH assay lysis buffer**

10% Triton X-100 (in PBS and filtered with a 0.22 µm sieve after preparation)

- **LDH assay storage buffer**

200 mM Tris-HCl (pH 7.3) + 10% Glycerol + 1% BSA (in milli-Q H_2O)

- **10X PBS**

13.7 M sodium chloride + 270 mM potassium chloride + 800 mM disodium hydrogenphosphate + 200 mM potassium dihydrogen phosphate (in deionized H_20) (pH 7.4)

- **Permeabilization buffer for IF stainings**

0.25 % Triton X-100 (in PBS)

- **Permeabilization buffer for TUNEL assay**

0.1 - 0.25 - 0.5 % Triton X-100 + 0.1% sodium citrate (in PBS)

- **50X TRIS-Acetate-EDTA (TAE) buffer (DNA gelelectrophoresis buffer)**

2 M TRIS + 1 M acetic acid + 50 mM EDTA (in deionized H_20)

3.1.10. Kits for cell and molecular biological analyses

Bioanalyzer RNA Analysis	Agilent
CellTox™ Green Cytotoxicity Assay	Promega
CytoTox-Glo™ Cytotoxicity Assay	Promega
Direct-zol™ RNA MicroPrep	Zymo Research
GeneRacer Kit	Invitrogen
HotStarTaq DNA Polymerase Kit	Qiagen
In Situ Cell Death Detection Kit, Fluorescein	Roche
LDH-Glo™ Cytotoxicity Assay	Promega
Pierce™ BCA Protein Assay Kit	Thermo Fisher Scientific
pSTBlue-1 AccepTor™ Vector Kit	Merck Millipore
QIAquick Gel Extraction Kit	Qiagen

Qubit® RNA HS Assay Kits	Life Technologies (Thermo Fisher Scientific)
Quick DNA Microprep Kit	Zymo Research
Quick DNA Miniprep Plus Kit	Zymo Research
Quick-RNA™ Microprep Kit	Zymo Research
RNAqueous® -Micro Total RNA Isolation Kit	Thermo Fisher Scientific
Superscript III First-Strand Synthesis System for reverse transcription PCR	Thermo Fisher Scientific
2x qPCRBIO SyGreen Mix Lo-ROX	PCRBIOSYSTEMS
T4 DNA Ligase	Thermo Fisher Scientific

3.1.11. Consumables for molecular biological analyses

Amicon® Ultra-0.5 mL 3K device - 3,000 MWCO	Merck Millipore
Amicon® Ultra-4 mL 3K device - 3,000 MWCO	Merck Millipore

3.1.12. Antibodies

3.1.12.1. Primary antibodies for IF

Table 1: **Primary antibodies for IF.**

Antibody	Supplier	Reactivity	Immunogen	Working dilution
Mouse anti-TJP ZO-1 (ZO1-1A12) (monoclonal)	Thermo Fisher Scientific	Human, Dog, Rhesus monkey	Human recombinant ZO-1 fusion protein encompassing amino acids 334-634	1:100
Rabbit anti- 5-HT3A (polyclonal) (from Kapeller *et al.* 2011 [58])	Eurogentec	Human	Peptidic sequence KGVRPVRDWRKPTTV of 5-HT3A	1:100

3.1.12.2. Secondary antibodies for IF

Table 2: **Secondary antibodies for IF.**

Antibody	Supplier	Conjugate	Working dilution
Goat anti-mouse IgG (H+L)	Invitrogen	Alexa Fluor 488	1:250
Goat anti-rabbit IgG (H+L)	Invitrogen	Alexa Fluor 568	1:250

3.1.12.3. Neutralizing antibodies

Table 3: Neutralizing antibodies.

Antibody	Supplier	Reactivity	Immunogen	Working concentration

Mouse monoclonal anti-IFN-γ R1/CD119	R&D SYSTEMS (Biotechne)	Human	Mouse myeloma cell line NS0-derived recombinant human IFN-γR1 Glu18-Gly245 (Accession # P15260.1)	1 - 48 µg/mL
Anti-IFNγ fully human IgG1 monoclonal antibody ("Emapalumab")	Kindly provided by Dr. Ercole Rao	Human	Binds to both free and IFNγR1-bound IFNγ. Impairs IFNγR1 and IFNγR2 interaction induced by IFNγ at the cell surface[59]	0.5 – 4 µg/mL
Anti-m/sTNFα recombinant fully human IgG1 monoclonal antibody ("Adalimumab")	Kindly provided by Dr. Ercole Rao	Human	N-terminal portion of m/sTNFα[60]	2.4 – 24 µg/mL

3.1.12.4. Neutralizing nanobodies

Table 4: Neutralizing nanobodies.

Nanobody	Supplier	Reactivity	Immunogen	Structure/mechanism of action	Working concentration
hTNFR1 Nanobody Alb-70-96 or TNF Receptor-One Silencer (TROS)	Kindly provided by Prof. Dr. Roosmarijn E. Vandenbroucke, VIB-UGent Center for Inflammation Research, Gent, Belgium	Human	Soluble human TNFR1 (hTNFR1)	Consists of Nb 70 (the only inhibitor of TNF/hTNFR1 signalling), Nb 96 (the one with the highest affinity for hTNFR1) and an anti-albumin Nb. All three are connected to each other with flexible $(G_4\text{-}S)_3$ linkers[61].	0.5 - 30 µM

3.1.13. Oligonucleotides

Table 5: Primers.

Primer name	Sequence (5' > 3')	Application
*ARF1*_for	GCCAGTGTCCTTCCACCTGTC	Conventional RT-PCR (reference gene)
*ARF1*_rev	GCCTCGTTCACACGCTCTCTG	
*SDHA*_for	TCGCACTGTGCATAGAGGAC	Conventional RT-PCR (reference gene)
*SDHA*_rev	ATGCCTGTAGGGTGGAACTG	
*TJP1*_for	TGCAAGTAGAGAGAGGAGCTTG	Conventional RT-PCR
*TJP1*_rev	TGCCAATCGAAGACCATATTC	
*HTR3A*_for	CCTGGTTCTGGAGAGAATCG	Conventional RT-PCR
*HTR3A*_rev	GGGCTCTTCTCGAAGTCCTG	
*HTR3B*_for	AGGCACCCCCTGGTCTATGT	Conventional RT-PCR
*HTR3B*_rev	CCACAGCACGTTGGGCCC	
*HTR3C*_for	TCCCCAGAGAAGAGTCCAGA	Conventional RT-PCR
*HTR3C*_rev	TGGATTCCACGATGAAGATG	
*HTR3D*_for	ATAAGCCAATGTGGGTGGTC	Conventional RT-PCR
*HTR3D*_rev	TGGGAGCAAGTCATTCATCA	

*HTR3E*_for	TGCTCCACTGCAACAGCCCG	Conventional RT-PCR
*HTR3E*_rev	CCCTGTCAGCTCTGCCTCCG	
*HTR3E/5-HT3C1*_for	ATGTTAGCTTTCATTTTATCACGGGC	Conventional RT-PCR. Full-length amplification of *HTR3E* and *5-HT3C1* transcripts.
*HTR3E/5-HT3C1*_rev	CCCTGTCAGCTCTGCCTCCG	
*HTR3Ea/HTR3Eb/HTR3EV3*_for	CTCGGTTTTCTGCTTCAAGG	Conventional RT-PCR. Full-length amplification of *HTR3Ea*, *HTR3Eb* and *HTR3EV3* transcripts.
*HTR3Ea/HTR3Eb/HTR3EV3*_rev	TCTGCCCTGCTGATACCTCT	
*VIL1*_for	ATTACCTGCTCTACGTTTGGCA	Conventional RT-PCR
*VIL1*_rev	AGTCTCTTGGTGTTGGCATAGG	
*KRT20*_for	ACGCCAGAACAACGAATACC	Conventional RT-PCR
*KRT20*_rev	ACCCCACCCCTTCTAATCAC	
*ACTA2*_for	ACCCACAATGTCCCCATCTA	Conventional RT-PCR
*ACTA2*_rev	GAAGGAATAGCCACGCTCAG	
*PROM1*_for	GCTGATGTTGAAACTGCTTGAG	Conventional and RT-qPCR
*PROM1*_rev	GCCCGCCTGAGTCACTAC	
*LGR5*_for	AGTCAGCTGCTCCCGAATC	Conventional and RT-qPCR
*LGR5*_rev	TGTAAAGGCCAGTGAATGCTC	
*LRIG1*_for	AGTTGACAGCGGTACCATCC	Conventional RT-PCR
*LRIG1*_rev	CTTTATAGGCGGTCCGTGTG	
*OLFM4*_for	CAGAGTGGAACGCTTGGAAT	Conventional RT-PCR
*OLFM4*_rev	CCTTGATCAGCTCGAAGTCC	
*HPRT1*_ RT-qPCR_for	TGATAGATCCATTCCTATGACTGTAGA	RT-qPCR (reference gene)
*HPRT1*_ RT-qPCR_rev	AAACATTCTTTCCAGTTAAAGTTGAG	
*SDHA*_ RT-qPCR_for	CCTGTCCTATGTGGACGTTG	RT-qPCR (reference gene)
*SDHA*_ RT-qPCR_rev	GTTTTGTCGATCACGGGTCT	
*ARF1*_ RT-qPCR_for	TTCGCCAACAAGCAGGAC	RT-qPCR (reference gene)
*ARF1*_ RT-qPCR_rev	CAGTTCCTGTGGCGTAGTGA	
*TNFRSF1A*_ RT-qPCR_for	CTCTCCACCGTGCCTGAC	RT-qPCR
*TNFRSF1A*_ RT-qPCR_rev	GGTGAGGGACCAGTCCAATA	
*TNFRSF1B*_ RT-qPCR_for	CGTCGGACTGGAGCTCTG	RT-qPCR
*TNFRSF1B*_ RT-qPCR_rev	GGGGCGTAGGGTGTAAATG	
*IFNGR1*_ RT-qPCR_for	ATGCCGAGATGGAAAAATTG	RT-qPCR
*IFNGR1*_ RT-qPCR_rev	TTTGCTTCTCCTCCTTTCTGA	
*IFNGR2*_ RT-qPCR_for	GTTTCAACACTATCGGAATGTGA	RT-qPCR
*IFNGR2*_ RT-qPCR_rev	GGGAGAGGAGAACCTGATGA	
*IL1R1*_ RT-qPCR_for	CCAAGAAGAATATGAAAGTGTTACTCA	RT-qPCR
*IL1R1*_ RT-qPCR_rev	TTCTTCACGTTCCTTGCATTT	
GeneRacer™ Oligo dT	GCTGTCAACGATACGCTACGTAACGGCATGACAGTG$(T)_{24}$	Priming of the first-strand cDNA synthesis in the RT reaction for the RACE sscDNA library preparation
GeneRacer™_Control Primer A_for	GCTCACCATGGATGATGATATCGC	5'/3' RACE PCR control gene (β-actin)
GeneRacer™_ Control Primer B.1_rev	GACCTGGCCGTCAGGCAGCTCG	5'/3' RACE PCR control gene (β-actin)
GeneRacer™ 5′ Primer_for	CGACTGGAGCACGAGGACACTGA	5' RACE PCR adaptor primer
GeneRacer™ 5′ Nested Primer_for	GGACACTGACATGGACTGAAGGAGTA	5' RACE Nested PCR adaptor primer

GeneRacer™ 3′ Primer_rev	GCTGTCAACGATACGCTACGTAACG	3’ RACE PCR adaptor primer
GeneRacer™ 3′ Nested Primer_rev	CGCTACGTAACGGCATGACAGTG	3’ RACE Nested PCR adaptor primer
*HTR3E*_5’ RACE_rev	TGCCTCCGCAGGGCCCGGCATCT	5’ RACE PCR *HTR3E* primer
*HTR3E*_5’ RACE Nested_rev	CCGGCATCTGCCCTGCTGATACCT	5’ RACE Nested PCR *HTR3E* primer
HTR3E_3’ RACE_for	CCACTGCAACAGCCCGGGGAGAT	3’ RACE PCR *HTR3E* primer
HTR3E_3’ RACE Nested_for	GGAAAATAAGGGCCCGGGTCTCA	3’ RACE Nested PCR *HTR3E* primer

3.1.14. Vector constructs

pSTBlue-1 Blunt Vector (#70188)	Merck Millipore (Novagen)

3.1.15. Hardware

Automated Inverted Microscope DMI4000B	Leica
2100 Bioanalyzer Instrument	Agilent
Biofuge fresco centrifuge	Heraeus
Biological Safety Cabinet Safe 2020	Thermo Fisher Scientific
Centrifuge 5418	Eppendorf
DS-11 FX+ (M/C/F) Spectrophotometer / Fluorometer	Denovix
Eclipse Ti Microscope with A1 confocal scanner	Nikon
EVOM^2 Epithelial Volt-Ohm-Meter with STX2 electrode set	World Precision Instruments, INC.
LB 960 Microplate Luminometer Centro	Berthold Technologies
Mastercycler vapo protect (thermal cycler)	Eppendorf
Microbiological incubator	WTB Binder
NuAire CO2 Incubator Series 5800	Ibs Tecnomara
Olympus BX53 Upright microscope	Olympus
QuantStudio™ 3 Real-Time PCR System 96-Well 0.2 mL Block	Applied Biosystems (Thermo Fisher Scientific)
QUANTUM Gel Documentation System	Peqlab
SP12 heating plate	MEDAX Nagel GmbH
Steri Cult CO_2 incubator	Thermo Fisher Scientific
Thermomixer comfort	Eppendorf

3.1.16. Software

Leica Application Suite Advanced Fluorescence 4.0.0.11706	Leica

MikroWin 2000	Berthold Technologies (Labsis)
NIS Elements Imaging Software 4.50.00	Nikon
Photoshop CS4 Vers. 11.0	Adobe
QuantStudio™ Design & Analysis Software v1.5.1	Applied Biosystems (Thermo Fisher Scientific)

3.1.17. Web databases and bioinformatics tools

DRUGBANK: https://www.drugbank.ca/

ENSEMBL genome browser: https://www.ensembl.org/index.html

Genecards: https://www.genecards.org/

HUGO Gene Nomenclature Committee: https://www.genenames.org/

IUPHAR/BPS Guide to PHARMACOLOGY: https://www.guidetopharmacology.org/

National Center for Biotechnology Information (NCBI): http://www.ncbi.nlm.nih.gov/

Nucleotide BLAST: https://blast.ncbi.nlm.nih.gov/Blast.cgi?PROGRAM=blastn&PAGE_TYPE=BlastSearch&LINK_LOC=blasthome

OligoAnalyzer 3.1: http://eu.idtdna.com/calc/analyzer

Primer3 (v. 0.4.0): http://bioinfo.ut.ee/primer3-0.4.0/primer3/

The Human Protein Atlas: https://www.proteinatlas.org/

UCSC Genome Browser, BLAT search and *in-silico* PCR: https://genome.ucsc.edu/

Universal ProbeLibrary Assay Design Center: https://lifescience.roche.com/en_de/brands/universal-probe-library.html#assay-design-center

3.2. Methods

3.2.1. Cell biological methods

3.2.1.1. Growth and maintenance in culture of T84 and CACO-2 cells

T84 and CACO-2 cells were always cultivated on 25 cm^2 polystyrene cell culture flasks, pre-coated with 10 µg/mL Collagen Type I (3 hrs at 37°C or overnight at 4°C) and passaged at 90% confluency. The cells were passaged by removing the culture media, washing one time (briefly) with pre-warmed 1X PBS and adding 1-2 mL of pre-warmed Trypsin-EDTA (0.25%) for cell detachment from the flask's surface and cell-cell dissociation. Trypsinization was performed for 15-20 min. at 37°C and stopped by the addition of pre-warmed Caco-2 and T84 culture medium, diluting the Trypsin at a ratio 1:3. For maintenance in culture, the cell suspension was split at a ratio 1:3-1:4 and seeded onto a new pre-coated flask (pre-washed three times with 1X PBS to get rid of the 60% EtOH) supplied with pre-warmed Caco-2 and T84 culture medium (high glucose). The cells were kept in culture at 37°C in a humidified atmosphere (95%) containing 5% CO_2

and 20% O_2. For hypoxic experiments, the same atmospheric conditions were kept but with an O_2 concentration of 1%. The media was changed every two days.

For the different experiments, CACO-2 was employed at passages ranging from 31 to 55 and T84 at passages ranging from 10 to 28.

3.2.1.2. Growth and maintenance in culture of FHC

FHC cells were always cultivated on 75 cm^2 polystyrene cell culture flasks without coating and passaged at 90% confluency. The cells were passaged by removing the culture media, washing one time (briefly) with pre-warmed 1X PBS and adding 2 mL of pre-warmed Trypsin-EDTA (0.05%) for cell detachment from the flask's surface and cell-cell dissociation. Trypsinization was performed for 7-10 min. at 37°C and stopped by the addition of pre-warmed FHC culture medium diluting the Trypsin at a ratio 1:3. After each cell dissociation, the suspension was centrifuged at 1300 rpm for 3 min., the growth media with Trypsin was aspirated and the pellet was resuspended in fresh FHC culture medium. For maintenance in culture, the cell suspension was split at a ratio 1:2 and seeded onto a new flask supplied with pre-warmed FHC culture medium. The cells were kept in culture at 37°C in a humidified atmosphere (95%) containing 5% CO_2. The media was changed every two days.

For the different experiments, FHC was employed at passage 7.

3.2.1.3. Trans Epithelial Electrical Resistance (TEER) measurements on transwell (TW) inserts

TEER is a technique employed in epithelial cell culture tissue models, in which a monolayer of cells is grown over a semipermeable membrane. In this two-dimensional organization, the establishment of an apical and a basolateral media compartments allows the measurement of the electrical resistance across the monolayer, employing an ohmmeter and a suitable pair of electrodes. As electrical currents are carried by ions in aqueous solutions, the resulting electrical resistance is a measure of the trans-epithelial ionic permeability (mainly cations given the negative characteristics of the paracellular route, and primarily Na^+ when working with cell culture medium)[62-64]. In a fluid-transporting epithelial monolayer, the TEER is indeed dominated by the high ionic conductance of the paracellular pathway, making of this measurement a sensitive indicator of the integrity of the intercellular junctional complexes that dictate the paracellular resistance[63]. In summary, measurement of the TEER allows the quantitative assessment of confluency (relative area of the surface of growth covered by the cells), and of the integrity of the three permeability pathways that account for the paracellular

resistance (barrier function) of polarizing monolayers (the pore, the leak and the unrestricted pathways).

The TEER was measured in all experiments employing an EVOM^2 volt-ohm-meter connected to an STX2 pair of electrodes suitable for the 6.5 mm (Ø) transwell inserts (figure 18, left).

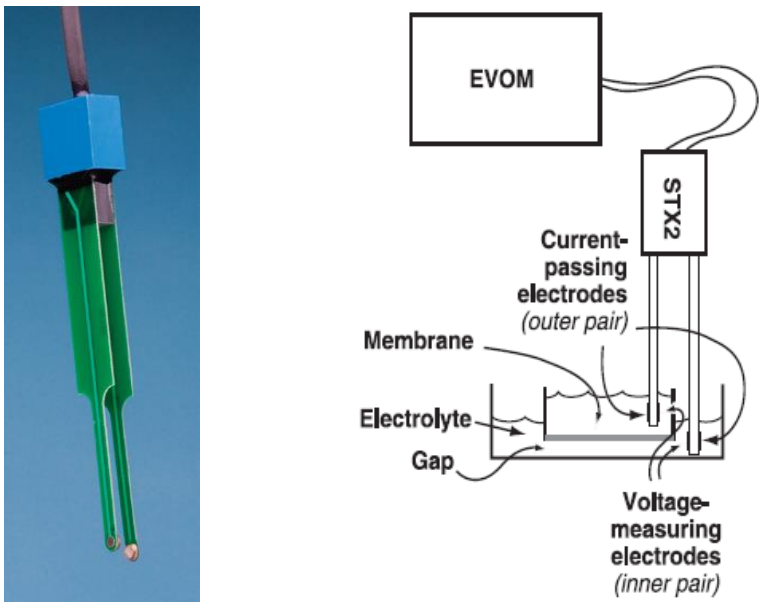

Figure 18: STX2 electrodes and diagram showing the positioning in a transwell chamber setup for measuring the TEER (from www.wpiinc.com)

Each stick of the STX2 (4 mm wide and 1 mm thick) contains an outer and an inner electrode: the outer electrodes are small silver (Ag) pads that pass current through the monolayer and the insert membrane, while the inner electrodes are small silver/silver chloride (Ag/AgCl) pellet voltage sensors[65,66] During the measurements one stick is immerged into the apical medium and the second one into the basal media (figure 18, right), an alternating current (AC) square wave of ±10 μA at 12.5 Hz is applied by the Ag electrodes and the voltage deflection is measured by the Ag/AgCl electrodes[65,66]. The measurements are then digitalized and the ohmic resistance is automatically computed in accordance to the Ohm´s law as the ratio of the measured voltage and the applied current (R=V/I).

The most relevant advantages of the measurements with the EVOM^2 are that **i)** are non-invasive (the AC current avoids adverse effects on the cells), **ii)** cover a wide range of resistances (1-9999 Ω) and **iii)** display a high resolution (1 Ω)[65,66].

For all experiments the procedure of measurement was the following:

1- the STX2 was sterilized in a sodium hypochlorite solution ~5 % active chlorine for 10 min.,
2- the STX2 was washed in pre-warmed 1X PBS for 5 min.,

3- the STX2 was immersed in pre-warmed media, the EVOM^2 was switched on in the resistance measuring mode and the electrodes were equilibrated for 15 min. until the display showed a resistance of ~20 Ω,
4- both the apical and basal culture media of the transwells were changed for a fresh pre-warmed one and the cells were equilibrated for 15 min. at 37°C in a humidified atmosphere (95%) containing 5% CO_2,
5- under the cell culture hood and keeping the plate temperature at 37°C with the help of a heating plate, the resistance of each transwell (including an empty one without cells, as a blank) was recorded at all three positions (figure 28 of section 4.1.2.).

The cell monolayers specific resistances (R_{TEER}) were calculated by subtracting the meter readings (R_{TOTAL}) to the reading of the experiment blank (R_{BLANK}) as shown in the formula:

$$\mathbf{R_{TEER}\,(\Omega) = R_{TOTAL} - R_{BLANK}}$$

The meter reading of the blank represents the sum of the resistance of the cell culture medium (R_{MEDIUM}), the resistance of the semipermeable membrane insert (R_{INSERT}), and the resistance of the electrode medium interface (R_{EMI})[65] (figure 19).

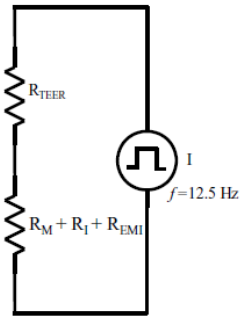

Figure 19: The total electrical resistance comprises the resistances of the cell monolayer (R_{TEER}), the cell culture medium (R_{MEDIUM}), the semipermeable membrane insert (R_{INSERT}), and the electrode medium interface (R_{EMI}). (from Srinivasan, B. *et al*., 2015)

As the resistance of a conductor is inversely proportional to its area (the one of the membrane insert in this case), is more convenient to report the product of the resistance and the area instead of just reporting the value in Ω. The unit "resistance x area" is independent of the area of the membrane employed so it may be used to compare data obtained from inserts of different sizes[66]. For each experiment, the R_{TEERs} were reported as **resistances of a unit area of 1 cm^2**, as shown in the formula:

$$\mathbf{R_{TEER}\ of\ a\ unit\ area\ (\Omega \cdot cm^2) = R_{TEER}\,(\Omega)\ x\ 0.33\ (cm^2)}$$

being 0.33 cm^2 the effective membrane area of the inserts employed.

3.2.1.4. FITC-Dextran 4 (FD4) and 70 (FD70) kDa permeability assays on TW inserts

The transport of molecules across the GI epithelium takes place either through the hydrophilic paracellular pathway or in a transcellular fashion by traversing the apical

and basolateral membranes of the epithelial cells. The paracellular transport involves only passive diffusion and exhibits a strong size-selectivity, whereas the transcellular transport can occur by passive, facilitated or active mechanisms and is less size-selective[62,67]. In general small, hydrophilic, passively transported solutes diffuse through the paracellular route, while hydrophobic compounds of bigger sizes are considered to cross the cell monolayer predominantly by the transcellular route[67].

The quantification of the transport of hydrophilic molecules across a cell monolayer is a method that can be employed to analyze the paracellular permeability and assess its size-selectivity. In fact, depending on their molecular size, these compounds can be exploited to test both solute and ion permeability through the "pore permeability pathway" (low molecular weights with a radius cutoff of <8Å) and macromolecules permeability through the "leak permeability pathway" (high molecular weights with a radius cutoff of <100Å), the "unrestricted pathway" (high molecular weights or entire microorganisms with no maximal radius cutoff) and the transcellular route[68,69]. This means that especially at low molecular weights this technique allows to confirm, by making use of non-ionic species, the information obtained by the TEER measurements concerning the epithelial barrier function and the overall integrity of the cell monolayer. Furthermore, the size-selectivity of the paracellular route can be evaluated in different cellular physiological conditions that may affect its permeability to high molecular weight molecules (that otherwise, in normal conditions, would be excluded from the paracellular space).

As for the TEER measurements, this kind of permeability assays can be performed only on an epithelial monolayer grown on a transwell insert format which consents the establishment of an apical and a basoleateral media compartments. The essential prerequisite for the quantification of the tranport is that the molecule of interest has to be labeled either with a fluorescent dye, a radioactive marker or an enzyme in order to be detectable.

In all the experiments in which the TEER was measured, a permeability assay was performed employing Dextran labelled with the fluorescent dye FITC of an overall average MW of 4 kDa and of 70 kDa. The choice of a fluorescent dye allows a rapid quantification but these tracers are less sensibly detected than radioactive and enzymatic markers, hindering the detection of subtle changes in the permeability. The major drawback of employing chemical dyes is that they render the tested cells unusable for further experiments[65].

The assay was performed initially in the same experimental cell culture media (early experiments with T84 and CACO-2) and was then optimized by carrying it out in the minimal buffer HBSS (without phenol red), aiming to avoid shifts in the absorption and

emission spectra as well as reductions of the quantum yield of the FITC. The following protocol was followed for all experiments:

1- the cell culture media was changed to a fresh one (done before the measurement of the TEER, which always preceded the assay) or to HBSS (after the measurement of the TEER),
2- 50 µL of 10 mg/mL FD4 and FD70 (2 mg/mL final concentration) were added to the 200 µL apical media of each transwell (including an empty one without cells, as a control of maximal permeability),
3- the plate was incubated in the dark, at 37°C in a humidified atmosphere (95%) containing 5% CO_2.
4- the transwell inserts were carefully removed without spilling apical media into the basal one,
5- the whole basal media of each transwell was collected and harvested at 4°C in the dark until the moment of the measurements (not more than one day after).

The florescence of the FD4 and FD70 (peaks of excitation and emission at wave lengths of 485 nm and 544 nm, respectively) that traversed the cell monolayers from the apical to the basolateral sides was measured on a Denovix DS-11 FX+ (M/C/F) spectrophotometer/fluorometer using the "Fluoro Std Assays" application. The Relative Fluorescent Units (RFUs) of a blank (only HBSS) were subtracted to the values of the samples and the effective FD4 and FD70 concentrations were extrapolated from a standard curve built with known concentrations (to which the blank was also subtracted). All the measurements fell within the linear range of the assay (0 to 1 mg/mL FD4 and FD70), so no dilution of the samples was necessary. For the experiments repeated in three biological replicas, the statistical analyses were carried out with a two-tailed paired T-test. Fold changes were calculated as:

$$Fold\ change = \frac{\text{average conc."treatment condition" – average conc."untreated condition"}}{\text{average conc."untreated condition"}}$$

3.2.1.5. IF staining of cells over glass coverslips

The cells grown over collagen-coated (section 3.2.1.1.) or acid-treated (fuming HCl for 15 days and then washed with autoclaved mQ H_2O) glass coverslips on a 24-well format. The cells were washed cautiously in 1-1,5 mL of 1X PBS after aspirating and discarding the culture media. The cells were either fixated shortly at RT°C for 15-20 min. in 4% PFA/1X PBS (500 µL/well). The PFA solution was discarded and the cells were shortly washed three times with 1 mL 1X PBS. A permeabilization step was performed incubating the cells in 0.1% Triton-X 100/1X PBS for 15 min. at RT°C (1 mL/well). After the permeabilization step, the blocking was performed to reduce the aspecific binding of the primary and secondary antibodies and minimize false-positive signals. The cells were incubated in 1% BSA/1X PBS for 1 hr at RT°C (1 mL/well). Successively the primary antibodies dilutions were prepared in 1% BSA/1X PBS and

25-50 µL of them were poured in single drops over a parafilm-covered plate. The coverslips were placed upside-down over single drops and incubated for 1 hr inside a humidified chamber at RT°C. Successively, the coverslips were transferred back to the 24 well plate upside-up and the excess of primary antibody was removed by three washes with 1X PBS (1 mL each). The incubations with the secondary antibodies were performed exactly in the same way as for the primary ones and three washes with 1X PBS (1 mL each) were done afterwards. The nuclear counterstaining was performed with Hoechst diluted 1:5000 in 1X PBS and incubating for 4 min. at RT°C in the dark. Afterwards, two washes were peformed with 1X PBS and two final ones with mQ H2O. The cells were mounted with Vectashield over a mounting glass slide.

3.2.1.6. IF staining of cells in two-dimensional epithelial-like structures grown over TW membranes

The cells grown under certain experimental condition were washed cautiously in 1,5 mL of 1X PBS after aspirating and discarding the culture media. Depending on the experiment, the whole cell monolayer of a single insert membrane or only half of it was processed. In both cases, the membrane was kept attached to the transwell during the first steps of the process. After the wash with PBS, the cells were either fixated shortly at RT°C for 15-20 min. or overnight at 4°C in 2% PFA/1X PBS (1,5 mL/transwell). The PFA solution was discarded and the cells were shortly washed three times with 1,5 mL 1X PBS. In order to make the epitopes accessible to the primary antibodies on T84 and CACO-2 monolayers, a permeabilization step was performed incubating the cells in 0.25% Triton-X 100/1X PBS for 15 min. at RT°C (1,5 mL/transwell). The harsh permeabilization treatment was performed considering that these two intestinal epithelial carcinoma cell lines manifest a high proliferation rate even after establishing cell-cell contact interactions, which make them grow forming domes (of multiple cell layers) and giving to the epithelial-like structure a three-dimensional configuration in certain regions. After the permeabilization step, the blocking was performed to reduce the aspecific binding of the primary and secondary antibodies and minimize false-positive signals. The cells were incubated in 1% BSA/1X PBS for 30 min. at RT°C (1,5 mL/transwell). Successively the primary antibodies dilutions were prepared in 1% BSA/1X PBS and 25-50 µL of them were poured in single drops over a parafilm-covered plate. The membranes were cut out of the transwell inserts, placed upside-down over single drops and incubated for 1 hr inside a humidified chamber at RT°C. Successively, the membranes were transferred back to the 24 well plate, upside-up, and the excess of primary antibody was removed by three washes with Tween 0.1%/1X PBS (300 µL each). The incubations with the secondary antibodies were performed

exactly in the same way as for the primary ones and three washes with Tween 0.1%/1X PBS (300 µL each) were done afterwards. The nuclear counterstaining was performed with Hoechst diluted 1:5000 in 1X PBS and incubating for 4 min. at RT°C in the dark. Afterwards, two washes were peformed with 1X PBS and two final ones with mQ H_2O. The cells were mounted with Vectashield or Aqua Poly/Mount over a mounting glass slide in accordance to the following order:

COVERSLIP
Mounting medium
Cells monolayer
Insert membrane
Mounting medium
MOUNTING GLASS

The imaging was done at the Leica Automated Inverted Microscope DMI4000B.

3.2.1.7. Lactate dehydrogenase (LDH) necrotic/necroptotic assay

The extent of cell Necrosis and Necroptosis that took place upon the different treatments was assessed at the whole monolayer level by applying the LDH-Glo™ Cytotoxicity Assay from Promega. This assay allows the quantification of the cytosolic enzyme LDH that is released into the culture media only by cells presenting an impaired plasma membrane (hallmark of Necrosis and Necroptosis). The quantification is based on a bioluminescent reaction in which the final emission of light depends indirectly on the enzymatic activity of the LDH as shown in figure 20.

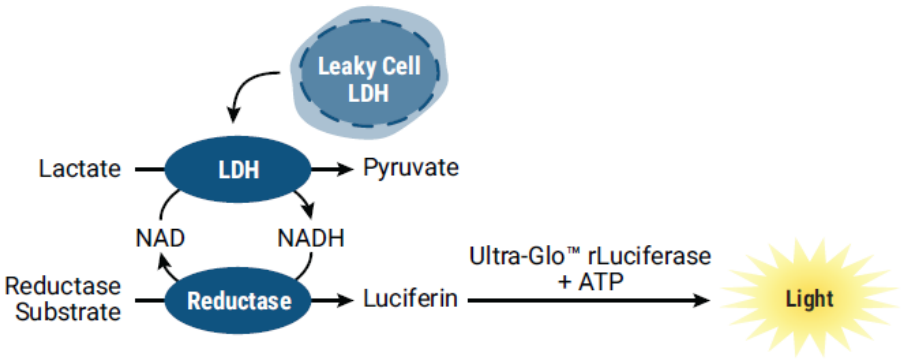

Figure 20: The reaction mix of the LDH assay contains Lactate, NAD^+, Reductase, Reductase Substrate, Ultra-Glo™ rLuciferase and a sample of diluted cell culture media. If the sample contains LDH, its activity will provide the necessary NADH for the production of Luciferin by the Reductase. The resulting luciferase-mediated production of light is proportional to the amount of LDH in the sample (from www.promega.com).

At a certain time-point after a certain treatment of the cells, the hereunder protocol was followed for all experiments:

1- A control condition of maximal plasma membrane impairment and maximal LDH release was established on a single untreated monolayer by applying 1X LDH Lysis Buffer in the culture media on both apical and basolateral sides and incubating for 15 min. at 37°C in a humidified atmosphere (95%) containing 5% CO_2.
2- The complete apical media of each single monolayer was transferred from each transwell into different Eppendorf tubes and mixed thoroughly.
3- 2 µL of each apical media were transferred into 48 µL of LDH Storage Buffer, mixed thoroughly and then harvested at -80°C until further processing.
4- At the moment of the measurement the samples were thawed and further diluted in LDH Storage Buffer (final dilution of the apical media of 1:100).
5- The quantification of the LDH was done in accordance to the manufacturer's instructions on 96-well plates made of Teflon (previously sterilized with Ethanol 70%, cleaned with an overnight treatment of Triton X-100 0.1% and washed for 30 min. under a VE-H_2O flow). The Relative Luminescence Units (RLUs) of the different conditions were subtracted to the blank that consisted on the media of a TW without cells.

At every experiment, a standard curve was built in accordance to the manufacturer's instructions as an overall experimental positive control and in order to corroborate that all diluted samples fall within the linear range of the assay.

3.2.1.8. TUNEL apoptotic assay

In order to quantify the extent of Apoptosis resulting either from the extrinsic and the intrinsic pathways and clearly distinguish apoptotic from necroptotic cells, the *In Situ* Cell Death Detection Kit, Fluorescein of Roche was applied to the monolayers upon the different experimental treatments.

The cleavage of the genomic DNA that takes place at later apoptotic stages prior to the formation of apoptotic bodies[70] can be quantified by the incorporation of fluorescently labeled nucleotides to the 3'-OH termini of double and single stranded breaks. Because of its mechanism of action, this assay is also termed TUNEL for "Terminal deoxynucelotidyl transferase (TdT)- mediated dUTP nick end labeling". The TUNEL reaction preferentially labels DNA strand breaks generated during Apoptosis in a template-independent manner allowing the *in situ* identification of fixed apoptotic cells by fluorescent microscopy[71].

At a specific time-point after a certain treatment, whole monolayers were processed in accordance to the manufacturer's instructions for adherent cells, with the following modifications:

1- Two additional (modified) cell permeabilization treatments were tested for the same reasons explained in the section 1.2.1.5: a permeabilization buffer for TUNEL assay with 0.25% Triton X-100 and another with 0.5% Triton X-100, both applied for 15 min. at RT°C.
2- The membranes were cut out of the transwell inserts after the post-permeabilization washes and the incubation with the TUNEL reaction mix was performed as described in the section 1.2.1.5 for primaries and secondaries antibodies.

3- The nuclear counterstaining and the final mounting of the cells over a mounting glass slide were performed as described in the section 1.2.1.5.

In all experiments and permeabilization conditions, a positive control was established in accordance to the manufacturer´s instruction.

All processed monolayers were analyzed by confocal fluorescent microscopy on an Eclipse Ti Microscope with an A1 confocal scanner (Nikon).

3.2.1.9. BrdU cell proliferation assay

The extent of cell proliferation during the differentiation processes was quantified *in situ* on the monolayers with the 5-Bromo-2´-deoxy-uridine Labeling and Detection Kit I of Roche.

This kit allows the identification by IF of cells which are actively synthesizing their DNA at a certain time-point. The assay consists on the addition into the culture media of 5-bromo-2´-deoxy-uridine (BrdU), which will be incorporated into the DNA of proliferating cells, in the place of thymidine. After a specific time of incubation with BrdU, the cells are fixed in acidic ethanol and the ones that were at an active proliferating state are identified with a monoclonal antibody for BrdU and a suitable secondary antibody labeled with a fluorescent dye. Noteworthy, the preparation buffer of the primary antibody contains specific nucleases which allow the access to BrdU after fixation in acidic ethanol[72].

At a certain experimental condition, whole monolayers were processed in accordance to the manufacturer's instructions for adherent cells, with the following modifications:

1- To define the optimal incubation time with the BrdU labeling medium, different times were tested in accordance to the specific cell´s doubling time. For T84 a doubling time of 33.9 hrs was considered[73] so the incubation times of 12, 24 and 36 hrs were tested.
2- The membranes were cut out of the transwell inserts after the post-fixation washes and the incubations with the primary and secondary antibodies were performed in the same way as described in the section 1.2.1.5.
3- As a secondary antibody a goat anti-mouse IgG (H+L) labeled with Alexa Fluor 488 was employed (Table 2).
4- The nuclear counterstaining and the final mounting of the cells over a mounting glass slide were performed as described in the section 1.2.1.5.

The imaging of all processed monolayers was performed at the Leica Automated Inverted Microscope DMI4000B.

3.2.2. Molecular biological methods

3.2.2.1. Total RNA isolation

3.2.2.1.1. Phenol-Chloroform extraction

A standard procedure of Phenol-Chloroform total RNA extraction was followed employing the TRIzol™ Reagent in accordance to the manufacturer´s instructions. This method was employed for undifferentiated T84 cell pellets.

3.2.2.1.2. Direct-zol™ RNA MicroPrep

For RNA isolation out of Monocytes cell pellets ($3x10^5$ - $3x10^6$ cells), this kit was employed in accordance to manufacturer´s instructions.

3.2.2.1.3. Quick-RNA™ Microprep Kit and RNAqueous®-Micro Kit

Both kits were used in accordance to manufacturer´s instructions for total RNA isolation out of the epithelial cells grown and differentiated over transwell membrane inserts under the different experimental conditions. As in both kits the lysis buffers contain only guanidinium thiocyanate without phenol, the integrity of the membranes was preserved avoiding the contamination of the final RNA samples with impurities.
In brief, single transwell membranes were cut out of the inserts and immersed in the appropriate volume of lysis buffer, vortexed and stored at -80°C. For certain experiments multiple transwell membranes under exactly the same experimental conditions were pulled together (the lysis buffer volume was adjusted accordingly) and treated in the same way. At the moment of the isolation, the membranes in lysis buffer were thawed, vortexed and centrifuged. The protocol was followed in accordance to the manufacturer´s instructions loading only the lysed cells into the column.
In all RNA isolations, the DNaseI treatment was included in accordance to manufacturer´s instructions.

3.2.2.2. RNA quantification and integrity check

Quantity and quality of the purified RNAs were assessed on a Denovix DS-11 FX+ (M/C/F) spectrophotometer/fluorometer employing the “RNA” application.
RNA samples with low concentrations and low values of the ratio abs 260/230 nm and the T84 RNA employed for the 5´-3´RACE cDNA library synthesis were quantified with the Qubit® RNA HS Assay Kits following the manufacturer´s instructions.

The integrity of the T84 RNA employed for the 5´-3´RACE cDNA library synthesis was checked with an Agilent 2100 Bioanalyzer Instrument and the Bioanalyzer RNA Analysis kit in accordance to the manufacturer´s instructions.

3.2.2.3. cDNA synthesis

The first strand synthesis of total RNA was performed with the Superscript III First-Strand Synthesis System for reverse transcription PCR kit from Thermo Fisher Scientific. The protocol was followed in accordance to the manufacturer´s instructions but including always either Oligo$(dt)_{20}$ (2.5 µM final concentration) and Random Hexamer (2.5 ng/µL final concentration) primers in the reaction mix. The RNA input was always 1 µg and after the whole procedure, the ss-cDNA samples were diluted 1:5 in mQ autoclaved H_2O, either for conventional and for RT-qPCR experiments.

In the cases in which at least one of the RNA samples to be compared had not enough material for an input of 1 µg, the inputs of all the samples were normalized to a lower amount or the final cDNA dilution of the sample with an input of less than 1 µg was reduced accordingly.

For all reverse transcriptions, a negative control reaction was set by adding mQ H_2O to the reaction mix in the place of the RNA template.

3.2.2.4. Conventional RT-PCR

Semi-quantitative gene expression analyses (at mRNA level) were carried out by conventional RT-PCRs, employing the HotStarTaq DNA Polymerase Kit from Qiagen. The reactions were performed in accordance to the manufacturer´s instructions and the input of ss-cDNA template in each reaction mix was always ~25 ng (except for cases in which there was not enough material for performing the reverse transcription out of 1 µg of RNA).

The primers for conventional RT-PCR (see Tables 5 and S1) were all designed in order to fulfill the following requirements:

- reach a Tm of 60°C,
- have a length of ~20 bp,
- present a GC content of ~60%,
- span an intron (the longest possible in order to exclude genomic DNA amplification),
- give an amplicon of >100 bp.

As positive controls of amplification ss-cDNA derived from cell lines or tissues with known mRNA expression (obtained from The Human Protein Atlas) or recombinant vectors, carrying the gene of interest were employed.

The results were analyzed by running 10 µL of each amplification in 1% (≥1 kb amplicons) to 2% (0.1-1 kb amplicons) agarose gels.

3.2.2.5. RT-qPCR

For quantitative gene expression analyses (at mRNA level), RT-qPCRs were carried out employing the QuantStudioTM 3 Real-Time PCR System 96-Well 0.2 mL Block from Applied Biosystems.

The primers for RT-qPCR (see Tables 5 and S2) were all designed in order to fulfill the following requirements:

- reach a Tm of 60°C,
- have a length of ~20 bp,
- present a GC content of ~60%,
- span an intron (the longest possible in order to exclude genomic DNA amplification),
- give an amplicon of ≤100 bp.

All reaction mixes were prepared in a final volume of 20 µL as follows:

- 2x qPCRBIO SyGreen Mix Lo-ROX (PCRBIOSYSTEMS): 10 µL,
- Primers FOR/REV pre-mix (10 µM each): 0.4 µL,
- mQ autoclaved H_2O: 7.6 µL,
- ss-cDNA: 2 µL (~20 ng)

The running program was set as follows:

1) 95°C for 2 min.,
2) 95°C for 2 seconds,
3) 60°C for 20 seconds,
4) repeat steps 2) and 3) for 39 cycles.

In all experiments the method of quantification was a relative quantification to a standard curve built for each set of primers out of serial dilutions of a template known to express the gene of interest (Figures S1 to S8 of the Supplementary Material). To this end, the experiment type at the QuantStudioTM 3 Real-Time PCR System was set to "Standard Curve" and after the run the calculation of the quantities was performed automatically by importing the standard curves of interest in the section "Standard Curves Settings".

For the runs in which the standard curves were built, a genomic DNA control (normal patient) and a mQ autoclaved-H_2O control were included for each pair of primers in the place of the template. In those experiments two technical replicas were prepared for each condition.

For the relative quantification runs a mQ autoclaved-H_2O control was included for each pair of primers in the place of the template and three technical replicas were prepared for each condition. The calculated quantities for each gene of interest in each

experimental condition were normalized to the mean quantities of the standard genes *SDHA*, *ARF1*, *HPRT1* in the same experimental conditions. Each experiment was repeated in three biological replicas, the statistical analyses were carried out with a two-tailed paired T-test and the fold changes were calculated as:

$$Fold\ change = \frac{\text{average quantity "treatment condition" – average quantity "untreated condition"}}{\text{average quantity "untreated condition"}}$$

3.2.2.6. Transcriptome expression profiling: RNA sequencing

Total RNA of T84 in the condition of interest was isolated employing the Quick-RNA™ Microprep Kit. An eventual contamination with genomic DNA (gDNA) was prevented by performing an "in column" digestion with DNAaseI in accordance to the manufacturer's instruction. The obtained RNA was quantified employing the Qubit® RNA HS Assay Kit, the quality was assessed at the spectrophotometer (expected abs. 260/280 of 2.0 and expected abs. 260/230 of 2.0-2.2) and the integrity was checked employing the Bioanalyzer RNA Analysis kit (expected RNA Integrity Number of 9-10).

The sequencing of the total mRNA populations of the single experimental conditions was carried out by GeneWiz (www.genewiz.com) via polyA-tail selection and enrichment as described in Figure 21.

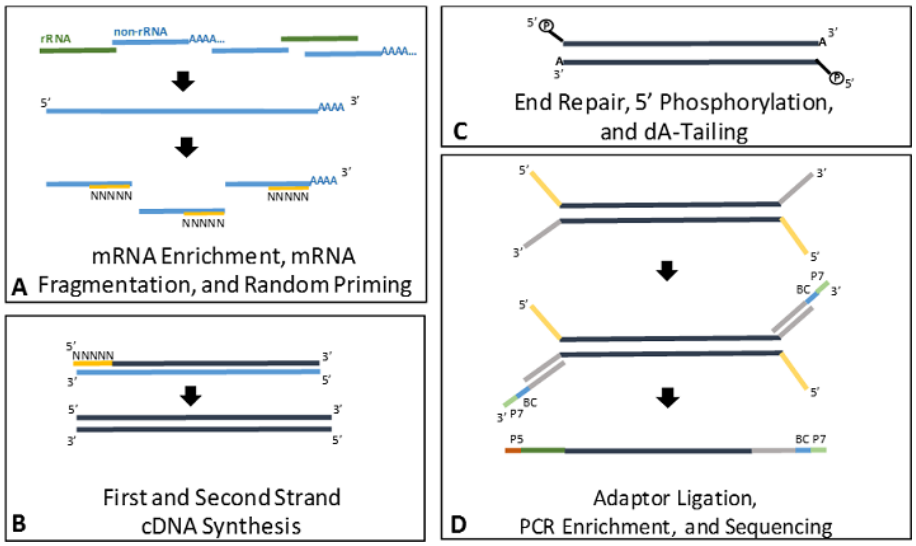

Figure 21: RNAseq of only mRNAs via polyA selection and enrichment (from www.genewiz.com).

The company provided a list of unique gene hit counts (unique reads that fell within exon regions) for each total mRNA population (of each experimental condition), calculated by using "featureCounts" from the "Subread package v.1.5.2". The normalization of the gene hit counts within each sample was carried out by GeneWiz using the "DESeq2 package" for R programming, which scaled them by a sample-

specific normalization factor that corresponds to the total gene hit counts in a sample. Samples with more total gene hit counts had their values decreased, while samples with less total gene hit counts had their values increased. The mean values of the normalized gene hit counts were calculated out of three biological replicas and the differential expression of the single genes was calculated for each specific comparison (in between different experimental conditions) as the Log2FoldChange:

$$Log2FoldChange = Log2\left(\frac{\text{Group 2 mean normalized counts}}{\text{Group 1 mean normalized counts}}\right)$$

where Group 2 refers to the experimental condition of interest and Group 1 refers to the untreated condition or the experimental condition of reference. Were considered significantly differentially expressed those genes that presented an absolute Log2FoldChange ≥2 in each specific comparison.

The statistical analyses of the RNAseq data provided by the company GeneWiz, employing the "package DESeq2" in R programming language, did not consider the three biological replicas per experimental condition and were performed on single biological replicas. For this, and for time reasons, the statistical significance of the Log2FoldChanges was not stated as should have been done, employing the Wald test (to obtain the p-values) and the Benjamini-Hochberg (to obtain the adjusted p-values). For the same reasons, the lfcSE (Log2FoldChange Standard Error) could not be calculated out of the Log2FoldChange mean values of the three biological replicas.

3.2.2.7. 5'/3' Rapid Amplification of cDNA Ends (RACE)

The RACE technique allows the amplification of the 5' and 3' flanking regions of a known internal cDNA sequence of a certain transcript. It consists on a series of PCRs that employ both forward (3' RACE) and reverse (5' RACE) primers of the internal known sequence and primers complementary to known oligonucleotide tags added to all the transcripts of the cell of interest.

3.2.2.7.1. Preparation of a total cDNA library labeled with known priming sites at both 5' and 3' ends

The first step of the whole procedure consisted on the preparation of a total cDNA library for the cell line of interest in which all the transcripts were labeled with known priming sites at both 5' and 3' ends (figure 22).

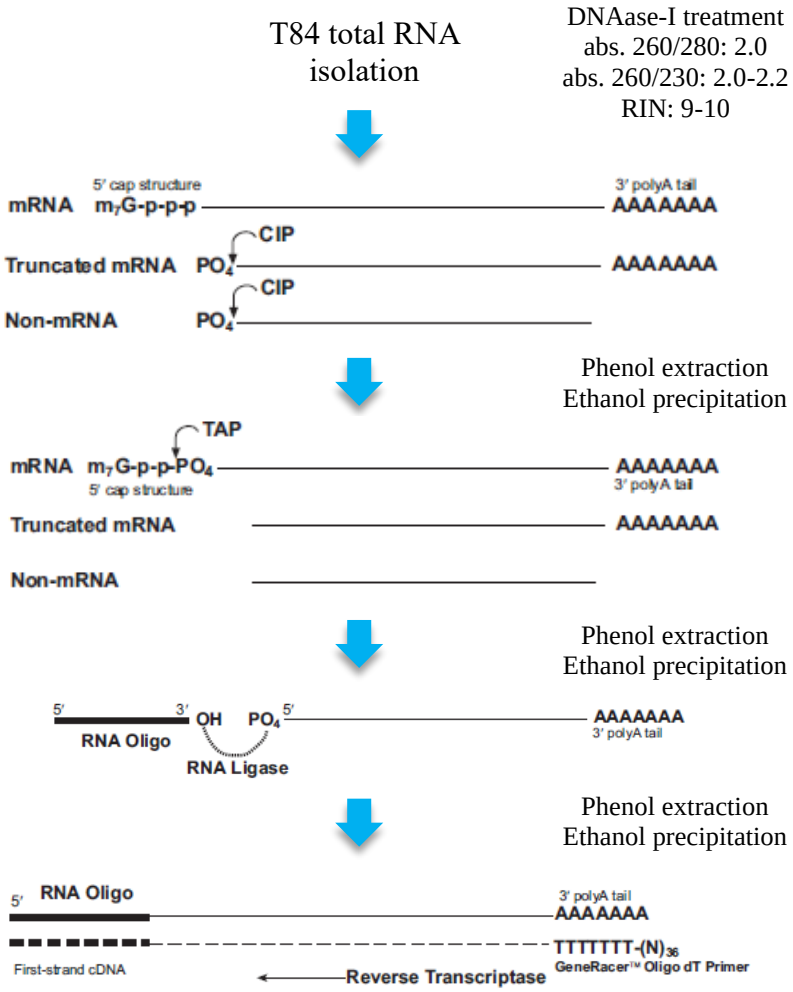

Figure 22: Schematic representation of whole procedure of preparation of the total sscDNA library with known priming sites at both 5' and 3' ends for 5'/3' RACEs. From Invitrogen GeneRacer™ Kit user manual (Version L, 8 April 2004, 25-0355).

In all experiments, the total RNA of the T84 cell line was isolated employing the Quick-RNA™ Microprep Kit or the Direct-zol™ RNA MicroPrep. An eventual contamination with gDNA was prevented by performing an "in column" digestion with DNAaseI in accordance to the manufacturer's instruction. The obtained RNA was quantified employing the Qubit® RNA HS Assay Kit, the quality was assessed at the spectrophotometer (expected abs. 260/280 of 2.0 and expected abs. 260/230 of 2.0-2.2) and the integrity was checked employing the Bioanalyzer RNA Analysis kit (expected RNA Integrity Number of 9-10).

The first reaction of the library preparation process required the Calf Intestinal Phosphatase for the removal of the 5' phosphates out of all cellular RNAs that lack the 5' cap (immature mRNAs, truncated mRNAs and non-mRNA RNA molecules). The following step consisted on the removal of the 5' cap structure out of all mature cellular mRNAs employing the Tobacco Acid Pyrophosphatase, leaving a 5' phosphate for the successive ligation reaction. In this reaction, an oligoribonucleotide with the 5' RACE known priming site was ligated to all decapped mature cellular mRNAs with the T4 RNA ligase. The final step consisted on a reverse transcription with Super Script III employing the GeneRacer™ Oligo dT Primer to obtain the sccDNA library with known priming sites at the 5′ and 3′ ends. In a second experiment the reverse transcription was performed with the gene-specific internal reverse primer when only the 5' RACE was followed.

3.2.2.7.2. 5' and 3' RACE PCRs

Considering that the preparation of the sscDNA RACE library requires many steps that negatively affect the final yield of the labeled mRNAs (substrate of the final reaction of cDNA synthesis), two consecutives PCRs were ran for each 5' and 3' RACE PCRs: a Touchdown followed by a Nested PCR. The first Touchdown PCR consists on a series of cycles that start with a higher Tm (low specificity in the primers annealing) and gradually decreases to the Tm of the RACE primers (high specificity in the primers annealing), allowing an initial enrichment of the amplicon of interest for which low amounts of template are available.

The primers were designed following the manufacturer's instructions (section 8.4). The reaction mixes of both Touchdown and Nested PCRs were prepared in accordance to the manufacturer's instructions of the HotStarTaq DNA Polymerase. The template of the Touchdown PCR was 1 µL of RACE cDNA library, whereas for the Nested PCR 1 µL of Touchdown post-PCR product was employed.

The running program for the Touchdown 5' and 3' RACE PCRs for *HTR3E* was set as follows:

1) 95°C for 15 minutes,
2) 94°C for 30 seconds,
3) 74°C for 2 minutes,
4) repeat steps 2) and 3) for 5 cycles,
5) 94°C for 30 seconds,
6) 72°C for 2 minutes,
7) repeat steps 5) and 6) for 5 cycles,
8) 94°C for 30 seconds,
9) 65°C for 30 seconds,
10) 72°C for 2 minutes,
11) repeat steps 8), 9) and 10) for 25 cycles,

12) 72°C for 10 minutes

The second is a Nested PCR performed with another pair of primers pairing the immediate 3' sequences that follow the sequences of the initial 5'/3' RACE primers. The goal of the Nested PCR is to enrich only the specific amplicon of interest out of the less specific initial pre-amplification carried out with the Touchdown PCR.

The running program for the Nested 5' and 3' RACE PCRs for *HTR3E* was set as follows:

1) 95°C for 15 minutes,
2) 94°C for 30 seconds,
3) 65°C for 30 seconds,
4) 72°C for 2 minutes,
5) repeat steps 2), 3) and 4) for 40 cycles.

Figure 23 graphically depicts these two consecutive PCRs for both 5' and 3' RACEs.

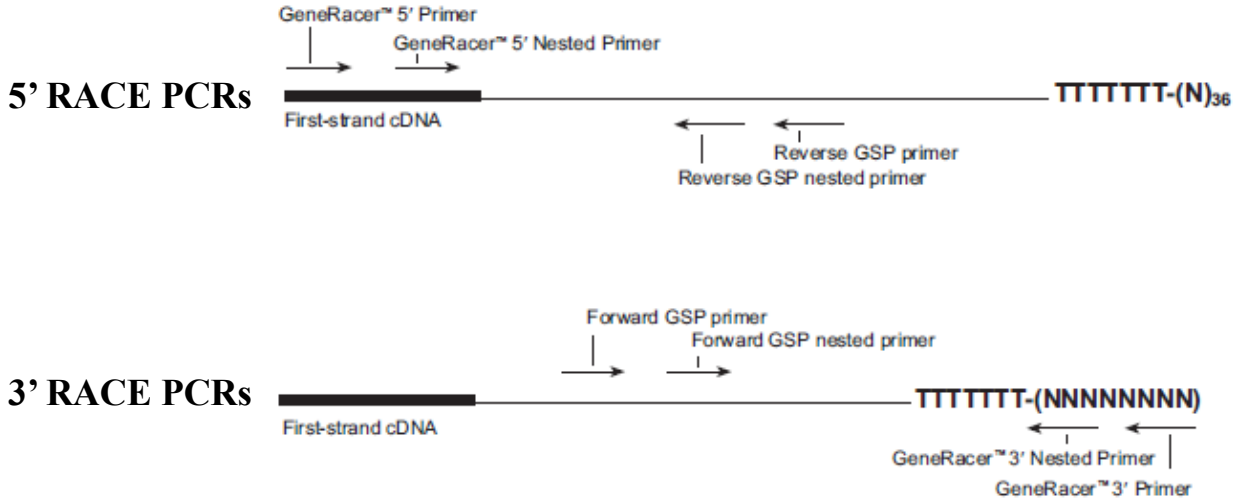

Figure 23: Schematic representation of both Touchdown and Nested 5' and 3' PCRs. From Invitrogen GeneRacer™ Kit user manual (Version L, 8 April 2004, 25-0355).

3.2.2.7.3. Cloning and sequencing of 5' and 3' RACE PCR fragments

The products of each 5' and 3' RACE Nested PCRs reaction (25 µL per reaction) were analyzed by gel electrophoresis (employing a 2% agarose gel) and the bands of interest were excised with a scalpel.

The post-PCR DNA of the bands was extracted and purified from the agarose gel employing the QIAquick Gel Extraction Kit in accordance to the manufacturer's manual.

The amplification reaction with the HotStarTaq DNA Polymerase release DNA products with blunt ends, so in order to clone the post-PCR DNA products the

pSTBlue-1 AccepTor™ was employed. The ligation reaction mix (final volume 10 µL) was prepared as follows:

- pSTBlue-1 AccepTor™ (50 ng/µL): 1 µL
- Purified DNA from band: 4 µL,
- 2X ligation pre-mix: 5 µL,

The reaction was ran at 16°C for 5 hrs.

The ligated vector/band DNA was employed to transform Chemocompetent NovaBlue cells applying the following protocol:

1) chemocompetent NovaBlue cells were thawed on ice for 2-5 min. and mixed without vortexing,
2) 1 µL of ligation reaction was added to the cells suspension and mixed without vortexing,
3) the cells suspension was kept on ice for 5 min.,
4) the transformation was performed by a heat shock at 42°C for 30 seconds,
5) to allow the recovery of the cells 250 µL of SOC medium was added to the cells suspension and this one was incubated at 37°C for 30 min.,
6) the transformed cells suspension was plated on an LB plate with ampicillin and IPTG/ X-Gal,
7) the transformed cells were allowed to grow over the plates overnight at 37°C.

Colonies formed by non-recombinant cells appeared blue (functional lacZ gene at the Multiple Cloning Site and hydrolysis of the chromogenic substrate X-gal by β-galactosidase) while the recombinant ones appeared white (insertion of the post-PCR DNA in the Multiple Cloning Site and within the lacZ gene).

In order to properly identify the colonies derived from cells that incorporated the recombinant ligated vector, single white colonies were picked up and dissolved in 15 µL of LB medium with ampicillin. A Colony PCR was performed employing 5 µL of each dissolved colony as a template. The reaction mixes were prepared followed the HotStarTaq DNA Polymerase manufacturer's instructions. The respective pair of Nested RACE PCR primers were employed each colony. The running program for the Colony PCRs was set as follows:

1) 95°C for 15 minutes,
2) 94°C for 30 seconds,
3) 65°C for 30 seconds,
4) 72°C for 2 minutes,
5) repeat steps 2), 3) and 4) for 40 cycles.

The colonies that gave rise to the expected amplification of the bands of interest were pre-inoculated in 5 mL of LB medium with Ampicillin and incubated at 37°C overnight shaking at 200 rpm.

Total plasmidic DNA was isolated from the pre-inoculations employing the Quick DNA Miniprep Plus Kit from Zymo Research, following the manufacturer's instructions.

From each plasmidic DNA 1 µg was sequenced with the Sanger method employing the primers T7_prom and M13_fwd (www.genewiz.com) specific for the multiple cloning site of pSTBlue-1 AccepTor™.

3.2.2.8. Protein concentration and quantification

The concentration of the nanobody TROS (MW of 42.87 kDa) was performed with Amicon filters of 3 kDa MWCO cellulose membranes of 4 and 0.5 mL. All filters were blocked with 1% Milk/mQ H_2O overnight at RT°C, in order to avoid the adsorption of the nanobody to the cellulose membrane. Washes with mQ H_2O to get rid of the excess of blocking proteins, and a pre-equilibration with PBS were performed before loading the nanobody. The whole process was subdivided in an initial concentration on 4 mL Amicon filters followed by a final concentration on the 0.5 mL ones. The times and speed of centrifugation in both steps were defined empirically (and in accordance to the characteristics of the employed centrifuges and rotors) in order to optimize the concentration without exposing the nanobody to the cellulose membrane for longer times (to avoid the adsorption).

On all flow-throughs and eluates of partially concentrated and fully concentrated fractions, the total protein quantification was performed with the Pierce™ BCA Protein Assay Kit following the manufacturer's instructions.

4. RESULTS

4.1. *In vitro* differentiation of T84 and CACO-2 cell lines into a two-dimensional epithelial-like structure

In order to establish an *in vitro* model of the intestinal epithelium my first goal was to define a human epithelial cell line to work with and the optimal conditions for its differentiation.
The differentiation experiments performed are summarized in the Table 6.

Table 6: T84 and CACO-2 differentiation experiments and conditions.

Differentiation experimental setup	Substrate	Coating/pre-treatment	Oxygen concentration (%)	Cell densities ($x10^3$ cells/cm^2)	Days of growth
Coverslips in normoxia	Glass	Collagen Type I 10 µg/mL	20	37 – 87 – 125 – 150	Until 100% confluency
		HCl 37% for 14 days			
TW inserts in normoxia	Polycarbonate membrane of 3 µm porosity	Collagen Type I 10 µg/mL	20	180 – 240 – 290 – 360 – 480	1 to 10 or 1 to 20
TW inserts in hypoxia	PET membrane of 0.4 µm porosity	Collagen Type I 10 µg/mL	1	360	1 to 10
	Polycarbonate membrane of 3 µm porosity	Matrigel 150 µg/mL – 1 mg/mL – 3 mg/mL			

4.1.1. *In vitro* differentiation trials of T84 and CACO-2 over a glass substrate: normoxic conditions

In a very first set of pilot experiments in standard normoxic cell culture conditions, I simply seeded T84 and CACO-2 at different cell densities over glass coverslips pre-treated with Collagen Type I 10 µg/mL overnight at 4°C or with Hydrochloric Acid 37% for 14 days at RT°C and let to grow until confluency. When the cells reached 100% confluency they were fixed and immunostained for the differentiation marker ZO-1 (ZO1-1A12, monoclonal antibody) and counterstained with Höchst 33342.
The IF stainings depicted in figure 24 summarize the first set of pilot differentiation experiments for CACO-2. Three different seeding densities were applied: 37, 87, 125 and 150 $x10^3$ cells/cm^2. As there was not a significant difference in between them regarding the times for reaching confluency nor regarding the expression and localization of ZO-1, the most representative images have been chosen but not for all densities.

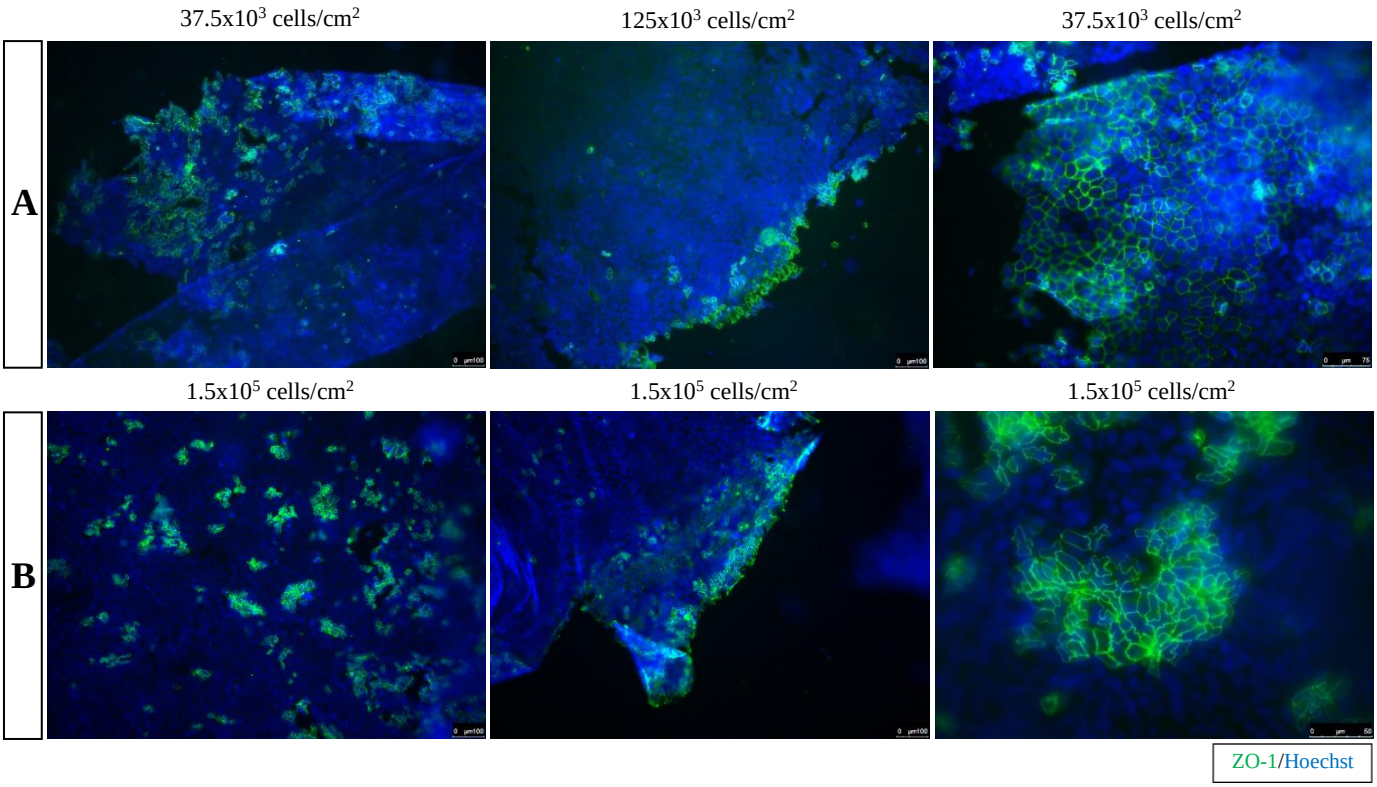

Figure 24: IF staining of CACO-2 (passage 55) grown over glass coverslips and imaging by widefield microscopy. In the green channel (ex: 460-500 nm / em: 512-542 nm) staining for ZO-1 (Alexa Fluor 488), and in the blue channel (ex: 340-380 nm / em: 450-490 nm) nuclei counterstaining (Hoechest). A) CACO-2 seeded at different densities over collagen-coated glass coverslips and grown for 13 days. Scale bar of 100 µm for the first two images and of 75 µm for the one at the far right. B) CACO-2 seeded at different densities over acid-treated glass coverslips and grown for 7 days. Scale bar of 100 µm for the first two images and of 75 µm for the one at the far right.

In addition to the *in situ* IF staining of ZO-1, an mRNA expression analysis was carried out by conventional RT-PCR from an experiment of seven days of growth ran over coverslips pre-coated with Collagen Type I, from an initial seeding density of 150 x10^3 cells/cm^2 (figure 25). The expression of the differentiation marker *TJP1* (coding for ZO-1) was analyzed together with the expression of the standard genes *SDHA* and *ARF1* (as controls for the evaluation of the quality of the RNA input material and of the correct establishment and development of the cDNA synthesis and PCR reactions).

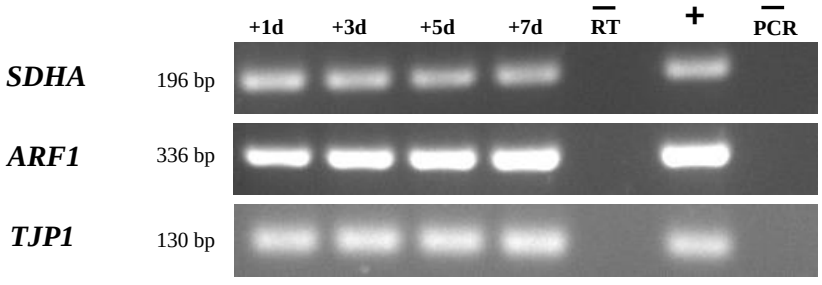

Figure 25: Conventional RT-PCR for *TJP1* (primers *TJP1*_for/_rev) of CACO-2 (passage 55) grown for seven days over glass coverslips coated with Collagen Type I. *ARF-1* (primers *ARF1*_for/_rev) and *SDHA* (primers *SDHA*_for/_rev) were amplified as standard genes. The positive control consisted on CACO-2 cells grown over collagen-coated plastic on a T25 format at 100% confluency.

The IF stainings depicted in figure 26 summarize the first set of pilot differentiation experiments for T84 grown for 7 days over glass. In this case only one seeding density (150 x10^3 cells/cm^2) is presented as, again, no significant difference was observed in between the different tested ones.

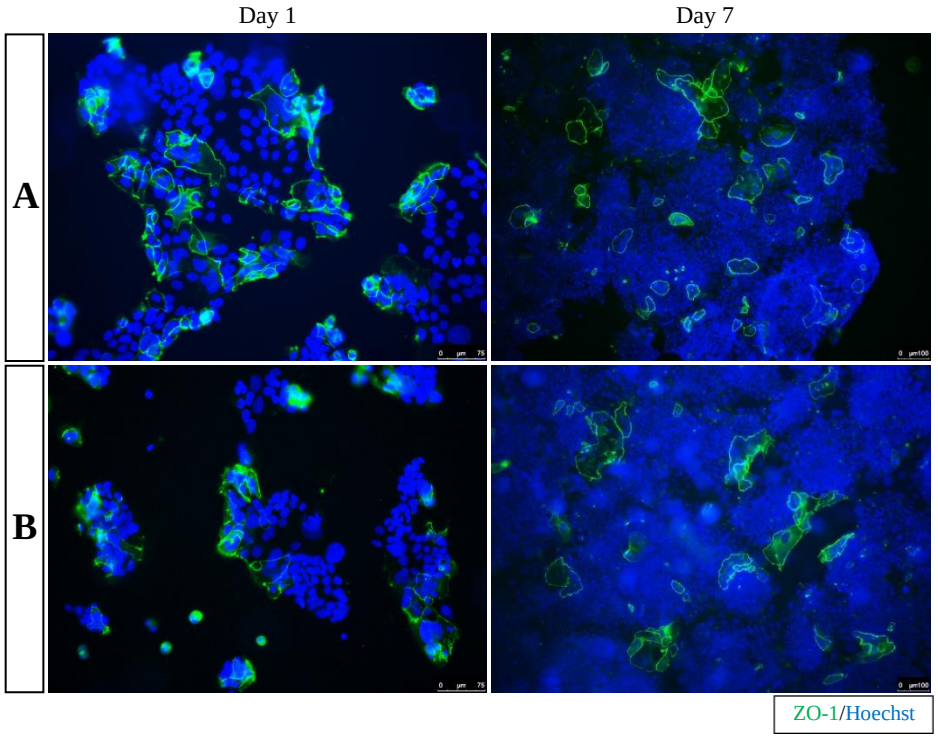

Figure 26: IF staining of T84 (passage 17) grown over glass coverslips and imaging by widefield microscopy. In the green channel (ex: 460-500 nm / em: 512-542 nm) staining for ZO-1 (Alexa Fluor 488), and in the blue channel (ex: 340-380 nm / em: 450-490 nm) nuclei counterstaining (Hoechest). A) T84 seeded at 1.5x10^5 cells/cm^2 over collagen-coated glass coverslips and grown for 1 and 7 days. Scale bar of 75 µm for the first image and of 100 µm for the one at the right side. B) T84 seeded at at 1.5x10^5 cells/cm^2 over acid-treated glass coverslips and grown for 1 and 7 days. Scale bar of 75 µm for the first image and of 100 µm for the one at the right side.

In order to complement the information obtained with the *in situ* IF staining of ZO-1, also for T84 an mRNA expression analysis was carried out by conventional RT-PCR from an experiment of seven days of growth ran over coverslips pre-coated with Collagen Type I from an initial seeding density of 150 x10^3 cells/cm^2 (figure 27). The expression of *TJP1* was analyzed together with the one of the standard genes *SDHA* and *ARF1*.

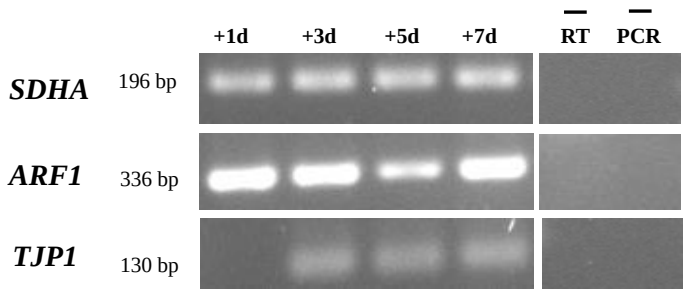

Figure 27: Conventional RT-PCR for *TJP1* (primers *TJP1*_for/_rev) of T84 (passage 17) grown for seven days over glass coverslips coated with Collagen Type I. *ARF-1* (primers *ARF1*_for/_rev) and *SDHA* (primers *SDHA*_for/_rev) were amplified as standard genes.

From this first set of experiments it appeared very clear that the simple seeding over glass coverslips did not allow for a proper and homogeneous differentiation of these two epithelial cell lines. Even though a basal, constant expression of *TJP1* was observed at the mRNA level (at day one for T84 some problem during the PCR cycles might have happened), a relatively diffused staining of ZO-1 in a ring-like pattern (functional latero-apical localization) was only observed at the borders of the final confluent monolayers. These borders were still attached to the central regions but partially suspended in the growth medium (so in contact with media from two sides). As mentioned before it has been reported that a basal expression of ZO-1 is observed in epithelial cells even at undifferentiated conditions, whereas its functional localization is only achieved upon differentiation. A clear difference was not observed in between coverslips pre-coated with Collagen Type I and coverslips pre-treated with fuming hydrochloric acid, but a slightly higher extent of IF staining was observed in the first condition (and of course this condition mimics better the substrate over which these cells grow *in vivo*).

4.1.2. *In vitro* differentiation of T84 and CACO-2 over semipermeable membranes: normoxic and hypoxic conditions

Given the poor results obtained by growing the cells over a glass substrate, I decided to establish the differentiation of T84 and CACO-2 in accordance to the literature[74-77] by growing them over semi-permeable supports filled with growth media from both apical and basolateral sides. The TW cell culture inserts not only allow to grow the cells in this manner but also to perform key electrophysiological and permeability assays for assessing both the cell confluency and the barrier function level (a direct consequence of the epithelial cells differentiation).

For every differentiation experiment both cell lines were passaged and expanded as described in the section 1.2.1.1. and then seeded onto Corning® Transwell® cell culture inserts with a porous (0.4 or 3.0 μm pores) polycarbonate membrane of 6.5 mm (Ø) and 0.33 cm^2 (cell growth area) (figure 28). The insert membranes were always pre-coated with 10 μg/mL of Collagen from rat tail Type I for 3 hrs at 37°C or overnight at 4°C or with Matrigel at different concentrations and times of incubation at 37°C.

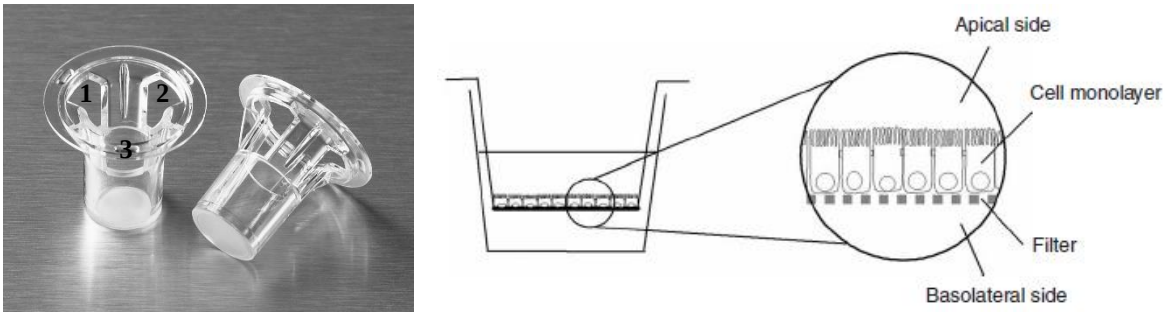

Figure 28: The TW chamber setup. Single inserts (left) with three open spaces for positioning the STX2 electrode (section 3.2.1.3). Scheme (right) describing the position of the cells monolayer and of the apical and basolateral media compartments (from Hubatsch, I. *et al.*, 2007).

Differentiation seeding tests were performed starting from various cell densities and growing the cultures for different time intervals in accordance to the literature[75,78]. In these time course experiments different measurements were performed *in situ* on a subset of TWs, while from other TWs the cells were processed for further analyses. The following activities (in order) were carried every other day for T84 and every second day for CACO-2:

1- the TEER was monitored as described in the section 3.2.1.3.,
2- a permeability assay using FD4 was performed as described in the section 3.2.1.4.,
3- the expression at the protein level and the cellular localization of TJP1 were analyzed by IF stainings as described in the section 3.2.1.6.
4- the expression of *TJP1* was monitored at regular intervals by conventional RT-PCR.

Differentiation tests for CACO-2 were performed by seeding $1.8x10^5$ and $3.6x10^5$ cells/cm^2 over Collagen-coated Corning® Transwell® cell culture inserts with a porous (3.0 µm pores) polycarbonate membrane of 6.5 mm (Ø) and 0.33 cm^2 (cell growth area), and letting them grow for 20 days in standard normoxic cell culture conditions, in accordance to the literature[75,77].

Figure 29 depicts a differentiation curve of CACO-2 (seeding density of $3.6x10^5$ cells/cm^2) obtained by measuring the TEER and performing a FD4 permeability assay every second day, for a single biological replica.

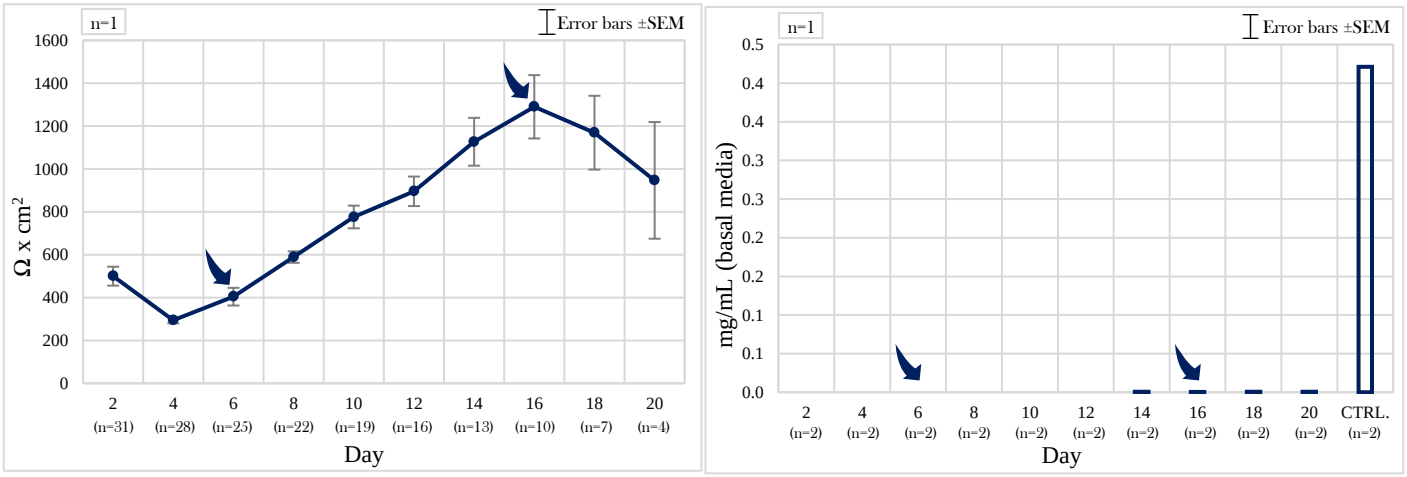

Figure 29: TEER measurements (Ω x cm^2) (left) and FD4 permeability assay (mg/mL) (right) for a differentiation experiment of CACO-2 (passage 34) over TW inserts. Error bars ±SEM of the technical replicas indicated in brackets. The left arrows indicates the estimated onset of differentiation (time point when 100% confluency was reached), and the right ones indicate the completion of the differentiation process. The control of maximal permeability for the FD4 assay corresponds to a TW insert without cells.

As many factors affect the behavior of the cells in culture, especially at sub-differentiating stages, it is not reasonable to calculate the mean values of the TEER values in between biological replicas in this kind of time-resolved experiments. That is why the outcome of a single biological replica is presented. The measurement of the TEER over 20 days of growth clearly show an initial increase of resistance given by the solely cell confluency and then a further, more pronounced, increase given the cell differentiation and the establishment of the barrier function (figure 29, left). The resistance given by the 100 % cell confluency in this kind of intestinal epithelial cell line is at around ±330 Ω x cm^2, so the remaining increase up to ±1290 Ω x cm^2 is determined by the cell differentiation.

In the same differentiation experiment with CACO-2, a FD4 permeability assay was performed every second day (figure 29, right). I would have expected to observe a gradual decrease of the permeability towards this molecular species concomitant to the reaching of the cell confluency and then to the differentiation. Nevertheless, no detectable initial high permeability was observed. This result is in accordance with the high proliferative capacity observed for CACO-2 (at least for the clone employed by me), by far higher than the one observed for T84. CACO-2 reached confluency a few days after seeding (independently of the seeding densities applied) and tended to form domes by growing over each other. This can be the reason for the lack of detectable permeability from day 2.

The IF stainings for ZO-1 depicted in figure 30 summarize the differentiation experiments for CACO-2 (seeding density of 3.6 x 10^5 cells/cm^2) at passage 34 over TW inserts. In addition, the IF stainings obtained in another experiment with a passage 31 (seeding density of 1.80 x 10^5 cells/cm^2) are presented.

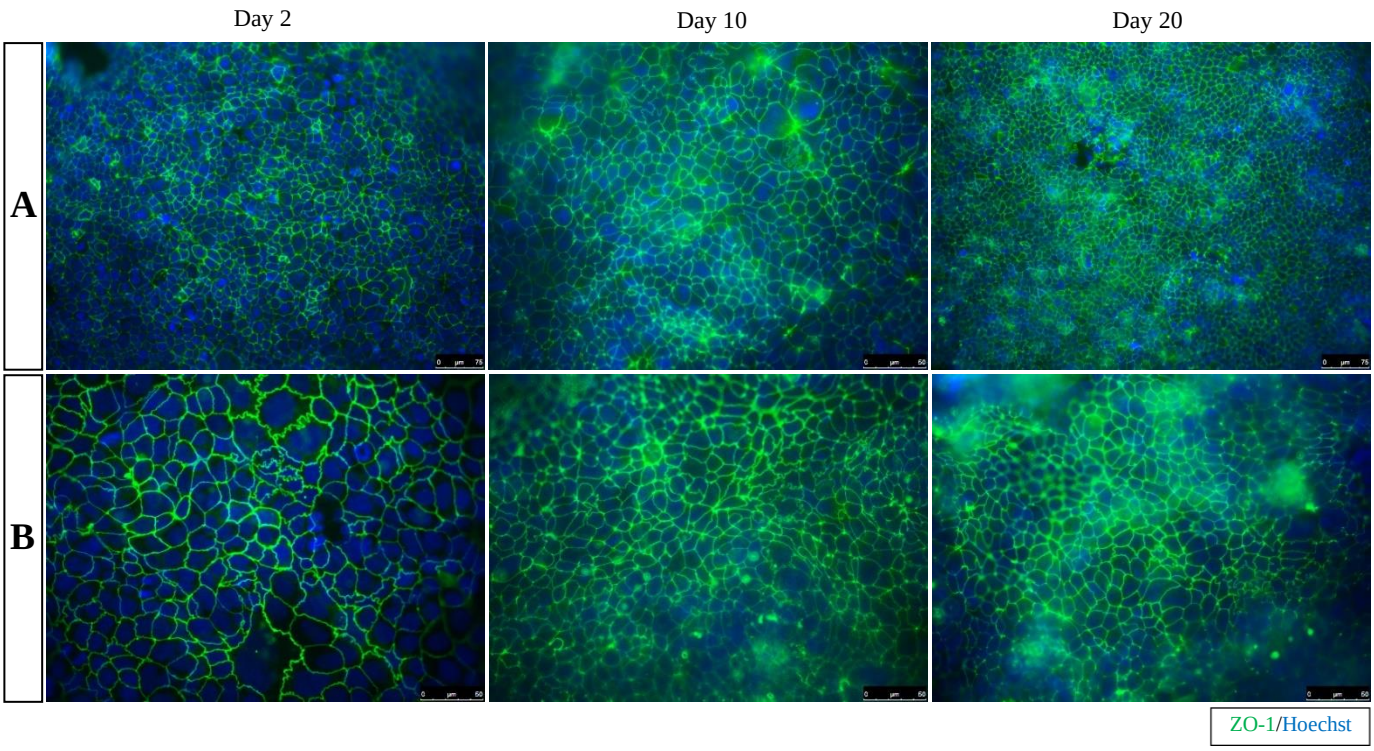

Figure 30: IF staining of CACO-2 (passages 34 and 31) grown over collagen-coated TW membranes of 3 µm porosity and imaging by widefield microscopy. In the green channel (ex: 460-500 nm / em: 512-542 nm) staining for ZO-1 (Alexa Fluor 488), and in the blue channel (ex: 340-380 nm / em: 450-490 nm) nuclei counterstaining (Hoechest). Negative controls included in section 8.8. A) CACO-2 seeded at $3.6x10^5$ cells/cm^2 and grown for 2, 10 and 20 days. Scale bar of 75 µm for the first image and last image and of 50 µm for the one in the middle. B) CACO-2 seeded at at $1.8x10^5$ cells/cm^2 and grown for 2, 10 and 20 days. Scale bars of 50 µm.

The images obtained show a drastic improvement with respect to the IF stainings performed with CACO-2 grown over glass. This is the confirmation that the proper localization of ZO-1, and so the epithelial differentiation, is only achieved when the cells are grown over semi-permeable supports. ZO-1 was detected at the latero-apical plasma membrane (this could eventually be confirmed by a Z-stack in confocal microscopy) presenting a signal with a clear ring-like pattern. The images at low magnification (figure 30 A, first one to the left and the last one at the right side) show that the signal was diffused over the whole monolayer.

An mRNA expression analysis of *TJP1* was carried out by conventional RT-PCR from the experiment with CACO-2 at passage 34 (seeding density of 180 $x10^3$ cells/cm^2) grown for 20 days (figure 31).

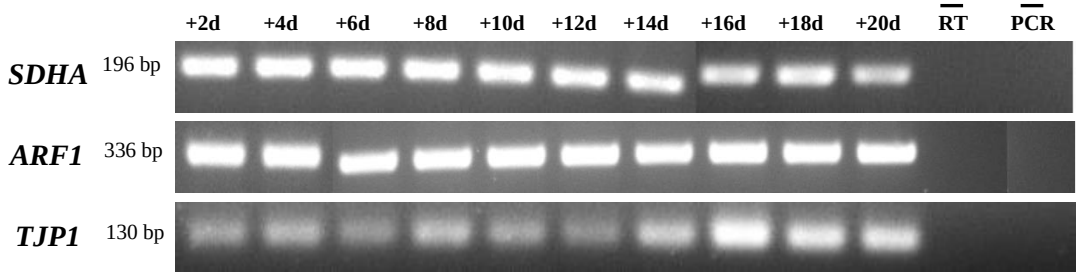

Figure 31: Conventional RT-PCR for *TJP1* (primers *TJP1*_for/_rev) of CACO-2 (passage 34) grown for twenty days over TW inserts. *ARF-1* (primers *ARF1*_for/_rev) and *SDHA* (primers *SDHA*_for/_rev) were amplified as standard genes.

The mRNA expression analyses clearly showed that ZO-1 is basally expressed from the very beginning at sub-differentiating stages, and until the end of the differentiation process. Being this a semiquantitative technique, it is not possible to conclude an increase of expression at fully differentiating stages (+14 to +20 days), even though the signal of the *TJP1* band was slightly more intense at those time-points.

In a following set of experiments, I performed differentiation tests for T84 by seeding 2.9 x 10^5 and 3.6 x 10^5 cells/cm^2 over the same Collagen-coated Corning® Transwell® cell culture inserts with a porous (3.0 µm pores) polycarbonate membrane of 6.5 mm (Ø) and 0.33 cm^2 (cell growth area), and letting them grow for 10 days in standard normoxic cell culture conditions, in accordance to the literature[74,78]. A differentiation curve of T84 at passage 28 (seeding density of 3.6 x 10^5 cells/cm^2) obtained by measuring the TEER and performing a FD4 permeability assay every day is shown on figure 32. As for CACO-2, a single biological replica is presented.

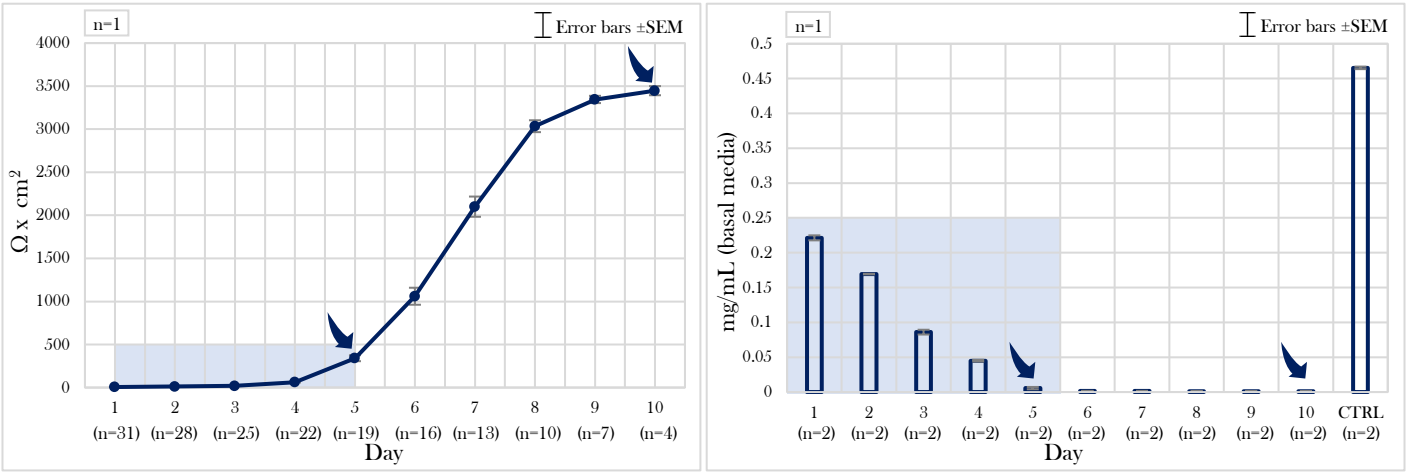

Figure 32: TEER measurements (Ω x cm^2) (left) and FD4 permeability assay (mg/mL) (right) for a differentiation experiment of T84 (passage 28) over TW inserts. Error bars ±SEM of the technical replicas indicated in brackets. The left arrow indicates the estimated onset of differentiation (time point when 100% confluency was reached), and the right one indicates the maximal TEER value achieved so the completion of the differentiation process. The light blue area corresponds to sub-confluent, sub-differentiating stages where slight changes of the TEER correspond to significant changes in the permeability of FD4. The control of maximal permeability for the FD4 assay corresponds to a TW insert without cells.

The differentiation curves of T84 (for other biological replicas at different cell passage numbers) showed a clearer and more defined pattern than the ones obtained with CACO-2. An initial increase of TEER determined by the cell confluency (from 0 to ±330 Ω x cm^2) and then a second, more pronounced, increase given the cell differentiation and the establishment of the barrier function (from ±330 Ω x cm^2 to ±3500 Ω x cm^2) (figure 32, left). Furthermore, the variance in between different

monolayers was by far lower and the final resistance achieved was by far higher, than the ones observed for CACO-2.

The FD4 permeability assay for the same differentiation experiment with T84 at passage 28 (seeding of $3.6x10^5$ cells/cm^2), also showed a better outcome than the one achieved with CACO-2. A gradual decrease of permeability concomitant to the establishment of cell confluency (reached at around day 5) was observed. From day 5 to 10 the permeability was imperceptible (figure 32, right).

For the same experiment with T84 at passage 28 (seeding of $3.6x10^5$ cells/cm^2) I performed an IF staining of ZO-1 (figure 33). The IF stainings obtained in another experiment with a passage 15 (seeding 3.6 x 10^5 cells/cm^2) are also included.

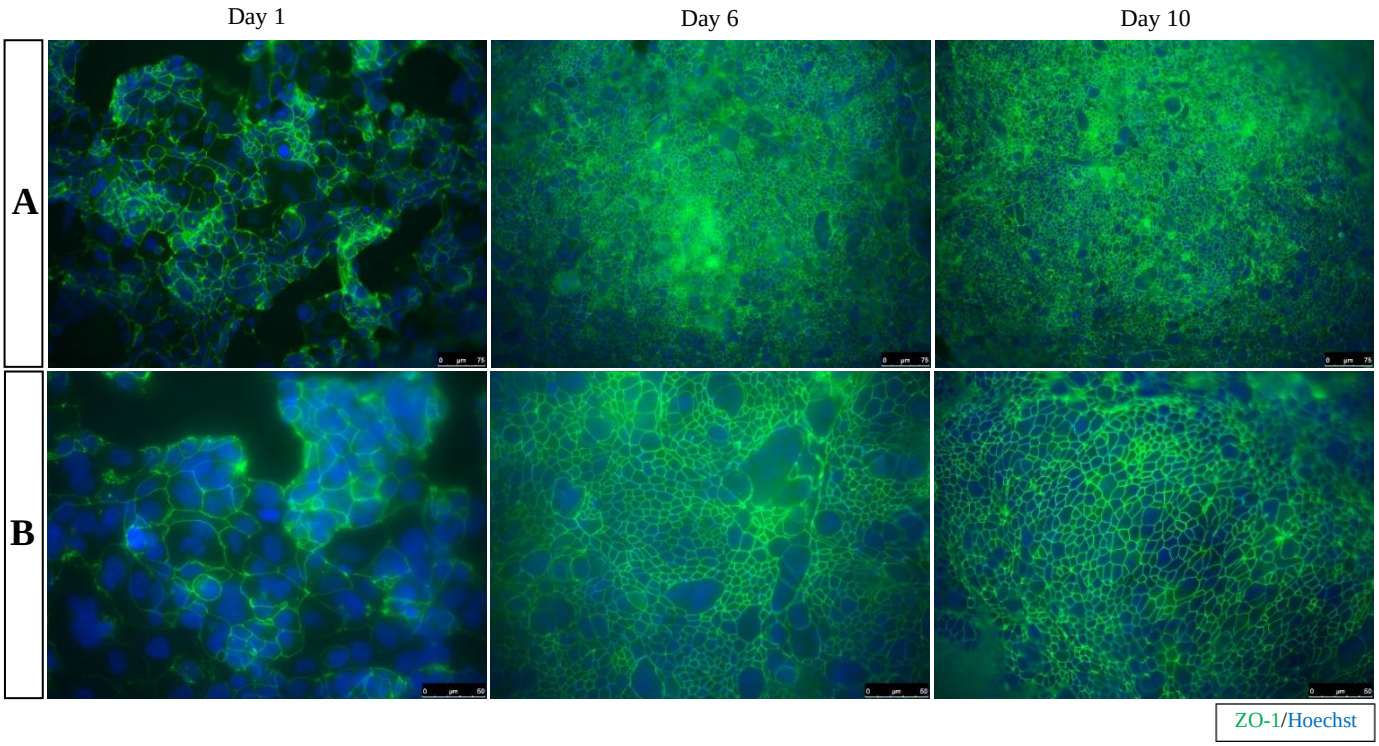

Figure 33: IF staining of T84 at passages 28 and 15 grown over collagen-coated TW membranes of 3 µm porosity and imaging by widefield microscopy. In the green channel (ex: 460-500 nm / em: 512-542 nm) staining for ZO-1 (Alexa Fluor 488), and in the blue channel (ex: 340-380 nm / em: 450-490 nm) nuclei counterstaining (Hoechest). Negative controls included in section 8.8. A) T84 seeded at $3.6x10^5$ cells/cm^2 and grown for 1, 6 and 10 days. Scale bar of 75 µm. B) T84 seeded at at $3.6x10^5$ cells/cm^2 and grown for 1, 6 and 10 days. Scale bars of 50 µm.

Also in this case, the IF staining for ZO-1 was drastically improved with regards to the experiments performed over glass. This clearly demonstrates that also for T84 the growth over semi-permeable inserts is fundamental for promoting the epithelial differentiation in a 2D structure. As happened with CACO-2, is evident that after reaching confluency these cells do not stop proliferating (being transformed cell lines), so they overgrow forming domes where both the signal of the nuclear marker and of the ZO-1 overlap. From the images obtained with T84 can be evidenced that at sub-confluent, sub-differentiating conditions, the size and the morphology of the cells is highly heterogeneous, and

that this completely changes at differentiating conditions. The images at low magnification (figure 33 A, day 1, 6 and 10) clearly show that, also in this case, the staining of ZO-1 is diffused over the whole surface of growth, so the whole monolayer differentiates in a synchronized way (compare with the stainings of the cells grown over glass, where only at peripheric regions there was signal).

To complete the characterization of the differentiation of T84, an mRNA expression analysis for *TJP1* was carried out by conventional RT-PCR from the experiment at a passage 28 (seeding of $3.6x10^5$ cells/cm^2) grown for 10 days (figure 34).

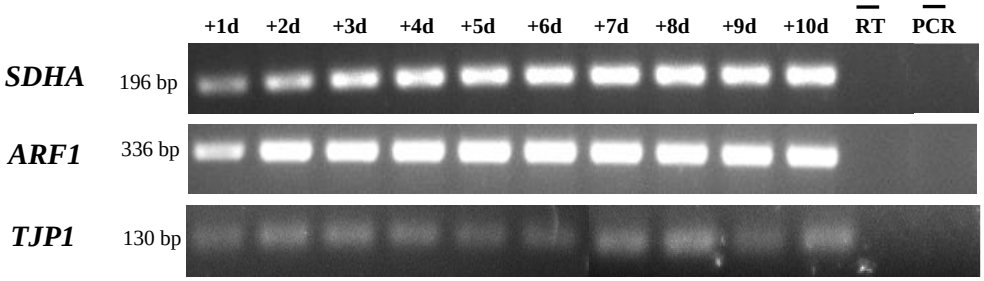

Figure 34: Conventional RT-PCR for *TJP1* (primers *TJP1*_for/_rev) of T84 (passage 28) grown for ten days over TW inserts. *ARF-1* (primers *ARF1*_for/_rev) and *SDHA* (primers *SDHA*_for/_rev) were amplified as standard genes.

The results show that also for the T84 cell line grown over TW inserts the expression of *TJP1* appears constant from the very beginning until the completion of the differentiation process. It is not possible to conclude an increase of expression at fully differentiating stages (+7 to +10 days) with this technique, but again a slightly higher signal of the band was observed at those time-points.

Considering the overall outcome of this second differentiation experiment, I have chosen T84 as the optimal cell line to continue working with. First of all, it needed less days for reaching high TEER values, presenting a low inter-TW variance. Furthermore, given the not so high proliferating capacities (in comparison with CACO-2), there was a range of resistances (a time-window in the differentiation curve at sub-differentiating stages) at which significant changes in the permeability of FD4 were observed. The importance of this is clarified in the section 4.4.

In order to include in the pipeline a cell proliferation assay, a BrdU cell proliferation assay was performed during the differentiation process of T84. As described in the section 3.2.1.9. a first experiment was ran in order to define the optimal incubation with BrdU labeling medium in accordance to the doubling time of T84 (33.9 hrs). After 2, 6 and 9 days post-seeding the assay was performed incubating the cells for 12, 24 and 36 hrs with BrdU labeling medium. Considering the results of this first experiment (data not shown) and taking into consideration the literature (Van der Werf *et al.*, 2012[79]) an incubation time of 24 hrs was chosen to proceed working with. In an experiment with a passage 26 of T84 grown over polycarbonate membranes (3.0 μm pores) a BrdU assay was performed after 2, 4 and 8 days of growth post-seeding and a decrease of positive cells was observed following the establishment of confluency and the differentiation process (figure 35).

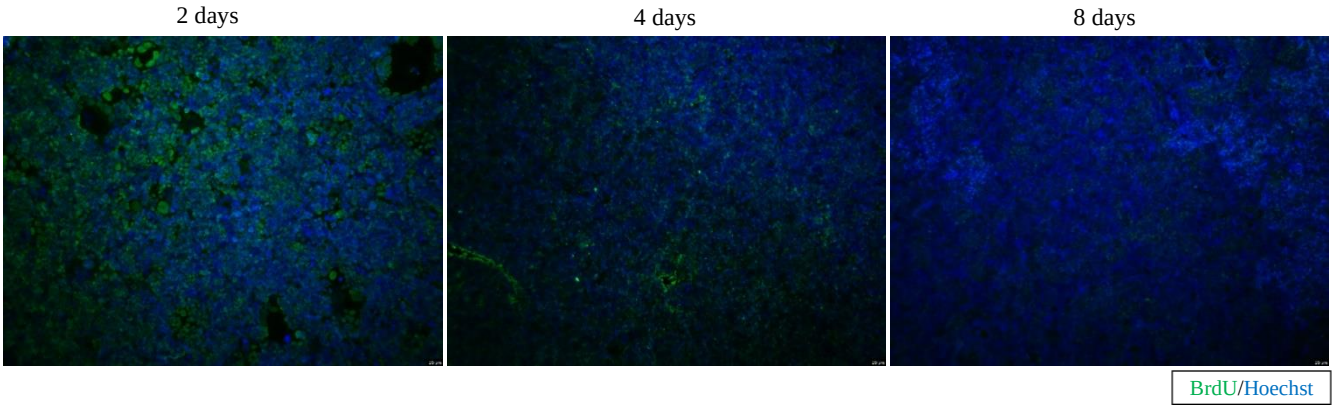

Figure 35: BrdU assay of T84 (passage 26) grown over TW inserts and incubated for 24 hrs with BrdU labeling medium. Imaging by widefield microscopy (representative images). In the green channel (ex: 460-500 nm / em: 512-542 nm) staining for BrdU (Alexa Fluor 488), and in the blue channel (ex: 340-380 nm / em: 450-490 nm) nuclei counterstaining (Hoechst). Scale bar of 20 µm.

The negative controls (Figure S13 of the Supplementary Material) confirm that the signal in the green channel is specific for BrdU positive cells.

Aiming to obtain a more physiologically relevant model of the intestinal epithelium, I decided to improve the differentiation of T84 by growing it not only over TW inserts but also in hypoxic conditions in accordance to the literature[15]. In order to mimic this drastic decrease of the O_2 partial pressure observed *in vivo* at the tip of the villi and understand if it had positive effects over the epithelial differentiation process in my *in vitro* model, I ran a differentiation test by seeding T84 cells at $3.6x10^5$ cells/cm^2 over cell culture inserts with a PET membrane (0.4 µm pores) of 6.5 mm (Ø) and 0.33 cm^2 (cell growth area), and letting them grow for 10 days in hypoxic cell culture conditions (atmospheric O_2 concentration of 1%) measuring the TEER every 24 hrs. A part from the regular coating with 10 µg/mL of Collagen from rat tail Type I for 3 hrs at 37°C (implemented in all the other experiments presented in this thesis), two coating strategies were tested with Matrigel® Basement Membrane Matrix Growth Factor Reduced. Three total protein concentrations of Matrigel (150 µg/mL, 1 and 3 mg/mL) were tested and applied with two different coating strategies: the "thin gel" coating strategy consisted on the addition of a minimal volume (16.5 µL) of Matrigel necessary to cover the 0.33 cm^2 of the membrane and then incubating at 37°C for 30 mins without aspirating the coating, whereas the "thin layer" coating strategy consisted in the addition of a higher volume (50 µL) per membrane and then incubating at 37°C for 1:30 hrs aiming to completely evaporate the solvent (PBS).

A differentiation curve of T84 at passage 24 grown in the aforementioned conditions was obtained by measuring the TEER every day and is shown in figure 36.

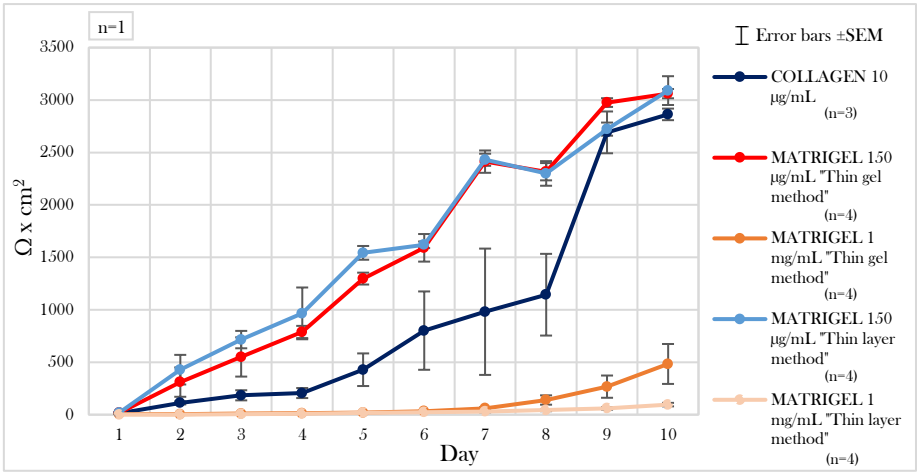

Figure 36: TEER measurements (Ω x cm²) for a single differentiation experiment of T84 (passage 24) over TW inserts (PET 0.4 µm pore), in 1% O_2 atm. and with five different coating methods. Error bars ±SEM of the technical replicas indicated in brackets.

The 1:30 hrs of incubation in the "thin layer" coating strategy were not enough to fully evaporate the coating volume so it had to be aspirated. The very reduced volume applied in the "thin gel" coating strategy evaporated during the 30 mins. of coating at 37°C, for the 150 µg/mL concentration (for the 1 mg/mL concentration it gelified). So, both "thin gel" and "thin layer" methods for 150 µg/mL were totally comparable. As the 1 mg/mL concentration gelified fast in both "thin gel" and "thin layer" coating methods, both conditions are also comparable. The 3 mg/mL concentration also determined a fast gelification of the coating volume. The plot shows that the best differentiation curves were obtained with Matrigel at 150 µg/mL applied with both coating strategies. The coating with 3 mg/mL determined no detectable increase of TEER in the time of growth so the values were not plotted.

In order to check if T84 was still forming domes growing in hypoxic conditions I stained the nuclei (with Hoechest) of an untreated monolayer (passage 21) grown for five days (TEER of 1296.57 Ω x cm^2) at 1% O_2 atm. over a polycarbonate membrane (3 µm pores). Employing a confocal microscope, a Z-stack (25 focal planes) was obtained and a representative 3D reconstruction of a single field of view is shown in figure 37.

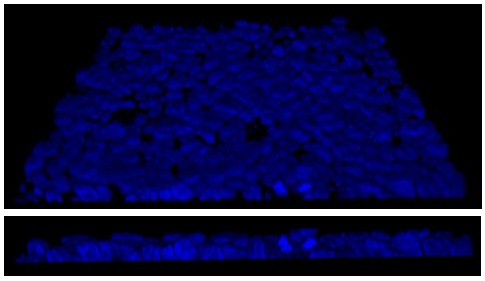

Figure 37: 3D reconstruction of a Z-stack built out of 25 focal planes of a Hoechest staining of T84 (passage 21) grown for five days in 1% O_2 atm. (1296.57 Ω x cm^2). A single field of view is depicted at three angles of the 3D reconstruction. The lowest image shows the reconstruction of the section of the sample along the Z-axis.

The 3D reconstruction of the Z-stack shows that T84 did not form domes in these growing conditions and the acquired tissue-configuration approximated more to a monolayer.

4.2. Characterization of T84 and CACO-2 regarding the expression of *HTR3* genes and identification of a putative novel *HTR3E* transcript variant

In order to start the characterization of the serotonergic receptor system in this intestinal epithelial *in vitro* model, I decided to check the expression at the mRNA level of the 5-HT3Rs gene family (*HTR3A/B/C/D/E* genes) on T84 and CACO-2 cells during the whole differentiation process over TW inserts.

The conventional RT-PCR from an experiment with CACO-2 at a passage 31 (seeding density of 180 x 10^3 cells/cm^2) grown for 20 days is presented in figure 38.

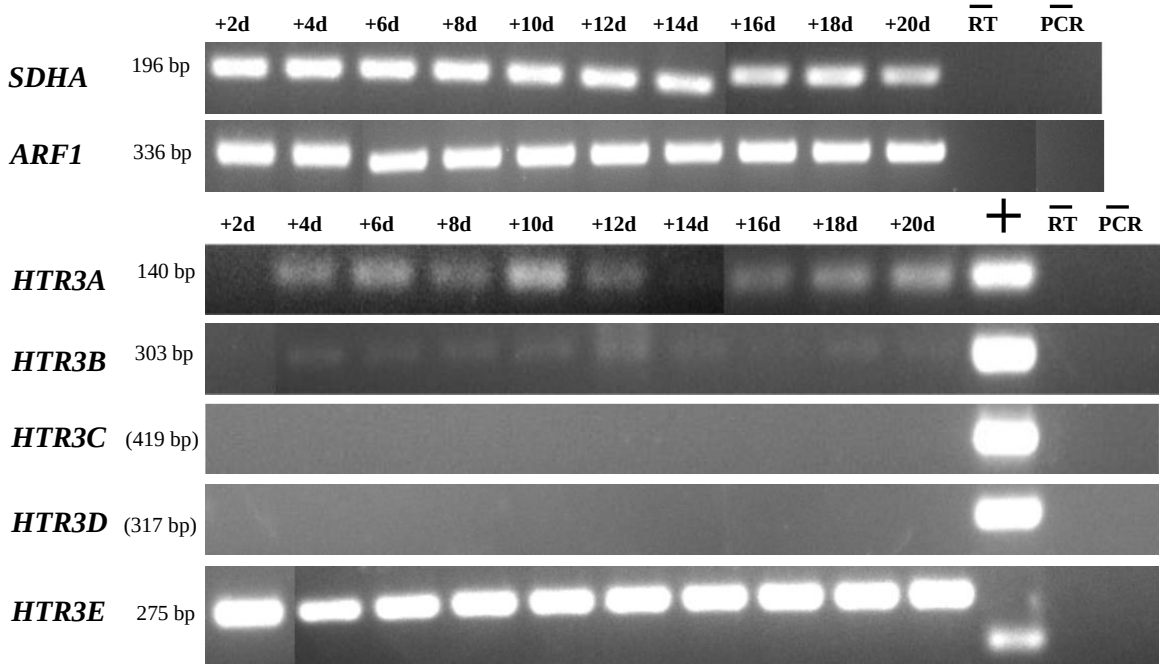

Figure 38: Conventional RT-PCR of *HTR3A/B/C/D/E* (primers *HTR3A/B/C/D/E*_for/_rev) for CACO-2 (passage 31) grown for twenty days over TW inserts. The positive controls consist on the amplification of 10 ng of recombinant-plasmidic cDNA of the gene of interest. *ARF1* (primers *ARF1*_for/_rev) and *SDHA* (primers *SDHA*_for/_rev) were amplified as standard genes.

The results showed that *HTR3A/B* were expressed almost at all time points, so not following the differentiation process. On the other hand, *HTR3E* was also expressed at a constant level at all time points but at higher extent compared to the other *HTR3* genes, considering the intensity of the signal of the bands. Important to note is that, regarding the amplification of *HTR3E*, the amplicon obtained from the cell's cDNA sample was larger than the one obtained with the positive control recombinant cDNA. *HTR3C* and *D* were not expressed at all, or their expression was imperceptible with this semi-quantitative method.

The same experiment was performed for T84 at a passage 28 (seeding density of 3.6 x 10^5 cells/cm^2) and the results are shown in figure 39.

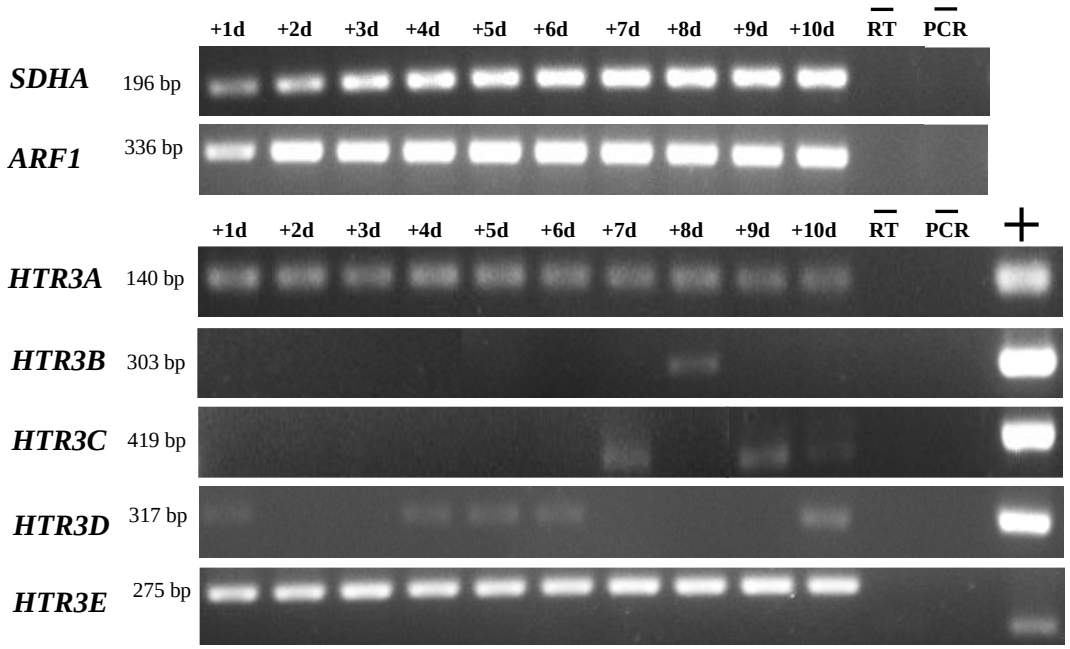

Figure 39: Conventional RT-PCR of *HTR3A/B/C/D/E* (primers *HTR3A/B/C/D/E*_for/_rev) for T84 (passage 28) grown for 10 days over TW inserts. The positive controls consist on the amplification of 10 ng of recombinant-plasmidic cDNA of the gene of interest. *ARF1* (primers *ARF1*_for/_rev) and *SDHA* (primers *SDHA*_for/_rev) were amplified as standard genes.

In the T84 cell line *HTR3A* and *HTR3E* were expressed almost constantly while the other genes were expressed without following a differentiation pattern. Regarding *HTR3E*, as again the amplicon obtained was bigger than the expected, I realized that I was presumably dealing with an unexpected alternative spliced isoform.

The primers employed in the conventional RT-PCRs for the *HTR3E* gene (*HTR3E*_for/_rev) were designed in order to amplify the 3' region of exon 7 and the 5' region of exon 8 (conserved in all described splicing variants as stated in[80]), spanning the last intron that was expected to not be amplified from the cell's cDNA. The expected amplicon (the one amplified from the positive control's cDNA sample) size was of 136 bp, and the size of the obtained amplicon was of 275 bp. In order to confirm or discard that possibility that the last intron had been retained, the band of the 275 bp amplicon (out of the amplification of the T84's cDNA grown for 10 days over TW inserts) was extracted, the amplified DNA was isolated with the QIAquick® PCR Purification Kit and then sequenced with the Sanger method employing the same primers *HTR3E*_for/_rev. The results of the sequencing confirmed that the amplicon consisted of the 3' region of exon 7 and the 5' region of exon 8 with the last intron (intron 7, for the reference sequence) retained (see Figure S9 of the Supplementary Material).

The first step followed for the identification of the novel putative *HTR3E* splicing variant/s that gave rise to the 275 bp amplicon was to perform two RT-PCRs with two pair of primers designed for the amplification of the full length of the different actually described transcripts. Figure 40 describes graphically the RT-PCRs performed and the expected sizes of the amplicons that could be obtained with or without the retainment of the last intron.

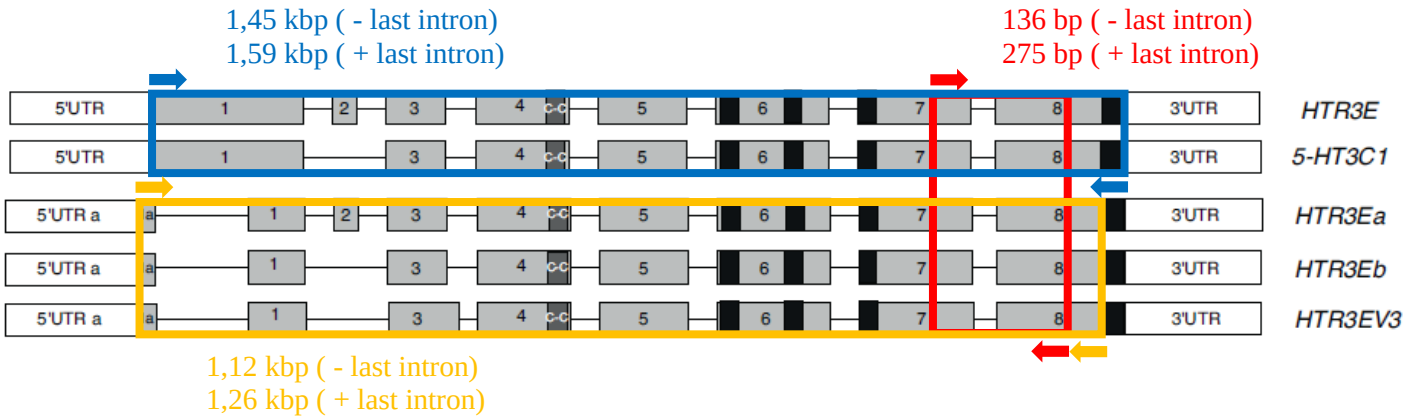

Figure 40: Design of conventional RT-PCRs of *HTR3E* with *HTR3E*_for/_rev (internal amplicon comprising exon 7 and 8 of all annotated splicing variants), *HTR3E/5-HT3C1*_for/_rev (full length amplicon of *HTR3E* and *5-HT3C1*) and *HTR3Ea/HTR3Eb/HTR3EV3*_for/_rev (full length amplicon of *HTR3Ea, HTR3Eb* and *HTR3EV3*). The image of the actually annotated splicing variant was obtained from Niesler, 2011.

The results of the full-length RT-PCRs described in figure 40, performed on cDNA from T84 passage 28 grown for 10 days over TW inserts, are depicted in figure 41.

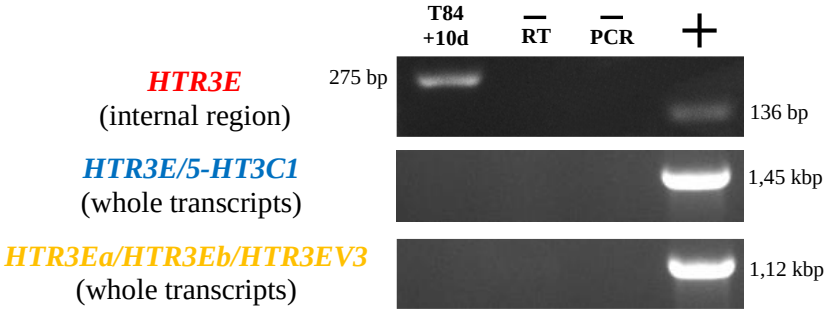

Figure 41: Conventional RT-PCRs of *HTR3E* with *HTR3E*_for/_rev (internal amplicon comprising exon 7 and 8 of all annotated splicing variants), *HTR3E/5-HT3C1*_for/_rev (full length amplicon of *HTR3E* and *5-HT3C1*) and *HTR3Ea/HTR3Eb/HTR3EV3*_for/_rev (full length amplicon of *HTR3Ea, HTR3Eb* and *HTR3EV3*). The RT-PCRs were run on cDNA from T84 (passage 28) grown for 10 days over TW inserts. The colors of the splicing variants names correspond to the colors of the amplicons depicted in figure 40. *ARF-1* (primers *ARF1*_for/_rev) and *SDHA* (primers *SDHA*_for/_rev) were amplified as standard genes (see figure 39).

The results obtained with the full-length amplifying pair of primers showed that the internal amplicon of 275 bp (obtained with *HTR3E*_for/_rev) did not belong to any of the actually annotated

splicing variants. In order to identify the flanking regions of the 275 bp internal amplicon I decided to perform a set of 5'/3'RACE-PCRs.

In a first 5'/3' RACE experiment a whole-cell sscDNAs library was obtained out of the RNA of a T84 passage 28 grown for 10 days over TW inserts employing the GeneRacer™ Oligo dT Primer in the RT step. Important to note is that in the RNA isolation procedure a DNAaseI treatment was performed in order to avoid the presence of genomic DNA in the sample and the quality (abs. 260/280= 2.11; abs. 260/230= 2.27) and the integrity (RIN=9.2) of the RNA were appropriate.

Before running the 5'/3' RACE PCRs with the internal primers *HTR3E*_for/_rev, I ran a control experiment for the standard gene *ACTB* (β-Actin) to evaluate the quality of the T84 RACE library (see Table S3 and Figure S10 of the Supplementary Material). Given the positive results obtained with the control 5'/3'RACE PCRs, I proceeded with the Touchdown and Nested PCRs for the *HTR3E* internal amplicon. The 5' RACE PCR was performed with the primers GeneRacer™ 5′ Primer_for and the *HTR3E*_5' RACE_rev first and successively with the pair GeneRacer™ 5′ Nested Primer_for and the *HTR3E*_5' RACE Nested_rev. The results are depicted in figure 42.

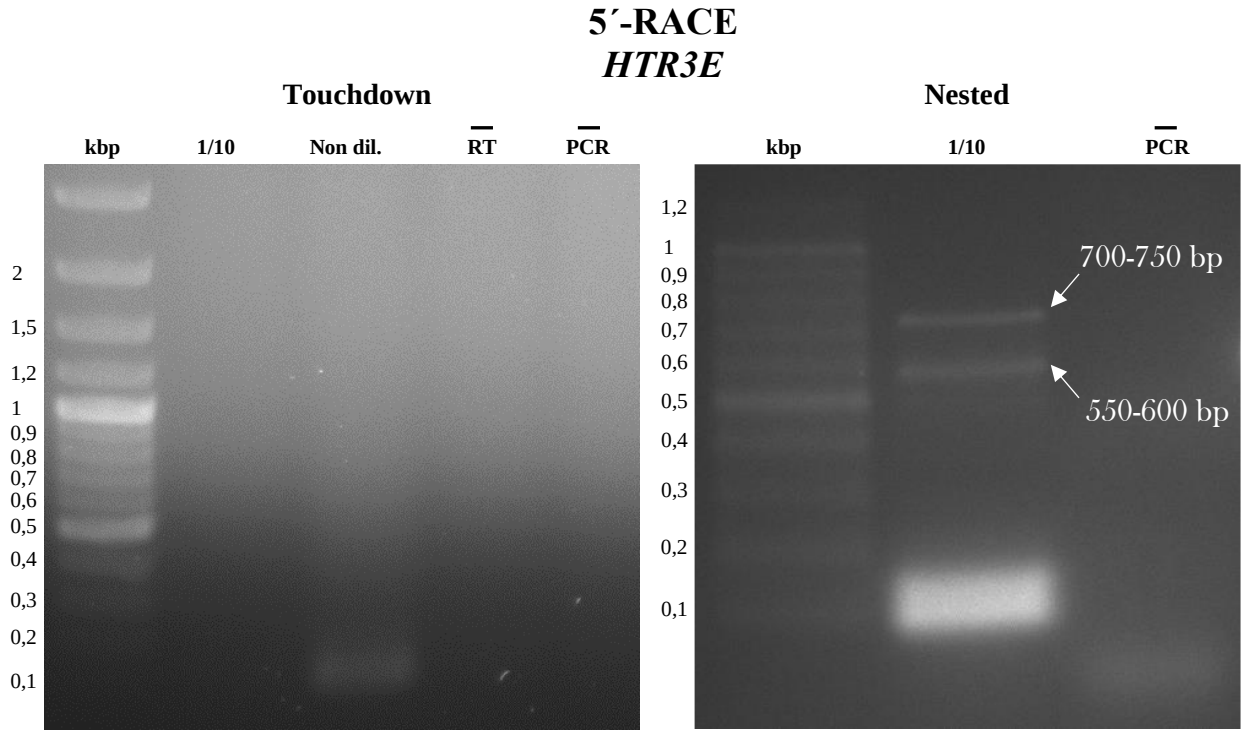

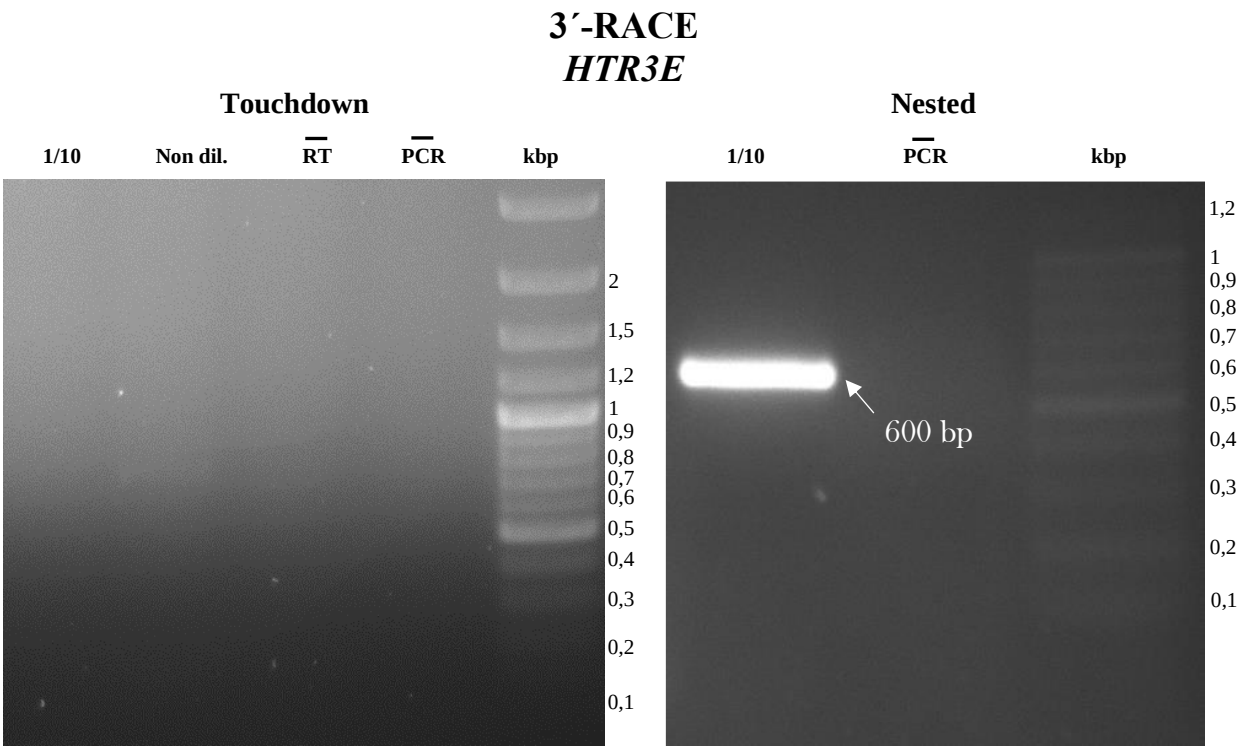

Figure 42: 5'/3' RACE PCRs (Touchdown and Nested) for novel putative *HTR3E* transcript variant/s from a RACE sscDNA library prepared from T84 passage 28 grown for 10 days over TW inserts. Two dilutions of the RACE sscDNA library were employed in order to define the optimal condition for obtaining the best amplification out of the two consecutive PCR rounds. Two clear products were obtained with the 5' RACE PCR (a 700-750 bp band and 550-600 bp band) and a single product was obtained with the 3' RACE PCR (600 bp band). The agarose gel electrophoresis was ran with 25 µL of post-PCR for each amplification.

The two 5'RACE bands (of 700-750 bp and of 550-600 bp) and the 3'RACE band (of 600 bp) were excised and the post PCR DNA was extracted with the QIAquick® PCR Purification Kit. The post PCR DNA was ligated in a pSTBlue-1 vector carrying blunt ends, and the recombinant vector was employed to transform Nova Blue Chemo-competent cells. The transformed cells were plated over solid, antibiotic-selective, LB-agar and let to grow overnight at 37°C. Colonies derived from clones that were successfully transformed with the ligated plasmid and carrying the 5'/3' RACE fragments at the MCSs, were identified following the Blue/White X-Gal/IPTG screening procedure. The isolated colonies were further screened by Colony PCR employing the pair of primers designed for the nested 5'/3' RACE PCRs. Single positive colonies were pre-inoculated in liquid, antibiotic-selective, LB and grown overnight. A total DNA isolation (genomic and plasmidic) was carried out for the different cultures employing the Quick DNA Miniprep Plus Kit. The isolated DNAs were sequenced with the Sanger method employing primers flanking the MCS (T7_prom and M13_fwd). The results showed that the band of 600 bp obtained with the 3' RACE PCR carried a sequence conserved at the 3' end of all the annotated *HTR3E* splicing variants (see Supplementary Material). Regarding the 5' RACE PCR, the band of 700-750 bp was not possible to be cloned (no positive

bacterial colony could be isolated) and the band of 550-600 bp consisted of an aspecific amplification for the *SNRPB* locus (data not shown).

Given these results, another sscDNA RACE library has been prepared employing the *HTR3E*_5' RACE_rev in the RT reaction, for optimizing the obtainance of 5' RACE amplicons. The outcome the 5' RACE PCRs could not be improved (data not shown).

4.3. Characterization of the Fetal Human Colonic (FHC) cell line cell for its *in vitro* differentiation into a two-dimensional epithelial-like structure

In order to incorporate a "normal" epithelial cell line in the *in vitro* model (and validate the findings on T84 and CACO-2), I decided to characterize the FHC line (ATCC® CRL-1831™) and start working on its differentiation as mature colonic epithelial cells.

The first step was to remove the excess of fibroblasts present in the heterogeneous FHC cell population by differential plating over normal plastic plates. This simple technique consists on detaching the cells of interest from the growth plate by trypsinization, seeding them on a new plate, and after a certain time re-seeding the supernatant on a new plate. As the fibroblasts usually attach to the substrate earlier than other cell types, this procedure should in principle allow to separate the fibroblasts (that will attach mainly to the first plate) from the epithelial and other cell types (that will attach only to the second plate). In a first experiment, I tested two different times of seeding on the first plate, 15 and 30 mins. I let the cells of both plates grow until 100% confluency and then I isolated total RNA from them in order to perform a conventional RT-PCR for a series of relevant markers. I checked the expression of *ACTA2*, as a marker for fibroblasts, and *PROM1*, *LGR5*, *OLFM4* and *LRIG1* as intestinal epithelial stemness markers. An RT-PCR was also run for *VIL1* and *KRT20*, two markers for intestinal epithelial cell differentiation that were expected to not be expressed on the epithelial stem cells present in the FHC heterogenous cell population. The differential plating was performed for two independent cell lines of FHC passage 7 and the RT-PCRs (figure 43) were run for both the expected "fibroblasts" and the "other cells types" fractions obtained from the differential plating at two seeding times (15 and 30 mins).

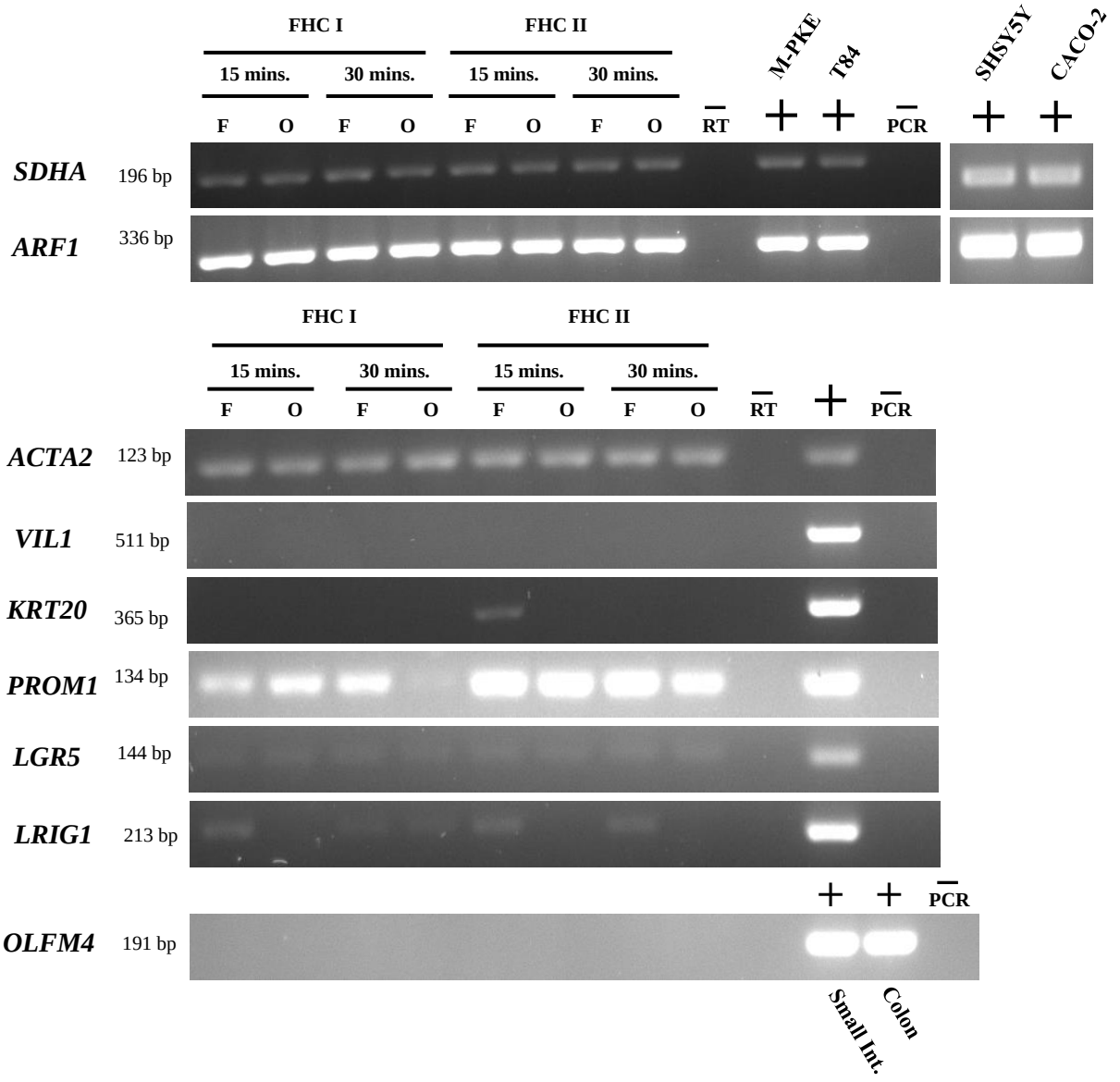

Figure 43: Conventional RT-PCR of *ACTA2, VIL1, KRT20, PROM1, LGR5, OLFM4, LRIG1* for two lines (I and II) of FHC passage 7. Total cDNA of both the cellular fractions with expected fibroblasts (F) and other cells (O) was employed for the RT-PCRs. The positive controls consist on the amplification of total cDNA of fibroblasts M-PKE p3 (for *ACTA2, OLFM4, LRIG1*), T84 p18 differentiated (for *VIL1* and *KRT20*), CACO-2 p30 undifferentiated (for *PROM1*), SHSY5Y p15 undifferentiated (for *LGR5*) and small intestine and colon total cDNA (for *OLFM4*). *ARF-1* and *SDHA* were amplified as standard genes.

The results clearly showed that the differential plating (at least for those two seeding times) is not sufficient for separating the fibroblast from the different intestinal epithelial cell types present in the heterogenous population. Even though the conventional RT-PCR is a semi-quantitative method, it appeared clear that the expression of *ACTA2* was maintained at the same level in both cellular fractions, at both differential plating times, and in both passage 7 cell lines of FHC. The stemness condition of the intestinal epithelial cells present in the heterogeneous population was confirmed by

the observed expression of key intestinal epithelial stem cell markers such as *PROM1*, *LGR5* and *LRIG1*, and by the lack of expression of the two intestinal epithelial differentiation markers *VIL1* and *KRT20*. *LRIG1*, marker for both intestinal epithelial stem cells and fibroblasts, was observed expressed in both fractions of the sorting. *OLFM4*, another epithelial stemness marker, did not give any detectable expression.

A first, very simplistic, attempt of differentiating the intestinal epithelial stem cells present in the FHC population was done by seeding them at three different densities (60, 150 and 300 x 10^3 cells/cm^2) over TWs with a polycarbonate membrane with pores of 3 µm, with and without coating with Collagen 10 µg/mL. Confluency and the establishment of the barrier function was assessed by measuring the TEER every other day for 30 days. The resistances did not increase significantly over the baseline values (TWs without cells, ±40 Ω x cm^2), even after 30 days of growth.

4.4. Establishment of the optimal pro-inflammatory input for determining the loss of barrier function

4.4.1. Barrier-impairment tests and dose-response curves of single cytokines and combinations

In order to establish an *in vitro* inflammatory model of the intestinal epithelium my first task was to define the optimal combination, concentrations and times of application of pro-inflammatory cytokines necessary to significantly disrupt a differentiated T84 monolayer.

Four different types of experiments were carried out, initially applying a combination and finally applying single cytokines. In all experiments the cells were seeded at the optimal density of 3.6 x 10^5 cells/cm^2. All of them consisted on the application of the cytokine challenge to only the basolateral compartments of two-dimensional epithelial-like structures (given the polarized distribution of the cognate receptors). The cytokines were always reconstituted in BSA 0.1% - PBS, so no control for the carrier buffer was performed.

In a first experiment, the two cytokines sTNFα and IL-1β were applied together at the concentrations of 12.5 and 10 ng/mL on T84 and CACO-2 monolayers that presented a TEER of ~330 Ω·cm^2 (onset of differentiation). The input was maintained for 72 hrs and thereafter was removed and the monolayer were kept in culture for other 72 hrs. The experiments were conducted in normoxia and coating the TWs with Collagen I at 10 µg/mL. The experimental design is schematically summarized in figure 44.

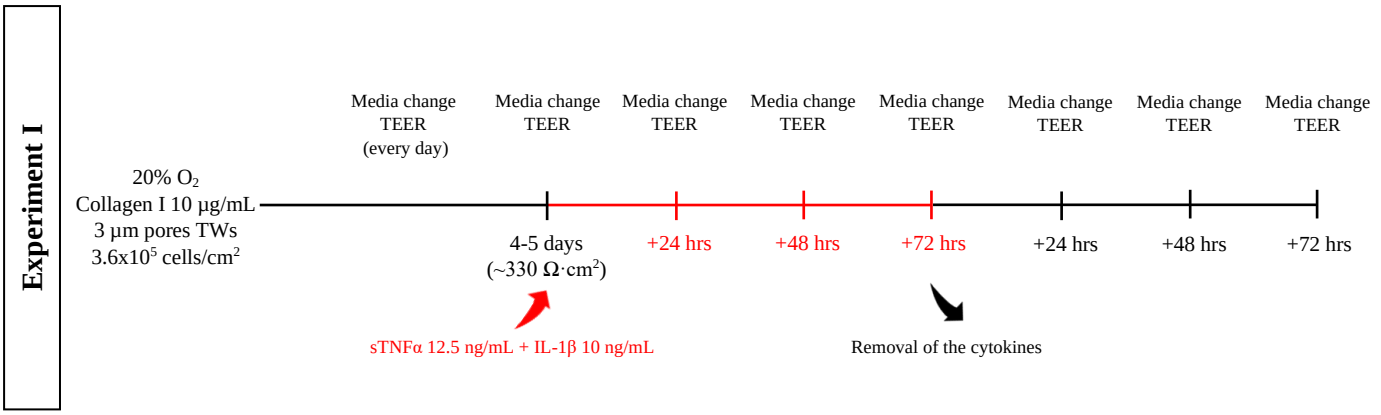

Figure 44: Schematic representation of a first barrier-impairment test with sTNFα and IL-1β on T84 and CACO-2 monolayers of ~330 Ω·cm². In red are indicated the time frames during which the monolayers were stimulated with the cytokines combinations from the basolateral side. Note: the different time frames depicted in the temporal axis are not in scale.

The results of this first experiment for T84 are depicted in figure 45 and the ones for CACO-2 in figure 46.

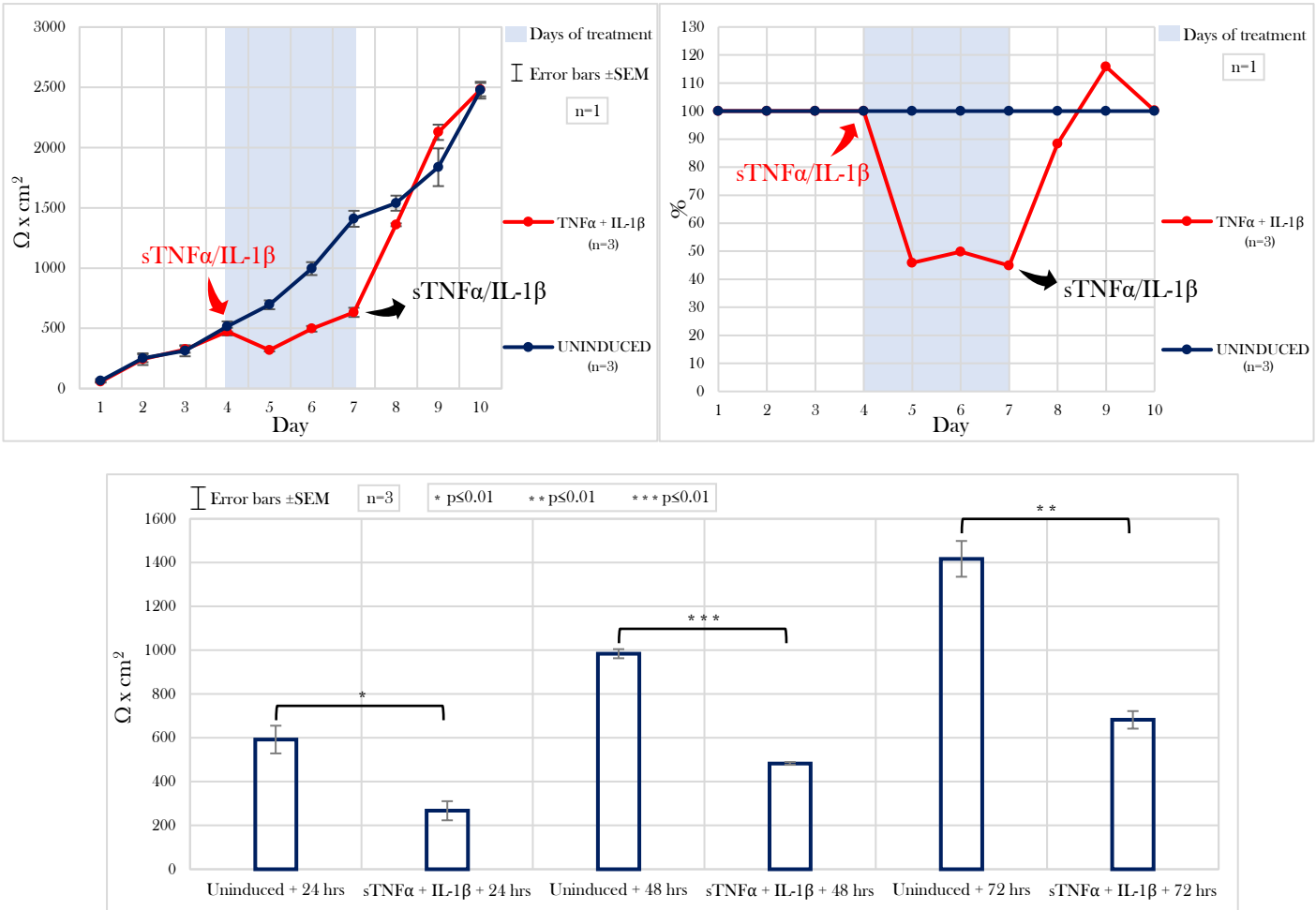

Figure 45: TEER measurements for the Experiment I ran with T84. Ω x cm² values (upper, left graph) and values normalized to the untreated condition (upper, right graph) from one single representative experiment with three

technical replicas per condition. Average values at 24, 48 and 72 hrs post-induction for n=3 (lower graph). Significance stated by a two-sided paired t-test. Error bars ±SEM.

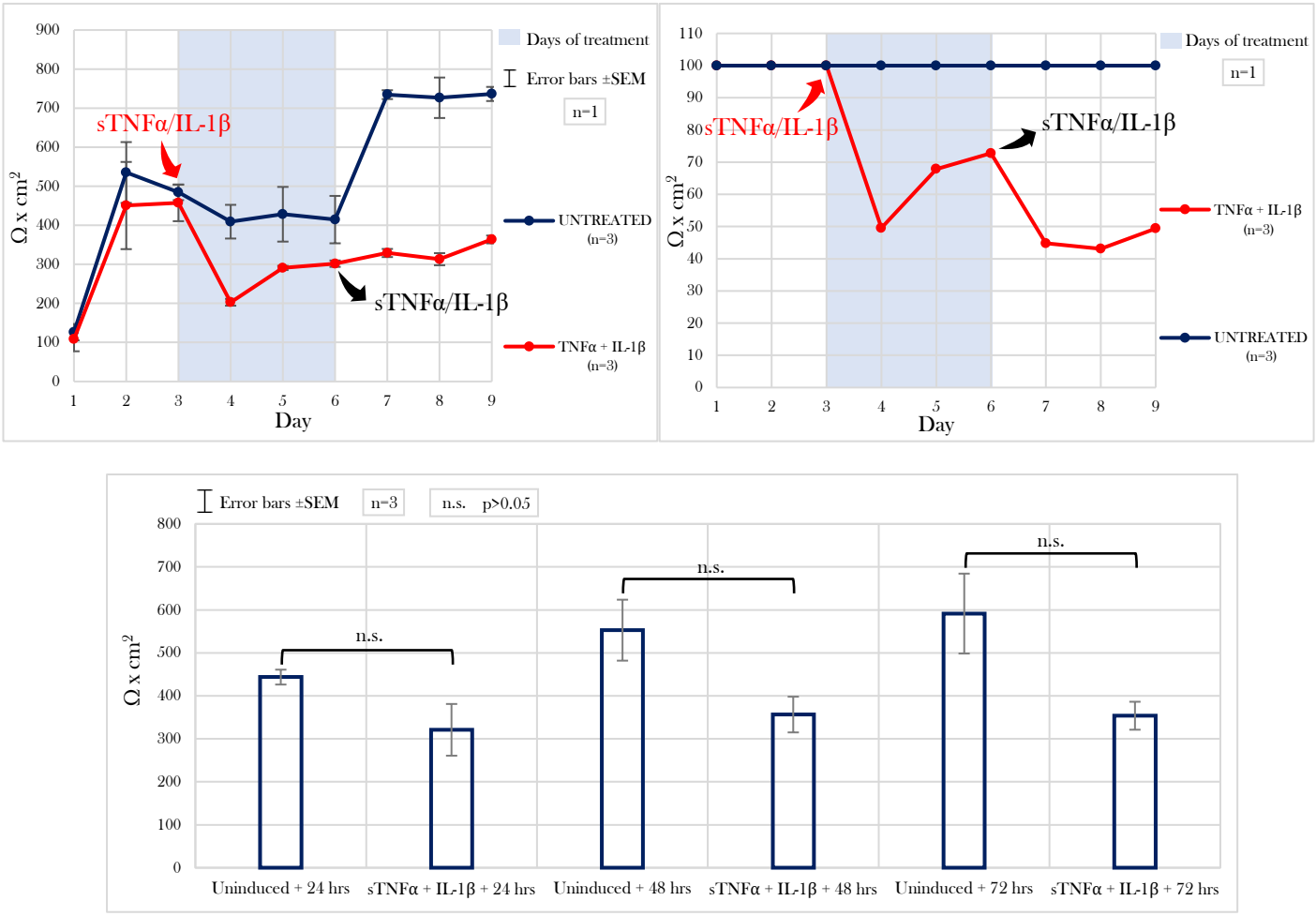

Figure 46: TEER measurements for the Experiment I ran with CACO-2. Ω x cm^2 values (upper, left graph) and values normalized to the untreated condition (upper, right graph) from one single representative experiment with three technical replicas per condition. Average values at 24, 48 and 72 hrs post-induction for n=3 (lower). Significance stated by a two-sided paired t-test. Significance stated by a two-sided paired t-test. Error bars ±SEM.

The results of this first experiment showed that the stimulus sTNFα 12.5 ng/mL and IL-1β 10 ng/mL applied at the onset of the differentiation process determined a statistically significant drop of TEER in both T84 ($p \leq 0.05$ at +24 hrs, $p \leq 0.001$ at +48 hrs and $p \leq 0.01$ at +72 hrs in a one-sided paired t-test, n=3) and CACO-2 ($p \leq 0.05$ at +24 hrs, +48 hrs and +72 hrs in a one-sided paired t-test, n=3) during the 72 hrs of application. T84 showed a lower variance between technical and biological replicas, reached higher TEER values and recovered faster (to the barrier function levels of the untreated condition) after the removal of the input. From this point onwards, I decided to continue working only with T84, being a more suitable cell line.

In a second experiment (figure 47) the two cytokines sTNFα and IL-1β were applied together at the concentrations of 12.5 and 10 ng/mL on T84 monolayers that presented a TEER of ~800 Ω·cm^2 (still not fully differentiating conditions). At that time point, the monolayers were challenged from the

basolateral side only, the induction was kept in standard cell culture conditions for three days and every 24 hrs the following activities were carried out in triplicates:

1- Establishment of the control for maximal LDH release in one technical replica for each 24 hrs time-point and running of the LDH assay.
2- TEER measurement.
3- Assessment of the FD4 permeability.

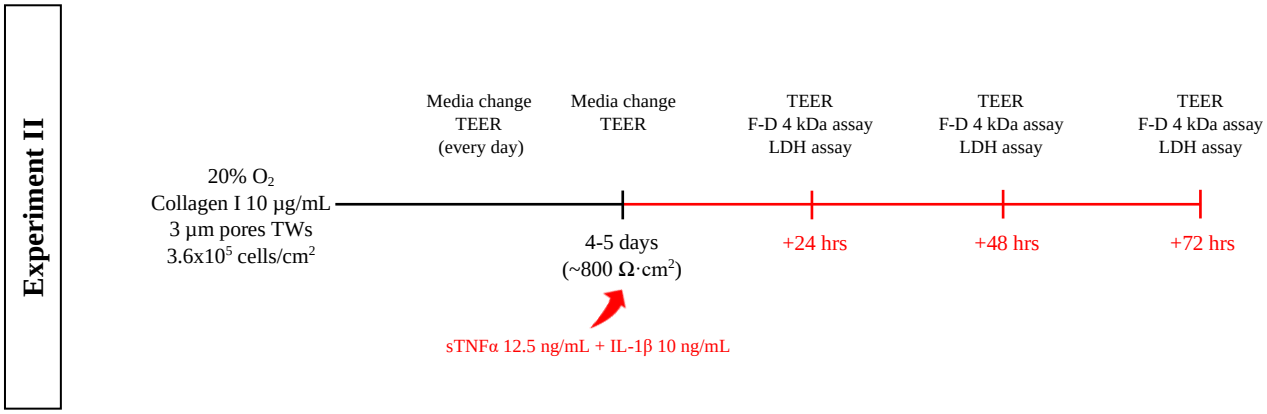

Figure 47: Schematic representation of the second barrier-impairment test with sTNFα and IL-1β on T84 monolayers of ~800 Ω·cm². In red are indicated the time frames during which the monolayers were stimulated with the cytokines combinations from the basolateral side. Note: the different time frames depicted in the temporal axis are not in scale.

The LDH assay quantifies the extent of cell death that culminates with the lysis of the plasma membrane. The two relevant mechanisms that lead to this outcome are the uncontrolled cell death by Necrosis and the programmed cell death by Necroptosis. The results of the LDH assay (figure 48) showed that the two cytokines sTNFα and IL-1β applied together at 12.5 ng/mL and 10 ng/mL each determined a statistically significant increase of either Necrosis and/or Necroptosis ($p \leq 0.05$ at each time point in a one-sided paired t-test, n=3). The increase of LDH determined by the cytokines at each time point, was of not more than 10% with respect to the untreated condition.

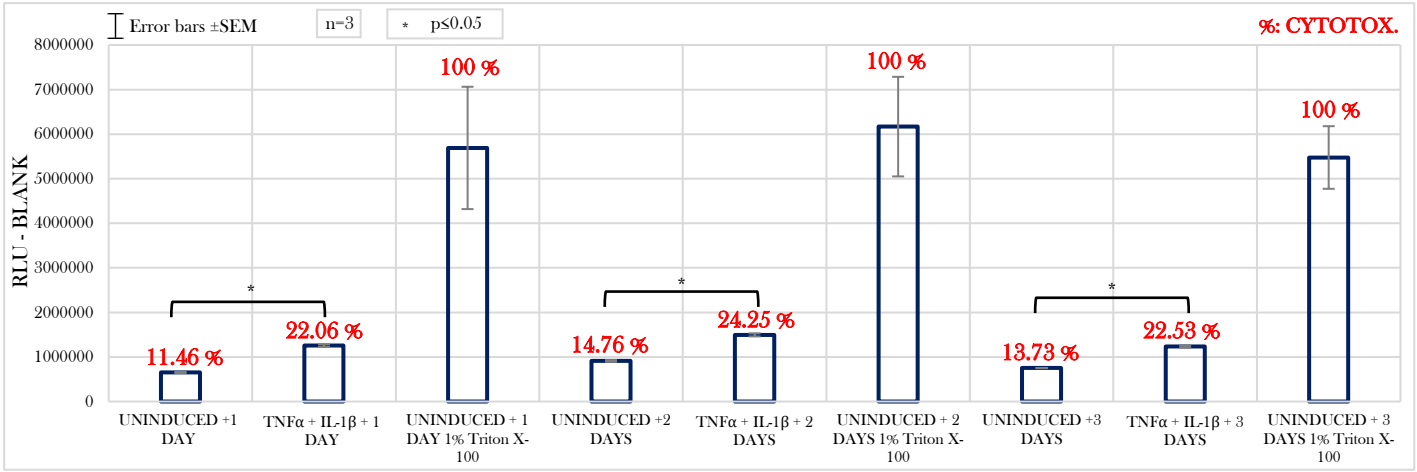

Figure 48: LDH assay for the Experiment II. RLUs of the different conditions subtracted to the blank. In red the percentage of Necrosis/Necroptosis normalized to a control of maximal cell membrane lysis. Significance stated by a two-sided paired t-test for n=3. Error bars ±SEM.

The results relative to the TEER measurements (figure 49) showed that the stimulus sTNFα 12.5 ng/mL and IL-1β 10 ng/mL applied at ~800 Ω·cm^2 determined a statistically significant drop of TEER at +24 hrs ($p \leq 0.001$) and at +48 hrs ($p \leq 0.05$), performing a two-sided paired t-test for n=3. After 72 hrs of application, the difference in between the induced and the uninduced conditions was not statistically significant.

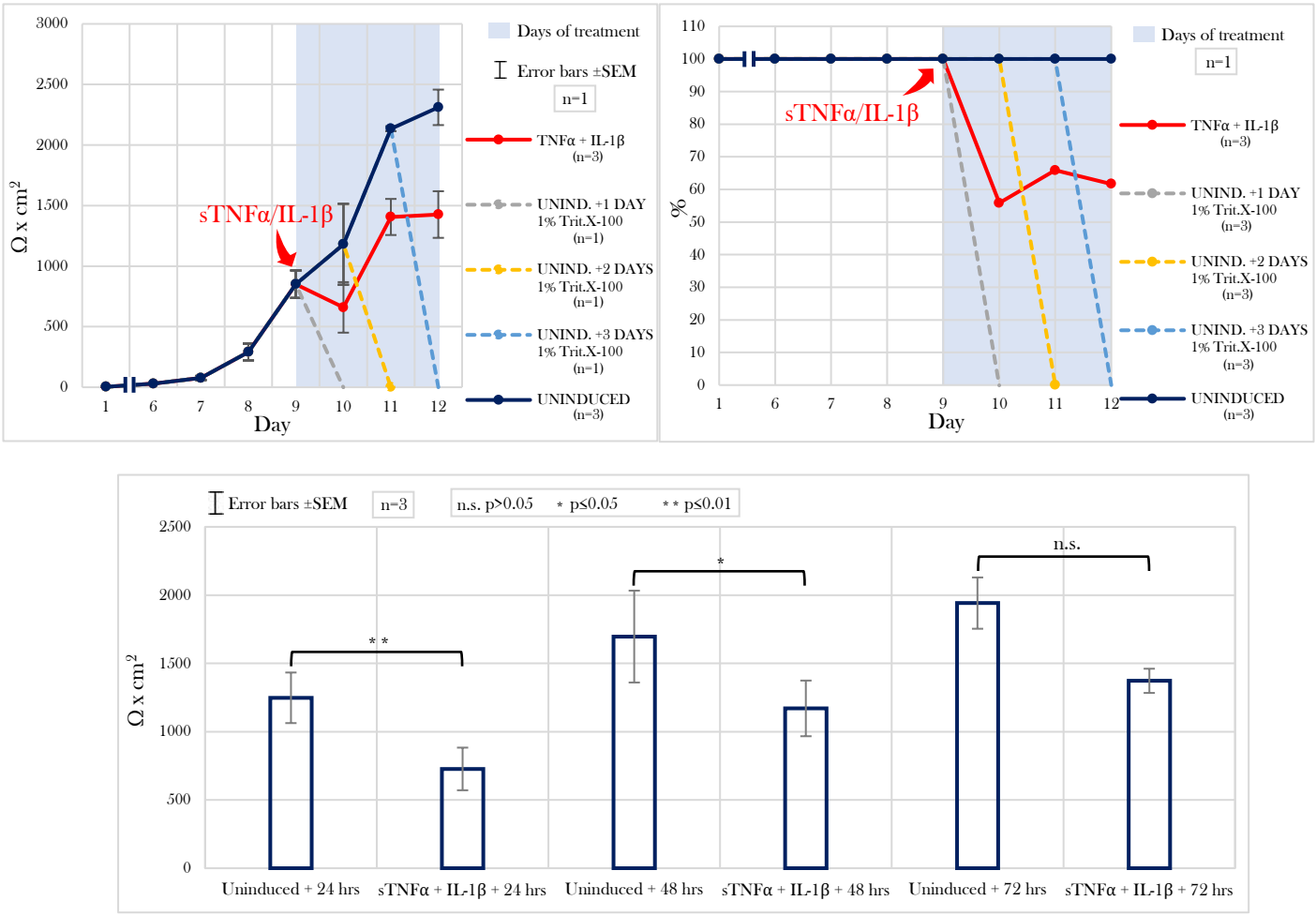

Figure 49: TEER measurements for the Experiment II. Ω x cm^2 values (upper, left graph) and values normalized to the untreated condition (upper, right graph) from one single representative experiment with three technical replicas per condition. Average values at 24, 48 and 72 hrs post-induction for n=3 (lower graph). Significance stated by a two-sided paired t-test. Error bars ±SEM.

The FD4 permeability assay (figure 50) (performed in the cell culture media) did not show a significant increase of permeability towards that molecular species at any time point.

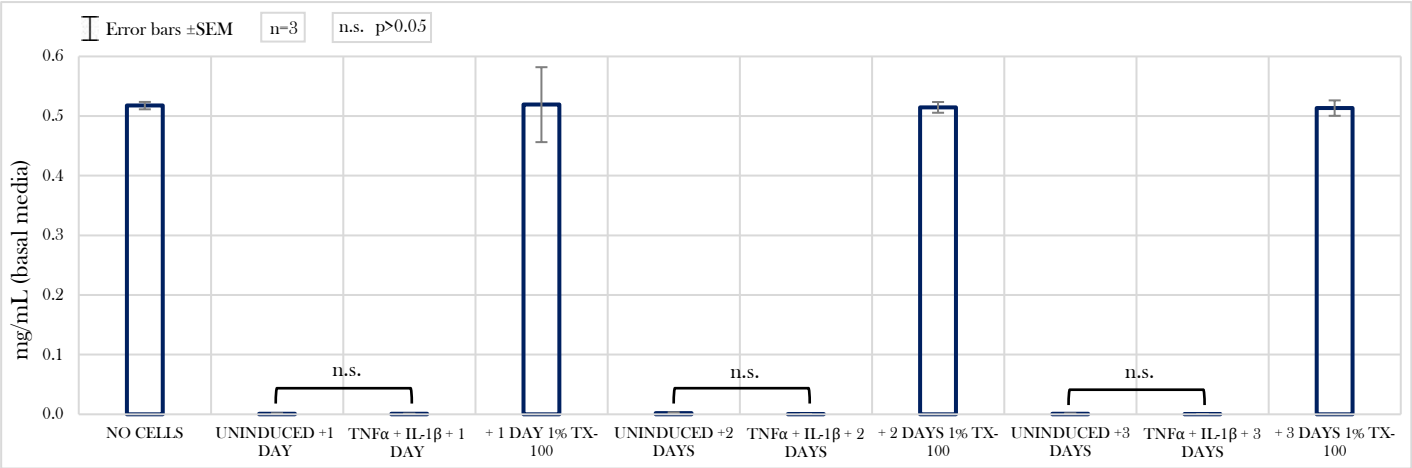

Figure 50: FD4 permeability assay for the Experiment II. Quantification reported in mg/mL. Significance stated by a two-sided paired t-test. Error bars ±SEM.

The third series of experiments (Figure 51) consisted on the growth of T84 for the necessary number of days (usually 7 to 10) in order to attain fully differentiating conditions at which the monolayers reached a more or less stable TEER of ~2500 $\Omega \cdot cm^2$ and the FD4 and FD70 kDa permeability assays determined a quantification of ~0.2-1 µg/mL and ~0.1 µg/mL respectively at the basolateral side. At that time point, the monolayers were challenged from the basolateral side only with a combination of sTNF-α and IL-1β at the concentrations of 10 ng/mL and 100 ng/mL each (experiment IIIa), or with a combination of sTNF-α and IFN-γ at the concentrations of 10 ng/mL and 100 ng/mL each (experiment IIIb), or with the single cytokines sTNF-α and IFN-γ at 100 ng/mL each (experiment IIIc). The induction was kept for 12 or 24 hrs in standard cell culture conditions and, in an endpoint fashion, the following analyses were carried out in triplicates:

1- Establishment of the control for maximal LDH release in one technical replica and running of the LDH assay.
2- TEER measurement.
3- Assessment of the FD4 permeability and/or of the FD70 permeability.

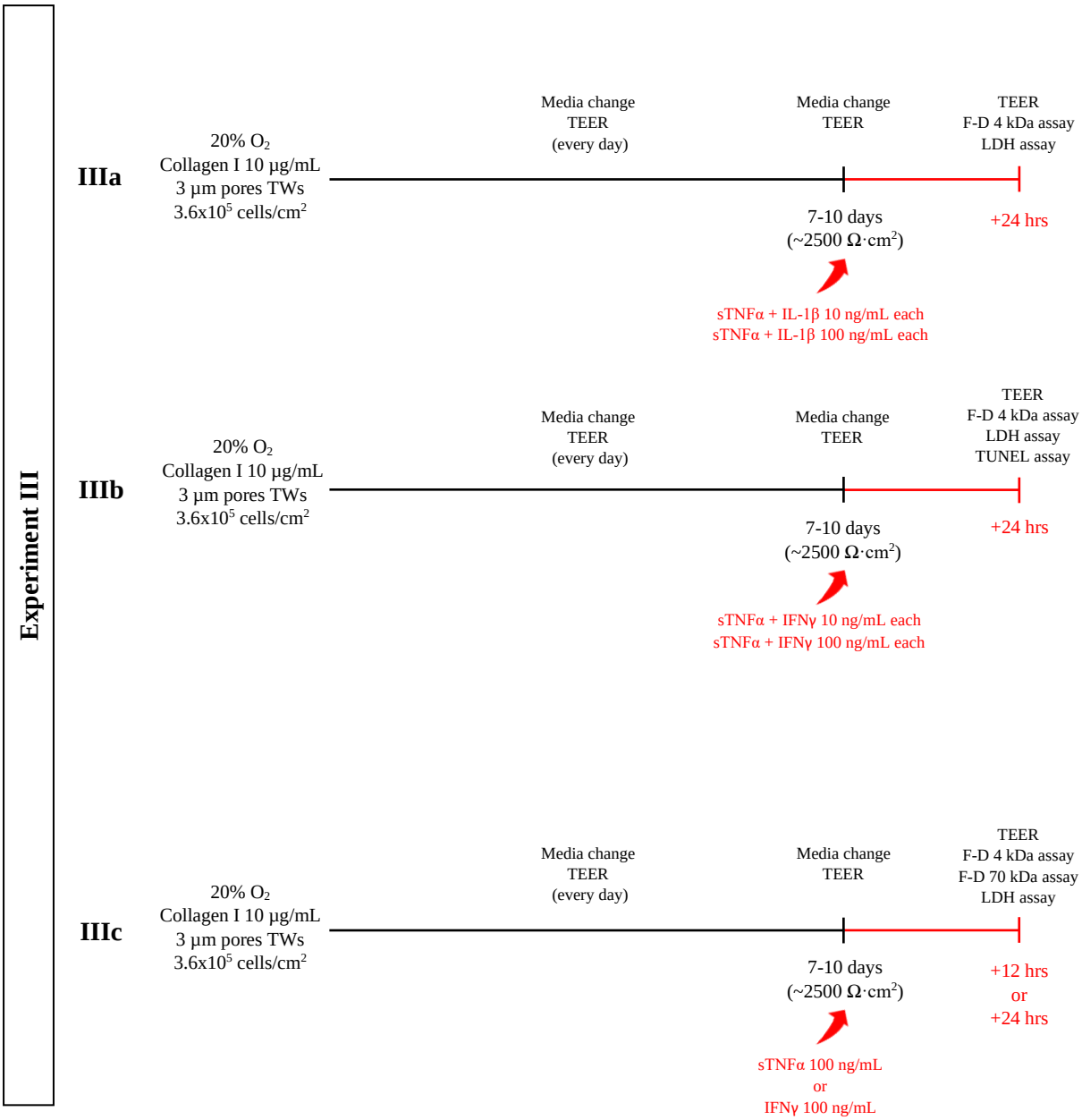

Figure 51: Schematic representation of the third barrier-impairment test with sTNFα/IL-1β, sTNFα/IFNγ and sTNFα or IFNγ on T84 monolayers of ~2500 Ω·cm². In red are indicated the time frames during which the monolayers were stimulated with the cytokines combinations from the basolateral side. Note: the different time frames depicted in the temporal axis are not in scale.

The experiments IIIa and IIIb were initially ran in parallel in one single biological replica. The results of the TEER measurements (figure 52) showed a clear dose-response effect for both cytokines combinations, with a clear more drastic barrier function impairing effect determined by sTNFα/IFNγ at 100 ng/mL. The experiment was repeated for this last cytokine combination and concentrations and the drop of TEER (to a mean value that represented only 14% of the uninduced condition) was found to be statistically significant ($p \leq 0.0001$, two-sided paired t-test, n=5).

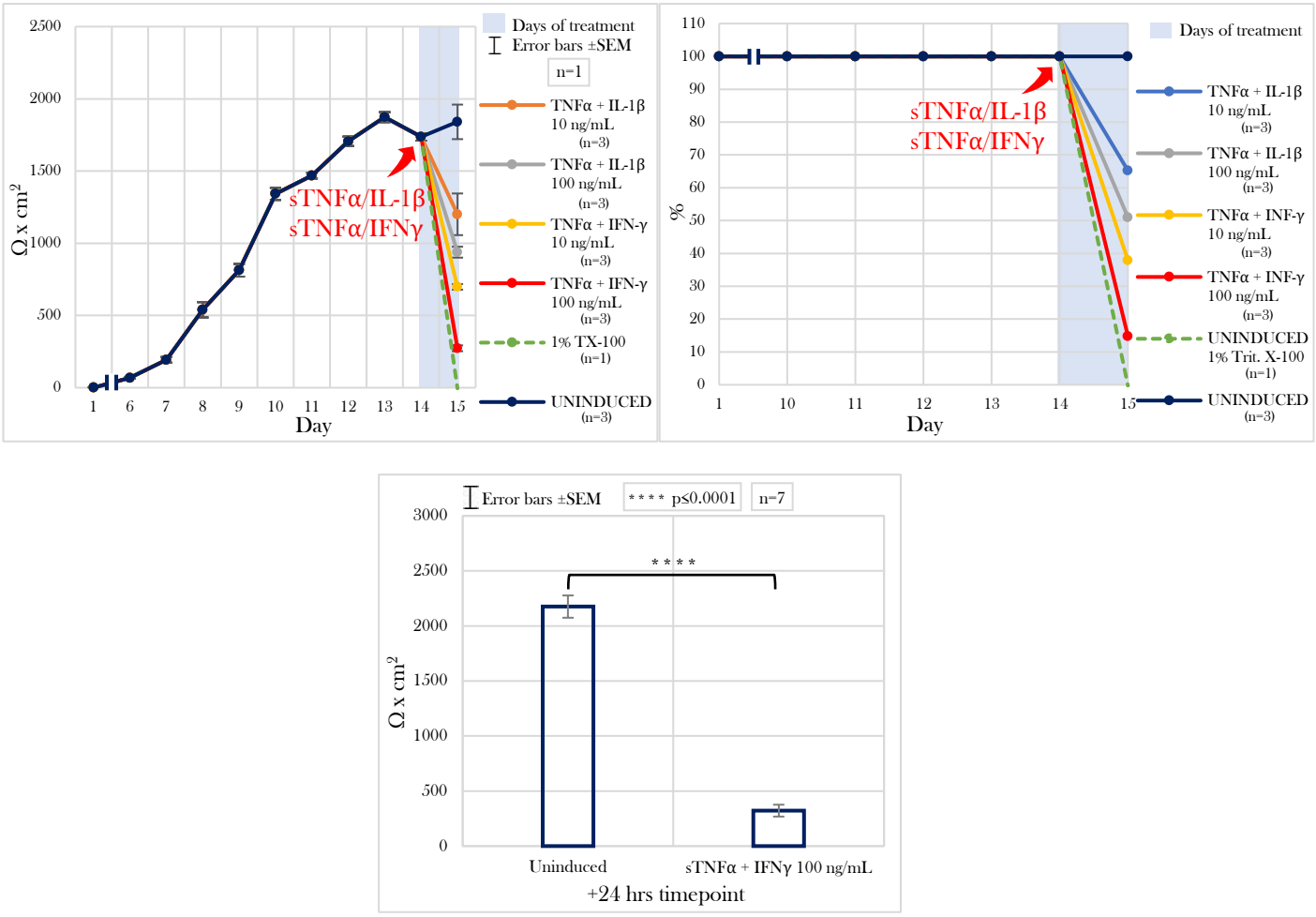

Figure 52: TEER measurements for the Experiment IIIa and IIIb. Ω x cm² values (average of all measurements from day 1 to day 14) (upper, left graph) and values normalized to the untreated condition (upper, right graph) from one single representative experiment with three technical replicas per condition The dashed lines indicate the controls of maximal cell membrane lysis for the LDH assay. Average values of seven biological replicas at the +24 hrs timepoint for sTNFα/IFNγ 100 ng/mL (lower graph). Significance stated by a two-sided paired t-test. Error bars ±SEM.

The FD4 permeability assay (figure 53), which gives a complementary insight about the size selectivity of the paracellular route (leak and unrestricted pathways), was not sensitive enough to show the extent of barrier impairment determined by the cytokine combination sTNFα/IL-1β in the first experiments, performed at sub-differentiating conditions in the cell culture media. Interestingly, the disruption of the fully polarized monolayer with sTNFα and IFNγ at 100 ng/mL determined a statistically significant 11,53-fold increase of the fluorescence-labeled Dextran in the basal media compared to the untreated condition ($p \leq 0.01$, two-sided paired t-test, n=7). Since the phenol red and the other components of the culture media seemed to interfere with the fluorescence signal of the FITC, I conducted the permeability assay with minimal media without phenol red Gibco™ HBSS before adding the FD4 to the apical side. Thereby, I could improve the quantification of the labeled Dextran, so the protocol was amended accordingly.

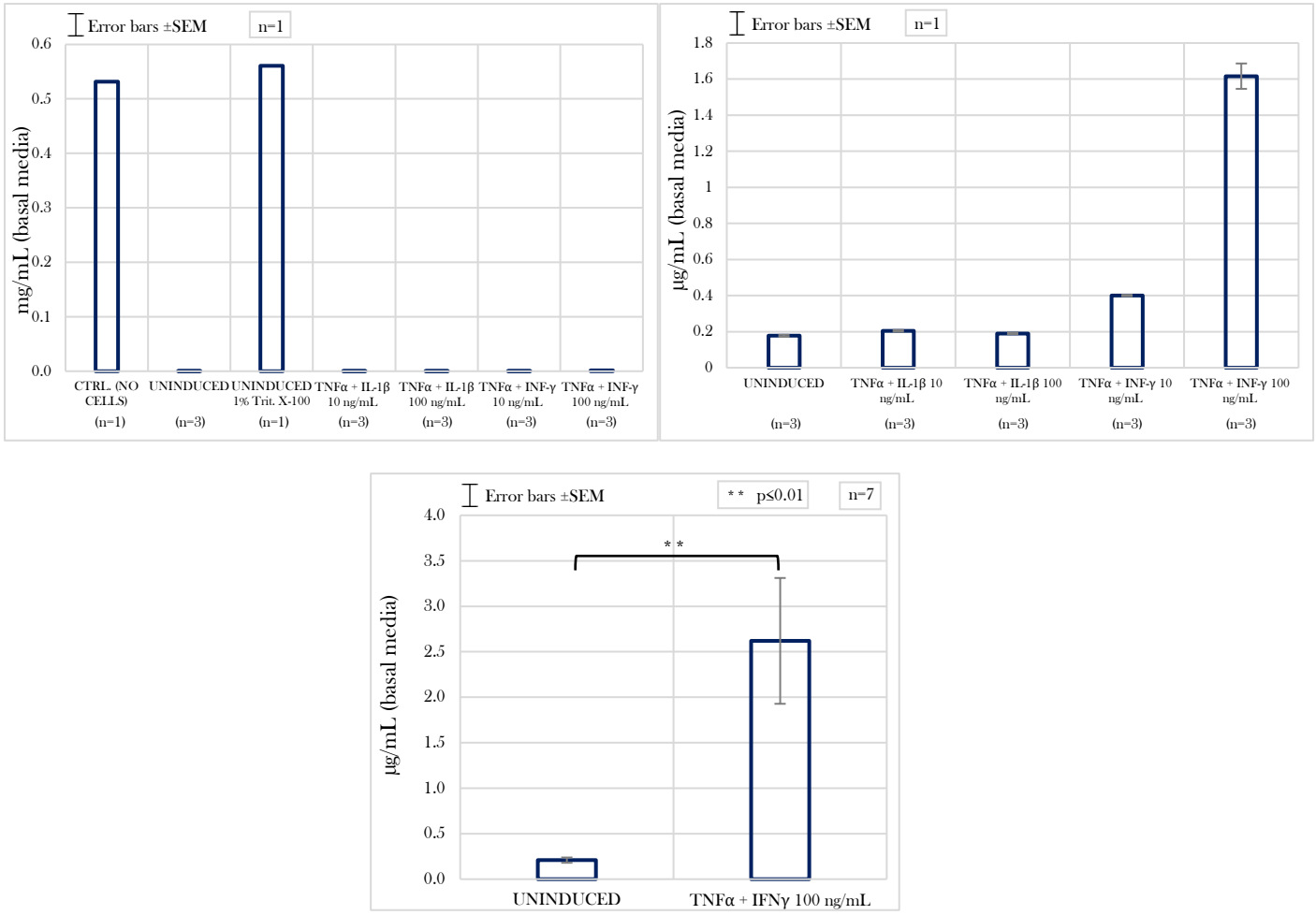

Figure 53: FD4 permeability assay for the Experiment IIIa and IIIb. Quantification reported in mg/mL or µg/mL. Results from one biological (upper graphs). Results for the combination sTNFα/IFNγ at 100 ng/mL in seven biological replicas (lower graph). Significance stated by a two-sided paired t-test. Error bars ±SEM.

The LDH assay ran for the experiments IIIa and IIIb (figure 54 upper graph) showed that the treatments with sTNFα/IL-1β and sTNFα/IFNγ did not increase the rate of Necrosis and/or Necroptosis significantly comparing with the uninduced monolayers. The combination sTNFα/IFNγ determined an increase of LDH in the media of 5-8% with regards to the uninduced condition (even though by subtracting the blank all the samples were close to background levels of LDH). By repeating the treatment sTNFα/IFNγ 100 ng/mL in five biological replicas (figure 54 lower graph) an increase of ~8% was observed with respect to the uninduced condition and this was statistically significant ($p \leq 0.05$, two-sided paired t-test). As stated for the combination sTNFα/IL-1β in the Experiment II, I assumed that there was not unexpected cytotoxicity involved and I ascribed the increase to be determined by the solely pro-necroptotic (affecting the unrestricted permeability pathway) effect of at least sTNFα.

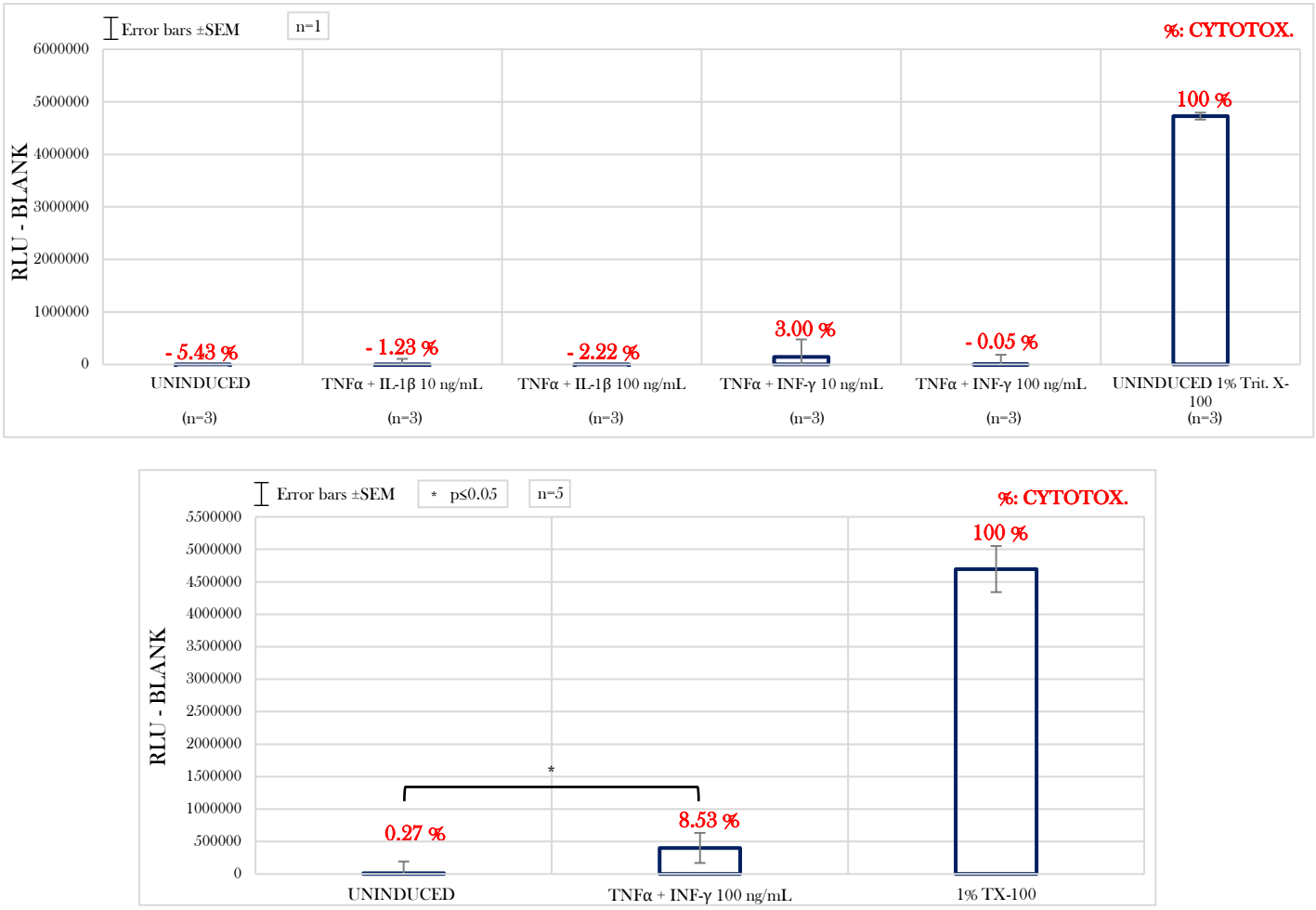

Figure 54: LDH assay for the Experiment III. RLUs of the different conditions subtracted to the blank. In red the percentage of Necrosis/Necroptosis normalized to a control of maximal cell membrane lysis. Results from one biological (upper graph). Results for the combination sTNFα/IFNγ at 100 ng/mL in five biological replicas (lower graph). Significance stated by a two-sided paired t-test. Error bars ±SEM.

The overall results of the experiments IIIa and IIIb showed that sTNFα/IFNγ at 100 ng/mL significantly impaired fully differentiated T84 monolayers, at a higher extent than the other combination, without inducing unwanted cytotoxic effects. The barrier impairing effects were properly detected with all the aforementioned assays.

In order to implement in the model an assay to selectively detect cell death by Apoptosis, and to evaluate the contribution of this process in the barrier impairment determined by sTNFα/IFNγ at 100 ng/mL, I ran a TUNEL assay following the same experimental setup of Experiment IIIb. A positive control of cells treated with DNAaseI did not show a complete, diffused chromatin staining with the fluorescent dye. A test of three different permeabilization treatments (0.1/0.25/0.5% Triton X100 for 15 mins at RT°C) clearly showed that the harshest treatment increased the number of TUNEL positive cells previously treated with DNAaseI, giving a hint that the access of the components of the reaction mix to the cells might be impaired (figure 55). The same experiment (cells grown for 10 days, induced with TNFα/IFNγ 100 ng/mL, for 24 hrs, from the apical side) performed on glass

coverslips showed that in the positive control, the weakest permeabilization treatment was sufficient to obtain a complete staining of DNAaseI treated cells, demonstrating that eventually the conditions of the cells on the TWs were the critical issue. No clear increase of TUNEL positive cells was observed on monolayers induced with sTNFα/IFNγ at 100 ng/mL, comparing with the untreated ones; neither on cells simply grown over glass, nor on cells differentiated over TWs (figure 55).

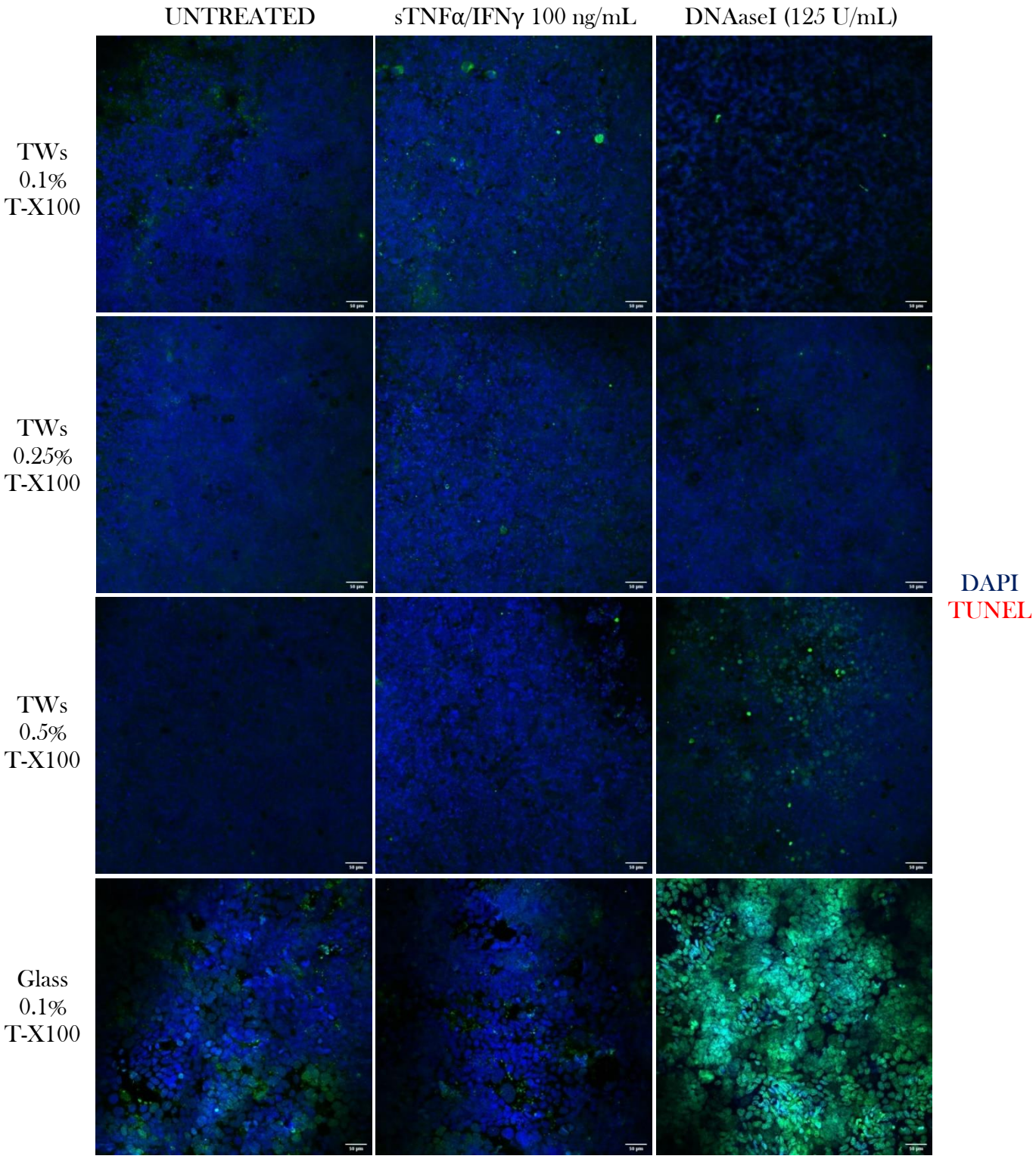

Figure 55: TUNEL assay on T84 (passage 19) grown over TWs or glass coverslips for 10 days (~2500 Ω x cm^2). Permeabilization test with T-X100 0.1, 0.25 and 0.5 % for cells fully differentiated on TWs and permeabilization with T-X100 0.1% for cells grown over coverslips for the same time. In the green channel (ex: 450 – 500 nm / em: 515 – 565 nm) TUNEL positive cells (Fluorescein), and in the blue channel (ex: 340-380 nm / em: 450-490 nm) nuclei counterstaining (DAPI). Scale bar of 50 µm. The images depict single representative fields of view for each condition

In order to dissect the barrier impairing effects determined by the combination sTNFα/IFNγ, I decided to run the experiment IIIc applying the single cytokines. In that way I could have evaluated the single contributions to the drastic phenotype observed in the experiment IIIb. In the experiment IIIc, sTNFα or IFNγ were applied basolaterally to fully differentiated monolayers, at 100 ng/mL each and for two different incubation times, 12 and 24 hrs.

The application of sTNFα for 12 hrs determined a statistically significant ($p \leq 0.0001$, two-sided paired t-test, n=6) drop of TEER to ±44% of the uninduced condition (figure 56). This drop of TEER was less pronounced than the one observed for the combination sTNFα/IFNγ applied at the same concentration for 24 hrs (figure 52).

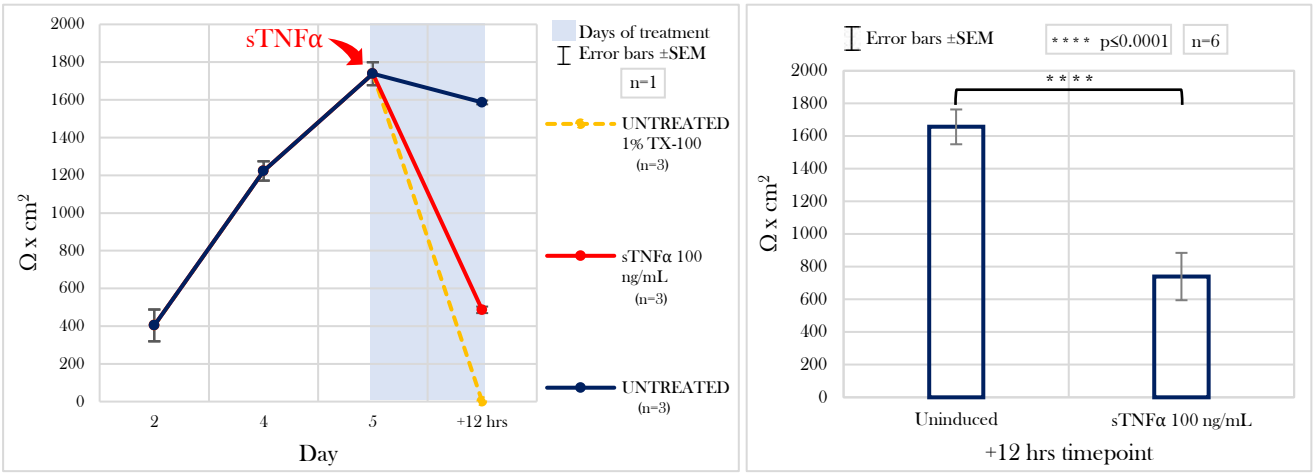

Figure 56: sTNFα applied for 12 hrs at fully differentiated stages: TEER measurements. The left graph shows the Ω x cm^2 over time from one single representative experiment with three technical replicas per condition. The right graph shows the average values for the two conditions, uninduced and sTNFα 100 ng/mL, at 12 hrs post-induction for n=6. Significance stated by a two-sided paired t-test. Error bars ±SEM.

The induction with sTNFα determined also a statistically significant ($p \leq 0.0001$, two-sided paired t-test, n=6) increase of permeability towards FD4 of 1.33-fold with regards to the uninduced condition (figure 57). This increase was lower than the one observed for the combination sTNFα/IFNγ applied at the same concentration for 24 hrs (figure 53).

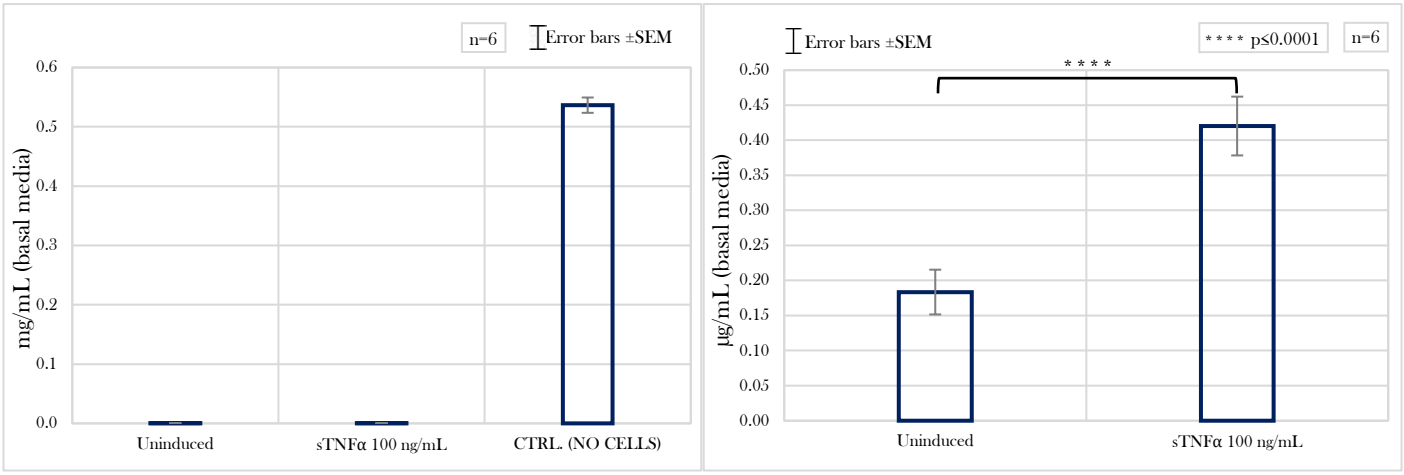

Figure 57: sTNFα applied for 12 hrs at fully differentiated stages: FD4 assay. Positive control of maximal permeability in mg/mL (left graph). Average values in µg/mL for the two conditions, uninduced and sTNFα 100 ng/mL, at 12 hrs post-induction for n=6 (right graph). Significance stated by a two-sided paired t-test. Error bars ±SEM.

In order to assess the unrestricted paracellular permeability pathway, I ran the FD70 assay in one biological replica (figure 58). An increase of permeability towards this molecular specie could not be observed in the aforementioned conditions, as I would have expected considering the nature of the cytokine.

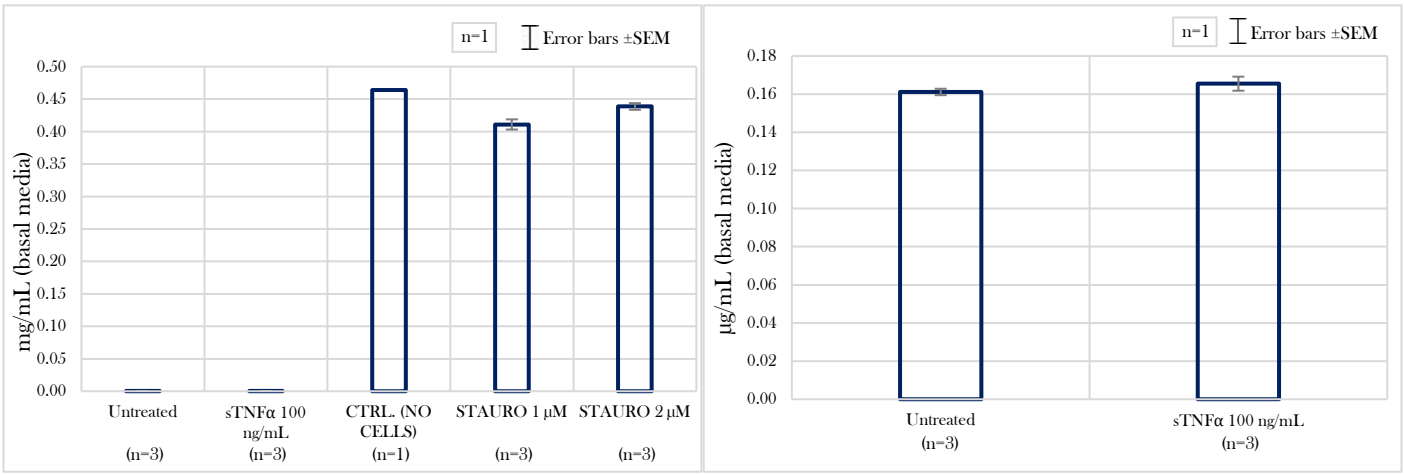

Figure 58: sTNFα applied for 12 hrs at fully differentiated stages: FD70 assay. Positive controls of maximal permeability: TW with no cells, and monolayers treated with two concentrations of Staurosporine, a chemical inductor of Apoptosis, in mg/mL (left graph). Average values in µg/mL for the two conditions, uninduced and sTNFα 100 ng/mL, at 12 hrs post-induction for n=1 (right graph). Error bars ±SEM.

The LDH assay, which quantifies the extent of plasma membrane lysis determined either by Necrosis and/or Necroptosis, showed that the induction with sTNFα determined a statistically significant ($p \leq 0.01$, two-sided paired t-test, n=6) increase of LDH in the apical media of 2-fold with regards to the uninduced condition (figure 59). As the percentage of cytotoxicity (calculated by normalizing to the control of maximal lysis) quantified in the monolayers treated with sTNFα was not greater than

10 (with respect to the one quantified in the uninduced monolayers), an undergoing Necrosis was excluded. The increase of 6% of cytotoxicity determined by sTNFα was very likely given only by an increase of Necroptosis. This increase was lower than the one observed for the combination sTNFα/IFNγ applied at the same concentration for 24 hrs (figure 54).

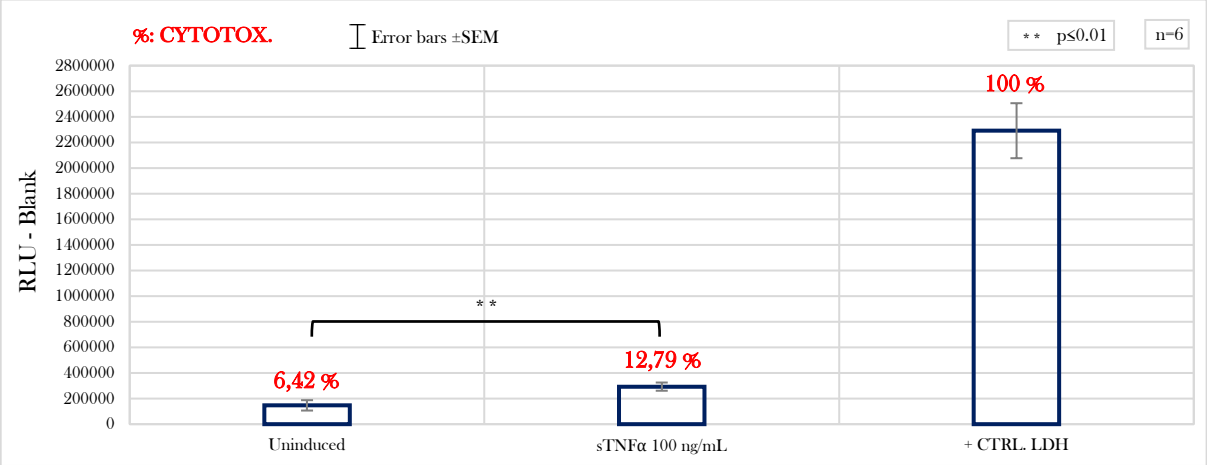

Figure 59: sTNFα applied for 12 hrs at fully differentiated stages: LDH assay. RLUs of the different conditions subtracted to the blank. In red the percentage of Necrosis/Necroptosis normalized to a control of maximal cell membrane lysis. Significance stated by a two-sided paired t-test for n=6. Error bars ±SEM.

The same experiment of induction with only sTNFα at 100 ng/mL was performed, extending the time of treatment with the cytokine from 12 to 24 hrs. This induction determined a slightly less pronounced drop of TEER (to 48% of the uninduced condition) but still statistically significant (p≤0.001, two-sided paired t-test, n=3) (figure 60).

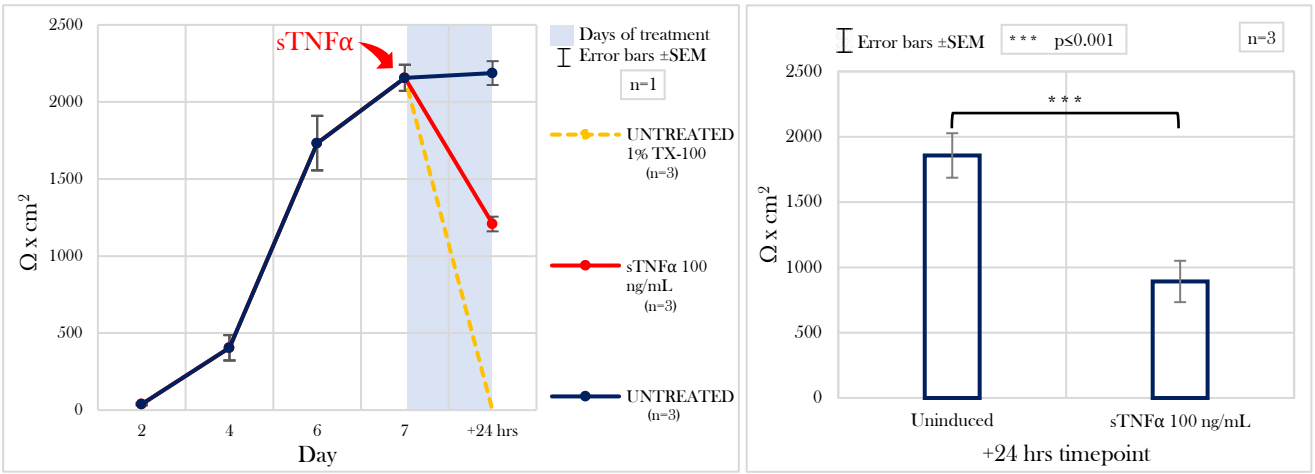

Figure 60: sTNFα applied for 24 hrs at fully differentiated stages: TEER measurements. The left graph shows the Ω x cm² over time from one single representative experiment with three technical replicas per condition. The right graph shows the average values for the two conditions, uninduced and sTNFα 100 ng/mL, at 24 hrs post-induction for n=3. Significance stated by a two-sided paired t-test. Error bars ±SEM.

Interestingly, the induction for 24 hrs determined also a less pronounced increase (0.88-fold) of the permeability towards FD4 comparing with the uninduced condition, which was not statistically significant ($p>0.05$, two-sided paired t-test, n=3) (figure 61).

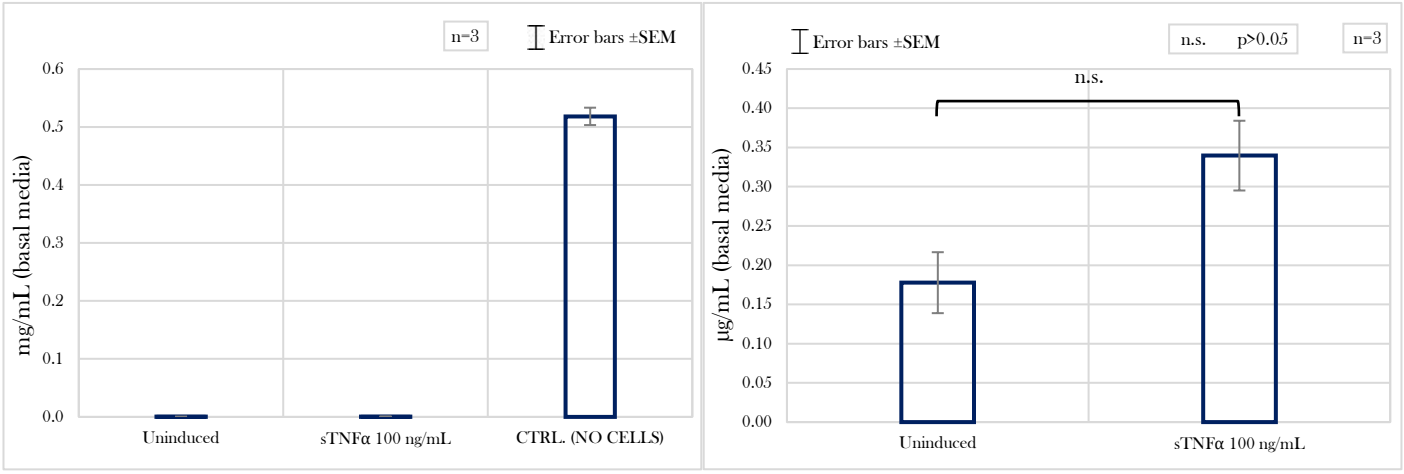

Figure 61: sTNFα applied for 24 hrs at fully differentiated stages: FD4 assay. Positive controls of maximal permeability (TW with no cells) in mg/mL (left graph). Average values in µg/mL for the two conditions, uninduced and sTNFα 100 ng/mL, at 24 hrs post-induction for n=3 (right graph). Error bars ±SEM.

In order to understand if an increase of permeability towards the FD70 was not observed after 12 hrs of induction simply due to the reduced incubation time, the assay was performed after 24 hrs of treatment. In one biological replica the experiment showed the same outcome, no increase of permeability (figure 62).

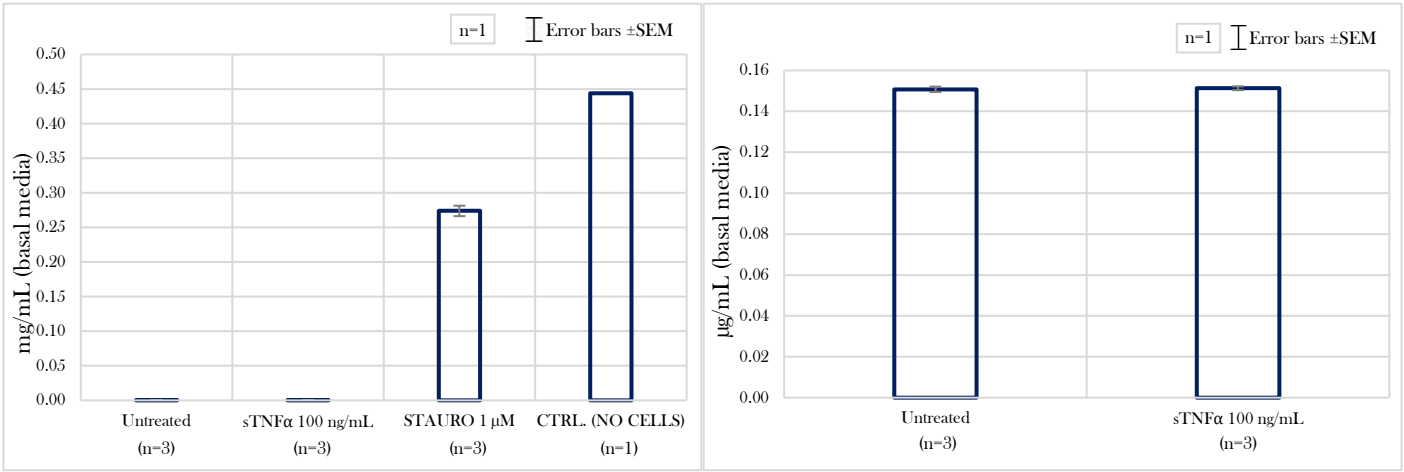

Figure 62: sTNFα applied for 24 hrs at fully differentiated stages: FD70 assay. Positive controls of maximal permeability: TW with no cells, and monolayers treated with two concentrations of Staurosporine, a chemical inductor of Apoptosis, in mg/mL (left graph). Average values in µg/mL for the two conditions, uninduced and sTNFα 100 ng/mL, at 24 hrs post-induction for n=1 (right graph). Error bars ±SEM.

Interestingly the LDH showed no significant increase of Necroptosis after 24 hrs of induction with sTNFα 100 ng/mL (figure 63).

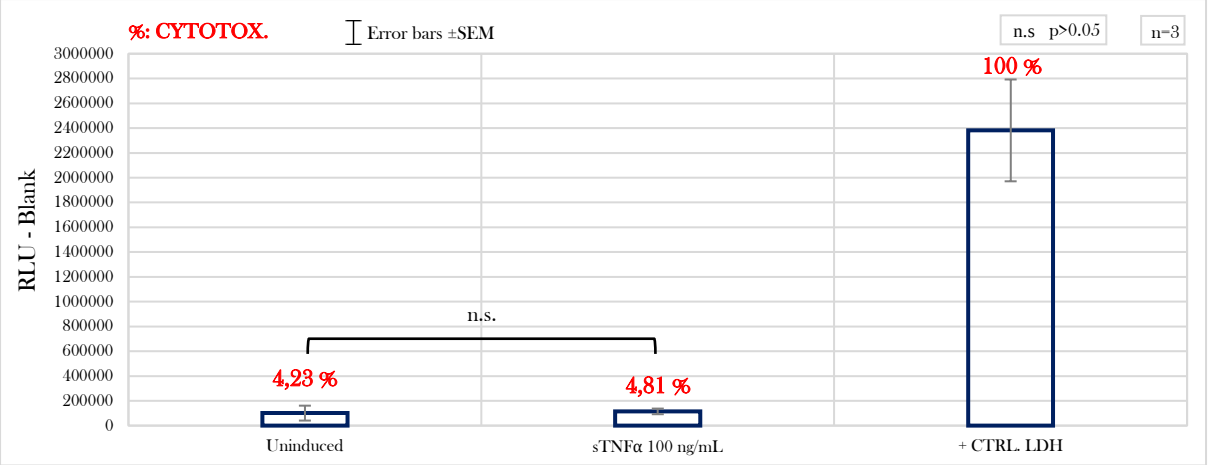

Figure 63: sTNFα applied for 24 hrs at fully differentiated stages: LDH assay. RLUs of the different conditions subtracted to the blank. In red the percentage of Necrosis/Necroptosis normalized to a control of maximal cell membrane lysis. Significance stated by a two-sided paired t-test for n=3. Error bars ±SEM.

The same kind of experiments were performed by inducing barrier disruption with only IFNγ at 100 ng/mL applied for 12 and 24 hrs on fully differentiated monolayers.

An induction with IFNγ for 12 hrs determined an average decrease of TEER to 68.19 % of the average value of the uninduced monolayers (figure 64). The drop appeared to not be statistically significant ($p>0.05$, two-sided paired t-test, n=3).

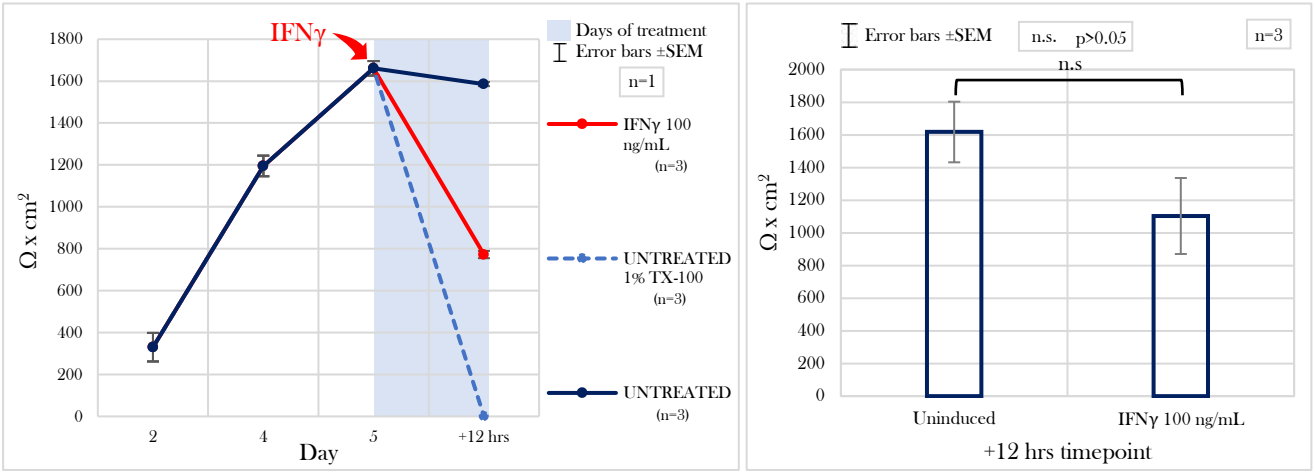

Figure 64: IFNγ applied for 12 hrs at fully differentiated stages: TEER measurements. The left graph shows the Ω x cm² over time from one single representative experiment with three technical replicas per condition. The right graph shows the average values for the two conditions, uninduced and sTNFα 100 ng/mL, at 12 hrs post-induction for n=3. Significance stated by a two-sided paired t-test. Error bars ±SEM.

The drop of TEER was accompanied by an increase of permeability towards FD4 of 0.62-fold in the treated monolayers with respect to the untreated ones (figure 65). The increase was statistically significant ($p\leq0.05$, two-sided paired t-test, n=3).

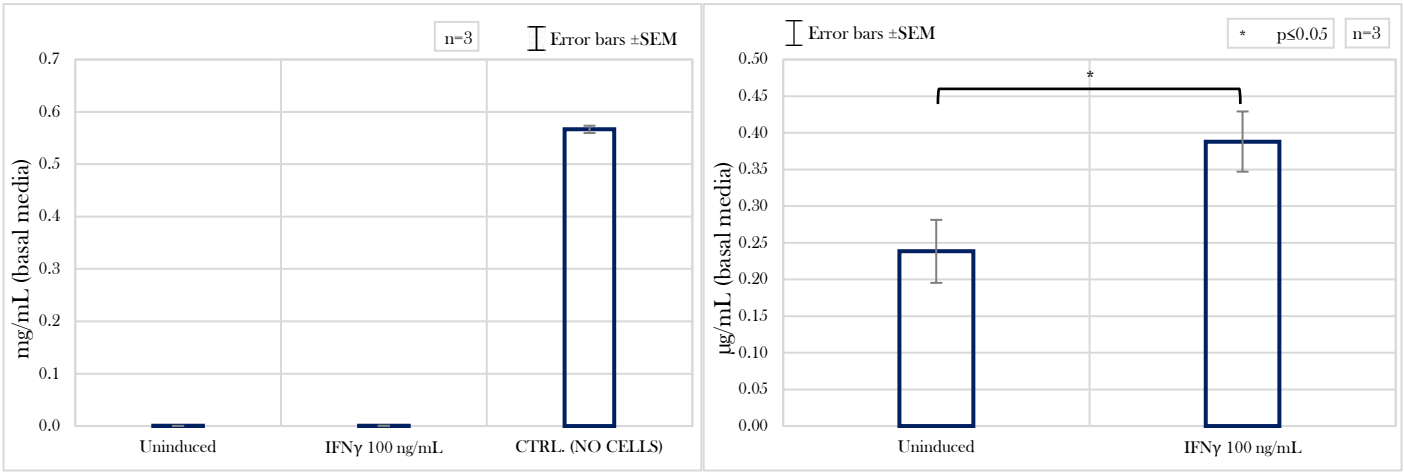

Figure 65: IFNγ applied for 12 hrs at fully differentiated stages: FD4 assay. Positive controls of maximal permeability (TW with no cells) in mg/mL (upper graph). Average values in µg/mL for the two conditions, uninduced and sTNFα 100 ng/mL, at 12 hrs post-induction for n=3 (lower graph). Error bars ±SEM.

From the measurement of the TEER and the FD4 assay appeared very clear that the barrier disruptive determined by IFNγ were less drastic than the ones determined by sTNFα in the same conditions. The LDH assay for assessing Necroptosis (affecting the unrestricted permeability pathway) showed a surprising result. A statistically significant ($p \leq 0.01$, two-sided paired t-test, n=3) decrease of the level of LDH in the apical media was observed (figure 66).

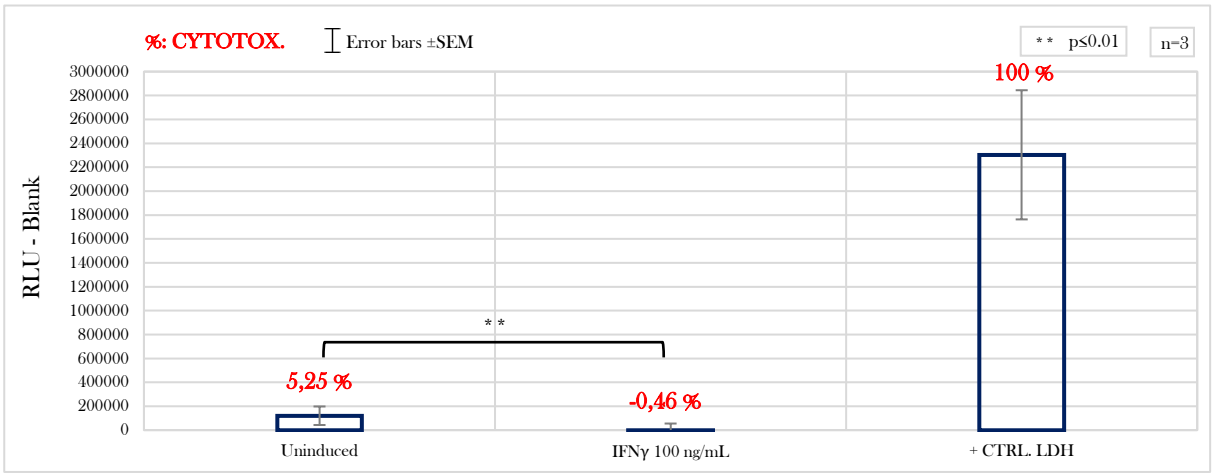

Figure 66: IFNγ applied for 12 hrs at fully differentiated stages: LDH assay. RLUs of the different conditions subtracted to the blank. In red the percentage of Necrosis/Necroptosis normalized to a control of maximal cell membrane lysis. Significance stated by a two-sided paired t-test for n=3. Error bars ±SEM.

The same experiment was performed with IFNγ applied at 100 ng/mL for 24 hrs. The drop of TEER was not statistically significant ($p > 0.05$, two-sided paired t-test, n=3) and the average value of the induced monolayers corresponded to 70% of the average of the uninduced condition (figure 67). This drop of 30% was comparable to one achieved by applying the cytokine for 12 hrs.

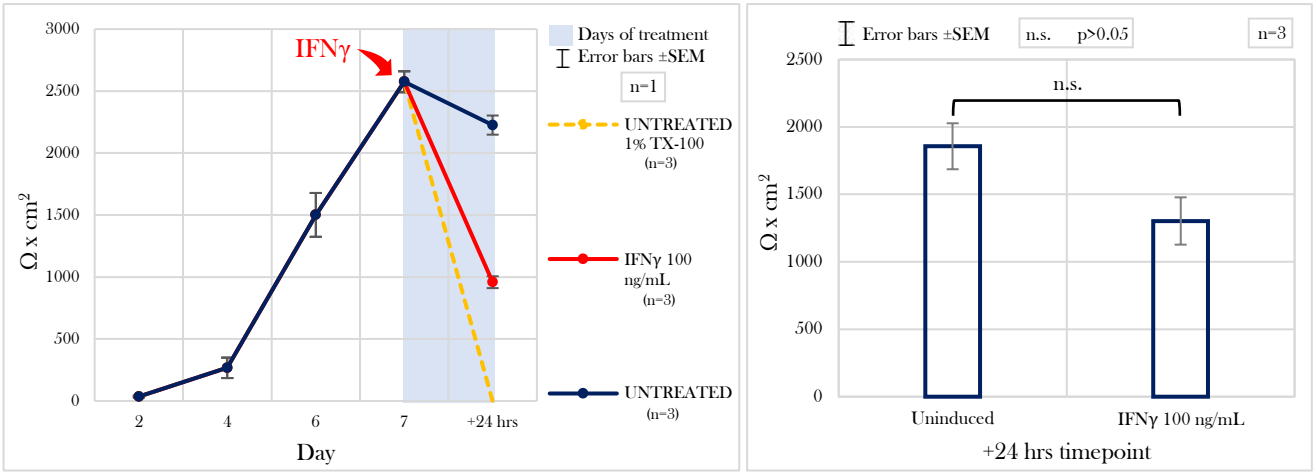

Figure 67: IFNγ applied for 24 hrs at fully differentiated stages: TEER measurements. The left graph shows the Ω x cm² over time from one single representative experiment with three technical replicas per condition. The right graph shows the average values for the two conditions, uninduced and sTNFα 100 ng/mL, at 24 hrs post-induction for n=3. Significance stated by a two-sided paired t-test. Error bars ±SEM.

An increase of permeability towards FD4 was observed also in this case (1.36-fold higher with regards to the uninduced condition) and it was higher than the one observed after 12 hrs of induction. Notwithstanding, the difference did not reach statistical significance (p>0.05, two-sided paired t-test, n=3) (figure 68).

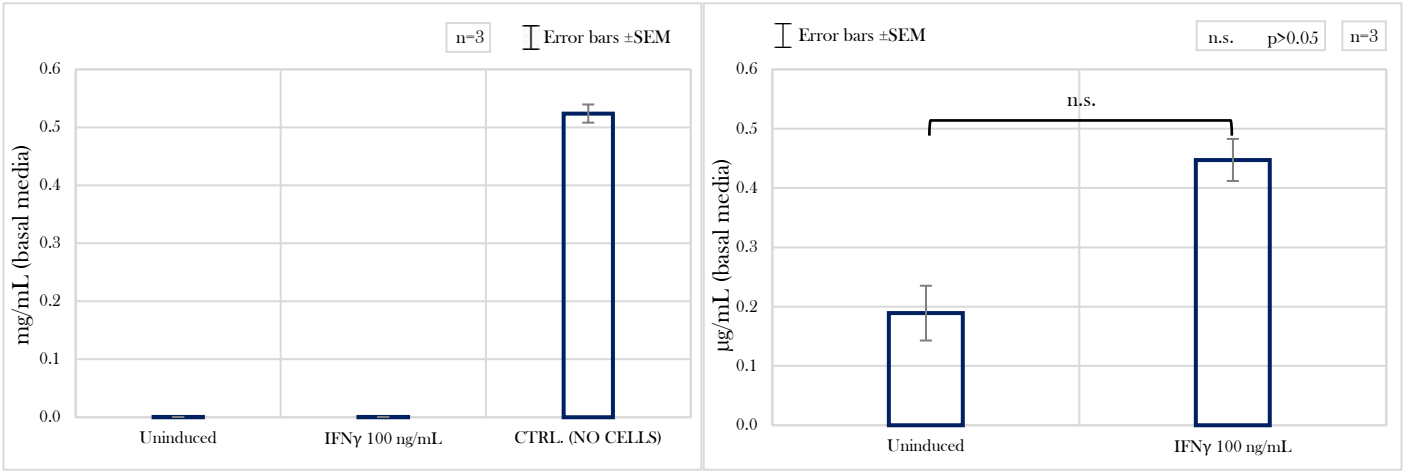

Figure 68: IFNγ applied for 24 hrs at fully differentiated stages: FD4 assay. Positive control of maximal permeability (TW with no cells) in mg/mL (left graph). Average values in µg/mL for the two conditions, uninduced and sTNFα 100 ng/mL, at 24 hrs post-induction for n=3 (right graph). Error bars ±SEM.

The LDH assay (figure 69) showed the same outcome also in this case but the difference observed in between induced and uninduced conditions did not reach statistical significance (p>0.05, two-sided paired t-test, n=3), as instead was reached with the induction for 12 hrs. The confirmation of this trend demonstrates that a reduction of LDH in the apical media is clearly determined by IFNγ and the reason of this phenomenon must be investigated.

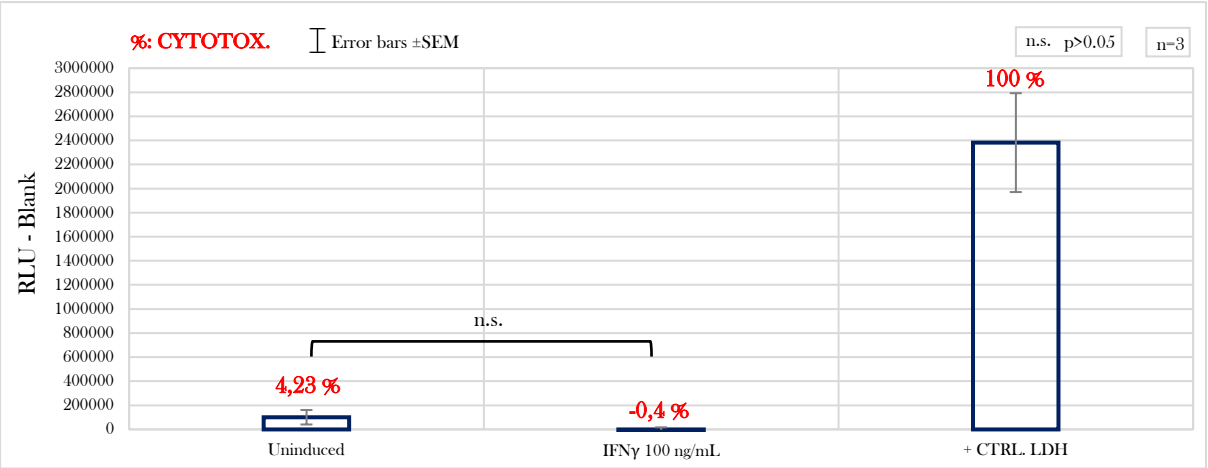

Figure 69: IFNγ applied for 24 hrs at fully differentiated stages: LDH assay. RLUs of the different conditions subtracted to the blank. In red the percentage of Necrosis/Necroptosis normalized to a control of maximal cell membrane lysis. Significance stated by a two-sided paired t-test for n=3. Error bars ±SEM.

Experiment IV consisted on the adaptation of the inflammatory model to the hypoxic conditions that resemble better the real physiological microenvironment. The titration of sTNFα, applied from the basolateral side on fully differentiated monolayer for 24 hrs, was performed by testing the concentrations 10, 50 and 100 ng/mL (figure 70).

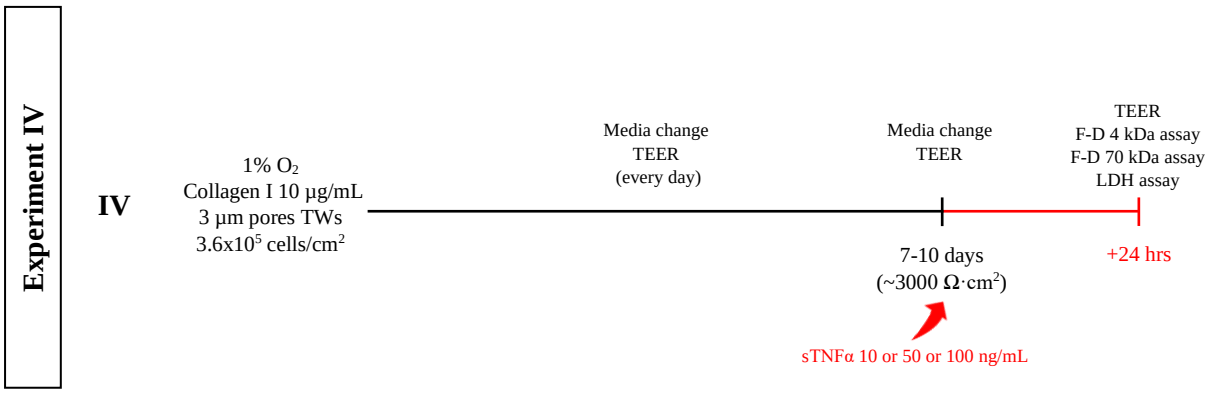

Figure 70: Schematic representation of the fourth barrier-impairment test with only sTNFα applied on fully differentiated monolayers of ~3000 Ω·cm² in 1% O_2 atm. In red are indicated the time frames during which the monolayers were stimulated with the cytokine from the basolateral side. Note: the different time frames depicted in the temporal axis are not in scale.

In the single biological replica of this pilot experiment the cells polarized quite fast and at +2 days a TEER of ±3200 Ω x cm² was achieved. The induction with the three different cytokine concentrations determined a drastic barrier disruption without following a clear dose-response pattern, being the concentration 50 ng/mL the one that determined the most drastic effect. A drop of TEER to 33.52 % of the uninduced condition was determined by the concentration 10 ng/mL, to 28.70 % of the uninduced condition by 50 ng/mL and to 42.74% of the uninduced condition by 100 ng/mL (figure 71).

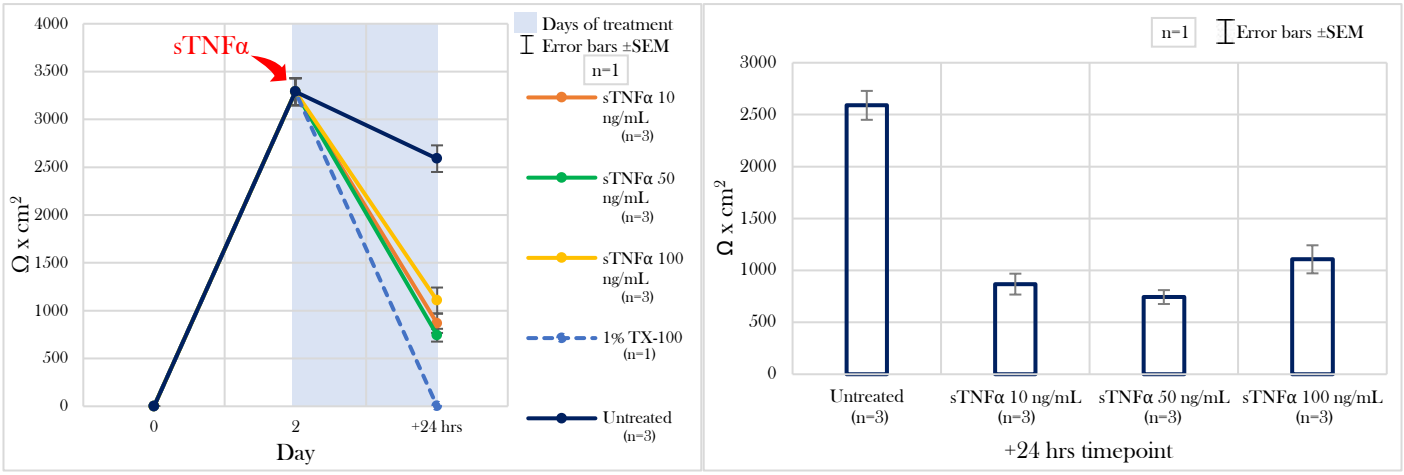

Figure 71: sTNFα applied for 24 hrs at fully differentiated stages in 1% O_2 atm: TEER measurements. Ω x cm^2 values over time from a single biological replica with three technical replicas per condition (left graph). Average values for the four conditions, untreated, sTNFα 10, 50 and 100 ng/mL, at 24 hrs post-induction (right graph). Error bars ±SEM.

The increase of permeability towards FD4 determined by sTNFα followed the same trend observed at the level of the TEER, with 50 ng/mL giving rise to the most prominent effect (figure 72). An increase of 1.22-fold with respect to the uninduced condition was observed for the concentration 10 ng/mL, of 2.46-fold with respect to the uninduced condition for 50 ng/mL and of 1.2-fold with respect to the uninduced condition for 100 ng/mL.

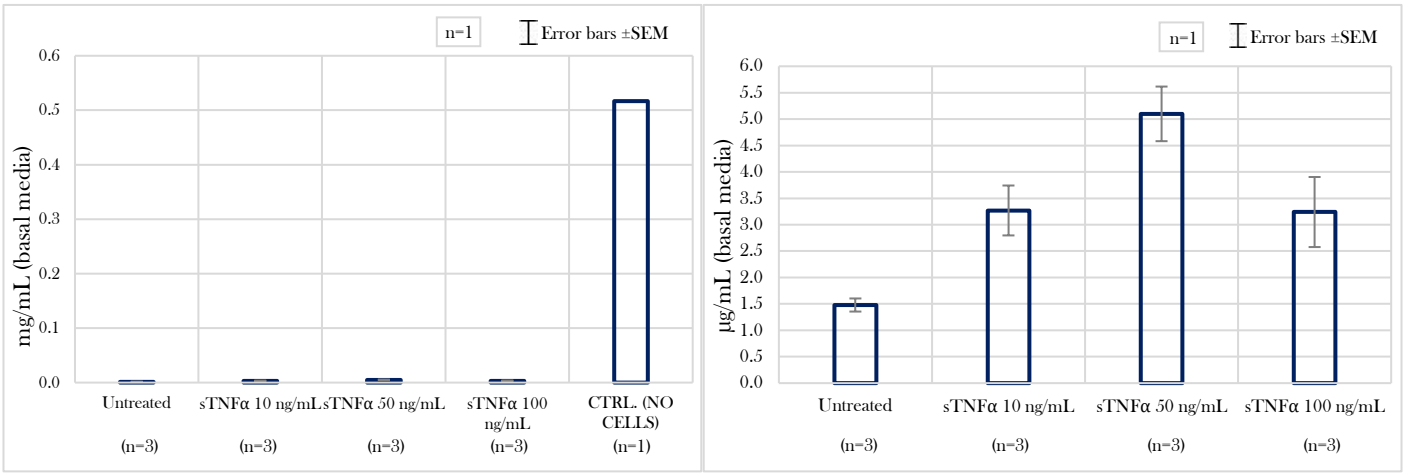

Figure 72: sTNFα applied for 24 hrs at fully differentiated stages in 1% O_2 atm: FD4 assay. Positive control of maximal permeability (TW with no cells) in mg/mL (left graph). Average values in µg/mL for the four conditions, uninduced and sTNFα 10, 50 and 100 ng/mL, at 24 hrs post-induction for a single biological replica with three technical replicas per condition (right graph). Error bars ±SEM.

The assessment of the FD70 permeability in the experiment IV (figure 73) showed that was indeed the multiple-layer configuration, acquired by T84 grown in normoxic conditions, to impair the outcome of this valuable assay. A significant increase of permeability of 0.86-fold with respect to the uninduced condition for the concentration 10 ng/mL, of 1.88-fold with respect to the uninduced

condition for 50 ng/mL and of 0.54-fold with respect to the uninduced condition for 100 ng/mL. The same trend observed at the TEER and at the FD4 assay was observed with the concentration 50 ng/mL determining the most drastic effect.

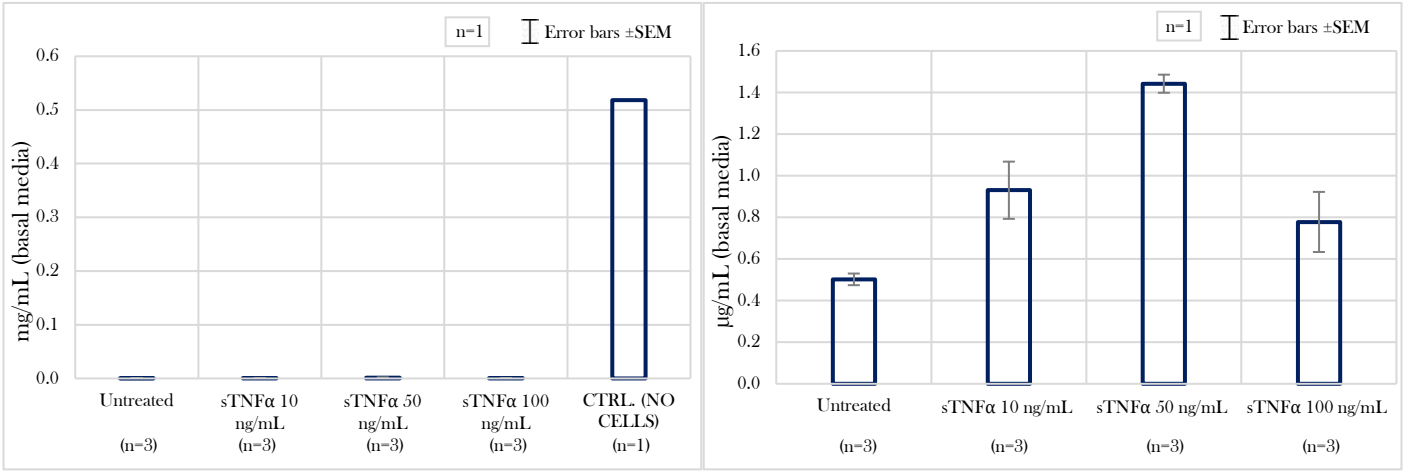

Figure 73: sTNFα applied for 24 hrs at fully differentiated stages in 1% O_2 atm: FD70 assay. Positive control of maximal permeability (TW with no cells) in mg/mL (left graph). Average values in µg/mL for the four conditions, uninduced and sTNFα 10, 50 and 100 ng/mL, at 24 hrs post-induction for a single biological replica with three technical replicas per condition (right graph). Error bars ±SEM.

Finally, an LDH assay was ran for the experiment IV. In line with the comparable experiment ran in normoxic conditions (figure 63), no relevant increase of Necroptosis was observed at any of the tested concentrations of sTNFα applied for 24 hrs with regards to the untreated condition (figure 74).

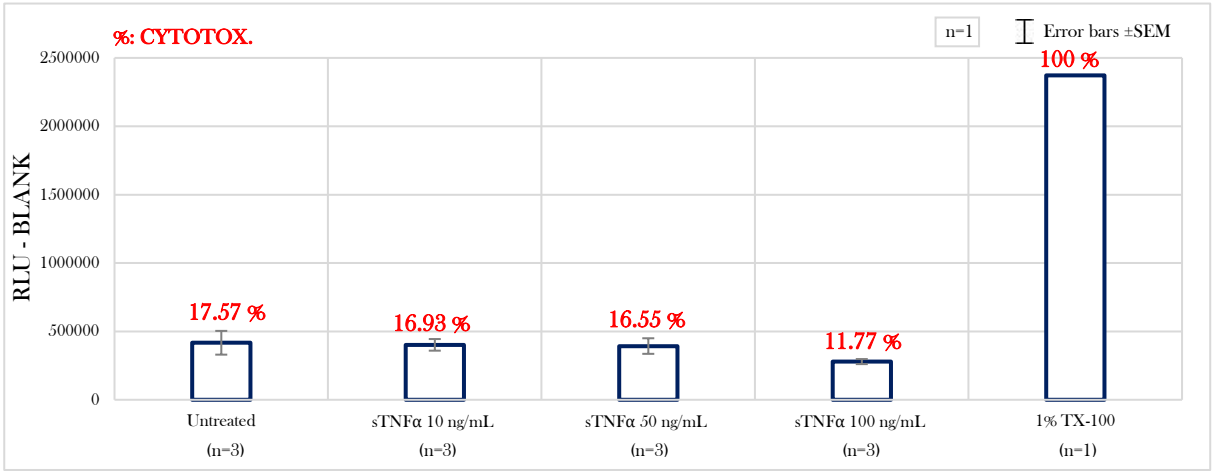

Figure 74: sTNFα applied for 24 hrs at fully differentiated stages in 1% O_2 atm: LDH assay. RLUs of the different conditions subtracted to the blank. In red the percentage of Necrosis/Necroptosis normalized to a control of maximal cell membrane lysis. One biological replica with three technical replicas per condition. Error bars ±SEM.

The titration of sTNFα in fully differentiated monolayers grown in hypoxic conditions did not show, for any of the assays applied, a clear dose-response trend.

4.4.2. Assessment of the expression of the cytokines cognate receptors in the optimal inflammatory model: untreated and sTNFα/IFNγ-induced conditions

The expression of the genes codifying for the receptors known to interact with the tested cytokines was assessed at the transcriptional level by RT-qPCR. The cells were grown to fully differentiated conditions (±2500 Ω x cm^2) and then challenged from the basolateral side for 24 hrs with sTNFα and IFNγ at 100 ng/mL each, the optimal pro-inflammatory cocktail defined with the experiment IIIb. After the 24 hrs of stimulation, total RNA was isolated from either uninduced and cytokines-induced cells employing the Quick-RNA™ Microprep Kit as described in the section 1.2.2.1.3. The cDNA synthesis from the whole cell transcriptome was performed as described in the section 1.2.2.2. The expression of the genes *TNFRSF1A*, *TNFRSF1B*, *IFNGR1*, *IFNGR2*, *IL1R1* was quantified in both uninduced and sTNFα/IFNγ-induced conditions by RT-qPCR (figure 75) as described in the section 1.2.2.4. The normalization was done with the standard genes *SDHA*, *HPRT1* and *ARF1*. The statistical analyses were carried out with a two-tailed paired T-test over three biological replicas and the fold changes were calculated as explained in section 3.2.2.5.

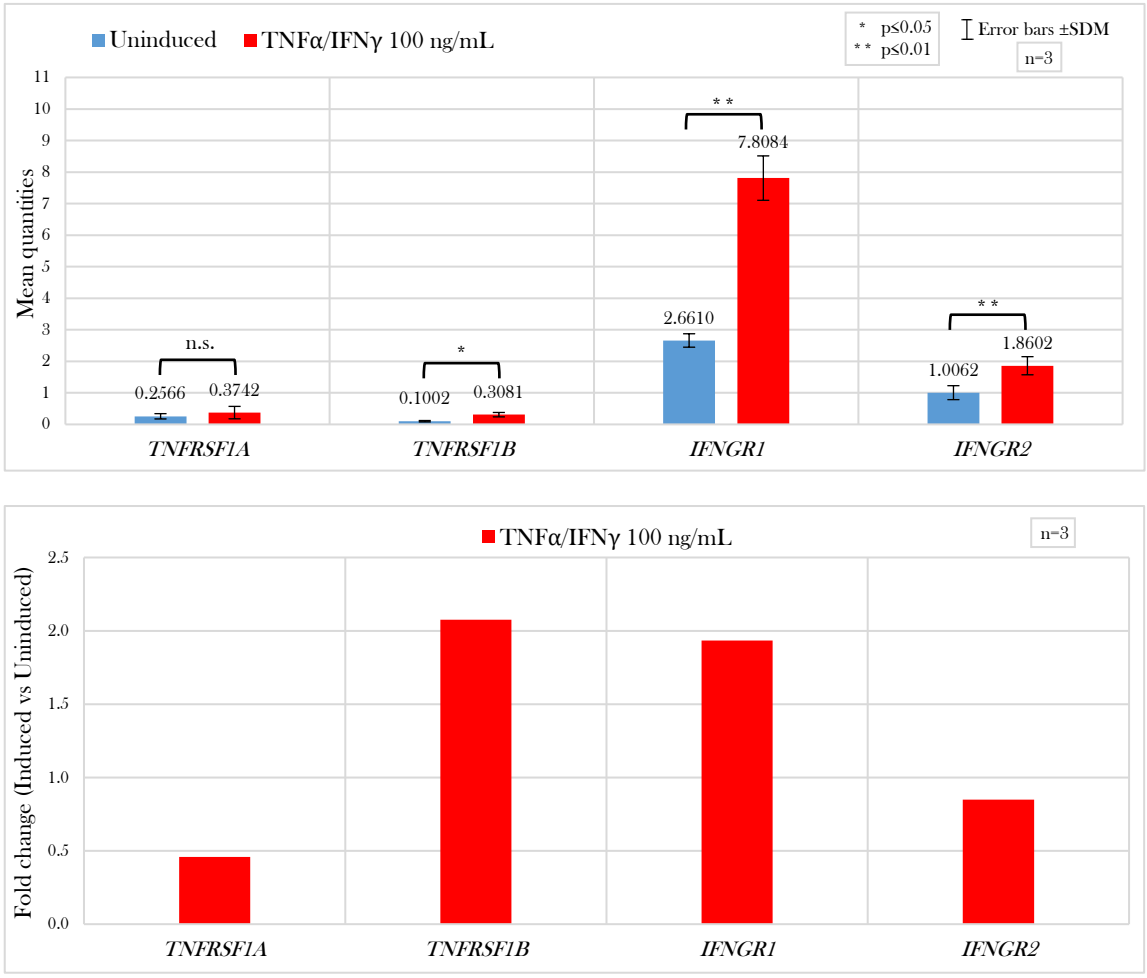

Figure 75: RT-qPCR for *TNFRSF1A*, *TNFRSF1B*, *IFNGR1*, *IFNGR2* performed on T84 cells grown for 10 days over TW membranes and treated basolaterally with sTNFα and IFNγ at 100 ng/mL each for 24 hrs. The uppest

graph shows the mean quantities normalized to *SDHA*, *HPRT1* and *ARF1*. Significance stated with a two-sided paired t-test, n=3 (error bars ±SD). The lowest graph shows the fold changes (induced versus uninduced conditions) for each gene.

The results of this experiment showed that the receptor genes *TNFRSF1A*, *TNFRSF1B*, *IFNGR1*, *IFNGR2* are expressed on uninduced fully differentiated cells. Furthermore, the expression of all genes increased upon a 24 hrs induction with sTNFα and IFNγ, and for *TNFRSF1B* ($p \leq 0.05$), *IFNGR1* ($p \leq 0.01$) and *IFNGR2* ($p \leq 0.01$) the increase was statistically significant (two-sided paired t-test, n=3).

As *IL1R1* has been found to be expressed at a hardly detectable levels, the qRT-PCRs were repeated without diluting the total cDNA to get quantifiable amounts. As very low expression levels of this receptor were observed (see Figure S14 of the Supplementary Material), it was not possible to drive conclusions about an eventual positive regulatory loop determined by the induction with sTNFα and IFNγ (anyway, the differential expression observed upon induction with the cytokines was statistically not significant).

4.5. Pharmacological interference experiments

4.5.1. Pharmacological interference experiments for controls of maximal barrier function protection upon the induction with IFNγ

4.5.1.1. Competitive antagonism of IFNγ with regards to barrier function by neutralizing the ligand in solution: titration of Emapalumab

In order to completely shut down the IFNγ signalling in my *in vitro* model, I employed the therapeutical monoclonal antibody Emapalumab which binds to both free and IFNγR1-bound IFNγ and impairs the interaction in between IFNγR1 (monomer containing the ligand binding site) and IFNγR2 (monomer containing the domains involved in the signal transduction), induced by IFNγ at the cell surface (figure 76).

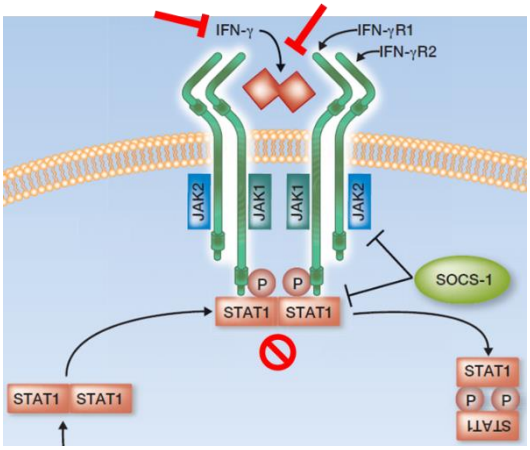

Figure 76: Graphical representation of the mechanisms of action of the antibody Emapalumab (in red). It can bind either to the free and to the IFNγR1-bound IFNγ. Adapted from Zaidi and Merlino, 2011.

The titration of Emapalumab for defining the optimal concentration for the control experiment was performed in one biological replica as schematically depicted in figure 77. The concentrations 0.5, 1, 2 and 4 µg/mL were defined in accordance to the literature[81] and applied to the basolateral sides of fully polarized monolayers for 6 hrs; afterwards, the cells were induced from the basolateral side with IFNγ at 100 ng/mL for 24 hrs (in the presence of the antibody) and the different functional assays for assessing barrier function were carried out.

Titration of Emapalumab

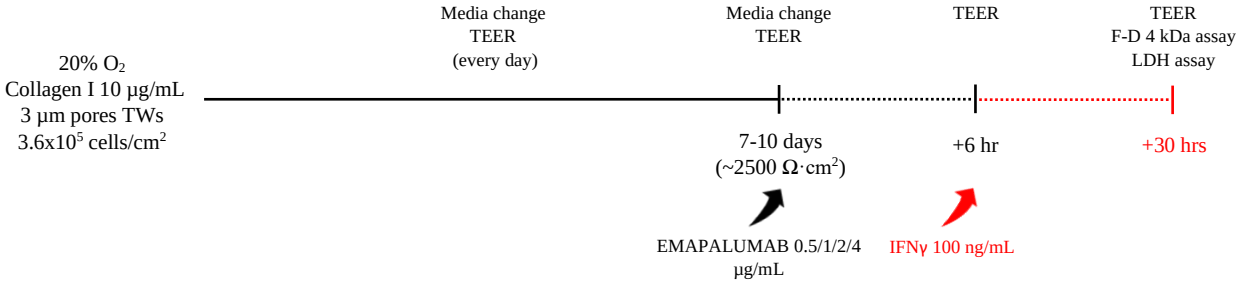

Figure 77: Schematic representation of the titration experiment for Emapalumab on fully differentiated monolayers (~2500 Ω·cm^2) induced with IFNγ 100 ng/mL for 24 hrs, in normoxia. In red are indicated the time frames during which the monolayers were stimulated with the cytokine from the basolateral side. Note: the different time frames depicted in the temporal axis are not in scale.

The measurement of the TEER showed, at all concentrations of Emapalumab, an almost total protection versus the drop of resistance determined by IFNγ alone to 43 % of the uninduced condition. The co-treatment with Emapalumab at 0.5 µg/mL brought the TEER to 93.9 %, at 1 µg/mL to 89.6 %, at 2 µg/mL to 88.4 % and 4 µg/mL to 95.6 % of the uninduced condition (figure 78).

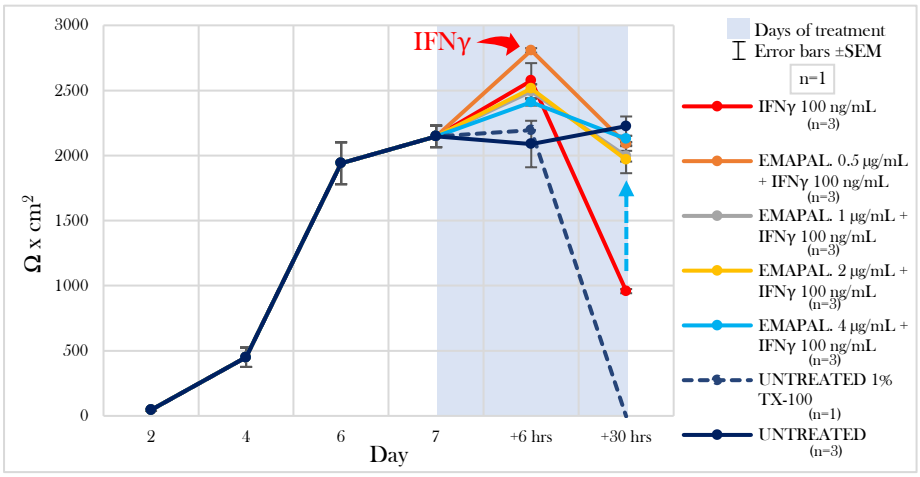

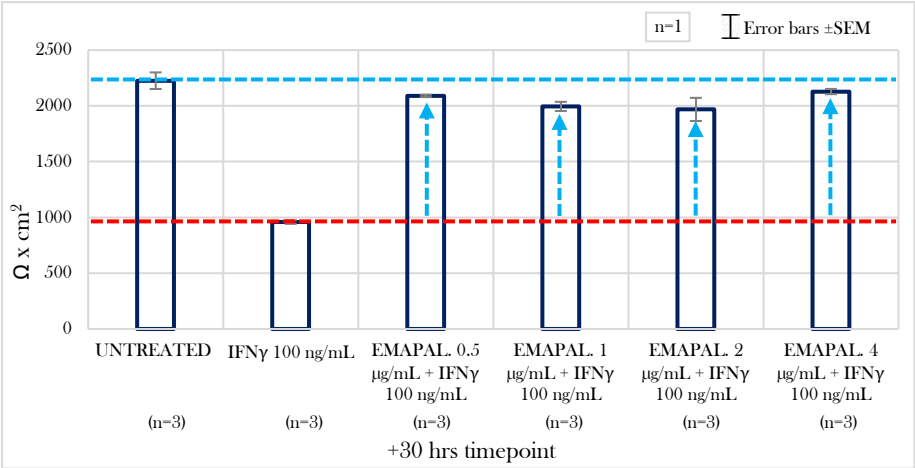

Figure 78: Titration of Emapalumab: TEER measurements. Ω x cm^2 values over time from the single biological replica with three technical replicas per condition (upper graph). Average values for the six conditions ("untreated", "IFNγ alone", "co-treatment with Emapalumab at 0.5, 1, 2 and 4 µg/mL") at 24 hrs post-induction induction, for a single biological replica with three technical replicas per condition (lower graph). Error bars ±SEM.

The complete protection of the barrier function impairment determined by IFNγ was also clearly observed at the level of the FD4 permeability, upon co-treatment with Emapalumab at all tested concentrations. Whereas IFNγ applied alone determined a 2.64-fold increase of permeability with regards to the uninduced condition, the co-treatments with Emapalumab at all tested concentrations determined no significant increase of permeability with regards to the uninduced condition (figure 79).

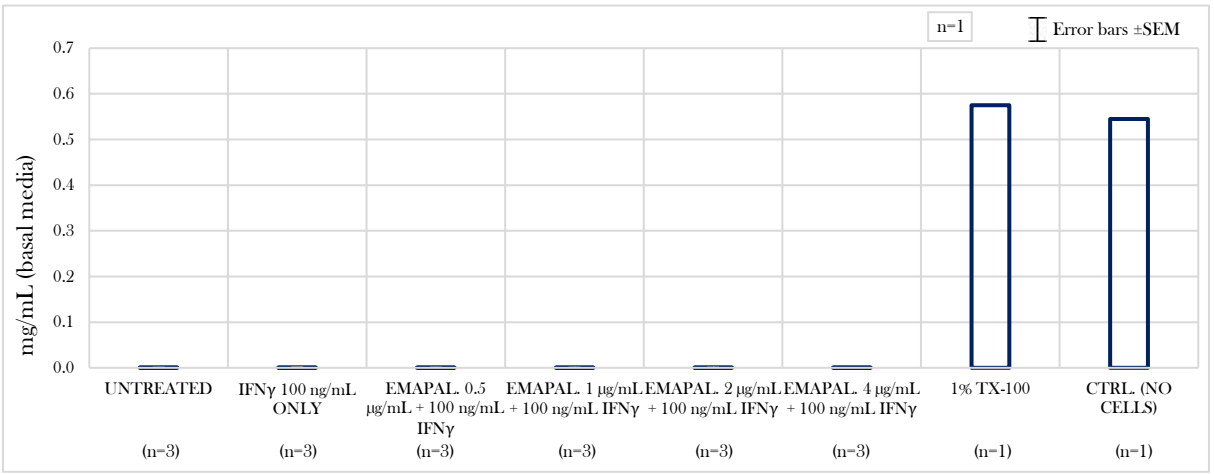

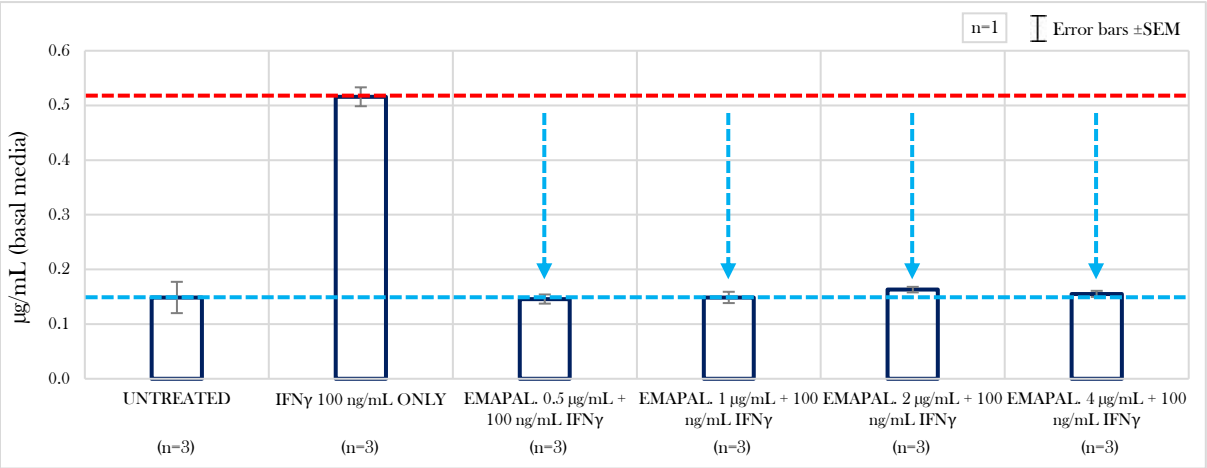

Figure 79: Titration of Emapalumab: FD4 assay. Positive control of maximal permeability (TW with no cells and monolayers treated with 1% TX-100) in mg/mL (upper graph). Average values in µg/mL for the six conditions ("untreated", "IFNγ alone", "co-treatment with Emapalumab at 0.5, 1, 2 and 4 µg/mL") at 24 hrs post-induction induction, for a single biological replica with three technical replicas per condition (lower graph). Error bars ±SEM.

The LDH assay showed no increase of cytotoxicity in any experimental condition. This result resembled what was observed in the experiment IIIc and also demonstrated that the working concentrations of Emapalumab determined no undesired effect (figure 80).

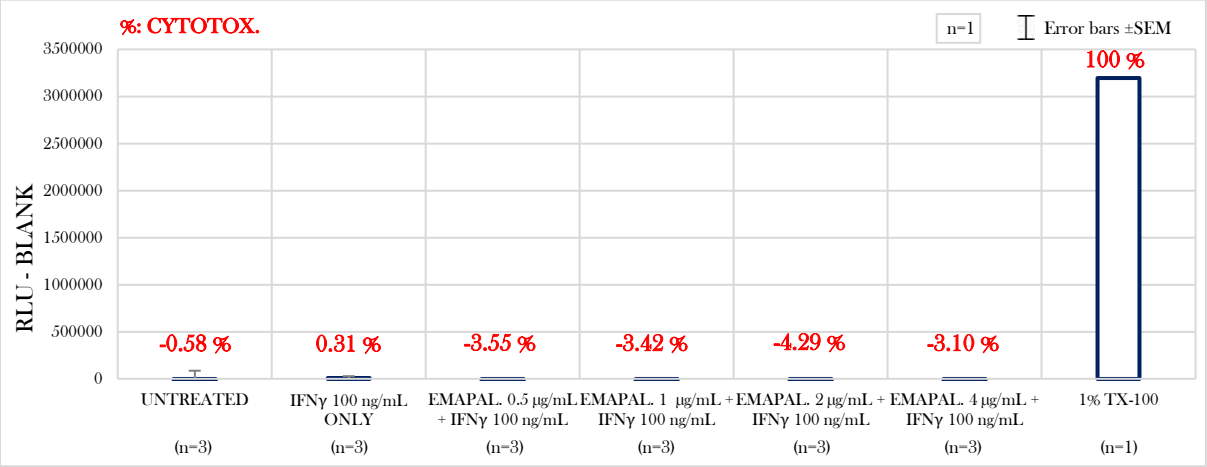

Figure 80: Titration of Emapalumab: LDH assay. RLUs of the different conditions subtracted to the blank. In red the percentage of Necrosis/Necroptosis normalized to a control of maximal cell membrane lysis. One biological replica with three technical replicas per condition. Error bars ±SEM.

Considering the overall outcome of the experiment of titration of Emapalumab in the presence of IFNγ at 100 ng/mL, I chose the concentration 4 µg/mL to continue working with, given the fact that it determined the highest protection at the level of the TEER. All concentrations determined comparable levels of protection in all assays and no unwanted effect of cytotoxicity was observed.

4.5.1.2. Full competitive antagonism of IFNγ with regards to barrier function by neutralizing the ligand in solution: Emapalumab at the optimal working concentration

Once defined 4 µg/mL as the optimal concentration of Emapalumab in the specific experimental conditions, the full neutralization of the the IFNγ signalling was repeated in three biological replicas (figure 81).

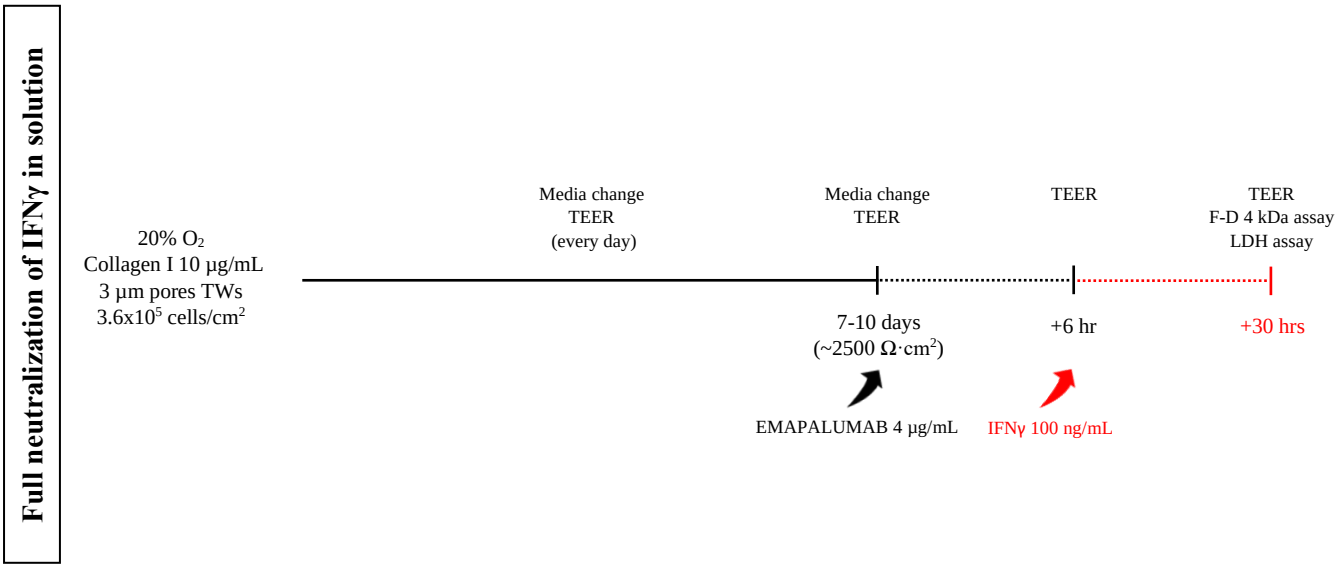

Figure 81: Schematic representation of the replication of the modulation with the optimal concentration of Emapalumab pre-applied for 6 hrs on fully differentiated monolayers (~2500 Ω·cm^2), which were then induced with IFNγ 100 ng/mL for 24 hrs, in normoxia. In red are indicated the time frames during which the monolayers were stimulated with the cytokine from the basolateral side. Note: the different time frames depicted in the temporal axis are not in scale.

The measurement of the TEER demonstrated a full protection towards the impairment determined by IFNγ. The average values for the three biological replicas showed a drop of resistance determined by IFNγ applied alone to 69.68 % of the untreated condition, whereas the co-treatment with Emapalumab at 4 µg/mL brought to a value slightly higher (105.4 %) than the one of the untreated condition (figure 82). Notwithstanding the full protection and in line with the experiment IIIc, no difference in between the three conditions was statistically significant ($p>0.05$, two-sided paired t-test, n=3).

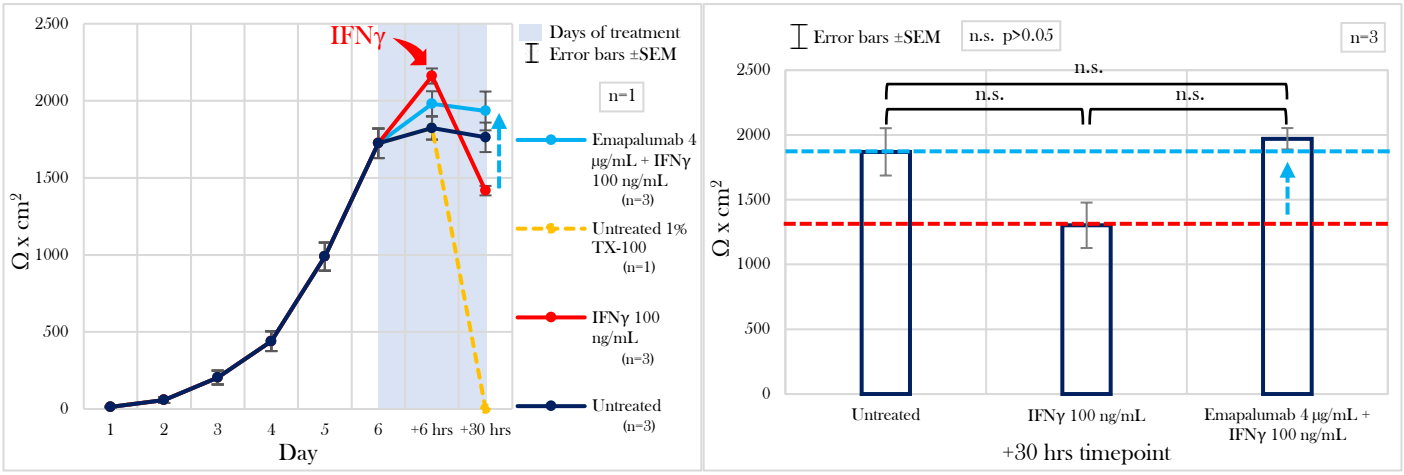

Figure 82: Full neutralization of IFNγ in solution: TEER measurements. Ω x cm² values over time from a single representative biological replica with three technical replicas per condition (left graph). Average values for the three conditions ("untreated", "IFNγ alone" and "co-treatment with Emapalumab at 4 µg/mL") at 24 hrs post-induction induction, for n=3 (right graph). Significance stated by a two-sided paired t-test. Error bars ±SEM.

The FD4 permeability assay demonstrated an almost full protection towards the increase of permeability determined by IFNγ applied alone (1.36 times higher than the one for the untreated condition) (figure 83). Also at this level, notwithstanding the observed full protection and in line with the experiment IIIc, no difference in between the three conditions was statistically significant (p>0.05, two-sided paired t-test, n=3).

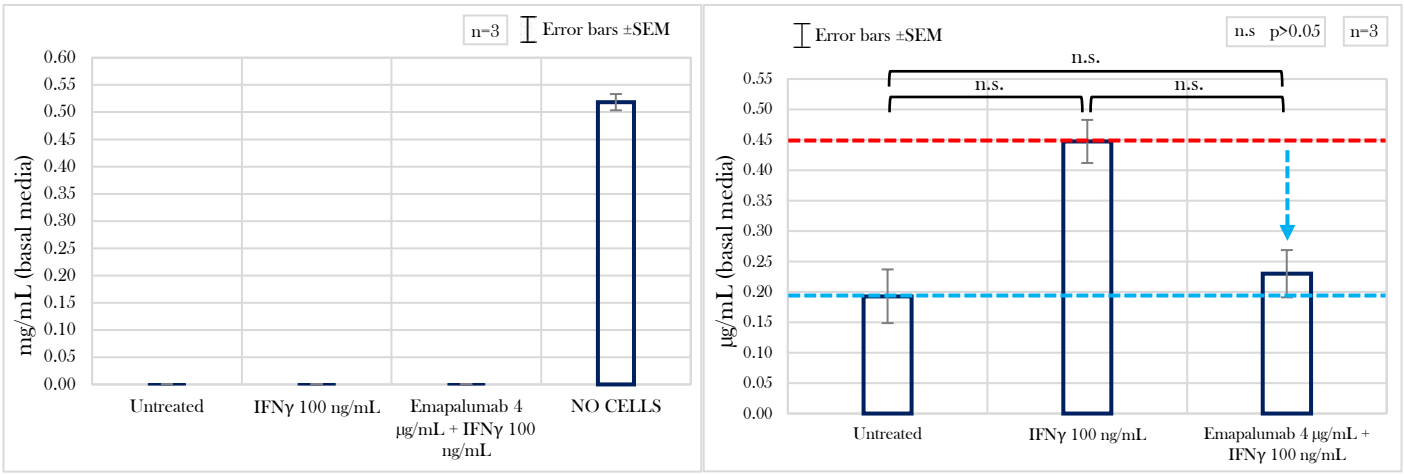

Figure 83: Full neutralization of IFNγ in solution: FD4 assay. Positive control of maximal permeability (TW with no cells) in mg/mL (left graph). Average values in µg/mL for the three conditions ("untreated", "IFNγ alone" and "co-treatment with Emapalumab at 4 µg/mL"), for n=3 (right graph). Significance stated by a two-sided paired t-test. Error bars ±SEM.

The LDH assay showed that the decrease of LHD in the apical media determined by IFNγ alone (the same one observed in the experiment IIIc) was not restored by the co-treatment with Emapalumab at 4 µg/mL, as I would have expected (figure 84). The pairwise differences in between the values of all conditions were not statistically significant (p>0.05, two-sided paired t-test, n=3).

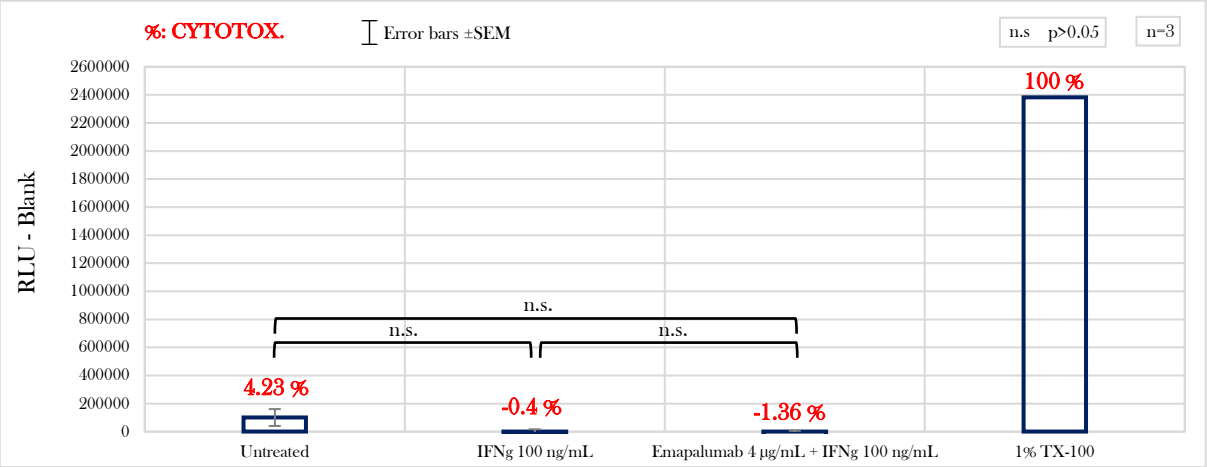

Figure 84: Full neutralization of IFNγ in solution: LDH assay. RLUs of the different conditions subtracted to the blank. In red the percentage of Necrosis/Necroptosis normalized to a control of maximal cell membrane lysis. Significance stated by a two-sided paired t-test for n=3. Error bars ±SEM.

4.5.1.3. Competitive orthosteric antagonism of INGR1: titration of α-INGR1/CD119

A second control experiment that aimed to completely shut down the IFNγ singnaling in my *in vitro* model consisted on the competitive orthosteric antagonism of IFN-γR1 (or INGR1, the monomer that contains the ligand-binding site in the INGR1/2 functional heteromeric complex) employing the monoclonal antibody α-INGR1/CD119 from R&D Systems (# P15260.1) (see figure 85).

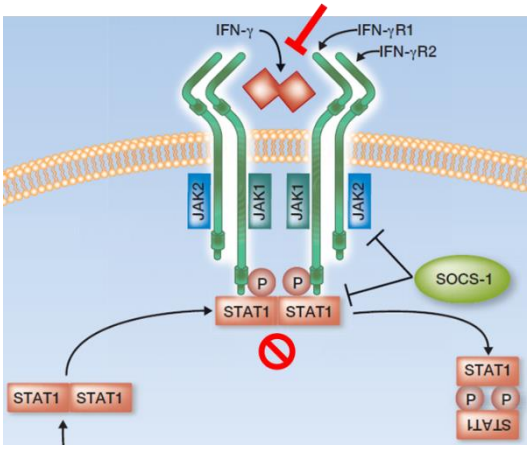

Figure 85: Graphical representation of the mechanism of action of the antibody α-INGR1/CD119 (in red). It can bind and occupy the ligand binding site of INGR1 interfering with the binding of IFNγ. Adapted from Zaidi and Merlino, 2011.

The titration of α-INGR1/CD119 was performed in three different experiments (one biological replica each) and the working plan is schematically summarized in figure 86.

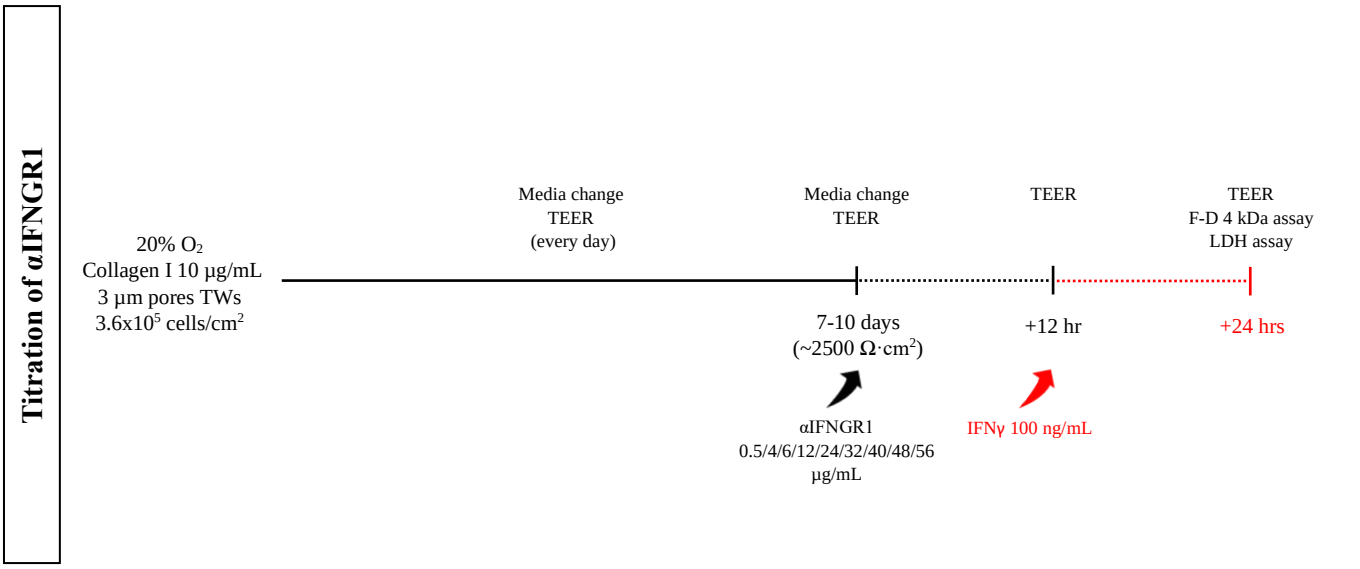

Figure 86: Schematic representation of the titration experiment for α-INGR1/CD119 on fully differentiated monolayers (~2500 Ω·cm^2) induced with IFNγ 100 ng/mL for 24 hrs, in normoxia. In red are indicated the time frames during which the monolayers were stimulated with the cytokine from the basolateral side. Note: the different time frames depicted in the temporal axis are not in scale.

The initial (lowest) titration points (0.5, 4 and 6 µg/mL) were defined in accordance to the literature[82] and the results of this first experiment are not included. The TEER measurements showed that none of the applied concentrations of α-INGR1/CD119 determined a barrier function protection against the impairment caused by IFNγ alone. Disregarding this, the TEER values slightly increased in a dose-dependent manner among the monolayers co-treated with the different concentrations of α-INGR1/CD119. Even though no protection was observed at the TEER level, a slight barrier function protection was observed at the level of the FD4 permeability assay following a dose-response effect (opposite to the one observed by measuring the TEER). As explained in the Introduction, changes in permeability towards ions are not always reflected by changes in permeability towards the FD4 (especially when they are subtle, as in this case). The LDH assay showed a decrease of LDH on the apical media of the monolayers treated with IFNγ only, as observed in the previous experiments performed with this cytokine. The monolayers co-treated with α-INGR1/CD119 showed comparable values to the ones observed for the "IFNγ only" condition.

As the first range of concentrations tested did not determine a significant barrier protective effect, I decided to shift the titration range upwards and test the concentrations 12, 48 and 48 µg/mL in a biological replica. The TEER measurement showed this time a clear barrier protective effect determined by the new set of concentrations (figure 87). IFNγ applied alone determined a drop to 48.7 % of the untreated condition, whereas the co-treatment with α-INGR1/CD119 at 12 µg/mL determined a drop to 69.38 %, at 24 µg/mL to 81.36 % and at 48 µg/mL to 67.13 % of the untreated condition. A clear dose-response effect was not observed as the protection determined by the highest concentration tested was of a lesser extent that the one determined by the two lower concentrations.

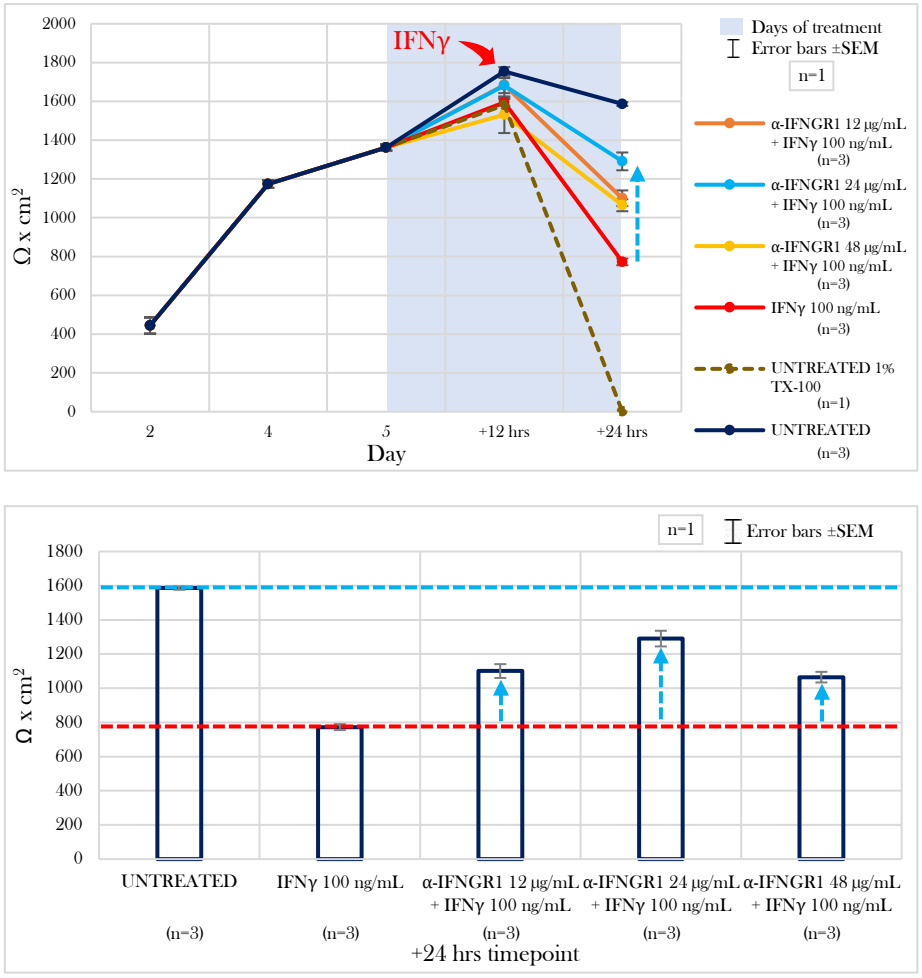

Figure 87: Second titration of α-INGR1/CD119: TEER measurements. Ω x cm² values over time from the single biological replica with three technical replicas per condition (upper graph). Average values for the five conditions ("untreated", "IFNγ alone", "co-treatment with α-INGR1/CD119 at 12, 24 and 48 µg/mL") at 24 hrs post-induction induction for a single biological replica with three technical replicas per condition (lower graph). Error bars ±SEM.

The FD4 permeability assay showed also a clear barrier-protective effect, comparable at all tested concentrations (figure 88). IFNγ applied alone determined a permeability towards this molecular species 1.2-fold higher than the one measures for the untreated condition. The co-treatments with α-INGR1/CD119 determined a permeability ±0.5-fold higher than the one of the untreated monolayers.

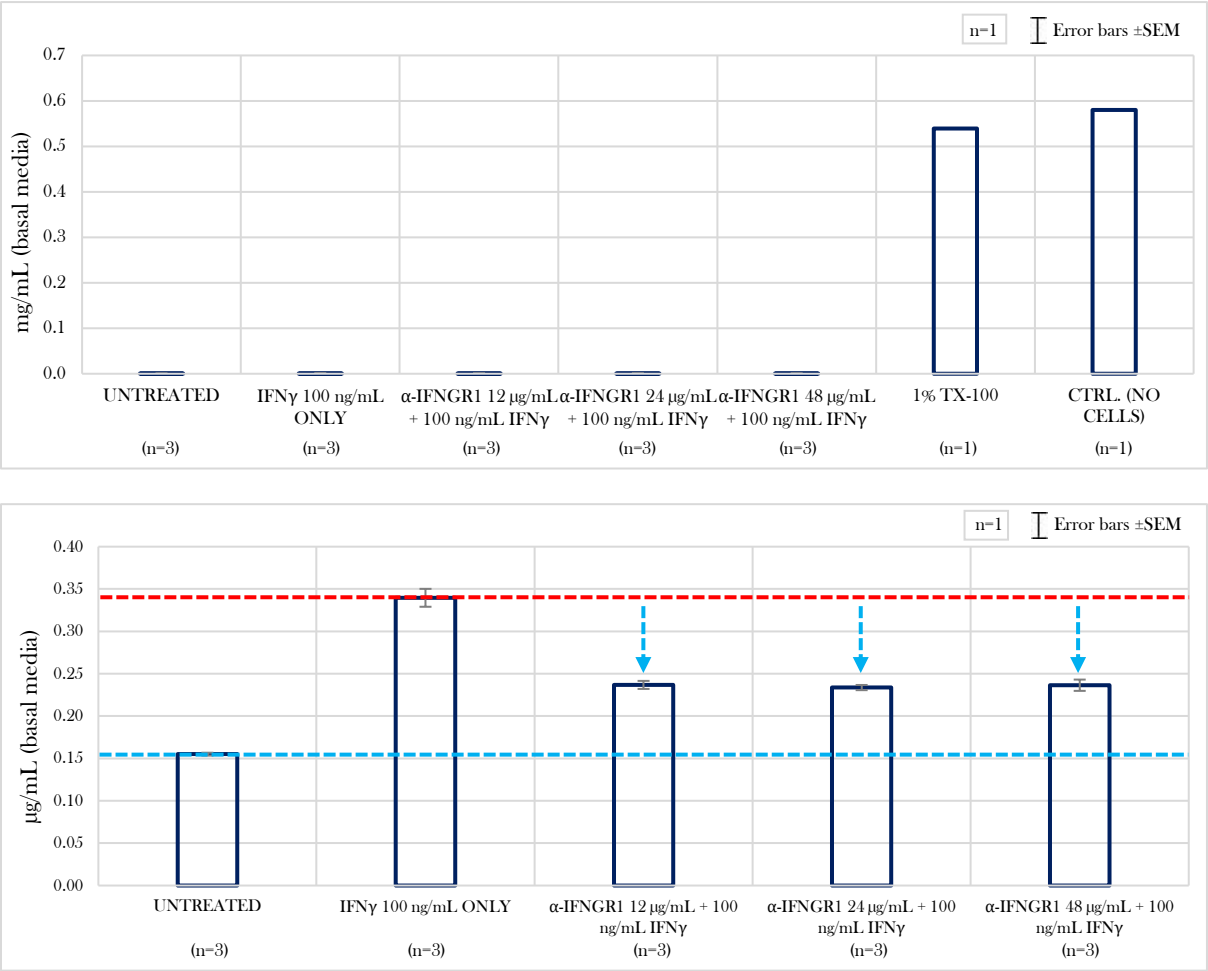

Figure 88: Second titration of α-INGR1/CD119: FD4 assay. Positive control of maximal permeability (TW with no cells and monolayers treated with 1% TX-100) in mg/mL (upper graph). Average values in µg/mL for the six conditions ("untreated", "IFNγ alone", "co-treatment with α-INGR1/CD119 at 12, 24 and 48 µg/mL") at 24 hrs post-induction induction, for a single biological replica with three technical replicas per condition (lower graph). Error bars ±SEM.

The LDH assay showed a drop of LDH in the apical media from 11.11 % on the untreated monolayers to 3.91 % at the monolayers treated only with IFNγ, in line with the previous experiments. This drop was not reversed by any of the co-treatments with α-INGR1/CD119, all of which showed very low levels of LDH (figure 89).

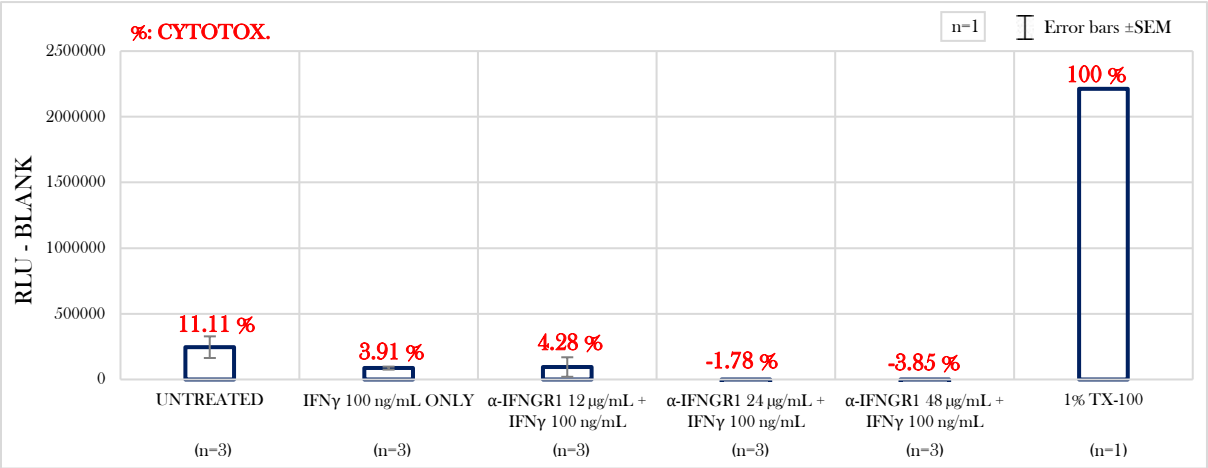

Figure 89: Second titration of α-INGR1/CD119: LDH assay. RLUs of the different conditions subtracted to the blank. In red the percentage of Necrosis/Necroptosis normalized to a control of maximal cell membrane lysis. One biological replica with three technical replicas per condition. Error bars ±SEM.

As the concentrations tested in the second experiment of titration did not determine an unwanted cytotoxic effect, I decided to extend the range to higher values, meaning 24, 32, 40 and 56 µg/mL, running the experiment in one biological replica. As the experiment did not show a clear overall improvement of the barrier protection, the results were included in the Supplementary Material (Figures S15 to S17). The TEER measurements showed, at first glance, that the untreated monolayers underwent a (random) drastic decrease of resistance from the timepoint +12 hrs to the timepoint + 24 hrs. The tested concentrations of α-INGR1/CD119 determined a barrier protective effect which followed a dose-response fashion. The FD4 permeability assay showed that all concentrations determined a comparable barrier-protective effect, and a clear dose-response effect was not observed at this level. Finally, the LDH assay showed basal levels of LDH (comparable to the levels present in the blank) in the apical media for all the experimental conditions. By subtracting the blank, all RLU values became negative and the conditions treated with IFNγ showed values more negative than the one for the untreated condition, which meant lower levels of LDH. So the outcome was in line with the previous results.

4.5.2. Pharmacological interference experiments for the characterization of the TNFα/TNR1A/TNR1B signalling axis

4.5.2.1. Competitive antagonism of sTNFα with regards to barrier function by neutralizing the ligand in solution: titration of Adalimumab

A first pharmacological interference experiment concerning the TNFα/TNR1A/TNR1B signalling axis in my *in vitro* model, consisted of a control of full neutralization of sTNFα in solution. This was done employing Adalimumab, an α-s/mTNFα monoclonal antibody that can bind to the N-terminal portion of both sTNFα and mTNFα, neutralizing their activity before they can engage the cognate receptors (figure 90).

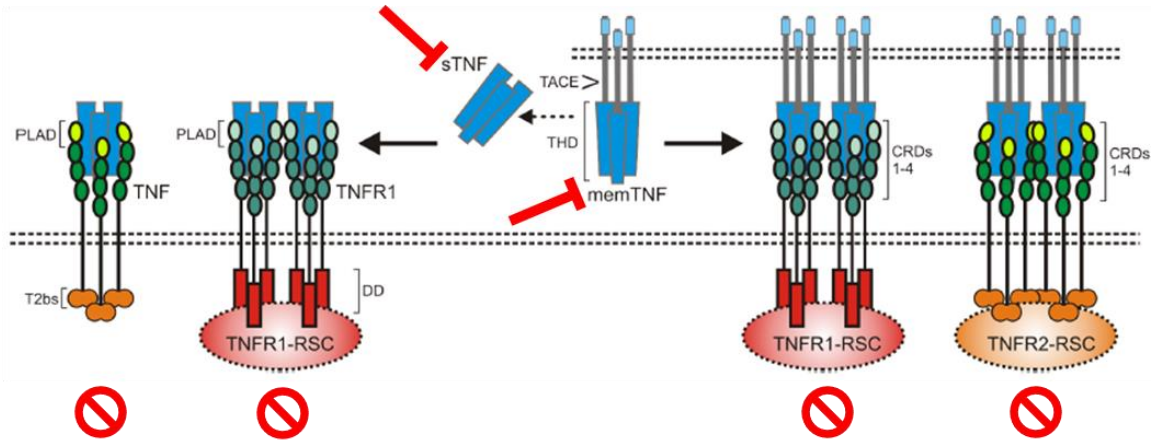

Figure 90: Graphical representation of the mechanisms of action of the antibody Adalimumab (in red). It can bind either to the free sTNFα and to the free mTNFα, completely shutting down the whole TNFα signalling. Adapted from Wajant and Siegmud, 2019.

In order to establish the optimal working concentration of Adalimumab for a maximal neutralization of sTNFα with regards to barrier function, I defined a set of concentrations from the literature[82] and adapted them to my working conditions (100 ng/mL of sTNFα; T84 cell line at fully differentiating conditions). The titration of Adalimumab was performed in one biological replica, in normoxia, as schematically depicted in figure 91. A pre-treatment for 12 hrs with the concentrations 2.4, 4.8, 9.6, 19.2 and 24 µg/mL of Adalimumab was followed by an induction (co-treatment) for other 12 hrs with sTNFα at 100 ng/mL. At the timepoint +24 hrs, the TEER was measured and the FD4 and the LDH assays were performed.

Titration of Adalimumab

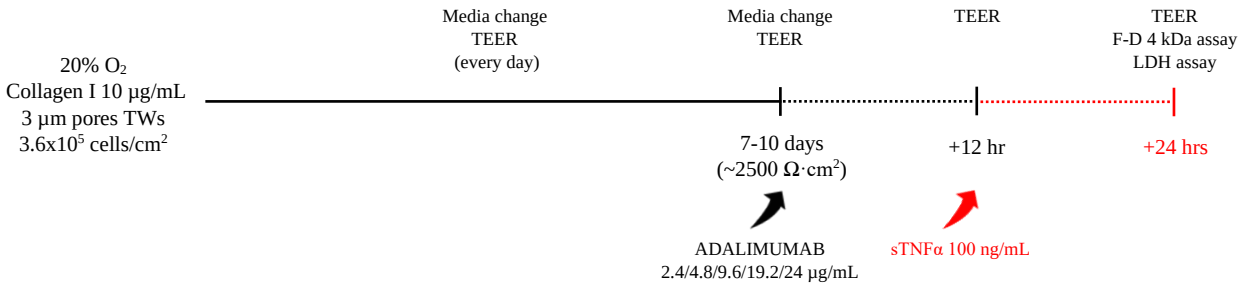

Figure 91: Schematic representation of the titration experiment for Adalimumab on fully differentiated monolayers (~2500 Ω·cm^2) induced with sTNFα 100 ng/mL for 12 hrs, in normoxia. In red are indicated the time frames during which the monolayers were stimulated with the cytokine from the basolateral side. Note: the different time frames depicted in the temporal axis are not in scale.

The results obtained by measuring the TEER showed that all concentrations of Adalimumab fully protected the drop of resistance determined by sTNFα alone to 10.64 % of the untreated condition. The co-treatment with Adalimumab at 2.4 µg/mL brought the TEER to 95.57 %, at 4.8 µg/mL to 106.97 %, at 9.6 µg/mL to 103.13 %, at 19.2 µg/mL to 106.4 %, and at µg/mL 24 to 108.72 % of the untreated condition (figure 92). A random decrease of TEER was observed for all conditions from the timepoint +12 hrs to the timepoint +24 hrs. As explained before this usually takes place at fully differentiated conditions, so was not taken into consideration (as also took place in the untreated condition).

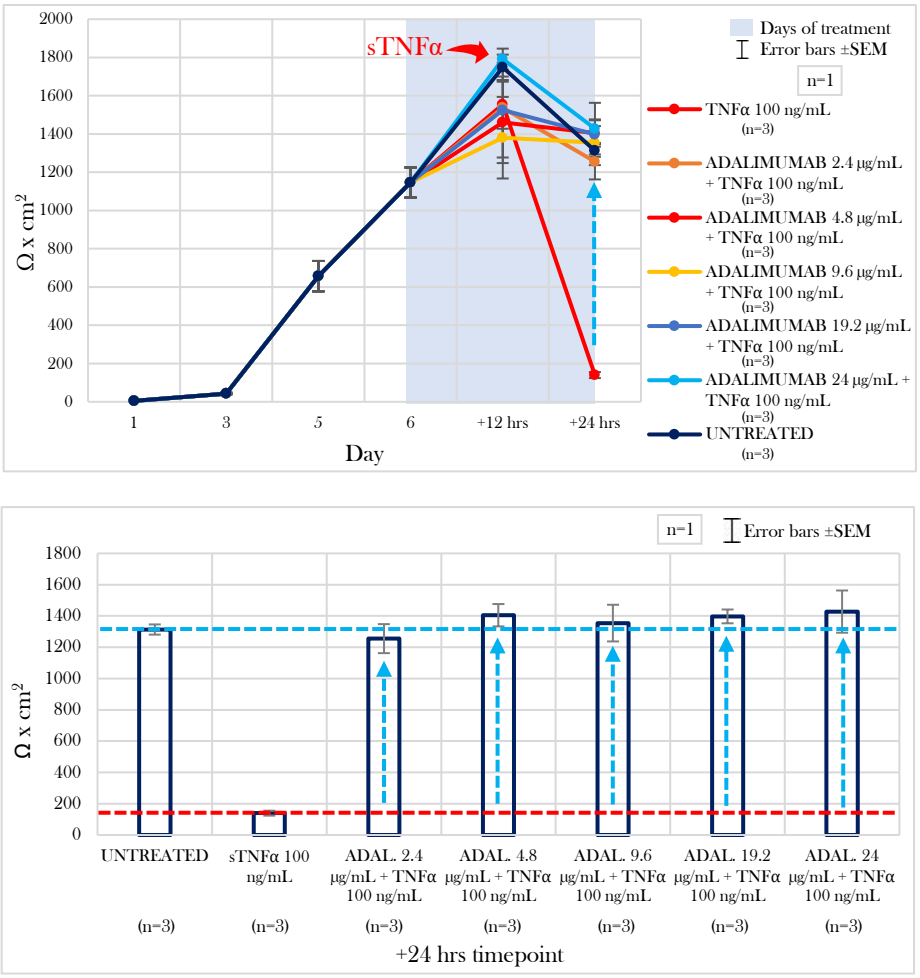

Figure 92: Titration of Adalimumab: TEER measurements. Ω x cm² values over time from the single biological replica with three technical replicas per condition (upper graph). Average values for the seven conditions ("untreated", "sTNFα alone", "co-treatment with Adalimumab at 2.4, 4.8, 9.6, 19.2 and 24 µg/mL") at 12 hrs post-induction induction, for a single biological replica with three technical replicas per condition (lower graph). Error bars ±SEM.

The FD4 permeability assay showed the same outcome of full barrier function protection at every concentration tested. sTNFα applied alone determined an increase of permeability of 0.86-fold with regards to the uninduced condition, the co-treatments with Adalimumab at all tested concentrations determined no significant increase of permeability with regards to the uninduced condition (figure

93). Minor increases in permeability (Adalimumab at 9.6 and 24 µg/mL) could have been determined by a minimal experimental error.

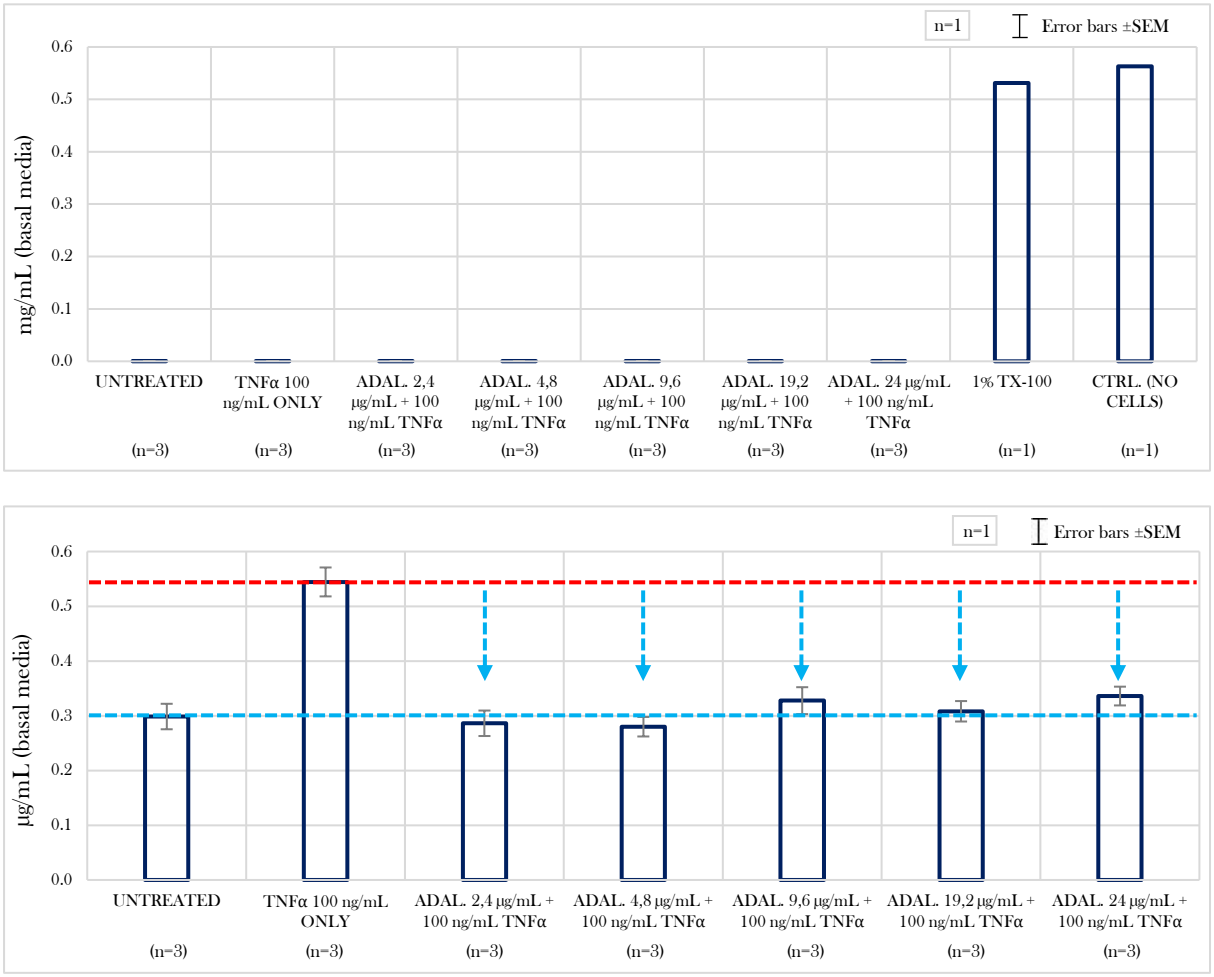

Figure 93: Titration of Adalimumab: FD4 assay. Positive control of maximal permeability (TW with no cells and monolayers treated with 1% TX-100) in mg/mL (upper graph). Average values in µg/mL for the seven conditions ("untreated", "sTNFα alone", "co-treatment with Adalimumab at 2.4, 4.8, 9.6, 19.2 and 24 µg/mL") at 12 hrs post-induction induction, for a single biological replica with three technical replicas per condition (lower graph). Error bars ±SEM.

The LDH assay consented me to not only assess the effect of the pharmacological modulation with regards to the pro-necroptotic effect determined by sTNFα (experiment IIIc), but also to monitor for an eventual unwanted cytotoxic (mainly Necrosis) effect, determined by the tested concentrations (figure 94). An increase of 4.37 % of LDH (normalized to the positive control) was determined by sTNFα, comparing to the untreated condition. This increase was not observed in any of the conditions of co-treatment with Adalimumab (at 2.4 µg/mL there was a slight increase but not significant due to the high variance within the three technical replicas).

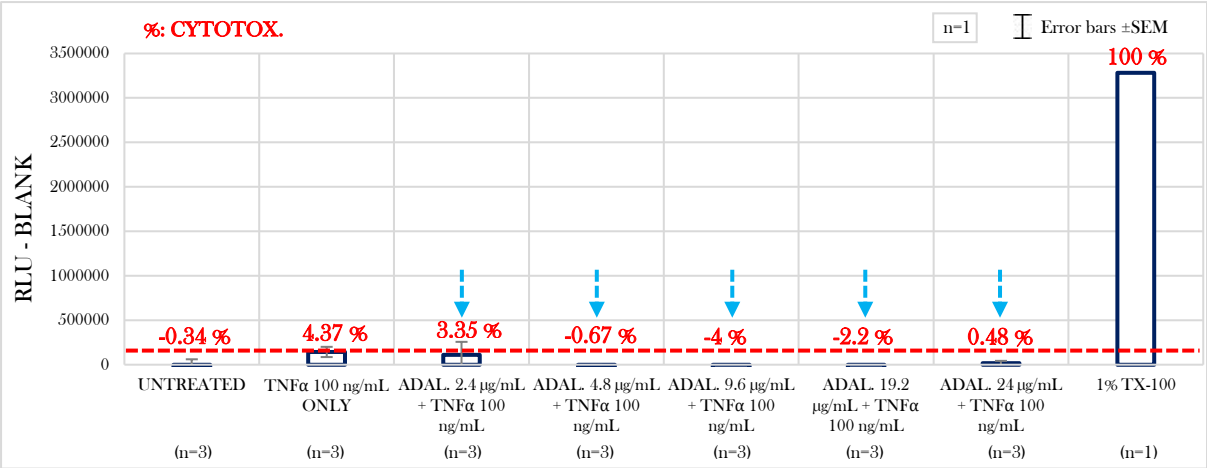

Figure 94: Titration of Adalimumab: LDH assay. RLUs of the different conditions subtracted to the blank. In red the percentage of Necrosis/Necroptosis normalized to a control of maximal cell membrane lysis. One biological replica with three technical replicas per condition. Error bars ±SEM.

The titration of Adalimumab demonstrated that all tested concentrations were equally effective in protecting the shifts determined by the induction with sTNFα: the drop of TEER, the increase of permeability towards FD4 and the increase of LDH in the apical media. The protections observed with all assays were complete; a nullification of the effects determined by sTNFα was determined by Adalimumab. I decided to continue working with the concentration 24 µg/mL as it determined the highest protection at the level of the TEER.

4.5.2.2. Full competitive antagonism of sTNFα with regards to barrier function by neutralizing the ligand in solution: Adalimumab at the optimal working concentration

Once the optimal working concentration was defined, I performed a pilot experiment (one biological replica) of full protection but slightly changing the experimental design followed for the titration experiment. Given the fact that the induction with sTNFα for 24 hrs determines milder effects than for a 12 hrs induction as explained before, I decided to abandon this experimental design but the results are worth to be shown (see Figure S18 to S21 of the Supplementary Material), as they confirm the outcome of the titration experiment at the highest concentration. In this pilot experiment, fully differentiated monolayers were pre-treated with Adalimumab at 24 µg/mL for 6 hrs (equilibration time) and then co-treated with sTNFα at 100 ng/mL for 24 hrs. The measurement of the TEER and the FD4 permeability assay showed an almost full protection towards the barrier function impairment determined by sTNFα applied alone. The LDH assay showed a not so prominent increase of LDH in the apical media upon induction with sTNFα alone for 24 hrs comparing to the untreated condition (in line with the experiment IIIc). A decrease of LDH (anti-necroptotic effect) was observed upon co-treatment with Adalimumab at 24 µg/mL.

The results of the experiment of full neutralization of sTNFα with Adalimumab at 24 µg/mL, with an induction time of 24 hrs, was a first replication and confirmation of the outcome of the titration experiment. To accordingly replicate the full neutralization of sTNFα and assess if the barrier function protective effects reached a statistical significance, the same experimental pipeline applied for the titration experiment was followed in three biological replicas (figure 95). In this experiment, total RNA was isolated at the timepoint +24 hrs for the different conditions, in order to perform whole cell transcriptomic analyses by RNAseq.

Full neutralization of sTNFα in solution

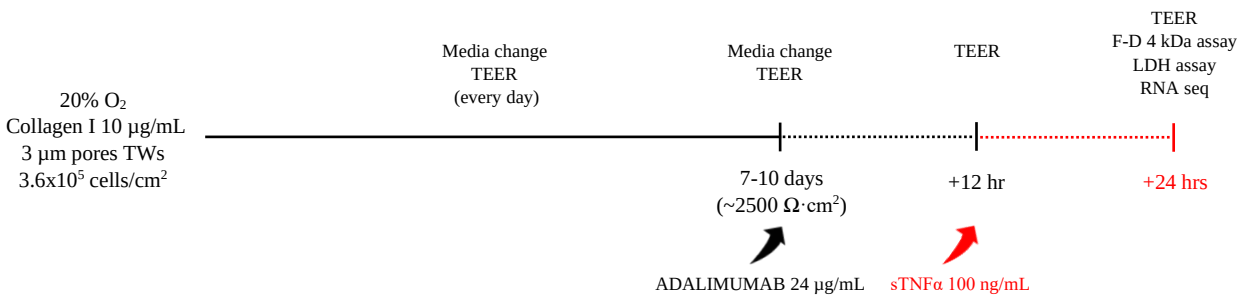

Figure 95: Schematic representation of the replication of the modulation with the optimal concentration of Adalimumab pre-applied for 12 hrs on fully differentiated monolayers (~2500 Ω·cm^2), which were then induced with sTNFα 100 ng/mL for 12 hrs, in normoxia. In red are indicated the time frames during which the monolayers were stimulated with the cytokine from the basolateral side. Note: the different time frames depicted in the temporal axis are not in scale.

The measurement of the TEER showed that the modulation with Adalimumab determined a full protection towards the impairment determined by sTNFα (figure 96). The average values for the three biological replicas showed a drop of resistance determined by sTNFα applied alone to 41.7 % of the untreated condition (drop of 58.3 %), and the co-treatment with Adalimumab at 24 µg/mL maintained the average TEER value at the same level (100.74 %) of the untreated condition. The difference observed in between the average values of the condition of co-treatment with Adalimumab at 24 µg/mL and the condition of induction with the sole sTNFα was statistically significant ($p \leq 0.05$, two-sided paired t-test, n=3). Was non-statistically significant the minimal difference in between the average values of the untreated condition and the condition of co-treatment with Adalimumab at 24 µg/mL ($p > 0.05$, two-sided paired t-test, n=3).

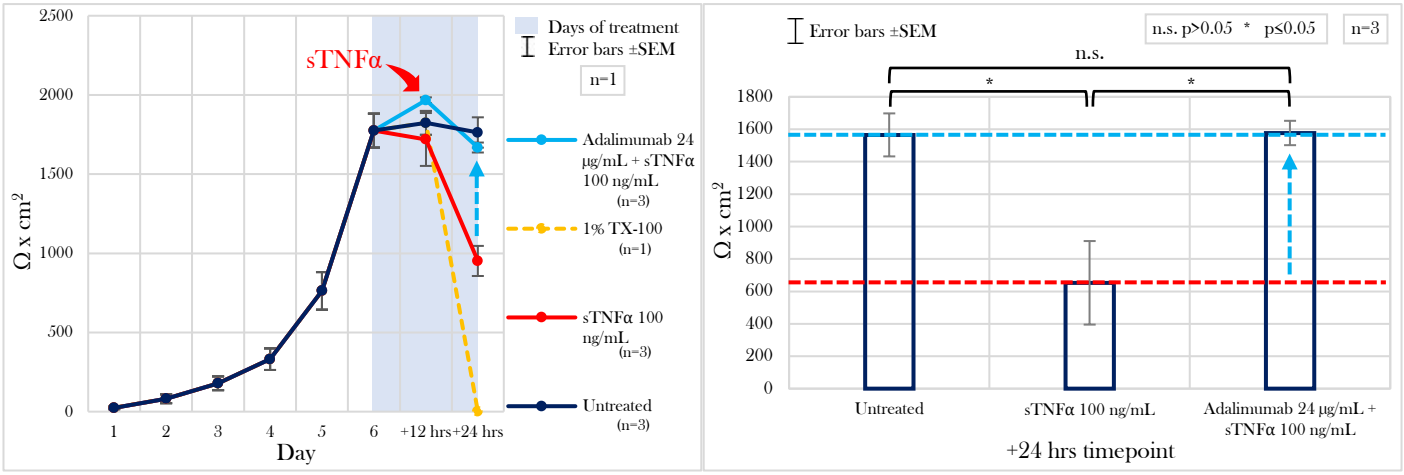

Figure 96: Full neutralization of sTNFα in solution: TEER measurements. Ω x cm² values over time from a single representative biological replica with three technical replicas per condition (left graph). Average values for the three conditions ("untreated", "sTNFα alone" and "co-treatment with Adalimumab at 24 µg/mL") at 12 hrs post-induction induction, for n=3 (right graph). Significance stated by a two-sided paired t-test. Error bars ±SEM.

A similar outcome was obtained with the FD4 permeability assay (figure 97). The average values of permeability showed a 1.08-fold increase determined by sTNFα applied alone with respect to the untreated condition. The co-treatment with Adalimumab at 24 µg/mL determined an average increase of permeability of only 0.13-fold with respect to the untreated condition (which represented only 12 % of the increase determined by sTNF applied alone). The difference observed in between the average values of the condition of co-treatment with Adalimumab at 24 µg/mL and the condition of induction with the sole sTNFα was statistically significant ($p \leq 0.01$, two-sided paired t-test, n=3). There was no difference in between the average values of the untreated condition and the condition of co-treatment with Adalimumab at 24 µg/mL ($p > 0.05$, two-sided paired t-test, n=3).

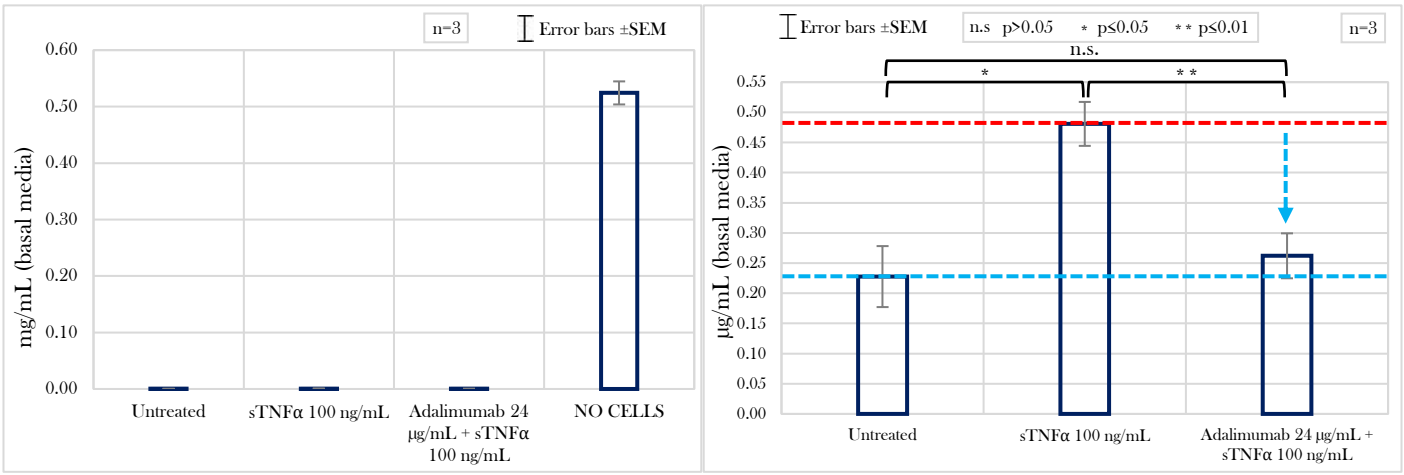

Figure 97: Full neutralization of sTNFα in solution: FD4 assay. Positive control of maximal permeability (TW with no cells) in mg/mL (left graph). Average values in µg/mL for the three conditions ("untreated", "sTNFα alone" and "co-treatment with Adalimumab at 24 µg/mL"), for n=3. Significance stated by a two-sided paired t-test (right graph). Error bars ±SEM.

Finally, the LDH assay showed that the co-treatment with Adalimumab at 24 µg/mL determined a complete normalization of the pro-necroptotic effect determined by sTNFα (figure 98). The difference observed in between the average RLU values of the condition of co-treatment with Adalimumab at 24 µg/mL and the condition of induction with the sole sTNFα was statistically significant ($p \leq 0.01$, two-sided paired t-test, n=3). The minimal difference observed in between the average RLU values of the condition of co-treatment with Adalimumab at 24 µg/mL and the untreated condition was non-statistically significant ($p > 0.05$, two-sided paired t-test, n=3).

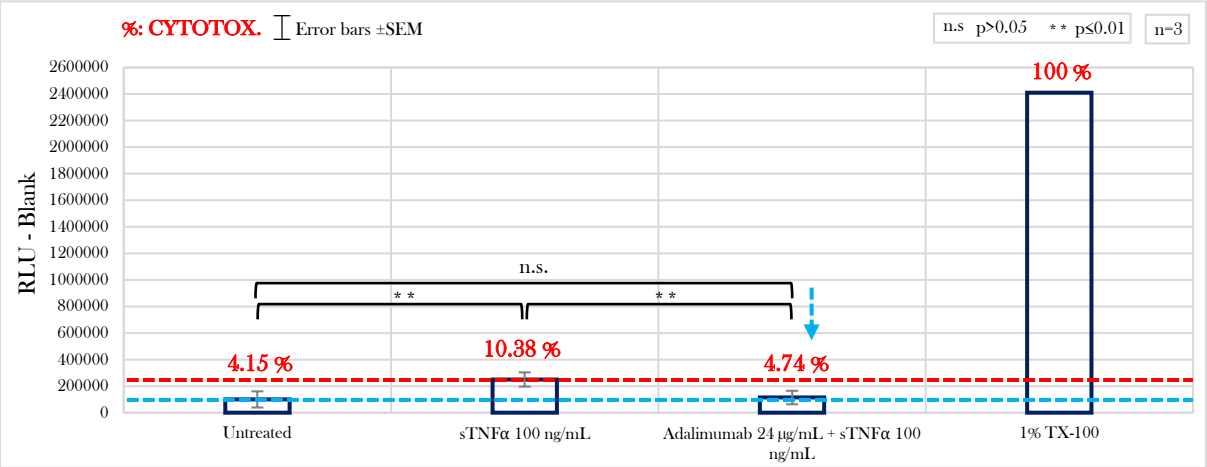

Figure 98: Full neutralization of sTNFα in solution: LDH assay. RLUs of the different conditions subtracted to the blank. In red the percentage of Necrosis/Necroptosis normalized to a control of maximal cell membrane lysis. Significance stated by a two-sided paired t-test for n=3. Error bars ±SEM.

4.5.2.3. Competitive orthosteric antagonism of TNR1A with regards to barrier function: titration of TROS

The selective competitive orthosteric antagonism of TNR1A in the presence of sTNFα (its natural ligand) was performed employing the hTNFR1 Nanobody Alb-70-96 or TNF Receptor-One Silencer (TROS), an inhibitor of the s/mTNFα-hTNFR1 interaction (figure 99). Nanobodies (Nbs) are small antigen-binding fragments derived from camelid heavy-chain antibodies that are devoid of light chains. They have advantages over the classical monoclonal antibodies such as their low molecular mass (42.8 kDa in the case of TROS), low immunogenicity, high affinity, solubility, and stability[61].

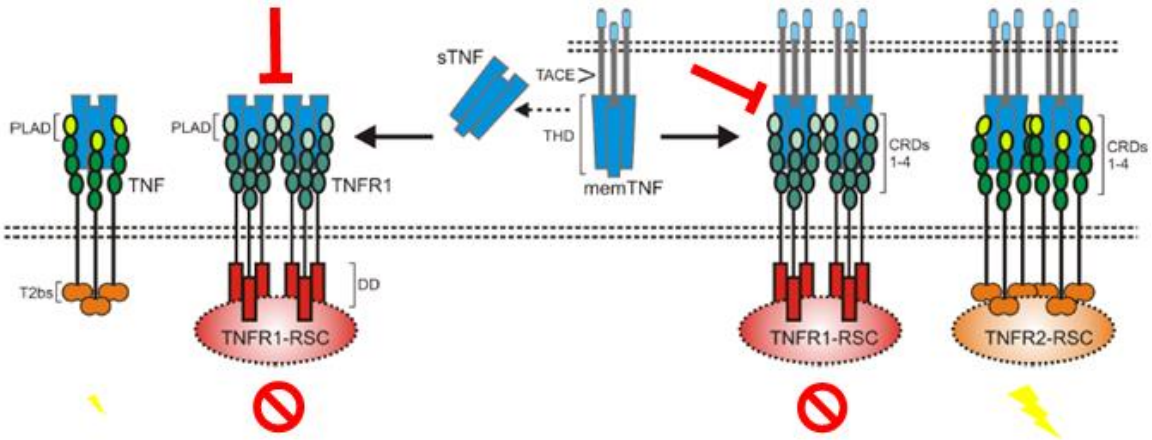

Figure 99: Graphical representation of the mechanisms of action of the Nanobody Alb-70-96 or TNF Receptor-One Silencer (TROS) (in red). It can bind to the ligand binding site of TNR1A interfering in its interaction with both sTNFα and mTNFα. The marginal activation, in the presence of sTNFα, and the full activation, in the presence of mTNFα, of TNR1B are kept (in yellow). Adapted from Wajant and Siegmud, 2019.

The titration of TROS started with a set of concentrations defined in accordance to the literature[61] and adapted to my working conditions (100 ng/mL of sTNFα; T84 cell line at fully differentiating conditions). In three different experiments (of one biological replica each), the working concentrations were gradually increased in order to achieve the optimal one (figure 100). The concentrations tested were 2, 2.5, 3.5, 10, 15, 20 and 30 µM. A pre-treatment with the different concentrations of TROS was performed for 12 hrs, after which a 12 hrs induction and co-treatment with sTNFα was carried out.

Titration of TROS

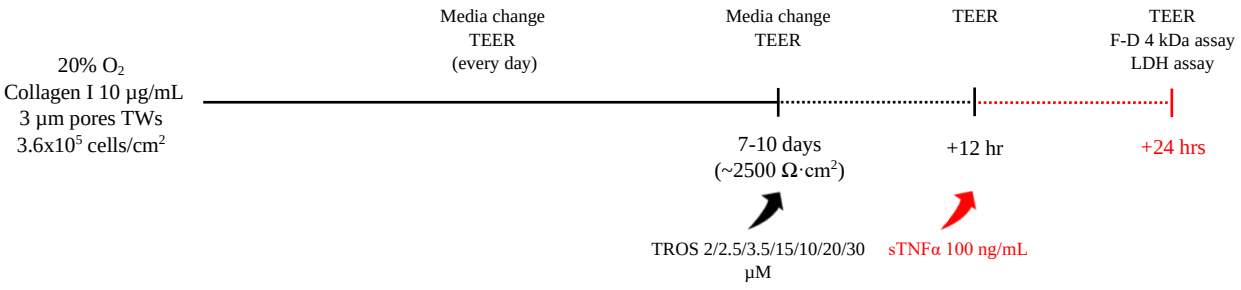

Figure 100: Schematic representation of the titration experiment for TROS on fully differentiated monolayers (~2500 Ω·cm^2) induced with sTNFα 100 ng/mL for 12 hrs, in normoxia. In red are indicated the time frames during which the monolayers were stimulated with the cytokine from the basolateral side. Note: the different time frames depicted in the temporal axis are not in scale.

In a first titration experiment, the concentrations 2, 2.5 and 3.5 µM were tested. The TEER measurements showed no significant protection versus the drop of resistance to 44.11 % of the untreated condition determined by the induction with the sole sTNFα (figure 101). It looked like the TEER values of the co-treatment conditions with TROS slightly increased following a dose-response fashion. A minimal, non-significant, protection versus the drop determined by sTNFα alone was observed for the co-treatment with TROS at 3.5 µM. It is important to notice the decrease of TEER for the untreated condition from the timepoint +12 hrs to the timepoint +24 hrs. As already explained for previous experiments, this random drop is non-informative and can take place at fully differentiated conditions.

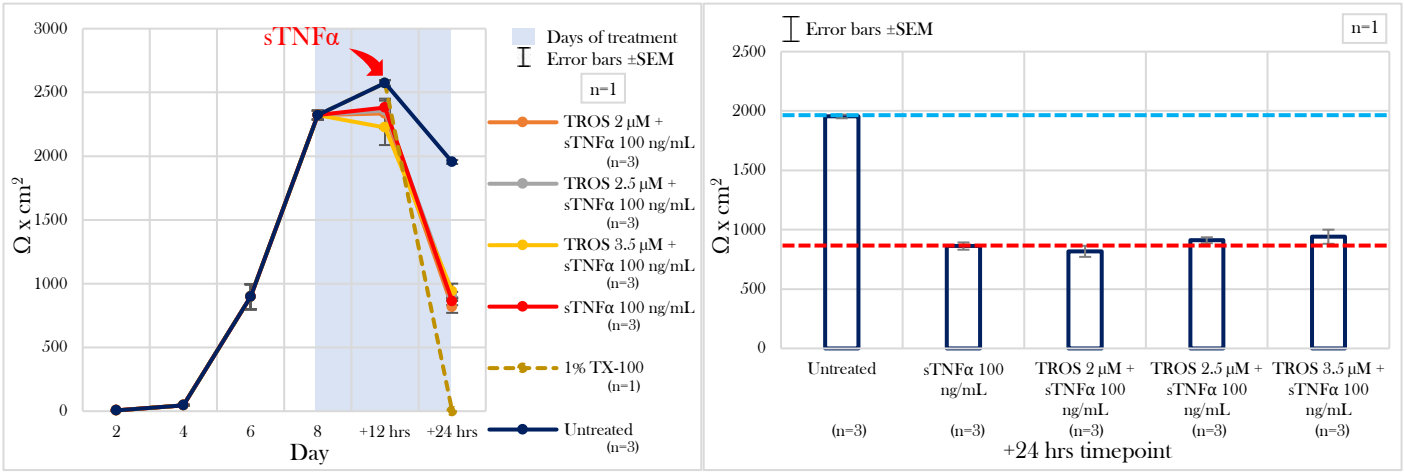

Figure 101: First titration of TROS: TEER measurements. Ω x cm² values over time from the single biological replica with three technical replicas per condition (left graph). Average values for the seven conditions ("untreated", "sTNFα alone", "co-treatment with TROS at 2, 2.5 and 3.5 µM") at 12 hrs post-induction induction, for a single biological replica with three technical replicas per condition (right graph). Error bars ±SEM.

The FD4 permeability assay showed instead a slight protective effect determined by the co-treatments with TROS versus the 1.46-fold increase of permeability determined by sTNFα applied alone, with respect to the untreated condition (figure 102). The co-treatment with TROS at 2 and 2.5 µM determined an increase of permeability of 0.96-fold (65.78 % of the increase determined by sTNF applied alone) with respect to the untreated condition, whereas at 3.5 µM a 1.15-fold increase (78.94 % of the increase determined by sTNF applied alone) was observed. So, the protective effect did not follow a dose-response pattern.

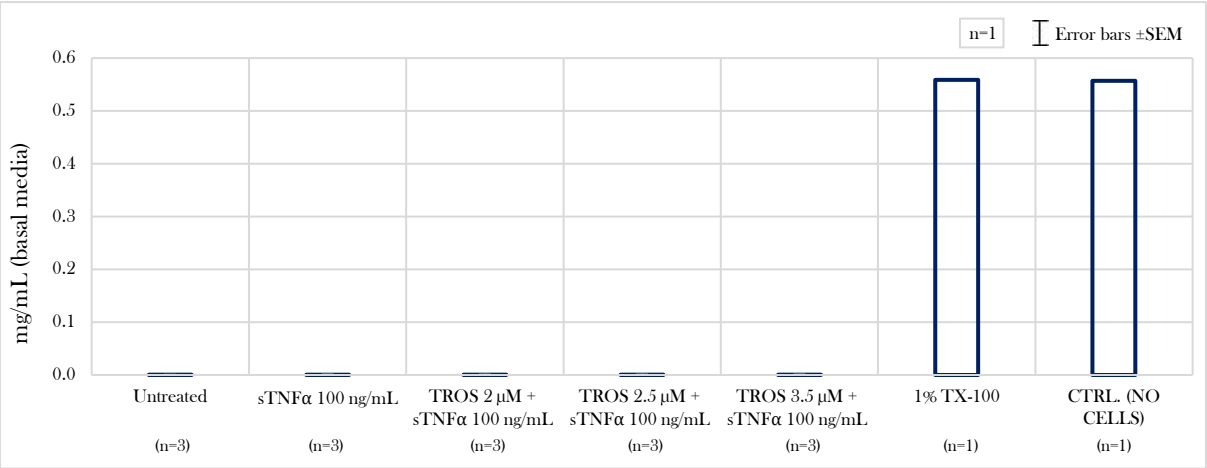

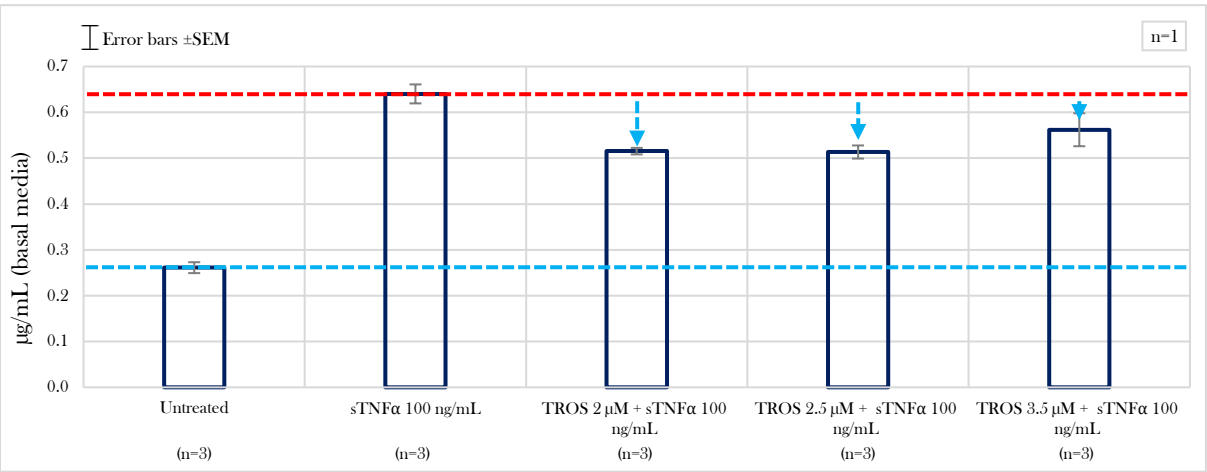

Figure 102: First titration of TROS: FD4 assay. Positive control of maximal permeability (TW with no cells and monolayers treated with 1% TX-100) in mg/mL (upper graph). Average values in µg/mL for the seven conditions ("untreated", "sTNFα alone", "co-treatment with Adalimumab at 2, 2.5 and 3.5 µM") at 12 hrs post-induction induction, for a single biological replica with three technical replicas per condition (lower graph). Error bars ±SEM.

The LDH assay (figure 103) did not show the expected significant increase of LDH in the apical media of the condition treated only with sTNFα with regards to the untreated condition. But a decrease of LDH with respect to the untreated condition (9.69 %) was observed for the co-treatments with TROS at 2.5 (5.23 %) and 3.5 (2.7 %) µM, following a dose-response pattern. Importantly, no cytotoxicity determined by TROS was observed.

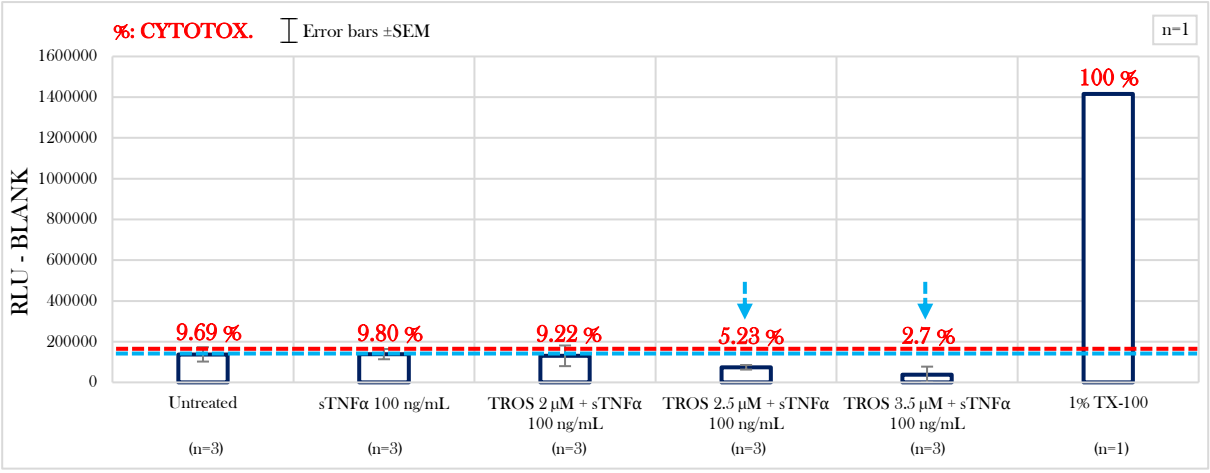

Figure 103: First titration of TROS: LDH assay. The RLUs of the different conditions subtracted to the blank. In red the percentage of Necrosis/Necroptosis normalized to a control of maximal cell membrane lysis. One biological replica with three technical replicas per condition. Error bars ±SEM.

As a result of this first titration experiment, I found no relevant barrier-protective effect at the TEER level determined by the aforementioned concentrations. A mild barrier protective effect at the level of the FD4 assay was observed but without following a dose-response fashion, and a mild anti-necroptotic effect was observed for the two higher concentrations.

Considering that no relevant overall barrier protective effect was determined at the TEER level by the aforementioned concentrations, and the fact that no cytotoxicity was observed, I decided to extend the titration range to much higher values. For doing so, I first had to concentrate the TROS from a stock concentration of 15 µM to higher values of around 150-250 µM in order to accordingly dilute it in the working cell culture media.

The second titration experiment of TROS consisted on the testing of the sole concentration 15 µM (due to a temporary lack of material). The results of this experiment showed that the initial range of concentrations was indeed too low to determine a detectable effect at the level of the overall barrier function of the 2D epithelial-like structure. The co-treatment with TROS at the concentration 15 µM was by far more effective than the previous ones and determined a clear barrier function protection: a drop of TEER of only 10 % with respect to the untreated condition (which could be given by the same random drop observed for the untreated condition from +12 to +24 hrs) versus the 70 % drop determined by sTNFα applied alone (figure 104).

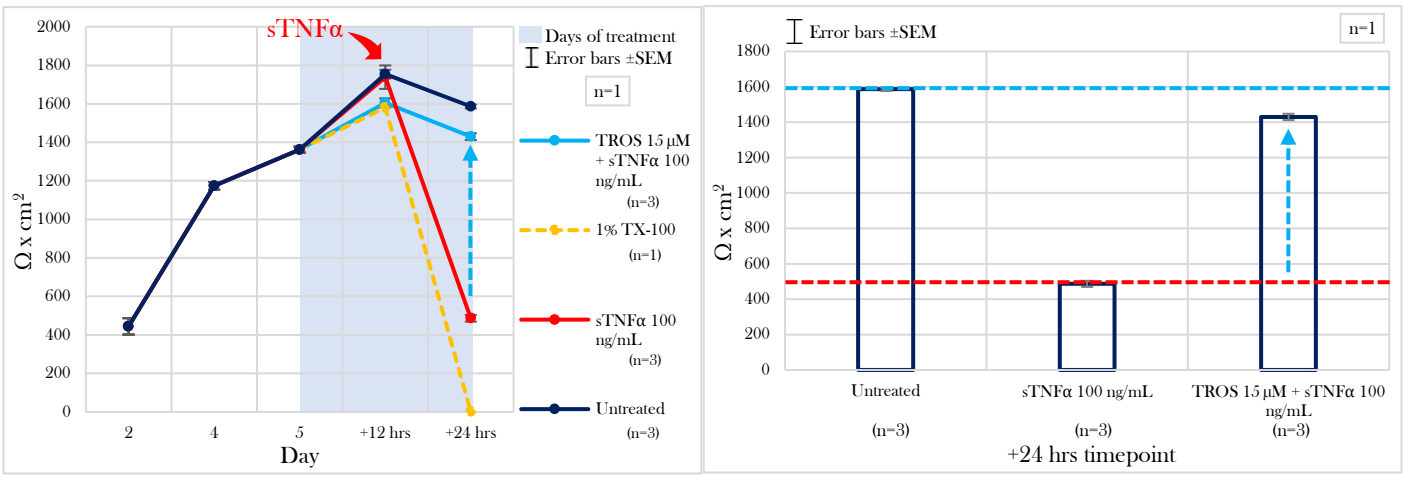

Figure 104: Second titration of TROS: TEER measurements. Ω x cm² values over time from the single biological replica with three technical replicas per condition (left graph). Average values for the three conditions ("untreated", "sTNFα alone", "co-treatment with TROS at 15 µM") at 12 hrs post-induction induction, for a single biological replica with three technical replicas per condition (right graph). Error bars ±SEM.

The FD4 permeability assay showed that sTNFα applied alone determined a 2-fold increase of permeability towards this molecular species with respect to the untreated condition, whereas the co-treatment with TROS 15 µM determined only a 0.8-fold increase. The increase of permeability determined by the co-treatment with TROS represented 40 % of the increase determined by sTNF applied alone, so a reduction of 60 % of the increase determined by the cytokine was observed (figure 105).

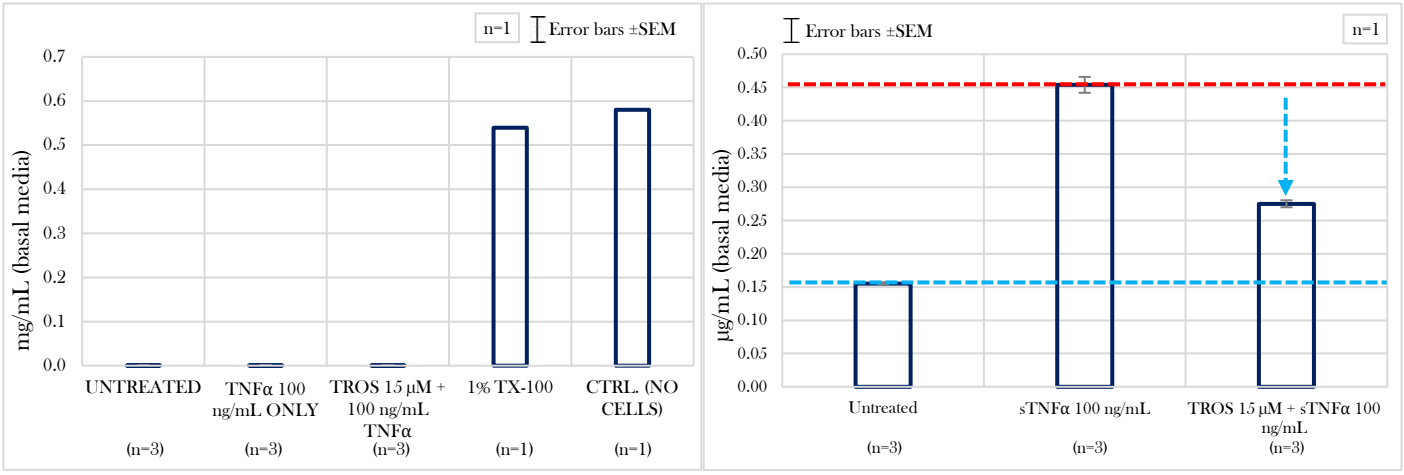

Figure 105: Second titration of TROS: FD4 assay. Positive control of maximal permeability (TW with no cells and monolayers treated with 1% TX-100) in mg/mL (left graph). Average values in µg/mL for the three conditions ("untreated", "sTNFα alone", "co-treatment with TROS at 15 µM") at 12 hrs post-induction induction, for a single biological replica with three technical replicas per condition (right graph). Error bars ±SEM.

The LDH assay showed a complete normalization of the pro-necroptotic effect determined by sTNFα (figure 106). Importantly, no unwanted cytotoxic effect was determined by the working

concentration at the timepoint +24 hrs, and the same could be concluded analyzing the TEER curve from day +5 to the time-point +12 hrs.

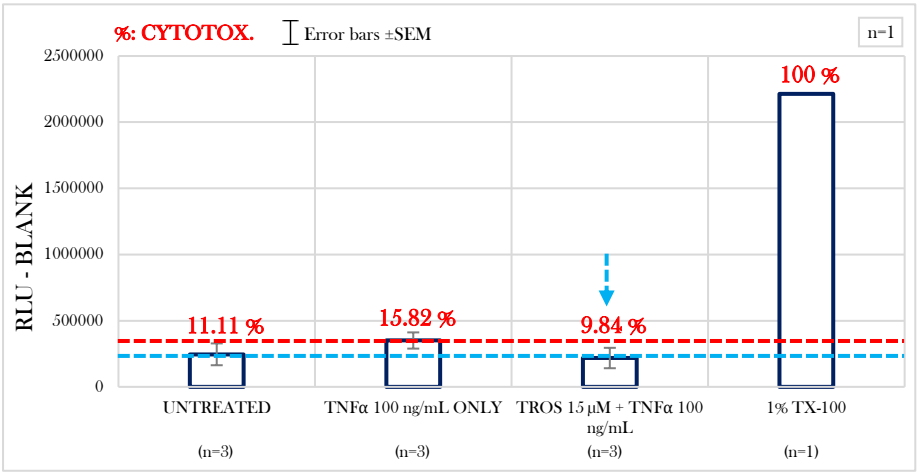

Figure 106: Second titration of TROS: LDH assay. RLUs of the different conditions subtracted to the blank. In red the percentage of Necrosis/Necroptosis normalized to a control of maximal cell membrane lysis. One biological replica with three technical replicas per condition. Error bars ±SEM.

The third and final titration experiment of TROS has been performed applying the concentrations 10, 20 and 30 µM in one single biological replica. The TEER measurements showed a clear barrier protective effect which followed a clear dose-response pattern, with 30 µM being the most effective (figure 107). The induction with sTNFα applied alone determined a drop of TEER to 51.33 % of the untreated condition (49 % drop), that was clearly protected by the co-treatments with TROS. At 10 µM the TEER dropped to 79.82 % (20.1 % drop), at 20 µM the TEER dropped to 91 % (9 % drop) and at 30 µM the TEER represented 102.05 % of the untreated condition.

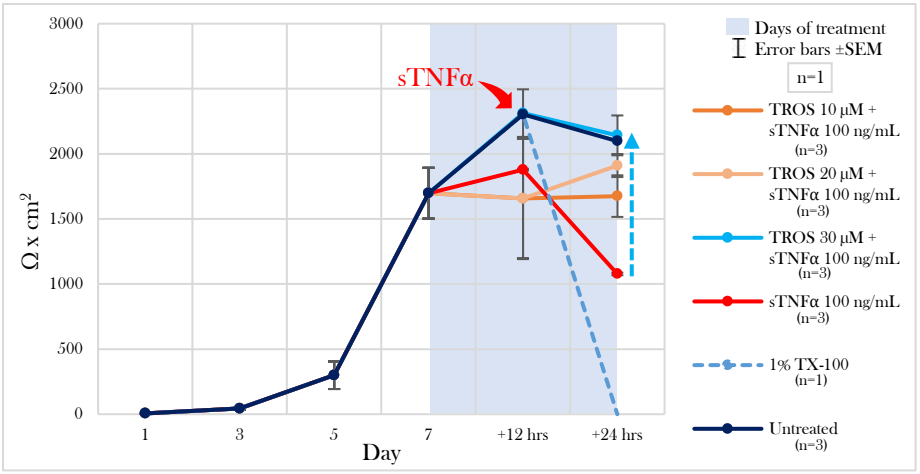

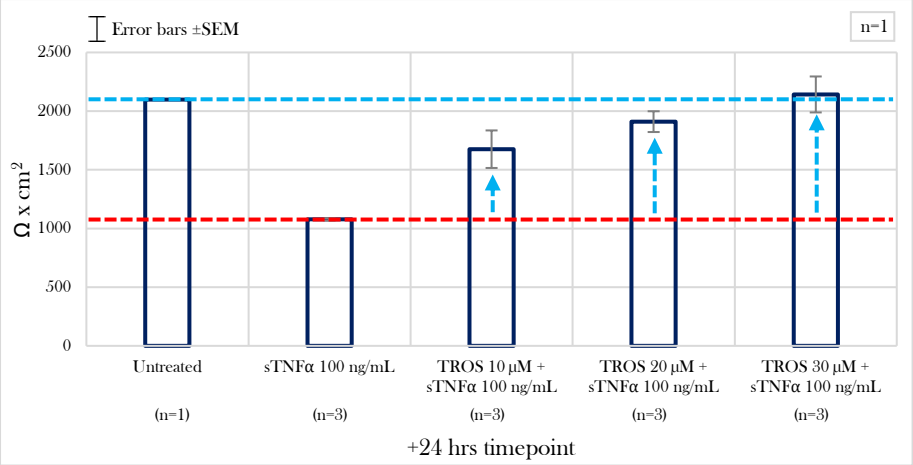

Figure 107: Third titration of TROS: TEER measurements. Ω x cm^2 values over time from the single biological replica with three technical replicas per condition (upper graph). Average values for the five conditions ("untreated", "sTNFα alone", "co-treatment with TROS at 10, 20 and 30 µM") at 12 hrs post-induction induction, for a single biological replica with three technical replicas per condition (lower graph). Error bars ±SEM.

The outcome of the FD4 permeability assay clearly reflected the TEER measurements. The application of sTNFα determined a 1.23-fold increase of permeability which was steadily and progressively protected by the co-treatments with TROS, following a dose-response pattern (figure 108). TROS applied at 10 µM determined a 1.05-fold increase of permeability (85.71 % of the increase determined by sTNFα alone), at 20 µM determined a 0.76-fold increase of permeability (61.9 % of the increase determined by sTNFα alone) and at 30 µM determined a 0.47-fold increase of permeability (38.09 % of the increase determined by sTNFα alone) with regards to the untreated condition.

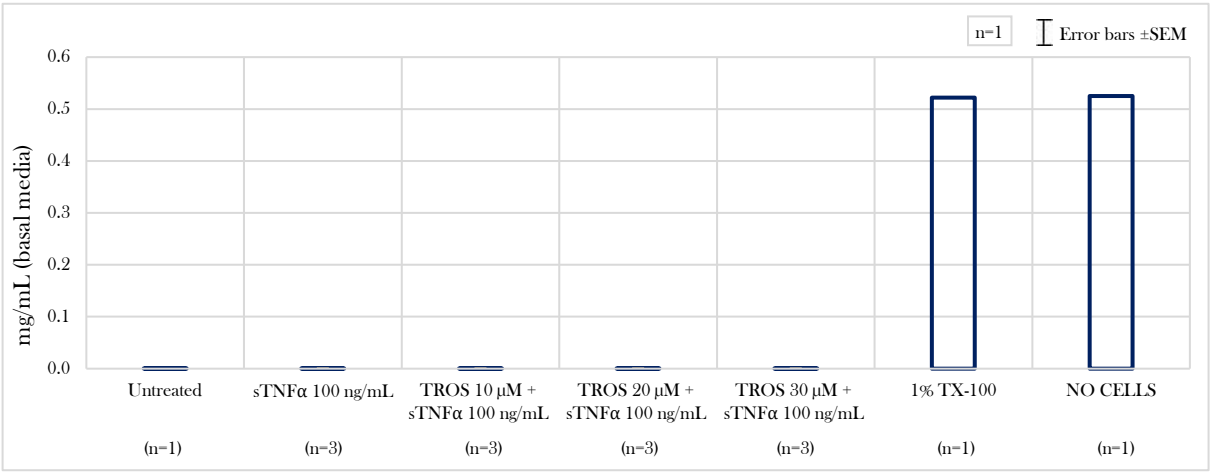

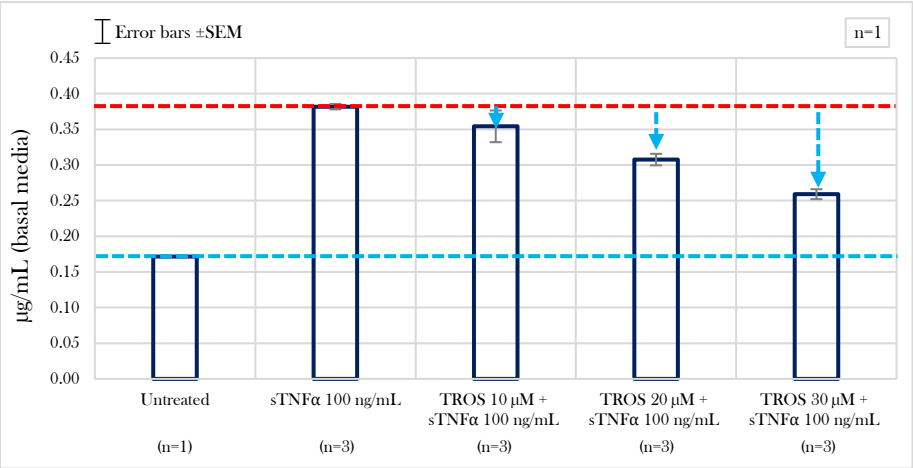

Figure 108: Third titration of TROS: FD4 assay. Positive control of maximal permeability (TW with no cells and monolayers treated with 1% TX-100) in mg/mL (upper graph). Average values in µg/mL for the five conditions ("untreated", "sTNFα alone", "co-treatment with TROS at 10, 20 and 30 µM") at 12 hrs post-induction induction, for a single biological replica with three technical replicas per condition (lower graph). Error bars ±SEM.

The LDH assay (figure 109) showed a clear anti-necroptotic effect determined by the three concentrations of TROS, which also followed a dose-response pattern. The concentrations 20 and 30 µM completely nullified the 10 % increase of LDH determined by sTNFα alone with respect to the untreated condition, and, importantly, did not show an unwanted cytotoxic effect.

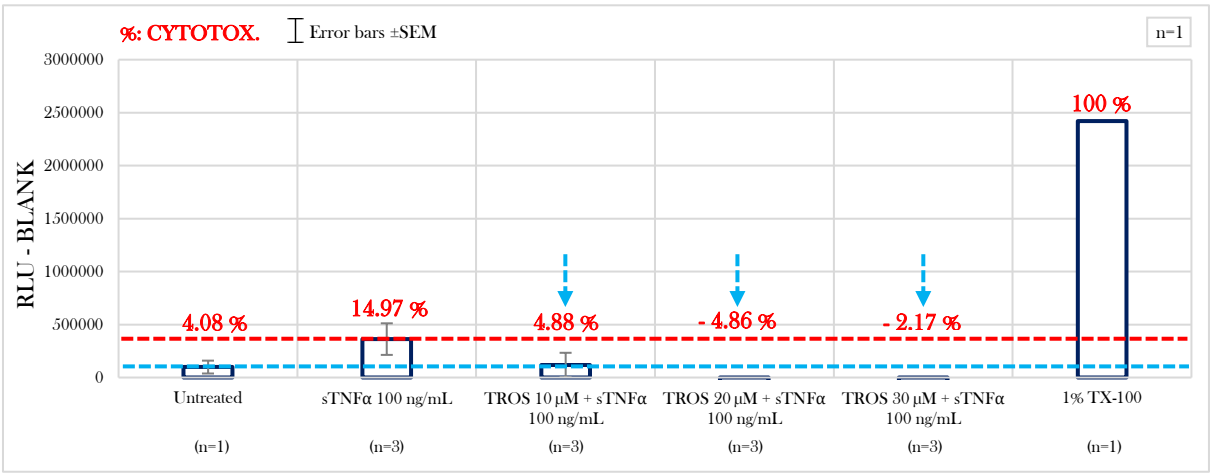

Figure 109: Third titration of TROS: LDH assay. RLUs of the different conditions subtracted to the blank. In red the percentage of Necrosis/Necroptosis normalized to a control of maximal cell membrane lysis. One biological replica with three technical replicas per condition. Error bars ±SEM.

4.5.2.4. Full competitive orthosteric antagonism of TNR1A with regards to barrier function: TROS at the optimal working concentration

Once established 30 µM as the optimal working concentration of TROS, I repeated the experiment of full antagonism of TNR1A in four biological replicas in order to assess if the differences observed were statistically significant. The experimental setup (figure 110) was exactly the same one followed

for the titration experiments. As for the full antagonism of sTNFα with Adalimumab, also in this experiment total RNA was isolated at the timepoint +24 hrs for the different conditions, in order to perform whole-cell transcriptomic analyses by RNAseq.

Full competitive antagonism of TNR1A

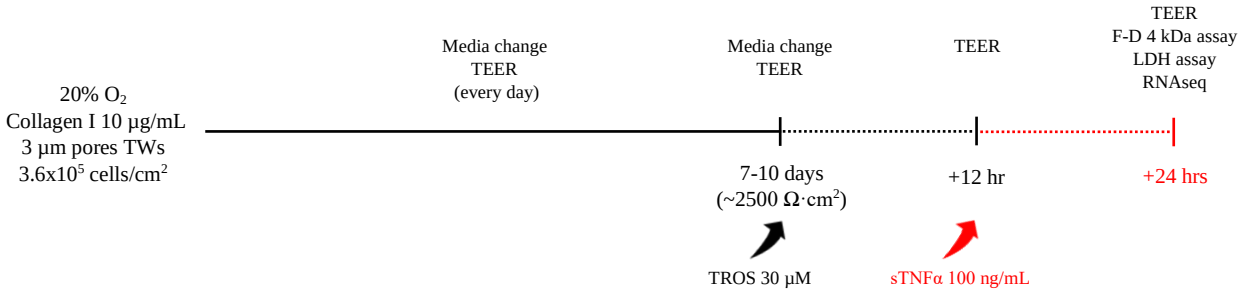

Figure 110: Schematic representation of the experiment for the full antagonism of TNR1A employing the optimal concentration of TROS pre-applied for 12 hrs on fully differentiated monolayers (~2500 Ω·cm^2), which were then induced with sTNFα 100 ng/mL for 12 hrs, in normoxia. In red are indicated the time frames during which the monolayers were stimulated with the cytokine from the basolateral side. Note: the different time frames depicted in the temporal axis are not in scale.

The result of this experiment at TEER level showed a full protection towards the impairment determined by sTNFα applied alone (figure 111). The average values for the four biological replicas showed a drop of resistance determined by sTNFα applied alone to 54.14 % of the untreated condition (drop of 44 %), which was fully protected by the co-treatment with TROS at 30 µM (with a TEER that represented 97.52 % of the untreated condition). The difference observed in between the average values of the condition of co-treatment with TROS 30 µM and the condition of induction with the sole sTNFα was statistically significant ($p \leq 0.01$, two-sided paired t-test, n=4). The minimal difference in between the average values of the untreated condition and the condition of co-treatment with TROS 30 µM was not statistically significant ($p > 0.05$, two-sided paired t-test, n=4).

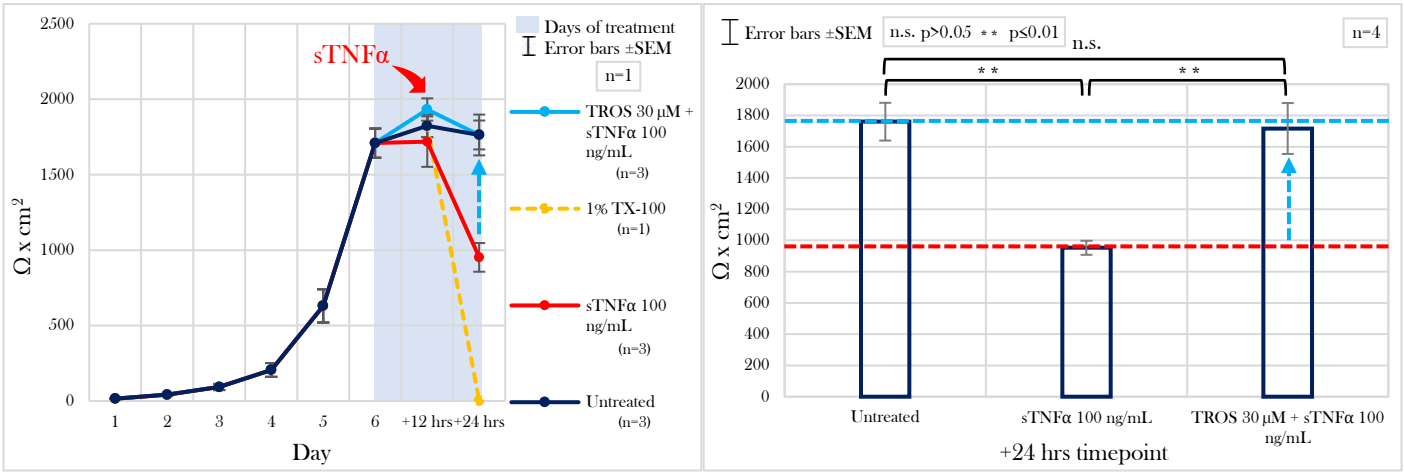

Figure 111: Full competitive antagonism of TNR1A with TROS µ30 M: TEER measurements. Ω x cm² values over time from a single representative biological replica with three technical replicas per condition (left graph). Average values for the three conditions ("untreated", "sTNFα alone" and "co-treatment with TROS at 30 µM") at 12 hrs post-induction induction, for n=4 (right graph). Significance stated by a two-sided paired t-test. Error bars ±SEM.

A prominent barrier function protection was also observed upon full antagonism of TNR1A with TROS 30 µM with the FD4 permeability assay (figure 112). A 1.37-fold increase of permeability determined by the cytokine applied alone was almost completely protected by the co-treatment with TROS 30 µM which determined only a 0.31-fold increase of permeability with respect to the untreated condition (only 22.72 % of the increase determined by sTNFα applied alone). The difference observed in between the average values of the condition of co-treatment with TROS 30 µM and the condition of treatment with sTNFα applied alone was statistically significant ($p \leq 0.05$, two-sided paired t-test, n=4). The minimal difference in between the average values of the untreated condition and the condition of co-treatment with TROS 30 µM was not statistically significant the ($p > 0.05$, two-sided paired t-test, n=4).

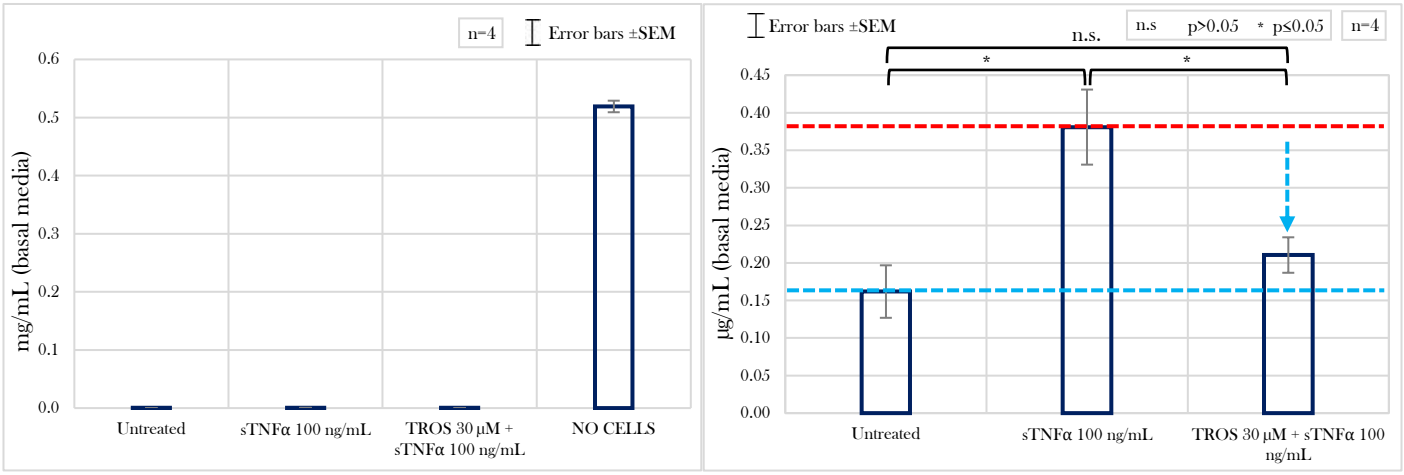

Figure 112: Full competitive antagonism of TNR1A with TROS µ30 M: FD4 assay. Positive control of maximal permeability (TW with no cells) in mg/mL (left graph). Average values in µg/mL for the four conditions ("untreated", "sTNFα alone" and "co-treatment with TROS at 30 µM"), for n=4 (right graph). Significance stated by a two-sided paired t-test. Error bars ±SEM.

The LDH assay (figure 113) showed that the full antagonism of TNR1A completely normalized the pro-necroptotic effect determined by sTNFα, and that the difference in between both conditions was statistically significant ($p \leq 0.05$, two-sided paired t-test, n=4).

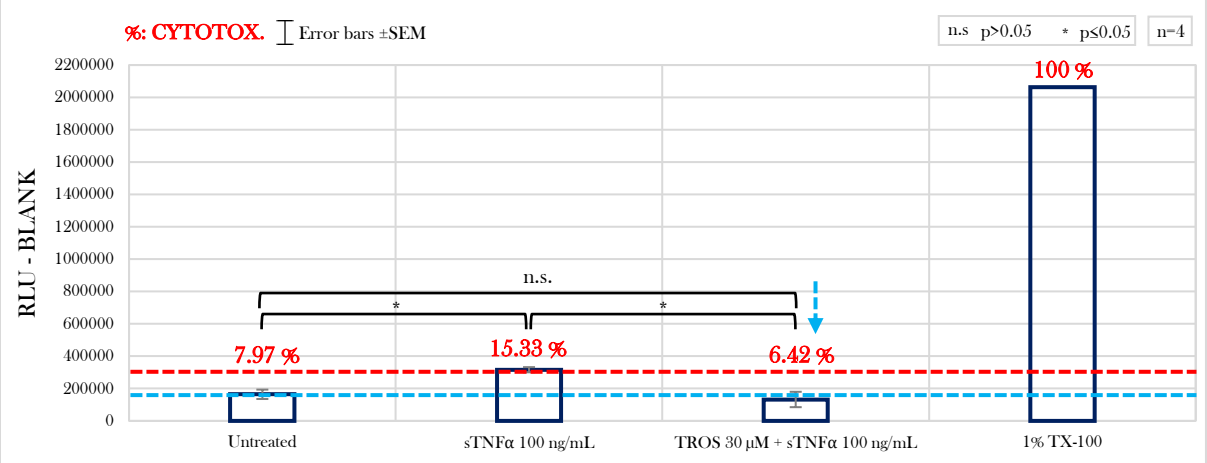

Figure 113: Full competitive antagonism of TNR1A with TROS µ30 M: LDH assay. RLUs of the different conditions subtracted to the blank. In red the percentage of Necrosis/Necroptosis normalized to a control of maximal cell membrane lysis. Significance stated by a two-sided paired t-test for n=4. Error bars ±SEM.

4.6. RNAseq: transcriptome expression profiling of the induction with sTNFα, of the full neutralization of the sTNFα signalling and of the full competitive orthosteric antagonism of TNR1A

In order to start gaining insights into the regulatory mechanisms involved in the barrier dysfunction determined by the sole activation of TNR1A, a whole-transcriptome expression analysis was performed by RNAseq. Total RNA was isolated from the three conditions “untreated”, “sTNFα 100 ng/mL” and “Adalimumab 24 µg/mL + sTNFα 100 ng/mL”, at the timepoint +24 hrs of the experiment of full neutralization of sTNFα in solution. The same was done for the three conditions “untreated”, “sTNFα 100 ng/mL” and “TROS 30 µM + sTNFα 100 ng/mL”, at the timepoint +24 hrs of the experiment of full competitive antagonism of TNR1A. The complete mRNA population of T84 in the single aforementioned experimental conditions was sequenced, and unique gene hit counts were obtained. The latter were employed for identifying the significantly differentially expressed genes (absolute Log2FoldChange of the normalized mean hit counts ≥ 2) within all the comparisons of the different experimental conditions, for each of the two experiments (n=3 for each). All the comparisons in between the different experimental conditions of the two aforementioned experiments, together with their respective significantly differentially expressed genes, are summarized in Table 7.

Table 7: RNAseq experiments. Differential expression comparisons and significantly differentially expressed genes (Log2FoldChange of normalized mean hit counts for n=3).

Experiment	Comparison	Differentially expressed genes Log2FoldChange ≥ +2 ⬆ Log2FoldChange ≤ - 2 ⬇	
I Full neutralization of sTNFα in solution with Adalimumab 24 µg/mL (figure 114)	sTNFα 100 ng/mL VS UNTREATED	⬆	*TNFRSF9, SPATA21, COL16A1, COL9A2, GBP4, CSF1, KCNA2, AC241585.3, SPRR1A, S100A3, AIM2, IGFN1, PHLDA3, C1orf147, OR7E91P, NEURL3, IL18R1, LINC01594, IL1A, CCL20, ADAMTS9, ARHGAP31, ADCY5, CHST13, LINC02068, LAMP3, KLHL5, CXCL8, CXCL1, CXCL3, CXCL2, CXCL10, TLR2, ANKRD33B, FYB1, CD74, MIR3142HG, N4BP3, AC034213.1, CD83, OR2I1P, UBD, TNF, LTB, NFKBIE, VNN1, AL356234.3, AL357060.1, TNFAIP3, FAM167A, FGF20, AC107959.3, TCIM, SDR16C5, LCN2, AL391056.1, SLC2A6, ASRGL1, BIRC3, GUCY1A2, DRGX, NFKB2, OLR1, TMEM52B, KRT7-AS, KRT87P, IL23A, LINC02384, DRAM1, LINC00943, LINC00944, NFKBIA, TNFAIP2, DUOXA2, FBN1, LINC02251, SYNGR3, IL32, ITGAM, SLC5A2, NOD2, CX3CL1, CNTNAP1, APCDD1, TGM3, PI3, AL021578.1, HMGB2P1, C3, ADGRE1, ICAM1, UNC13A, NPHS1, IFNL1, TEX101, RELB, PLA2G4C, IL4I1, PRKCG, CACNG8, TMEM211, NFAM1, AL022316.1, U62317.2, KLHDC7B*
		⬇	*AC141930.1, AC016735.1, SLC6A19, PDLIM4, PDE6A, SLC26A2, MRAP2, SLC26A3, KIF12, MOGAT2, ADAMTS15, VIM-AS1, ZNF488, CYP26A1, COL2A1, PIWIL1, CHP2, SLC13A2, LINC00668, COL5A3, CACNA1I*
	ADALIMUMAB 24 µg/mL VS sTNFα 100 ng/mL	⬆	*AC141930.1, AC016735.1, SLC6A19, MRAP2, AC004593.1, SLC18A1, KIF12, MOGAT2, ADAMTS15, VIM-AS1, CYP26A1, COL2A1, DTX3, CHP2, PCAT14, CACNA1I*
		⬇	*TNFRSF9, SPATA21, COL16A1, COL9A2, GBP4, CSF1, KCNA2, TSPAN2, S100A3, AIM2, NMNAT2, PHLDA3, C1orf147, NEURL3, IL18R1, IL1A, HOXD11, TM4SF20, CCL20, ADAMTS9, ARHGAP31, ADCY5, CHST13, LINC02068, KLHL5, CXCL8, CXCL1, CXCL3, CXCL2, CXCL10, TLR2, ANKRD33B, CD74, MIR3142HG, AC034213.1, CD83, OR2I1P, UBD, TNF, LTB, NFKBIE, VNN1, AL356234.3, AL357060.1, TNFAIP3, FAM167A, FGF20, SDR16C5, TMOD1, AL391056.1, PRRX2, PTGES, SLC2A6, RCC2P6, BIRC3, MMP10, GUCY1A2, DRGX, NFKB2, OLR1, TMEM52B, KRT7, KRT7-AS, KRT87P, IL23A, LINC02384, DRAM1, LINC00944, NFKBIA, TNFAIP2, DUOX2, DUOXA2, LINC02251, SYNGR3, IL32, SOCS1, AC106886.2, ITGAM, SLC5A2, NOD2, CX3CL1, RRAD, IL34, CNTNAP1, ICAM2, APCDD1, TGM3, PI3, HMGB2P1, C3, ADGRE1, ICAM1, ZSWIM4, UNC13A, NPHS1, TEX101, RELB,*

			PLA2G4C, IL4I1, PRKCG, CACNG8, NFAM1, AL022316.1, PANX2, U62317.2, KLHDC7B
	ADALIMUMAB 24 µg/mL VS UNTREATED	⬆	(None)
		⬇	(None)
II Full competitive antagonism of TNR1A with TROS 30 µM (figure 115)	sTNFα 100 ng/mL VS UNTREATED	⬆	*TNFRSF9, COL16A1, COL9A2, GBP4, CSF1, KCNA2, S100A9, S100A3, IGFN1, PHLDA3, C1orf147, OR7E91P, NEURL3, IL18R1, IL1A, CCL20, ADAMTS9, ARHGAP31, ADCY5, CHST13, LINC02068, KLHL5, CXCL8, CXCL1, CXCL3, CXCL2, CXCL10, TLR2, ANKRD33B, FYB1, CD74, MIR3142HG, AC034213.1, CD83, OR2I1P, UBD, TNF, LTB, AL354740.1, NFKBIE, VNN1, AL356234.3, AL357060.1, TNFAIP3, PGAM1P7, FAM167A, FGF20, AC107959.3, TCIM, SLC28A3, AL391056.1, SLC2A6, ASRGL1, RCC2P6, BIRC3, GUCY1A2, DRGX, NFKB2, OLR1, TMEM52B, KRT87P, IL23A, LINC02384, RPL10P12, DRAM1, LINC00943, LINC00944, NFKBIA, TNFAIP2, DUOX2, DUOXA2, LINC02251, SYNGR3, IL32, ITGAM, SLC5A2, NOD2, CX3CL1, RRAD, IL34, CNTNAP1, APCDD1, TGM3, PI3, AL021578.1, HMGB2P1, C3, ADGRE1, ICAM1, ZSWIM4, UNC13A, NPHS1, TEX101, RELB, PLA2G4C, IL4I1, PRKCG, CACNG8, TMEM211, NFAM1, AL022316.1, U62317.2, KLHDC7B*
		⬇	*AC141930.1, SLC6A19, PDE6A, SLC26A2, MRAP2, ELN, SLC26A3, AQP7, HRCT1, KIF12, MOGAT2, ADAMTS15, ZNF488, CYP26A1, COL2A1, BIN2, CCDC175, LINC02568, CHP2, AC026462.3, SLC13A2, LINC00668, COL5A3, CACNA1I*
	TROS 30 µM VS sTNFα 100 ng/mL	⬆	*AC141930.1, SLC6A19, SLC26A2, MOGAT2, ADAMTS15, CYP26A1, LINC02568, CHP2, CACNA1I*
		⬇	*TNFRSF9, CSF1, KCNA2, S100A3, IL1A, CCL20, ARHGAP31, CXCL8, CXCL1, CXCL3, CXCL2, ANKRD33B, MIR3142HG, AC034213.1, OR2I1P, UBD, TNF, LTB, NFKBIE, AL356234.3, AL357060.1, TNFAIP3, LINC02538, TCIM, AL391056.1, SLC2A6, BIRC3, MMP10, GUCY1A2, DRGX, OLR1, TNFAIP2, ITGAM, SLC5A2, NOD2, IL34, APCDD1, TGM3, PI3, HMGB2P1, C3, ICAM1, UNC13A, NPHS1, IL4I1, PRKCG, CACNG8, U62317.2, KLHDC7B*
	TROS 30 µM VS UNTREATED	⬆	*DRGX, LINC02384, IL34*
		⬇	*CYP1A1*

In the experiment of full neutralization of the sTNFα signalling with Adalimumab at 24 µg/mL, the induction for 12 hrs with the sole cytokine determined a significant deregulation of 126 genes, comparing with the untreated condition (comparison "sTNFα 100 ng/mL VS UNTREATED" in Figure 114). The majority of these genes were upregulated. The co-treatment with Adalimumab at 24 µg/mL determined a significant deregulation of 122 genes, comparing with the condition of

induction with the sole cytokine (comparison “ADALIMUMAB 24 µg/mL VS sTNFα 100 ng/mL” in Figure 114). All the genes deregulated by the cytokine alone were completely normalized in their expression by the co-treatment with Adalimumab at 24 µg/mL, considering that in the comparison “ADALIMUMAB 24 µg/mL VS UNTREATED” no gene was found to be significantly differentially expressed.

In the experiment of full selective competitive antagonism of TNR1A with TROS at 30 µM, 127 genes were significantly deregulated by the induction with sTNFα applied alone (comparison “sTNFα 100 ng/mL VS UNTREATED” in Figure 115). The co-treatment with TROS at 30 µM determined a significant differential expression of 58 genes comparing with the condition of sole induction with the cytokine (comparison “TROS 30 µM VS sTNFα 100 ng/mL” in Figure 115). Three of these genes were not fully normalized in their expression level by the co-treatment with TROS as demonstrated by the comparison “TROS 30 µg/mL VS UNTREATED” (Figure 115). One gene, *CYP1A1*, was found to be significantly downregulated by the co-treatment with TROS at 30 µM with respect to the untreated condition; an intensification of the downregulation determined by sTNFα applied alone (Figure 115).

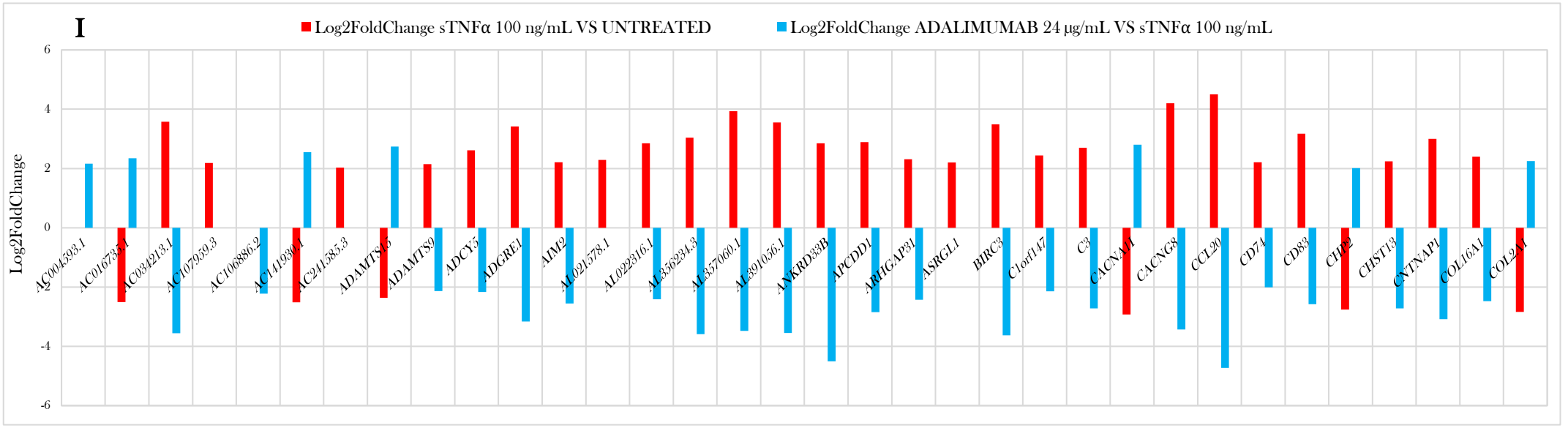
I
Log2FoldChange sTNFα 100 ng/mL VS UNTREATED
Log2FoldChange ADALIMUMAB 24 µg/mL VS sTNFα 100 ng/mL
Log2FoldChange
6
4
2
0
-2
-4
-6
AC004393.1
AC016735.1
AC034213.1
AC107959.3
AC106886.2
AC141930.1
AC241585.3
ADAMTS6
ADAMTS9
ADCY5
ADGRE1
AIM2
AL021578.1
AL022316.1
AL353934.3
AL357060.1
AL391056.1
ANKRD33B
APCDD1
ARHGAP31
ASRGL1
BIRC3
C1orf147
C3
CACNA1I
CACNG8
CCL20
CD74
CD83
CHI3
CHST13
CNTNAP1
COL16A1
COL24A1

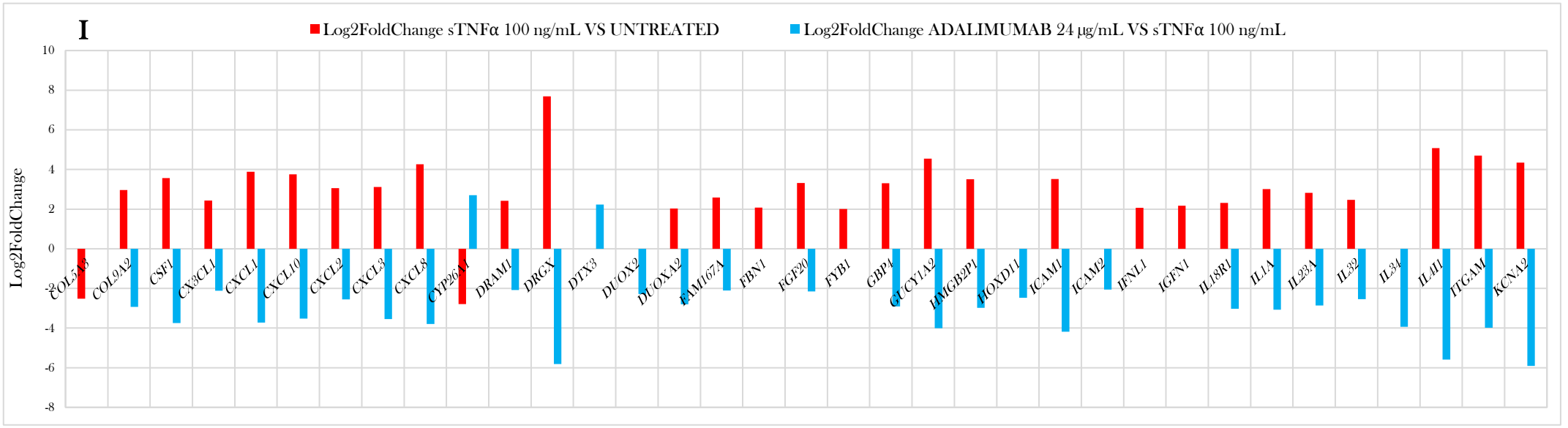
I
Log2FoldChange sTNFα 100 ng/mL VS UNTREATED
Log2FoldChange ADALIMUMAB 24 µg/mL VS sTNFα 100 ng/mL
Log2FoldChange
10
8
6
4
2
0
-2
-4
-6
-8
COL5A3
COL9A2
CSF1
CX3CL1
CXCL1
CXCL10
CXCL2
CXCL3
CXCL8
CYP26A1
DRAM1
DRGX
DTX3
DUOX2
DUOXA2
EMID2
FBN1
FGF20
FYB1
GBP4
GUCY1A2
HMGB2P1
HOXD11
ICAM1
ICAM2
IFNL1
IGFN1
IL18R1
IL1A
IL23A
IL32
IL34
ILHL
ITGA11
KCNA2

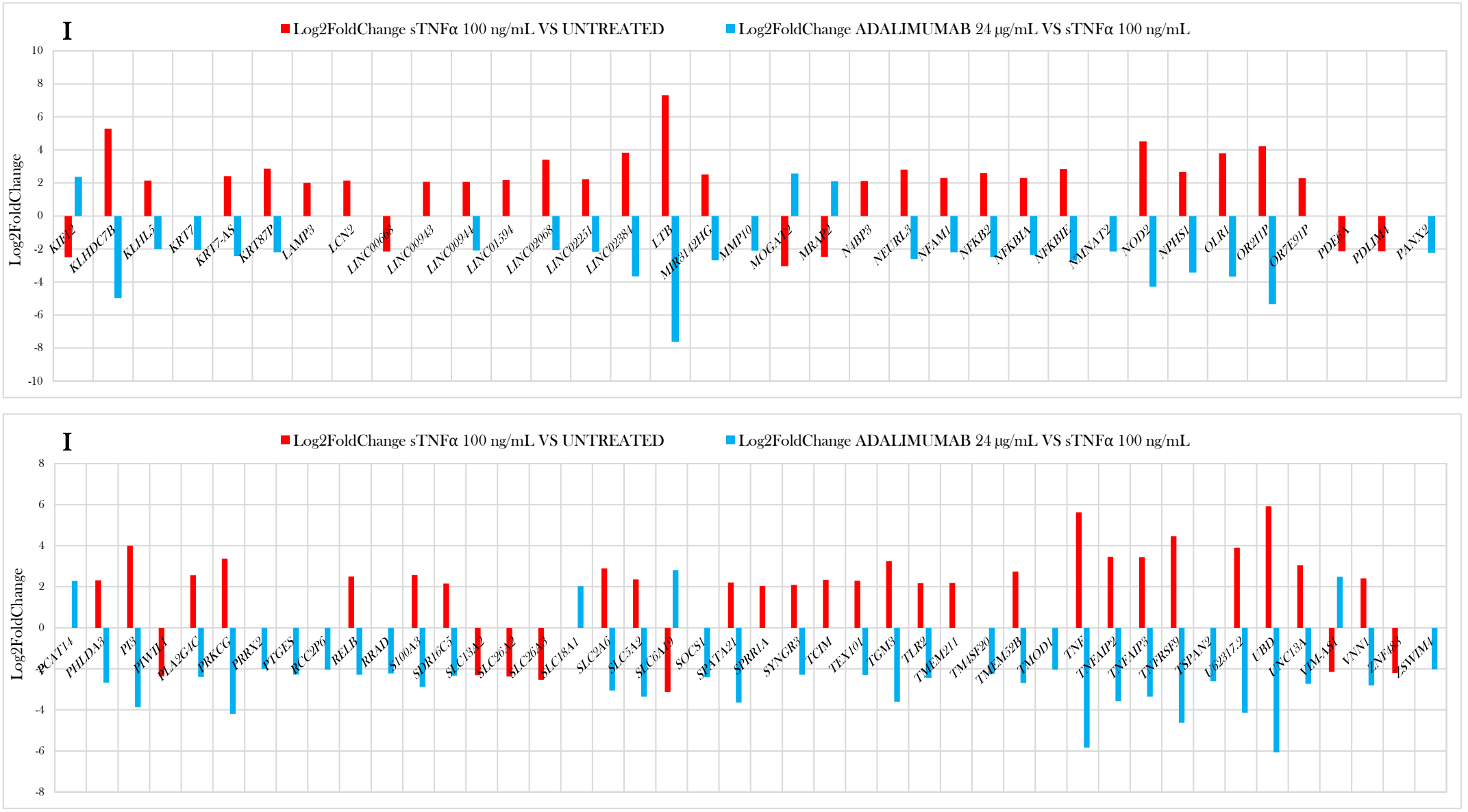

Figure 114: Differentially expressed genes (absolute Log2FoldChange of the normalized mean hit counts ≥ 2, for n=3) identified by RNAseq in the Experiment I (full neutralization of sTNFα in solution), at the timepoint +24 hrs. Comparisons "sTNFα 100 ng/mL VS UNTREATED" and "ADALIMUMAB 24 µg/mL VS sTNFα 100 ng/mL".

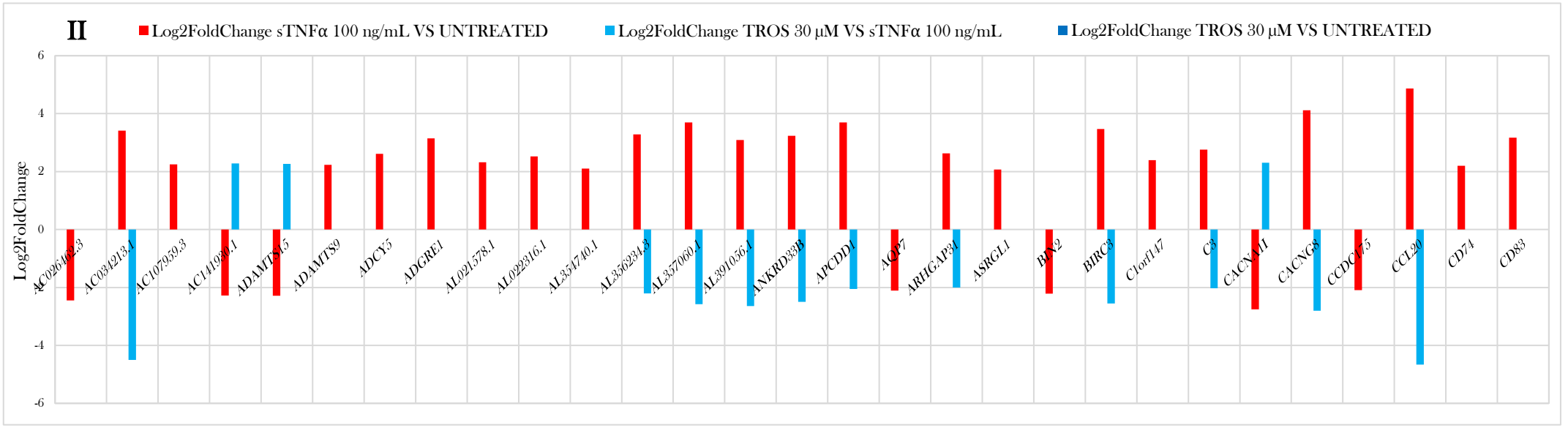
II
Log2FoldChange sTNFα 100 ng/mL VS UNTREATED
Log2FoldChange TROS 30 µM VS sTNFα 100 ng/mL
Log2FoldChange TROS 30 µM VS UNTREATED
Log2FoldChange
6
4
2
0
-4
-6
AC026462.3
AC034213.4
AC107959.3
AC141930.1
ADAMTS15
ADAMTS9
ADCY5
ADGRE1
AL021578.1
AL022316.1
AL354740.1
AL356234.3
AL357060.1
AL391056.1
ANKRD33B
APCDD1
AQP7
ARHGAP31
ASRGL1
BCN2
BIRC3
C1orf147
C3
CACNA1I
CACNG8
CCDC175
CCL20
CD74
CD83

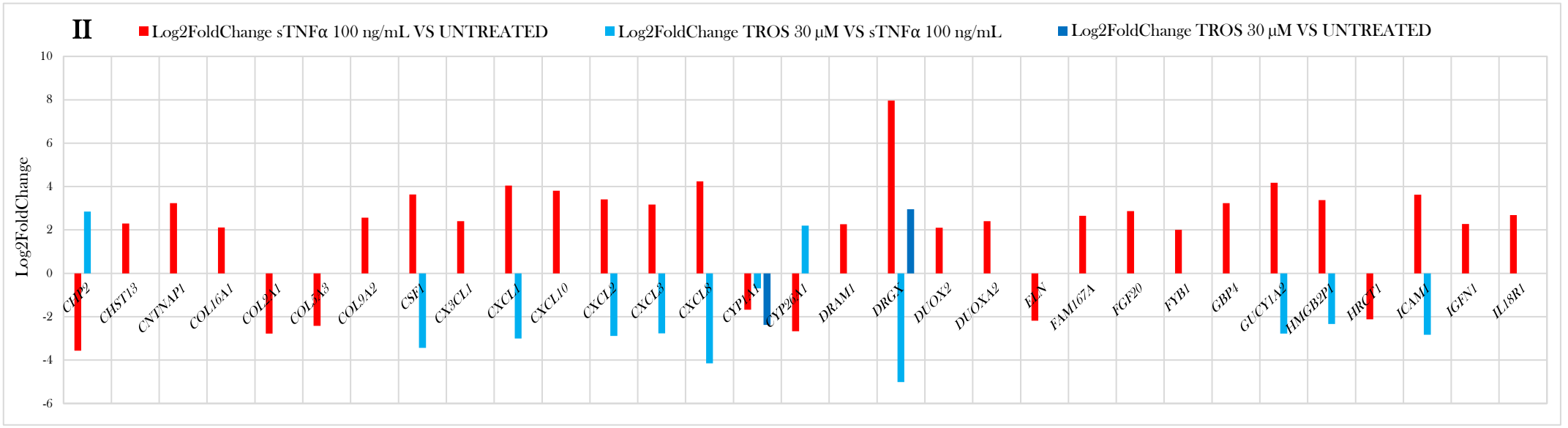
II
Log2FoldChange sTNFα 100 ng/mL VS UNTREATED
Log2FoldChange TROS 30 µM VS sTNFα 100 ng/mL
Log2FoldChange TROS 30 µM VS UNTREATED
Log2FoldChange
10
8
6
4
2
0
-2
-4
-6
CHP2
CHST13
CNTNAP1
COL16A1
COL24A1
COL3A1
COL9A2
CSF1
CX3CL1
CXCL1
CXCL10
CXCL2
CXCL3
CXCL8
CYP1A1
CYP26A1
DRAM1
DRGX
DUOX2
DUOXA2
ELN
FAM167A
FGF20
FYB1
GBP4
GUCY1A2
HMGB2P1
HRCT1
ICAM1
IGFN1
IL18R1

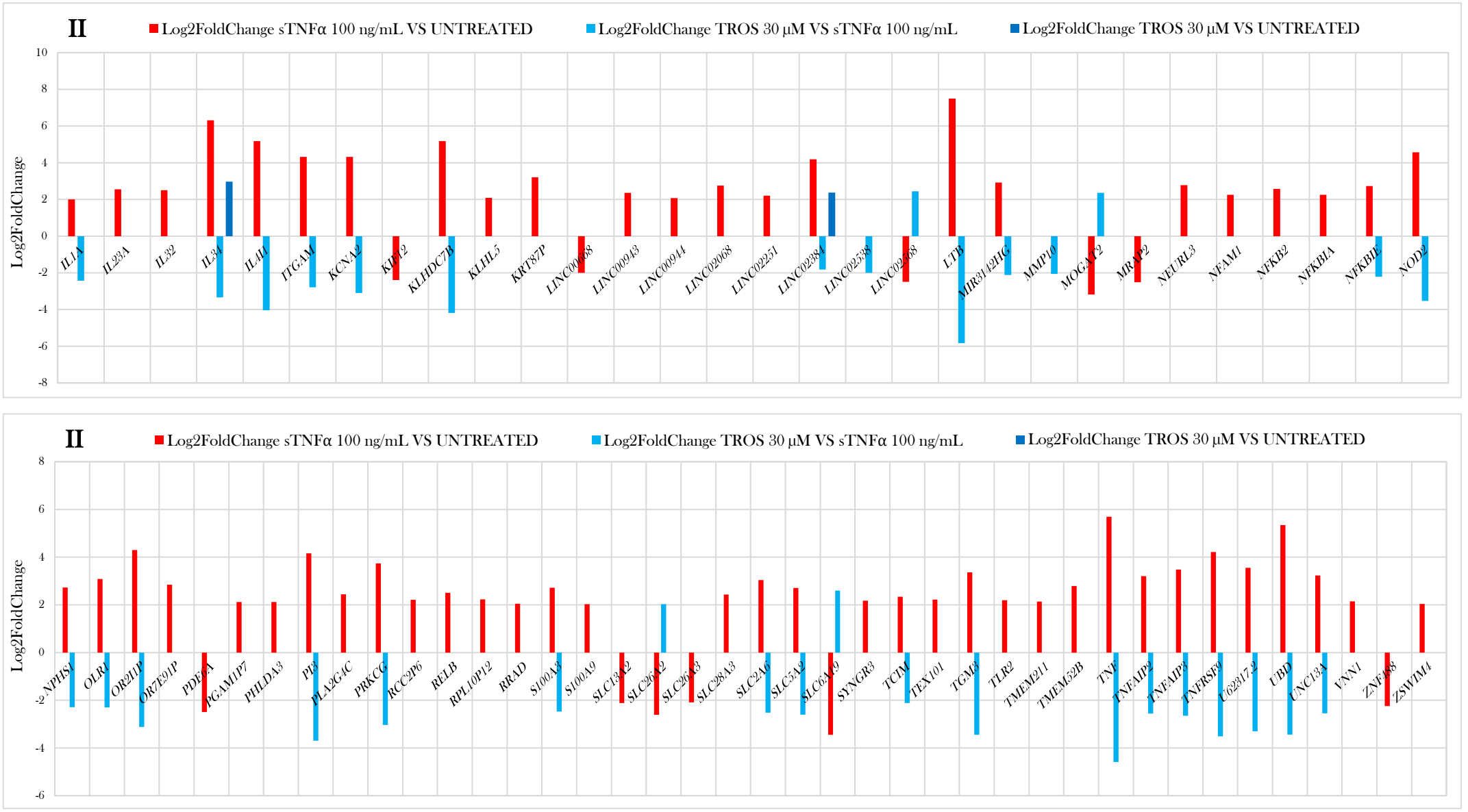

Figure 115: Differentially expressed genes (absolute Log2FoldChange of the normalized mean hit counts ≥ 2, for n=3) identified by RNAseq in the Experiment II (full competitive antagonism of TNR1A), at the timepoint +24 hrs. Comparisons "sTNFα 100 ng/mL VS UNTREATED", "TROS 30 µM VS sTNFα 100 ng/mL" and "TROS 30 µM VS UNTREATED".

The RNAseq data of the two aforementioned experiments allowed me also to analyze the differential expression of various genes of interest that did not reach the arbitrary threshold of significance (absolute Log2FoldChage≥2) but that could have anyway reached statistical significance. The analysis of the expression of *TNFRSF1A*, *TNFRSF1B*, *IFNGR1* and *IFNGR2* upon induction for 12 hrs with only sTNFα at 100 ng/mL is presented in Figure 116. It allowed me to complement the previous expression analyses by RT-qPCR in the presence of both sTNFα and IFNγ (figure 75).

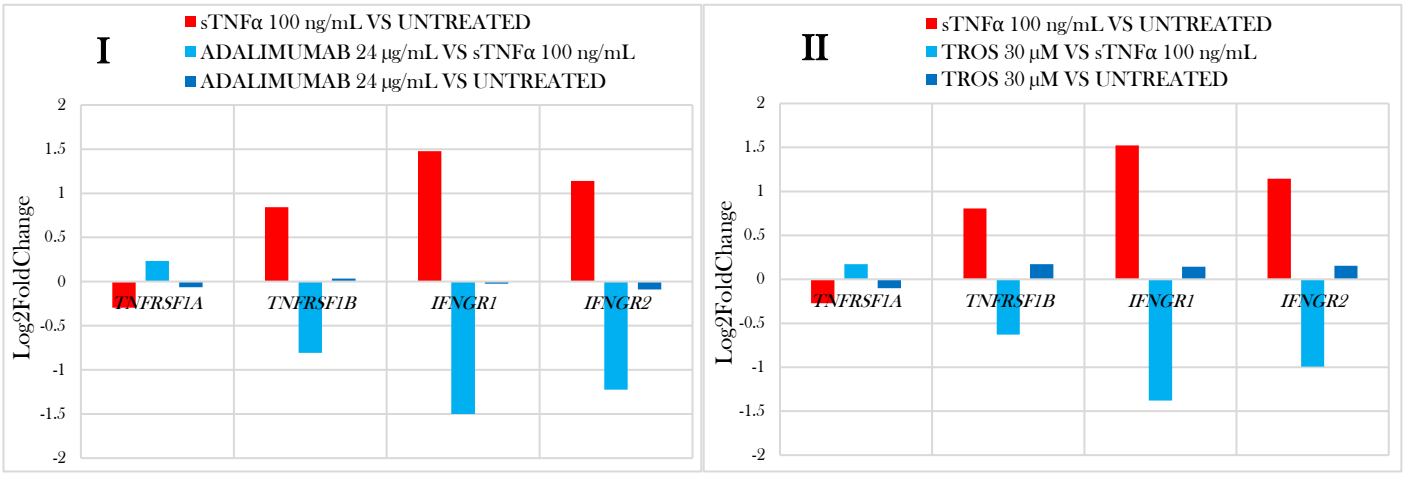

Figure 116: Differential expression of *TNFRSF1A*, *TNFRSF1B*, *IFNGR1* and *IFNGR2* (Log2FoldChange of the normalized mean hit counts, for n=3) assessed by RNAseq in the experiments of full neutralization of sTNFα in solution (I) and of full competitive antagonism of TNR1A (II), at the timepoint +24 hrs.

The induction with the sole sTNFα determined a differential expression of the aforementioned genes with regards to the untreated condition, but in none of the cases the absolute Log2FoldChange was greater than 2. In both experiments, a slight downregulation of *TNFRSF1A* (Log2FoldChanges of -0.27 and -0.29) and a moderate upregulation of *TNFRSF1B* (Log2FoldChanges of 0.8 and 0.84) were observed. A more prominent upregulation was observed for both *IFNGR1* (Log2FoldChanges of 1.47 and 1.52) and *IFNGR2* (Log2FoldChanges of 1.13 and 1.14). Importantly, the co-treatments with either Adalimumab 24 µg/mL and TROS 30 µM determined a complete restoration of the expression levels of all genes to the basal ones of the untreated condition.

Finally, I employed the RNAseq data to preliminarily analyze, in the different aforementioned experimental conditions, the expression of a series of functionally relevant genes that contribute in different ways to the intestinal epithelial barrier function. The analysis and the description of the results are schematically summarized in Table 8 and in Figure 117.

Table 8: RNAseq experiments I and II. Differential expression comparisons of functionally relevant genes in the context of intestinal epithelial barrier function.

Gene	Function of the protein	Exp.	Comparison	Log2Fold Change
			sTNFα 100 ng/mL VS UNTREATED	+0.43

CLDN1 (Claudin-1)	Intercellular TJP that regulates the pore permeability pathway. Defined as a "sealing" Claudin.	I	ADALIMUMAB 24 µg/mL VS sTNFα 100 ng/mL	-0.38
			ADALIMUMAB 24 µg/mL VS UNTREATED	+0.06
		II	sTNFα 100 ng/mL VS UNTREATED	+0.37
			TROS 30 µM VS sTNFα 100 ng/mL	-0.38
			TROS 30 µM VS UNTREATED	-0.01
CLDN2 (Claudin-2)	Intercellular TJP that regulates the pore permeability pathway. Defined as a "pore-forming" cation-selective Claudin.	I	sTNFα 100 ng/mL VS UNTREATED	+0.87
			ADALIMUMAB 24 µg/mL VS sTNFα 100 ng/mL	-0.24
			ADALIMUMAB 24 µg/mL VS UNTREATED	+0.63
		II	sTNFα 100 ng/mL VS UNTREATED	+0.93
			TROS 30 µM VS sTNFα 100 ng/mL	-0.71
			TROS 30 µM VS UNTREATED	+0.22
CLDN3 (Claudin-3)	Intercellular TJP that regulates the pore permeability pathway. Defined as a "sealing" Claudin.	I	sTNFα 100 ng/mL VS UNTREATED	-0.08
			ADALIMUMAB 24 µg/mL VS sTNFα 100 ng/mL	-0.07
			ADALIMUMAB 24 µg/mL VS UNTREATED	-0.15
		II	sTNFα 100 ng/mL VS UNTREATED	-0.22
			TROS 30 µM VS sTNFα 100 ng/mL	+0.06
			TROS 30 µM VS UNTREATED	-0.16
CLDN4 (Claudin-4)	Intercellular TJP that regulates the pore permeability pathway. Defined as a "pore-forming" anion-selective Claudin with an inconsistent function.	I	sTNFα 100 ng/mL VS UNTREATED	+0.25
			ADALIMUMAB 24 µg/mL VS sTNFα 100 ng/mL	-0.36
			ADALIMUMAB 24 µg/mL VS UNTREATED	-0.11
		II	sTNFα 100 ng/mL VS UNTREATED	+0.12
			TROS 30 µM VS sTNFα 100 ng/mL	-0.29
			TROS 30 µM VS UNTREATED	-0.17
CLDN7 (Claudin-7)	Intercellular TJP that regulates the pore permeability pathway. Defined as a "pore-forming" Claudin with an inconsistent charge-selectivity.	I	sTNFα 100 ng/mL VS UNTREATED	-0.27
			ADALIMUMAB 24 µg/mL VS sTNFα 100 ng/mL	+0.11
			ADALIMUMAB 24 µg/mL VS UNTREATED	-0.16
		II	sTNFα 100 ng/mL VS UNTREATED	-0.28
			TROS 30 µM VS sTNFα 100 ng/mL	+0.09
			TROS 30 µM VS UNTREATED	-0.18
CLDN9 (Claudin-9)	Intercellular TJP that might regulate the pore permeability pathway. It has an unknown function.	I	sTNFα 100 ng/mL VS UNTREATED	-1.61
			ADALIMUMAB 24 µg/mL VS sTNFα 100 ng/mL	+1.09
			ADALIMUMAB 24 µg/mL VS UNTREATED	-0.52
		II	sTNFα 100 ng/mL VS UNTREATED	-1.05
			TROS 30 µM VS sTNFα 100 ng/mL	+0.69
			TROS 30 µM VS UNTREATED	-0.35
CLDN11 (Claudin-11)	Intercellular TJP that regulates the pore permeability pathway. Defined as a "sealing" Claudin.	I	sTNFα 100 ng/mL VS UNTREATED	+0.79
			ADALIMUMAB 24 µg/mL VS sTNFα 100 ng/mL	-0.17
			ADALIMUMAB 24 µg/mL VS UNTREATED	+0.62
		II	sTNFα 100 ng/mL VS UNTREATED	+0.90
			TROS 30 µM VS sTNFα 100 ng/mL	-1.13
			TROS 30 µM VS UNTREATED	-0.23
CLDN12 (Claudin-12)	Intercellular TJP that might regulate the pore permeability pathway. It has an unknown function.	I	sTNFα 100 ng/mL VS UNTREATED	+0.05
			ADALIMUMAB 24 µg/mL VS sTNFα 100 ng/mL	-0.10
			ADALIMUMAB 24 µg/mL VS UNTREATED	-0.05
		II	sTNFα 100 ng/mL VS UNTREATED	+0.11
			TROS 30 µM VS sTNFα 100 ng/mL	-0.15
			TROS 30 µM VS UNTREATED	-0.04
CLDN15 (Claudin-15)	Intercellular TJP that regulates the pore permeability pathway. Defined as a "pore-forming" cation-selective Claudin.	I	sTNFα 100 ng/mL VS UNTREATED	+0.15
			ADALIMUMAB 24 µg/mL VS sTNFα 100 ng/mL	-0.14
			ADALIMUMAB 24 µg/mL VS UNTREATED	+0.01
		II	sTNFα 100 ng/mL VS UNTREATED	+0.12
			TROS 30 µM VS sTNFα 100 ng/mL	-0.20
			TROS 30 µM VS UNTREATED	-0.08

CLDN20 (Claudin-20)	Intercellular TJP that might regulate the pore permeability pathway. It has an unknown function.	I	sTNFα 100 ng/mL VS UNTREATED	+0.32
			ADALIMUMAB 24 µg/mL VS sTNFα 100 ng/mL	-0.03
			ADALIMUMAB 24 µg/mL VS UNTREATED	+0.28
		II	sTNFα 100 ng/mL VS UNTREATED	+0.11
			TROS 30 µM VS sTNFα 100 ng/mL	-0.06
			TROS 30 µM VS UNTREATED	+0.05
CLDN23 (Claudin-23)	Intercellular TJP that might regulate the pore permeability pathway. It has an unknown function.	I	sTNFα 100 ng/mL VS UNTREATED	+0.10
			ADALIMUMAB 24 µg/mL VS sTNFα 100 ng/mL	-0.26
			ADALIMUMAB 24 µg/mL VS UNTREATED	-0.16
		II	sTNFα 100 ng/mL VS UNTREATED	-0.07
			TROS 30 µM VS sTNFα 100 ng/mL	-0.08
			TROS 30 µM VS UNTREATED	-0.15
OCLN (Occludin)	Intercellular TJP which presence or absence at the TJ density regulates the leak permeability pathway.	I	sTNFα 100 ng/mL VS UNTREATED	-0.30
			ADALIMUMAB 24 µg/mL VS sTNFα 100 ng/mL	+0.08
			ADALIMUMAB 24 µg/mL VS UNTREATED	-0.22
		II	sTNFα 100 ng/mL VS UNTREATED	-0.36
			TROS 30 µM VS sTNFα 100 ng/mL	+0.24
			TROS 30 µM VS UNTREATED	-0.12
TJP1 (ZO-1)	Intracellular, scaffolding TJP which presence or absence at the TJ density regulates the leak permeability pathway.	I	sTNFα 100 ng/mL VS UNTREATED	+0.50
			ADALIMUMAB 24 µg/mL VS sTNFα 100 ng/mL	-0.29
			ADALIMUMAB 24 µg/mL VS UNTREATED	+0.20
		II	sTNFα 100 ng/mL VS UNTREATED	+0.47
			TROS 30 µM VS sTNFα 100 ng/mL	-0.31
			TROS 30 µM VS UNTREATED	+0.17
TJP2 (ZO-2)	Intracellular, scaffolding TJP which can also regulate gene expression at the nucleus.	I	sTNFα 100 ng/mL VS UNTREATED	+0.10
			ADALIMUMAB 24 µg/mL VS sTNFα 100 ng/mL	-0.16
			ADALIMUMAB 24 µg/mL VS UNTREATED	-0.05
		II	sTNFα 100 ng/mL VS UNTREATED	+0.05
			TROS 30 µM VS sTNFα 100 ng/mL	-0.04
			TROS 30 µM VS UNTREATED	+0.01
TJP3 (ZO-3)	Intracellular, scaffolding TJP.	I	sTNFα 100 ng/mL VS UNTREATED	-0.08
			ADALIMUMAB 24 µg/mL VS sTNFα 100 ng/mL	-0.09
			ADALIMUMAB 24 µg/mL VS UNTREATED	-0.17
		II	sTNFα 100 ng/mL VS UNTREATED	-0.11
			TROS 30 µM VS sTNFα 100 ng/mL	-0.02
			TROS 30 µM VS UNTREATED	-0.13
MYLK (Myosin Light Chain Kinase)	Master regulator of the leak permeability pathway: determines the delocalization of Occludin and ZO-1 out of the TJ density	I	sTNFα 100 ng/mL VS UNTREATED	-1.04
			ADALIMUMAB 24 µg/mL VS sTNFα 100 ng/mL	+0.97
			ADALIMUMAB 24 µg/mL VS UNTREATED	-0.06
		II	sTNFα 100 ng/mL VS UNTREATED	-1.35
			TROS 30 µM VS sTNFα 100 ng/mL	+1.2
			TROS 30 µM VS UNTREATED	-0.15
MKI67 (Antigen Ki67)	Nuclear protein, marker of cell proliferation. Present during the active phases of the cell cycle and absent in quiescent cells.	I	sTNFα 100 ng/mL VS UNTREATED	-0.04
			ADALIMUMAB 24 µg/mL VS sTNFα 100 ng/mL	+0.32
			ADALIMUMAB 24 µg/mL VS UNTREATED	+0.29
		II	sTNFα 100 ng/mL VS UNTREATED	-0.04
			TROS 30 µM VS sTNFα 100 ng/mL	+0.22
			TROS 30 µM VS UNTREATED	+0.18
PCNA (Proliferating Cell Nuclear Antigen)	Auxiliary protein of the DNA polymerase δ involved in the control of eukaryotic DNA replication. Marker of cell proliferation.	I	sTNFα 100 ng/mL VS UNTREATED	+0.27
			ADALIMUMAB 24 µg/mL VS sTNFα 100 ng/mL	-0.06
			ADALIMUMAB 24 µg/mL VS UNTREATED	+0.21
		II	sTNFα 100 ng/mL VS UNTREATED	+0.20
			TROS 30 µM VS sTNFα 100 ng/mL	+0.04

			TROS 30 µM VS UNTREATED	+0.23
TRADD (TNF receptor type 1-associated Death Domain protein)	Death domain-containing protein that takes part in the activation of the extrinsic apoptotic pathway.	I	sTNFα 100 ng/mL VS UNTREATED	-0.03
			ADALIMUMAB 24 µg/mL VS sTNFα 100 ng/mL	-0.06
			ADALIMUMAB 24 µg/mL VS UNTREATED	-0.09
		II	sTNFα 100 ng/mL VS UNTREATED	-0.03
			TROS 30 µM VS sTNFα 100 ng/mL	-0.09
			TROS 30 µM VS UNTREATED	-0.12
FADD (FAS-associated Death Domain protein)	Death domain-containing protein that takes part in the activation of the extrinsic apoptotic pathway.	I	sTNFα 100 ng/mL VS UNTREATED	+0.23
			ADALIMUMAB 24 µg/mL VS sTNFα 100 ng/mL	-0.25
			ADALIMUMAB 24 µg/mL VS UNTREATED	-0.02
		II	sTNFα 100 ng/mL VS UNTREATED	+0.20
			TROS 30 µM VS sTNFα 100 ng/mL	-0.25
			TROS 30 µM VS UNTREATED	-0.05
BAX (Bcl-2-associated X protein)	Pro-apoptotic protein that takes part in the activation of the intrinsic apoptotic pathway by regulating the permeability of the outer mitochondrial membrane.	I	sTNFα 100 ng/mL VS UNTREATED	+0.05
			ADALIMUMAB 24 µg/mL VS sTNFα 100 ng/mL	+0.05
			ADALIMUMAB 24 µg/mL VS UNTREATED	+0.10
		II	sTNFα 100 ng/mL VS UNTREATED	-0.01
			TROS 30 µM VS sTNFα 100 ng/mL	+0.02
			TROS 30 µM VS UNTREATED	+0.02
TP53 (Tumor protein P53)	Pro-apoptotic protein that regulates the transcriptional activation of the proteins PUMA and NOXA, which activate the intrinsic apoptotic pathway.	I	sTNFα 100 ng/mL VS UNTREATED	+0.55
			ADALIMUMAB 24 µg/mL VS sTNFα 100 ng/mL	-0.37
			ADALIMUMAB 24 µg/mL VS UNTREATED	+0.18
		II	sTNFα 100 ng/mL VS UNTREATED	+0.50
			TROS 30 µM VS sTNFα 100 ng/mL	-0.43
			TROS 30 µM VS UNTREATED	+0.08
BCL2 (B-cell lymphoma 2)	Anti-apoptotic protein that controls this intrinsic pathway by regulating the permeability of the outer mitochondrial membrane.	I	sTNFα 100 ng/mL VS UNTREATED	-0.47
			ADALIMUMAB 24 µg/mL VS sTNFα 100 ng/mL	+0.46
			ADALIMUMAB 24 µg/mL VS UNTREATED	-0.01
		II	sTNFα 100 ng/mL VS UNTREATED	-0.43
			TROS 30 µM VS sTNFα 100 ng/mL	+0.53
			TROS 30 µM VS UNTREATED	+0.11
MLKL (Mixed lineage kinase domain like pseudokinase)	Pro-necroptotic protein phosphorylated and activated by the complex RIPK1/3, which executes the lysis of the plasma membrane.	I	sTNFα 100 ng/mL VS UNTREATED	+0.53
			ADALIMUMAB 24 µg/mL VS sTNFα 100 ng/mL	-0.32
			ADALIMUMAB 24 µg/mL VS UNTREATED	+0.21
		II	sTNFα 100 ng/mL VS UNTREATED	+0.53
			TROS 30 µM VS sTNFα 100 ng/mL	-0.33
			TROS 30 µM VS UNTREATED	+0.20
RIPK1 (Receptor-interacting serine/threonine-protein kinase 1)	Pro-necroptotic protein that interacts with RIPK3 forming the "ripoptosome" that activates MLKL.	I	sTNFα 100 ng/mL VS UNTREATED	+0.03
			ADALIMUMAB 24 µg/mL VS sTNFα 100 ng/mL	-0.03
			ADALIMUMAB 24 µg/mL VS UNTREATED	0.00
		II	sTNFα 100 ng/mL VS UNTREATED	+0.03
			TROS 30 µM VS sTNFα 100 ng/mL	-0.06
			TROS 30 µM VS UNTREATED	-0.03
RIPK3 (Receptor-interacting serine/threonine-protein kinase 3)	Pro-necroptotic protein that interacts with RIPK1 forming the "ripoptosome" that activates MLKL.	I	sTNFα 100 ng/mL VS UNTREATED	-0.33
			ADALIMUMAB 24 µg/mL VS sTNFα 100 ng/mL	+0.46
			ADALIMUMAB 24 µg/mL VS UNTREATED	+0.12
		II	sTNFα 100 ng/mL VS UNTREATED	-0.31
			TROS 30 µM VS sTNFα 100 ng/mL	+0.10
			TROS 30 µM VS UNTREATED	-0.21

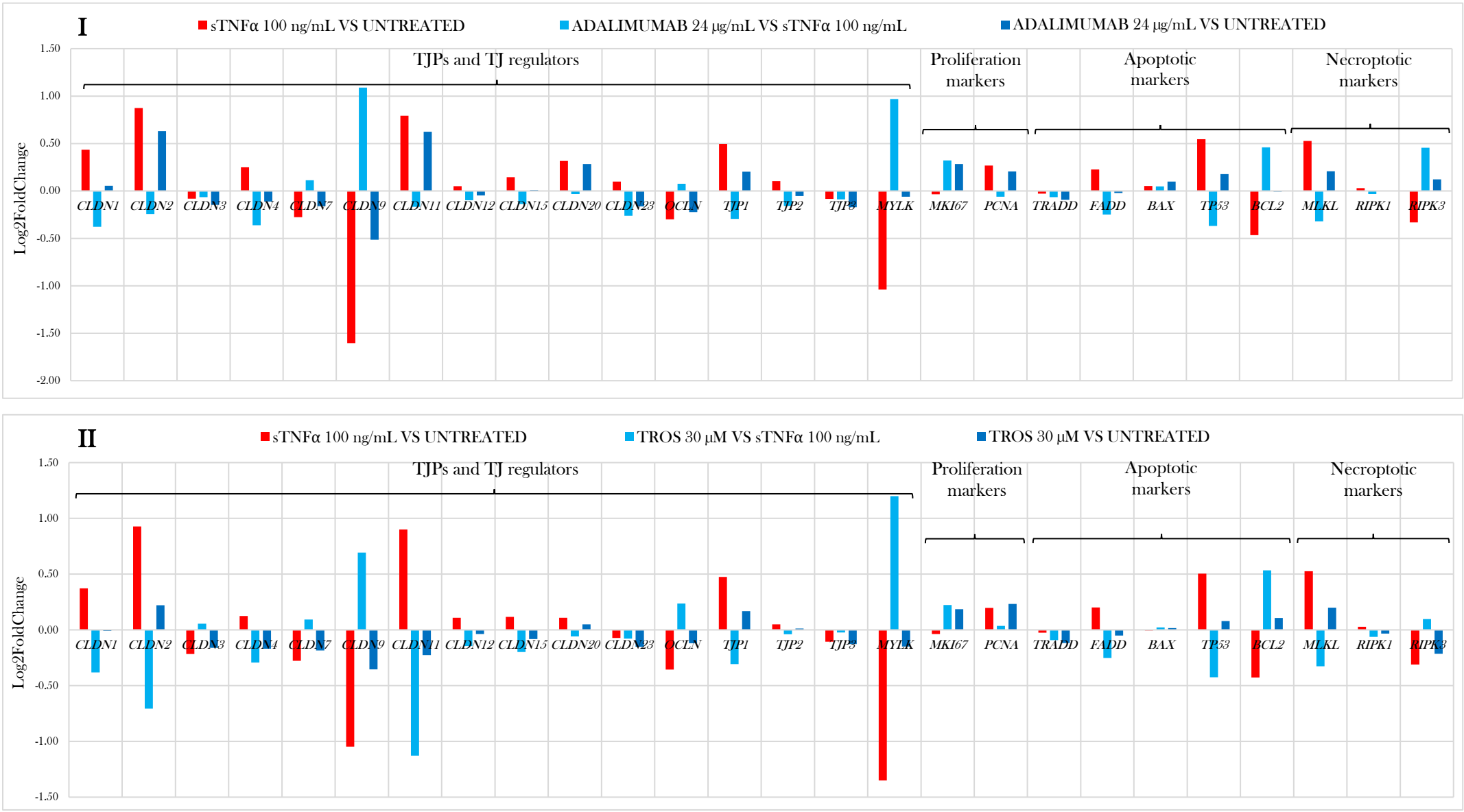

Figure 117: Differential expression (Log2FoldChange of the normalized mean hit counts, n=3) of functionally relevant genes in the context of intestinal epithelial barrier function assessed by RNAseq. Experiments of full neutralization of sTNFα in solution (I) and of full competitive antagonism of TNR1A (II), at the timepoint +24 hrs.

5. DISCUSSION

5.1. *In vitro* differentiation of T84 and CACO-2 cell lines into a two-dimensional epithelial-like structure

Different epithelial cell lines obtained from human biopsies are available on the market. These cells were originally dissociated and isolated from the primary tissue material and then transferred to *in vitro* cell culture conditions where they can be kept for few or for many passages reaching a state of so-called immortalization. Normal non-transformed cell lines have the advantage of representing better the original tissue physiological conditions but have the disadvantage of being less robust, meaning that can be kept in general for few (a dozen) passages in culture, are more reluctant to differentiate *in vitro* and are more sensitive to the different culture conditions. On the other side tumoral or transformed cell lines immortalize in cell culture (and can be kept for even 50-60 passages), differentiate easily and are more resistant to the various culture conditions. The important disadvantage of tumoral cell lines is that they carry drastic gene and chromosomal aberrations which confer them unique non-physiological properties. In the initial part of my work I defined the optimal differentiating conditions for T84 and CACO-2, two intestinal epithelial colorectal carcinoma cell lines that would have served as the first platform for the establishment of the inflammatory model of the intestinal epithelium and for the pharmacological interference experiments necessary to dissect the TNFα/TNR1A/TNR1B signalling axis. In accordance to the literature, although both cells derive from a colorectal carcinoma, the morphological and functional differentiation of CACO-2 recapitulates the characteristics of enterocytes (the absorptive cells of the small intestine), while differentiated T84 resemble at a higher extent the properties of colonocytes (the absorptive cells of the colon)[83].

In a first attempt to differentiate the T84 and CACO-2, the cells were simply grown until reaching confluency over glass coverslips, a suitable movable substrate for performing IF stainings. Cell confluency was considered the first essential prerequisite for the differentiation of epithelial cells into an epithelial-like structure and the variables tested to optimize the differentiation process were the seeding density and the coating of the glass substrate. Collagen Type I is the most abundant collagen type and it was employed to mimic an extracellular matrix or even the basement membrane (although in the second one the most abundant collagen type is the IV) with which the intestinal epithelial cells interact *in vivo*. The harsh acid treatment could have eventually served to prepare the glass surface for the attachment of the epithelial cells. The differentiation progress was monitored by conventional RT-PCR of *TJP1* and, very importantly, by IF staining of its protein, ZO-1. ZO-1 is a scaffolding TJP that is expressed at a basal level in epithelial cells and that reaches its functional latero-apical cytoplasmic location during the process of polarization and differentiation. This protein is in fact recruited to nascent adhesion sites by the formation of AJs and, once in that position, it

forms together with ZO-2 a membrane-attached scaffold that facilitates the formation and sub-apical positioning of Claudin strands and sequesters cytoskeleton and signalling proteins[84]. Being a key protein required for TJ formation and localization, its positioning at the latero-apical cytoplasm indicates the complete formation of the TJB, serving as a guide for assessing cell polarization and differentiation. The expression of *TJP1* at mRNA level that I observed in this first experiment demonstrated the basal expression of that gene disregarding of the differentiation status. Even at fully confluent stages, the simple seeding over an homogeneous substrate did not promote cell polarization and differentiation, as demonstrated by the absence of ZO-1 at its functional subcellular localization. The two coating strategies did not determine significant differences in the behavior of the cells, but of course Collagen I mimicked better the substrate over which these cells grow *in vivo*. Interestingly, a clear signal of ZO-1 at the latero-apical cytoplasm (following a ring-like shape) was observed only at the floating edges of the monolayers, giving a hint about the reason for the lack of differentiation.

The differentiation of T84 and CACO-2 as polarized epithelial monolayers was achieved by testing the key factors and conditions described in the literature[74-77]. At least for this kind of transformed cell lines, not only 100% confluency is a prerequisite for the differentiation but also the possibility for the cells to be in contact with growth media from two sides is a critical factor. These are the two cellular sides that become, upon differentiation, the apical and basolateral domains that account for both a structural and a functional polarization. When these cells reach confluency over permeable filter supports (also under standard normoxic cell culture conditions) they spontaneously differentiate acquiring a cylindrical polarized morphology with microvilli on the apical side, establishing functional TJs and AJs and expressing a series of relevant markers including genes coding for different TJPs, *CDH1* (cadherin-1), *VIL1* (villin-1), and *EGF-R* (Epidermal Growth Factor Receptor)[76,77], among others. By growing these cells over semi-permeable supports I could not only induce their differentiation but also monitor it with the key functional assays for assessing barrier function: the measurement of TEER with regards to ions and the quantification of the permeability towards fluorescently labeled Dextrans of different molecular weights. In these second series of differentiation experiments over semipermeable membranes, I applied the aforementioned functional assays and assessed the expression at mRNA level and the expression and localization at protein level of ZO-1 (*TJP1*). The establishment of barrier function was properly assessed with the permeability assays and the functional subcellular localization of ZO-1 at the latero-apical cytoplasm could be properly observed upon cell polarization, confirming the successful differentiation process. The expression of *TJP1* at mRNA was kept constant during the whole differentiation process for both cell lines confirming the results obtained in the first, failed, differentiation trial. The clear results obtained by growing the cells over TW inserts showed that the only way to push the epithelial differentiation in a synchronized manner was to grow the cells for several days after confluency and allowing them to be in direct contact with growth media from both the apical and the basolateral

sides. These two factors were sufficient for differentiating transformed intestinal epithelial cell lines that are more robust than normal cell lines and, even though are initially dedifferentiated, are not in a real condition of stemness (that would require other parameters to play with, as the modulation of different transcription factors). Out of the protocols applied for T84 and CACO-2 in normoxic conditions, it was possible to obtain fully differentiated intestinal epithelial monolayers in a 3D rather than in a 2D configuration. As clearly evidenced from the IF stainings, the highly proliferative, uncontrolled capacities of both cell lines determined the formation of domes, where there was an evident multiple-layer configuration. This was the main, or the only, disadvantage of the model, and had the following consequences: **i)** it did not perfectly resemble the real 2D configuration, **ii)** it impaired the outcome of the IF stainings (overlapping signals at widefield microscopy, irregularity of the cell layer/s given the presence of the domes, opacity of the samples, necessity to apply harsh permeabilizing treatments) and **iii)** it influenced the outcomes of the TEER and the permeability assays by a reason (multiple-layer) that went beyond the mechanisms that account for the intestinal barrier function *in vivo*. Comparing the results obtained for T84 and CACO-2 grown over TW inserts, I drove the following conclusions summarized in Table 9.

Table 9: Comparison of T84 and CACO-2 differentiation over TW inserts with 3.0 μm pores in normoxic conditions.

Parameter	**T84**	**CACO-2**
Days in culture for reaching a fully differentiating condition	7-10	16-20
Highest TEER values achieved	±3500 Ω x cm^2	±1290 Ω x cm^2
FD4 permeability	Decreased gradually concomitant to the differentiation process	Imperceptible from early time-points
Inter-TW variance	Low	High
Proliferative capacity and tendency to form domes	High	Very high
Cell homogeneity	Low at sub-differentiating and high at fully differentiating conditions	Low at sub-differentiating and high at fully differentiating conditions
Optimal or good seeding density	$3.6x10^5$ cells/cm^2	$3.6x10^5$ cells/cm^2

As explained in the Results section, I decided to continue working only with T84 as **i)** it needed less days for reaching high TEER values, **ii)** it presented a low inter-TW variance and **iii)** showed lower proliferating capacities than CACO-2 (tending to form less domes and exhibiting a time-window in the differentiation curve, at sub-differentiating stages, at which significant changes in the permeability of FD4 were observed).

Working with T84 over semipermeable membranes, I decided to run a pilot experiment in which I monitored the proliferative state of the cells during the differentiation process employing the BrdU assay. The outcome of the experiment demonstrated that the assay is a valuable tool for assessing this important cellular process at the basis of the epithelial repair and restitution capacities (essential for the maintenance of the contiguity of an epithelial monolayer and of its TJ network). The decrease of BrdU positive cells concomitant to the differentiation process confirms that a diminution of the proliferation rate takes place due to inhibition by cell-to-cell contact, as expected. However, the overgrowth of T84 after reaching confluency (formation of domes that corresponded to overlapping signals of the stained nuclei with Hoechst) demonstrated that cell proliferation was still taking place, at a lower rate, at these stages and that the cellular configuration in a tissue-like structure might have impeded the proper staining of BrdU positive cells (as happened for the TUNEL assay, section 4.3.1.).

A final improvement of the differentiation protocol was implemented, aiming to obtain a more physiologically relevant model of the intestinal epithelium, by growing T84 not only over TW inserts but also in hypoxic conditions. As explained in section 1.1.2.2.2. of the Introduction, the partial pressure of O_2 at the tip of the villus, where differentiated epithelial cells reside, is lower than at the crypt, where the stem cell niche is located. Decreasing the O_2 concentration in the cell culture atmospheric conditions would have not only induced the activation of regulatory mechanisms at the basis of the differentiation process, but would have also reduced the proliferative capacities of these cells as is observed for intestinal epithelial cells *in vivo* (from the initiation of the transit amplifying process to the completion of the differentiation process). Given the highly proliferative capacities of transformed cell lines as T84 and the recurrent formation of domes at different days of growth post-confluency, an important advantage of growing the cells in hypoxic conditions would have been the obtainment of a real cellular monolayer configuration. This configuration would have been not only more physiologically relevant but it would have also improved the outcome of the different permeability assays (by not impeding the diffusion of the different fluorescently labeled molecular species for reasons different than the level of barrier function), of the LDH assay (by allowing a proper diffusion of the LDH into the apical media) and of the IF stainings, the TUNEL (section 4.3.1) and the BrdU assays (by avoiding problems related with the opacity of a tissue-like cellular configuration and with antibody trapping). Furthermore, it would have eventually also improved the responsiveness of the monolayers (as a whole tissue entity) to pharmacological modulations from the basolateral side. In a pilot experiment, I tested not only the cell differentiation behavior in hypoxia but also a membrane porosity of 0.4 μm and different membrane coating strategies with Matrigel. The porosity of 0.4 μm was implemented aiming to avoid any possible migration of cells from the apical to the basolateral side of the insert membrane determining the eventual formation of a second cell monolayer with an opposite polarity towards the basolateral side. This was an important point to consider, as T84 derives from a lung metastasis of a colorectal carcinoma, and metastatic

cells are prone to degrade the extracellular matrix and migrate undergoing an Epithelial Mesenchymal Transition. The formation of a double monolayer, with an opposite polarity, would drastically impair the contact of the basal domains of both of them with the growth media, impairing the differentiation process and also the responsiveness to any stimulus applied from the basolateral side. The idea of the coating employing Matrigel was to mimic in the best way the intestinal epithelial basement membrane with regards to protein composition and configuration. Matrigel is a solubilized basement membrane preparation extracted from the Engelbreth-Holm-Swarm mouse sarcoma, composed of laminin, collagen IV, heparan sulfate proteoglycans and entactin/nidogen. By testing three different protein concentrations and two coating strategies, the goal was to obtain the thinnest possible ECM layer, homogeneously distributed over the membrane and with a high protein concentration to optimize the cell-to-matrix interactions. The results clearly showed that the coating strategies in which the thinnest possible layers were established (lowest concentrations that did not gelify fast) allowed the obtainment of the best differentiation curves. A very important result of this pilot experiment was the demonstration by confocal microscopy that T84 did not form domes in these growing conditions and that it acquired a tissue-configuration that approximated more to a real 2-dimentional one.

5.2. Characterization of T84 and CACO-2 regarding the expression of HTR3 genes and identification of a putative novel *HTR3E* transcript variant

As a parallel project for my Ph.D. thesis, I started the characterization of the serotonergic receptors system in this intestinal epithelial *in vitro* model.

Serotonin or 5-HT is a phylogenetically highly conserved neurotransmitter, hormone and paracrine signalling molecule. Nearly 95% of the total 5-HT of the human body is produced, stored and released by the GI epithelial enterochromaffin cells. Interacting with 15 different membrane receptors (5-HTRs), 5-HT regulates multiple physiological processes including immune functions by promoting the recruitment, activation and cytokine-production of innate immune cells and by activating and enhancing the proliferation of T- and B-cells[18,19]. At least five classes of 5-HTRs (1-4 and 7) are expressed in epithelial, immune, neuronal and muscle cells coordinating the intrinsic functions of the GI tract, promoting the growth and turnover of the GI epithelium[85] and regulating the GI immune responses. Even though 5-HT acts as a key pro-inflammatory molecule in this location[86-89], the function of most 5-HTRs have not been systematically evaluated in the context of IBD (especially at the level of the GI epithelium) and there are proofs of the multifaceted and opposed roles of each of them[57]. Taking into consideration that 5-HT is a pro-inflammatory molecule produced and stored in considerable amounts at the level of the GI mucosa, a possible role of it in the context of the GI epithelial barrier function could be hypothesized. The selective pharmacological modulation (either agonism or antagonism, as stated in Coates *et al*. 2017[57]) of the different 5-HTRs expressed by GI epithelial cells might lead to barrier function impairing or

protective effects. Out of the five 5-HTRs known to be expressed in GI epithelial cells, three of them (5-$HT_{3,4,7}$Rs) were found highly upregulated in Crohn's disease colonic biopsies[89], and are promising candidates for mediating most of the 5-HT signalling in these chronic inflammatory conditions.

As a first step to carry out the characterization of this signalling in intestinal epithelial barrier function, I decided to assess the transcription level of the 5-HTRs expected to be expressed by both CACO-2 and T84 cell lines (as intestinal epithelial cells), at the different stages of their differentiation process. By conventional RT-PCR I found that, out of the five members of the 5-HT3Rs gene family (*HTR3A/B/C/D/E* genes), CACO-2 expressed *HTR3A/B/E* at a similar extent at all time points of the differentiation process. On the other side, all members of the gene family were expressed by T84, some of them only at differentiated stages (*HTR3B/C*), others constantly at all time points of the differentiation process (*HTR3A/E*) and *HTR3D* not following a clear pattern.

The outcome of this expression analysis suggested T84 to be more suitable than CACO-2 as a cell line for the study of the 5-HT3Rs, at least, and presented another interesting result. The amplification of *HTR3E*, from both cell's cDNA samples, gave rise to an amplicon that was larger than the expected one (and obtained with the positive control recombinant cDNA), suggesting that the last intron had been retained (as the size of 275 bp corresponded exactly with that situation) and that a novel splicing variant of this gene was expressed by these cell lines. The sequencing of the obtained amplicon demonstrated that the last intron had been indeed retained, and two RT-PCRs with two set of primers designed for the amplification of the full length of *HTR3E* showed that the amplicon did not belong to any of the actually annotated splicing variants.

In order to identify the flanking regions of the obtained internal amplicon of HTR3E, I performed a 5'/3'RACE-PCR. The positive results obtained with the control 5'/3'RACE PCRs for *ACTB* confirmed the good quality of the starting material for the preparation of the whole-cell sscDNAs library, and the suitability of all the components of the kit for its preparation. The 3'RACE PCRs for the internal amplicon of *HTR3E* gave rise to a band which carried a sequence conserved at the 3' end of all the annotated *HTR3E* splicing variants. The 5'RACE PCRs, instead, gave rise to a band of 700-750 bp that could not be successfully cloned and sequenced, but that very probably contained the novel combination of exons of a new putative *HTR3E* splicing variant (see figures 40 and 41).

Given the expected difficulty of obtaining 5'RACE fragments, for an internal known sequence located a the 3' region of the locus, the experiment should be repeated further optimizing the cDNA synthesis step (as I did employing in this step the internal sequence reverse primer, instead of the Oligo-dT primer) and by optimizing the ligation of the RNA oligo at the 5'-end of all the cells mRNAs (in the process of preparation of the whole-cell sscDNAs library with known flanking sequences).

5.3. Characterization of the FHC cell line for its *in vitro* differentiation into a two-dimensional epithelial-like structure

Considering the negative aspects of working with a tumoral cell line, that not only carry chromosomal aberrations but that also tend to overgrow forming domes, I decided to start working on the establishment of the differentiation of a normal intestinal epithelial stem cell line, aiming to obtain a more physiologically relevant 2D *in vitro* model of the intestinal epithelium.

The FHC commercial cell line (ATCC® CRL-1831™) consists on an heterogeneous colonic cell population derived from human fetuses of 13 to 17 weeks of conceptual age. The cell line was established by Siddiqui and Chopra, 1984[90] who described it as a combination of epithelial cells that resemble the basal portion of colon crypts (colonic epithelial stem cells), goblet cells and fibroblasts. In accordance with the authors, the fibroblasts outnumber the epithelial cells and are required for the sustained proliferation and maintenance of the stemness condition of the last ones, so in a first experiment I tried to remove the excess of fibroblasts by differential plating. In order to evaluate, at least a semi-quantitatively, the separation of the two cell types (fibroblasts and all the other cell types), I monitored the expression of relevant markers by conventional RT-PCR in the two differential plating fractions. The expression of the fibroblast marker *ACTA2*, maintained at the same level in both cellular fractions, at two differential plating times, and in two independent cell lines of FHC (biological replicas), demonstrated straight away that this strategy was not successful in sorting the two aforementioned cell types. The two intestinal epithelial differentiation markers *VIL1* and *KRT20* were not expressed in any fraction, in line with the fact that the epithelial cells present in the FHC population were expected to be in an undifferentiated condition as reported by Siddiqui and Chopra, 1984 and considering that the cell culture conditions (substrate and media composition) would have never promoted any differentiation process. On the contrary, the key intestinal epithelial stem cell markers *PROM1*, *LGR5* and *LRIG1* were expressed, confirming the presence of intestinal epithelial stem cells in the FHC cell population. The expression of these markers in both cellular fractions confirmed that the differential plating strategy was not successful in separating fibroblast and intestinal epithelial stem cells. Even though *LRIG1* is an intestinal epithelial stemness marker, it was expected to be also expressed in fibroblasts (that is why as a positive control the total cDNA of M-PKE fibroblasts was used as a template). Interestingly, it was observed slightly more expressed in the expected fibroblasts fractions.

These results brought to the conclusion that a more sophisticated cell sorting protocol should be tested and defined before attempting to differentiate the intestinal epithelial stem cells over TW inserts. Indeed, a first trial of differentiation of the unsorted FHC cells by growing them over polycarbonate membrane with pores of 3 µm, in normoxia, showed no increase of TEER over the baseline, even after 30 days.

5.4. Establishment of the optimal pro-inflammatory input for determining the loss of barrier function

The establishment of the *in vitro* inflammatory model of the intestinal epithelium consisted on the definition of the optimal combination, concentrations and times of application of pro-inflammatory cytokines necessary to significantly disrupt a differentiated T84 monolayer, in order to mimic the barrier dysfunction that takes place *in vivo*. Four key requisites were taken into consideration for this purpose: **i)** employing concentrations comparable to the ones present in the literature, applied in a similar *in vitro* model (expected to be close to the pathophysiological concentrations taking action *in vivo*), **ii)** not causing an unwanted cytotoxic effect (that would have determined mainly a pro-necrotic effect), **iii)** being able to determine significant increases of paracellular permeability detectable with all TEER and FD4 and FD70 assays, starting from a differentiated/polarized condition, **iv)** integrating all the aforementioned requisites in order to adapt the model to the final goal of establishing a platform for pharmacological interference experiments.

The pro-inflammatory cytokines TNFα (soluble form), IFNγ and IL-1β were chosen as they are hallmarks of IBD and have been shown to be implicated in the impairment of the intestinal epithelial barrier-function in this context[53,55]. In accordance to the literature, these cytokines modulate mechanisms underlying all three paracellular permeability pathways by interacting with their cognate receptors, distributed in a polarized fashion at the plasma membranes of differentiated intestinal epithelial cells. The basolateral distribution of the cognate receptors has been shown for TNFα[56] and IFNγ[55], and the same was expected for IL-1β.

The definition of the optimal inflammatory model required four different series and typologies of experiments. The first two consisted on the induction with sTNFα and IL-1β at relatively low concentrations on monolayers not fully differentiated. The third one consisted on the application of the cytokines sTNFα and IFNγ in combination and alone, at high concentrations and at fully differentiated conditions. And the fourth type of experiment consisted on the application of only sTNFα at different concentrations, on fully differentiated monolayers, in hypoxic conditions.

In the first series of experiments (Experiment I) I tested in both T84 and CACO-2 an induction at the onset of the differentiation process, with both sTNFα and IL-1β, at concentrations in the range of the 10 ng/mL for each, and I evaluated the effects by measuring only the TEER every 24 hrs. The induction was kept for three days and then removed in order to evaluate how fast the barrier function impairment could be recovered. Considering the low variance in between technical and biological replicas, the statistically significant drop of TEER observed upon induction with the cytokines, the higher TEER values reached and the fast recovery (comparing with the untreated condition) observed after the removal of the input, I could confirm again T84 as the most appropriate cell line to continue working with.

As the induction at the onset of the differentiation process did not reflect in the best way the real pathophysiological process (keeping in mind that, *in vivo*, the barrier dysfunction determined by the cytokines takes place on fully polarized, differentiated cells), in the second series of experiments (Experiment II) a slight delay of the time point of induction was implemented (monolayers of ~800 $\Omega \cdot cm^2$). In these experiments I also incorporated the FD4 and the LDH assays. The increase of permeability with regards to the FD4 would have depended on whether the stimulus would have modulated the leak and unrestricted permeability pathways, and the increase of LDH in the apical media would have indicated an increase of Necrosis and/or Necroptosis that would have affected the unrestricted permeability pathway. The results of these second series of experiments showed that a statistically significant drop of TEER took place, at least after 24 and 48 hrs of induction, but it was not reflected by an increase of permeability towards the FD4. On the other side, a statistically significant increase of LDH in the apical media was observed at all time points. Taking into consideration the expected pro-necroptotic effect, at least for sTNFα[43], and the fact that the increase of LDH with respect to the untreated condition was of not more than 10% (generally accepted threshold for an eventual cytotoxic effect determined by a certain substance applied in an *in vitro* model), the observed increase of plasma membrane lysis was considered to be determined (mainly) by a necroptotic process.

Aiming to work at more physiologically relevant conditions and to reduce the TEER variance in between technical and biological replicas at the time point of induction, a third type of experiment (Experiment III) was performed in which the monolayers were allowed to fully polarize before applying the cytokines stimulus. The goals were to determine a significant barrier-dysfunction properly detectable with all the TEER and the FD4 and FD70 permeability assays (in order to then being able to employ these assays to assess a protection towards the deregulation of all three paracellular permeability pathways), employing concentrations comparable to the ones present in the literature and without causing an unwanted cytotoxic effect. Expecting the monolayer to be more reluctant to respond to the cytokine input at fully differentiating conditions, and considering that an increase of LDH of not more than 10 % was observed in the second set of experiments, higher concentrations were tested in this case. Furthermore, the cytokine combination sTNFα and IFNγ was incorporated as, in accordance to the literature[55,91,92], I expected them to manifest a synergistic effect and so, to determine a proper barrier disruption even on monolayers with high resistance values.

In the experiment IIIa and IIIb, the two cytokines combinations sTNFα/IL-1β and sTNFα/IFNγ were applied at either 10 ng/mL or 100 ng/mL each in order to directly define the optimal combination for my purposes. sTNFα/IFNγ at 100 ng/mL determined the most drastic effects on the epithelial barrier function of fully differentiated T84 monolayers. By repeating the experiment in multiple biological replicas, I found that either the decrease of TEER, the increase of permeability towards FD4 (the FD70 was not tested in this experiment) and the increase of LDH in the apical media were statistically significant. Importantly, in five biological replicas an average increase of LDH of ~8%

was observed with respect to the uninduced condition, allowing me to discard an unwanted cytotoxic effect for this cytokine combination and working concentration. Considering the capabilities of sTNFα/IFNγ at 100 ng/mL to significantly impair fully differentiated T84 monolayers, without inducing unwanted cytotoxic effects, and being possible the assessment of this process with all the aforementioned assays, I considered this cytokines combination and concentrations as an optimal one for mimicking the barrier dysfunction of the intestinal epithelium taking place in chronic inflammatory conditions. The upregulation of these proinflammatory cytokines is a hallmark of CD[40] and the concentration of 100 ng/mL for both was already employed by Schmitz *et al.* 1999[92] in comparable *in vitro* conditions.

On the same setup of the Experiment IIIb, I ran a TUNEL assay for quantifying the DNA double strand breaks, characteristic of the late apoptotic stages (that affect the unrestricted permeability pathway). This should have allowed me to assess the contribution of the activation of the extrinsic apoptotic pathway by sTNFα/IFNγ 100 ng/mL to the impairment of the monolayer (expected in accordance to the literature[43]). The result of this experiment demonstrated that the condition of the epithelial cells, fully differentiated over a TW membrane and forming a 3D rather than a 2D structure, intrinsically impaired the outcome of the chromatin staining of apoptotic cells. The positive control of cells grown over TW inserts and pre-treated with DNAaseI, gave a reasonable result only when the IF detection was performed together with a harsh permeabilizing treatment with TX-100. A proper positive control was only obtained when the same experiment was performed on cells simply grown over glass coverslips. Leaving aside the positive control (in spite of its crucial importance), no clear increase of TUNEL positive cells was observed on monolayers induced with sTNFα/IFNγ at 100 ng/mL, in any of the tested growth and permeabilizing conditions. Noteworthy, Petecchia *et al.* 2012[93] have shown that similar inflammatory conditions in another epithelial model (Calu3 airway epithelial cells treated with sTNFα 10 ng/ml, IL-4 5 ng/ml and IFNγ 50 ng/ml for 48 hrs) did not lead to an increase of TUNEL positive cells. They could show that apoptotic cells are extruded from epithelia by a process similar to the one taking place in Anoikis (a form of programmed cell death that occurs in anchorage-dependent cells when they detach from the surrounding extracellular matrix) fairly rapidly, so the quantification of DNA damage can be missed at any given time (by the washing out of late apoptotic cells). This might explain my results with the TUNEL assay (figure 55). On the contrary, Necroptosis could be assessed as the LDH released into the apical media by both floating and monolayer-associated cells could be easily quantified.

Even though the cytokine combination sTNFα and IFNγ determined a statistically significant barrier function impairment in fully differentiated monolayers, and resembles better the pathophysiological conditions of IBD (upregulation of different proinflammatory cytokines), I decided to run the experiment IIIc applying the single cytokines at fully differentiated stages. Doing so, I have characterized, in a clear way, the single cytokines signallings with regards to barrier function. The experiment IIIc was performed applying sTNFα or IFNγ to fully differentiated monolayers from the

basolateral side, at 100 ng/mL and for two different incubation times, 12 and 24 hrs. Considering that after defining the optimal conditions for the inductions, the work followed with different pharmacological modulations aiming to characterize the single cytokines signallings at different levels, the incubation time of 12 hrs was tested in order to not extend excessively the overall times of treatment (time of pre-treatment with a specific pharmacological modulator plus time of co-treatment with a certain cytokine).

The induction with sTNFα at 100 ng/mL for 12 hrs determined a statistically significant barrier function impairment at the levels of all three paracellular permeability pathways (figures 56, 57 and 59). As expected, the extent of impairment was lower than the one observed for the combination sTNFα/IFNγ (applied at the same concentration, but for 24 hrs), as this one is known to determine a synergistic pro-inflammatory and barrier disruptive effect. Importantly, the FD70 assay was implemented in this experiment and ran in one biological replica (figure 58), in order to assess the unrestricted paracellular permeability pathway (dominated by the rate of both Apoptosis and Necroptosis). Even though sTNFα is known to determine an increase of either Apoptosis and Necroptosis, mediated by TNR1A, an increase of permeability towards this molecular specie could not be observed in the aforementioned conditions, as I would have expected. Indeed, the increase of 6% of LDH in the apical media induced by sTNFα, and with high probability determined only by an increase of Necroptosis, was not reflected by an increase of permeability towards FD70. A first possible explanation for this was the fact that, as explained before, T84 is a highly proliferative cell line and, in the experiments ran under normoxic conditions, it grew forming multiple cell layers. This 3D configuration could have impeded, with high probability, the diffusion of this molecular species of 70 kDa MW, independently of the undergoing rate of Apoptosis and Necroptosis. This phenomenon would have been of course non-physiologically relevant and would have hidden an increase of paracellular permeability determined by the modulation of the unrestricted pathway. Further experiments were necessary to confirm this explanation, and to properly implement the FD70 assay (see below).

In order to evaluate if a prolongation of the incubation time could have intensified the barrier-disruptive effects determined by sTNFα applied alone, the same experiment was performed but letting the induction act for 24 hrs. This experiment would have been strictly comparable to the one of co-treatment with sTNFα and IFNγ, so the clear effects of the synergism in between the two cytokines could have been evidenced. The conclusion reached after the second experiment of barrier disruption with only sTNFα at 100 ng/mL was that an extension of the incubation time determined a milder effect (at all levels) than the one observed by inducing for 12 hrs. Even though the number of biological replicas was lower for the second experiment, the results are conclusive (n=3). An explanation for this milder effect could be the loss of biological activity of sTNFα over time in the cell culture media. The results of the two experiments with only sTNFα were positive as demonstrated that a shorter incubation time determined a more drastic barrier function impairment

at all levels. This would have allowed me not only to clearly assess an eventual barrier function protection in the subsequent pharmacological interference experiments aiming to dissect the TNFα/TNR1A/TNR1B signalling axis, but also to perform such experiments without excessively extending the overall times of treatment.

The set of experiments IIIc included also the sole induction with IFNγ at 100 ng/mL for both 12 and 24 hrs. From the measurement of the TEER and the FD4 assay, appeared very clear that the barrier disruptive effects determined by IFNγ were significantly less drastic than the ones determined by sTNFα in the same conditions. Unlike what was observed for sTNFα, the effects determined by the induction with IFNγ for 12 hrs, at the levels of the TEER and the FD4 assays, were comparable to ones observed after an induction for 24 hrs. Regarding the LDH assay a very interesting result, and novel in this context, was obtained. A statistically significant ($p \leq 0.01$, two-sided paired t-test, n=3) decrease of the level of LDH in the apical media was observed for an induction of 12 hrs, and a comparable effect (although not statistically significant) was observed after 24 hrs of induction. The interpretation of the results of the LDH assay appeared more complicated, as it has been shown that IFNγ reduces Necroptosis[94] although, as demonstrated before (figure 54) and in line with the literature, it contributes synergistically to the effects of TNFα (which determines a clear pro-necroptotic effect). The published anti-necroptotic effect of IFNγ could explain the observed statistically significant reduction of LDH in the apical media of the IFNγ-treated versus the uninduced monolayers. But, as in the uninduced monolayers no pro-necroptotic (nor pro-necrotic) stimulus was present, it should be defined wheatear the difference of LDH in between both conditions corresponds to an anti-necroptotic effect or if another phenomenon (or eventually an artifact) is taking place and both correspond to baseline levels of LDH (there is no reason for the untreated cells to undergo Necroptosis, as there is no engagement of death receptors).

In order to adapt the inflammatory model to the hypoxic conditions that, as explained in the section 4.1.2 resemble better the real physiological microenvironment that promote the intestinal epithelial cells differentiation at the distal portion of the villi, the pilot experiment IV has been performed. It consisted on the repetition of the titration of sTNFα applying the TEER, the FD4 and FD70 and the LDH assays. The incubation time of 24 hrs has been chosen for organizational reasons even though, as explained for the results of the experiment IIIc, the induction for 12 hrs determined a more drastic barrier disruption. The concentrations tested were 10, 50 and 100 ng/mL because, given the fact that T84 tended to acquire a real monolayer configuration in hypoxia, I expected the cells to be more sensitive and so more responsive to the cytokine challenge. As in hypoxic conditions the majority of the cells are positioned at the same level, I expected a better interaction of the cytokine with its cognate receptors at the basolateral domains and a full physiological response from the majority of these cells (which I assumed to not take place in a multiple layer configuration were the cells located at the higher levels of the single domes are, with high probability, not properly in contact with the basal media). The results of this pilot experiment confirmed, at first glance, that the cells are indeed

more responsive to the cytokine challenge in hypoxic conditions rather than in normoxia. Comparing figures 71 and 72, for a 24 hrs induction in hypoxia, with figure 60 and 61, for a 24 hrs induction in normoxia, it appeared evident that the concentration 10 ng/mL applied in hypoxia determined a more drastic effect, at the levels of the TEER and the FD4 assays, than the concentration 100 ng/mL applied in normoxia. Secondly, the result of the FD70 assay in the experiment IV (figure 73) clearly confirmed my hypothesis that the multiple-layer configuration, acquired by T84 grown in normoxic conditions, was the reason for the complete absence of an increase of permeability towards this molecular species even upon induction with sTNFα 100 ng/mL (figures 58 and 62). This clear improvement of the FD70 assay (at least in one biological replica) allowed me to implement it (only in hypoxic conditions) for assessing changes in the paracellular permeability determined by the modulation of the unrestricted pathway. The LDH assay did not show any significant increase of cytotoxicity, in line with the experiment of sole induction with sTNFα for 24 hrs in normoxia. Is important to underline that, for unexplainable reasons, none of the assays applied, showed a clear dose-response trend regarding the inductions with sTNFα. Indeed, the concentration 50 ng/mL showed the strongest effects and the concentration 100 ng/mL showed the mildest effects, in all assays.

Even though it is known from the literature that GI epithelial cells are able to respond to cytokines[53], I decided to confirm that the barrier function impairment observed in T84 upon induction with sTNFα, IFNγ and IL1β was mediated by cognate receptors of these cytokines. For doing so, I decided to assess the expression of the genes encoding for the receptors known to interact with the tested cytokines by RT-qPCR, at the transcriptional level. The expression of *TNFRSF1A*, *TNFRSF1B*, *IFNGR1*, *IFNGR2* and *IL1R1* was assessed in cells untreated and treated for 24 hrs with sTNFα and IFNγ at 100 ng/mL each, as done in the experiment IIIb. The results of this experiment showed that the receptor genes *TNFRSF1A*, *TNFRSF1B*, *IFNGR1*, *IFNGR2* were expressed in uninduced fully differentiated cells, indicating the reason of their responsiveness to the cytokines and confirming the usefulness of the cell line for the characterization of their roles with regards to intestinal epithelial barrier function. On the other side, the expression of all genes increased upon a 24 hrs induction with sTNFα and IFNγ, and for *TNFRSF1B*, *IFNGR1* and *IFNGR2* the increase was statistically significant. This positive regulatory loop for *TNFRSF1A* and *TNFRSF1B* has been described by Wang *et al.*, 2006[56] who found that IFNγ primes the expression of both genes at comparable extents, clarifying the reason for the already known (and described by me with the experiments IIIb and IIIc) synergistic effect of the combination sTNFα and IFNγ. The positive regulatory loop regarding *IFNGR1* and *IFNGR2* upon application of the sTNFα/IFNγ cocktail has not been described to my knowledge. In order to clearly show that IFNγ is at the basis of the positive regulation of *TNFRSF1A* and *TNFRSF1B*, the same experiment should be run by applying the single cytokines and not the cocktail. The same would be necessary in order to have a clearer image of the reasons behind the positive regulation of *IFNGR1* and *IFNGR2*. In section 5.6, the results of an RNAseq ran for the

single induction with sTNFα at 100 ng/mL for 12 hrs are discussed and analyzed in this regard. With respect to the expression of *IL1R1*, I found it to be very low and no significant change of expression was observed upon induction with the cytokines.

5.5. Pharmacological interference experiments

Before focusing on the characterization of the TNFα/TNR1A/TNR1B signalling axis in intestinal epithelial barrier function, I decided to verify the validity of the *in vitro* inflammatory model of the intestinal epithelium for pharmacological interference analyses. For this reason, I decided to establish control experiments of maximal achievable barrier protection by completely shutting down the cytokines signallings with pharmacological modulators. The possible ways to do so were the following: the competitive antagonism of the cytokines ligands in solution, the competitive orthosteric and the non-competitive allosteric antagonisms of the cytokines cognate receptors at the basolateral cell membranes and the blocking of the cytosolic signalling by targeting mediators of the signal transduction. In my Ph.D. thesis work I followed the competitive antagonism of the ligands in solution and the competitive orthosteric antagonism of the cognate membrane receptors.

Being the neutralization of the cytokines ligands in solution intrinsically the most efficient, but non-informative with respect to the receptors signalling (so non-suitable for pharmacological interference experiments), with those control experiments I wanted to observe the complete restoration of the three main parameters under regular analysis (in normoxia) for the assessment of the overall barrier-function in the 2D epithelial-like structures: the avoidance of the TEER drop, the maintenance of the basal paracellular permeability (at fully differentiated conditions) towards the FD4, and the conservation of the basal rate of cell death by Necrosis/Necroptosis. On the other side, the targeting of the cognate receptors at the basolateral plasma membranes would have acted as a proof of principle experiment showing that is possible to protect the barrier impairment induced by the cytokines (in the specific model) by pharmacological targeting of membrane receptors (the final goal to be achieved with the model). A positive outcome of this second approach would have also demonstrated the validity of the cytokines working concentrations (no side-effects determined through other pathways).

In order to simplify the experimental setup and to avoid a bias in the interpretation of the results, I decided in a first step to selectively neutralize the single cytokines and not to perform the co-neutralization of different cytokines applied in a cocktail. In all the experiments, the pharmacological modulators were pre-applied on fully differentiated monolayers before the application of the respective cytokines, so a protection to the cytokines effects was evaluated. I considered this approach to be more practical than performing the pharmacological interference after the cytokine induction and evaluating the recovery of the aforementioned parameters related to barrier function. Even though the “recovery approach” could have resembled better a potential therapeutical

procedure, it would have depended on the cells doubling time, on the times of TJ protein synthesis and on the times of the final TJs complexes formation, delaying the experimental analyses and introducing more complexity to the interpretation of the results. A pharmacological interference approach based on the pre-application of a certain modulator of a (protein) target of interest and on the consecutive evaluation of a protection, or of a further enhancement, towards a certain barrier function impairing stimulus (given for example by a different modulator for the same initial target), would have given a clear information about the role of the target of interest in this context.

For all the pharmacological interference experiments that I performed (control experiments and interference experiments for the characterization of the TNFα/TNR1/TNR1B signalling axis), the pharmacological modulators were selected aiming to achieve the highest possible selectivity and potency in the modulation. The maximal neutralizing concentration of the modulator of interest was defined in my *in vitro* model by setting up different dose-response experiments selecting the titration points in accordance to the expected maximal neutralization doses calculated from the IC_{50} values obtained from the literature (for other kind of functional assays, in other cellular models). The maximal response to the modulation, and so the optimal working concentration of the modulator, was inferred with the functional assays for assessing barrier function and controlling for an eventual unwanted cytotoxic effect with the LDH assay (a difference of 10 % with respect to the untreated condition was considered the threshold of maximal acceptable cytotoxicity).

5.5.1. Pharmacological interference experiments for controls of maximal barrier function protection upon the induction with IFNγ

The complete protection towards the barrier dysfunction determined by IFNγ on fully differentiated T84 monolayers, was achieved by neutralizing the ligand in solution employing the antibody Emapalumab. In a first titration experiment, four concentrations were chosen in accordance to the literature and pre-applied to the basolateral sides of fully polarized monolayers for 6 hrs. Successively, the monolayers were co-treated from the basolateral side with IFNγ at 100 ng/mL for 24 hrs and then a series of endpoint analyses were carried out by applying the different functional assays for assessing barrier function. As significant differences were not observed in between the incubation times of 12 and the 24 hrs with IFNγ (experiment IIIc), the second one has been chosen for organizational reasons. The 6 hrs of pre-treatment with Emapalumab represented an equilibration time of the cells with the media including the antibody. The results of the titration experiment demonstrated that all concentrations of Emapalumab determined a full protection towards the increase of paracellular permeability determined by the cytokine applied alone. This was clearly observed measuring the TEER and assessing the paracellular permeability towards FD4. In summary, all tested concentrations determined comparable levels of protection and there was no increase of cytotoxicity detected by the LDH assay (in none of the experimental conditions), so I

chose the concentration 4 µg/mL to continue working with, given the fact that it determined the highest protection at the level of the TEER.

With the chosen working concentration, I repeated the experiment in three biological replicas and I observed again a full protection at the levels of both TEER and FD4 permeability assays. Even though the average values demonstrated a clear full protection, the differences were not statistically significant with a two-sided paired T-test for the only three biological replicas. Is important to clarify that in all three biological replicas, at the timepoint of induction with the cytokine (+6 hrs), the monolayers not pre-treated but only induced presented (by chance) a significantly higher TEER. This fact reduced the extent to the drop of TEER (and the increase in permeability towards FD4) upon induction with the sole IFNγ, masking the full extent of the protection (clearly observed in the experiment of titration of the antibody). Regarding the LDH assay, a decrease of LDH in the apical media was observed upon induction with IFNγ and the same levels were quantified in the condition of co-treatment with Emapalulab at 4 µg/mL. Considering that the pairwise differences in between the values of all conditions were not statistically significant ($p>0.05$, two-sided paired t-test, $n=3$), I could in principle conclude that all of them corresponded to basal levels of LDH. I would have expected to observe a reversal of the slight decrease of LDH determined by IFNγ in the monolayers co-treated with Emapalumab at 4 µg/mL. Considering that the decrease of LDH determined by IFNγ was statistically significant for an induction time of 12 hrs (experiment IIIc), in the future I will repeat the experiment with Emapalumab applying an induction time of 12 hrs and evaluate the outcome in those conditions. In summary, the results of this experiment (and of the one of titration of Emapalumab) were a first demonstration of the validity of the *in vitro* inflammatory model, as a full barrier function protection was achieved.

Another control of barrier function protection upon the induction with IFNγ, was performed by competitive orthosteric antagonism of INGR1 (the monomer that contains the ligand-binding site in the INGR1/2 functional heteromeric complex) employing an R&D Systems antibody. Is important to clarify that this antibody was not designed for purely neutralizing purposes, as instead was the nanobody TROS employed for the neutralization of the activity of TNR1A. The titration of the α-INGR1/CD119 antibody, necessary to define the range of concentrations for a maximal effect of the antagonism in my specific *in vitro* model, required three different experiments.

In the first experiment, the range of concentrations tested (0.5, 4 and 6 µg/mL) did not determine any significant barrier protective effect at the TEER level and only a milder effect at the level of the FD4 permeability, so I decided to extend the titration range upwards.

The second set of concentrations tested (12, 48 and 48 µg/mL) demonstrated to be effective in the neutralization of the IFNγ signalling: a clear barrier function protection was observed at the level of the TEER (without following a dose-response fashion) and at the level of the FD4 permeability (a comparable extent of protection was determined by all tested concentrations). The LDH assay showed a prominent decrease of LDH in the apical media of the INFγ-treated condition with respect

to the untreated condition, which was not reversed by the co-treatments with the antibody. This outcome demonstrated that the new tested concentrations determined no cytotoxic effect, but it is unclear why, even though they determined a barrier function protection, they did not bring the LDH levels to the ones observed in the untreated cells. An eventual anti-necroptotic effect determined by IFNγ should have been reversed by the competitive antagonism with the antibody.

With the last titration experiment (24, 32, 40 and 56 µg/mL) the aim was to define a working concentration of maximal barrier function protection and to eventually see a clear dose-response effect. In this experiment a technical issue was encountered as the untreated monolayers (and very probably also the other ones) underwent a drastic decrease of resistance from the timepoint +12 hrs to the timepoint + 24 hrs. This phenomenon, which somehow hinders the barrier function impairment determined by the cytokine, has been observed in several experiments when the monolayers are fully differentiated and might be due to a reorganization of the cells and of the TJ network. The outcome of the experiment showed anyway a barrier-protective effect that followed a dose-response fashion only for the TEER measurements. A full protection was observed neither by measuring the TEER nor with the FD4 assay, and the LDH assay showed basal levels of apical LDH for all conditions.

Even though a full protection was not achieved, the importance of the three experiments of titration of α-INGR1 was the demonstration that was possible to protect the barrier function impairment determined by a cytokine, in the specific model, by targeting a cognate membrane receptor.

5.5.2. Pharmacological interference experiments for the characterization of the TNFα/TNR1A/TNR1B signalling axis

The main object of this PhD thesis is the initiation of the full characterization of the TNFα signalling in the context of intestinal epithelial barrier function. As explained in the introduction, the TNFα signalling is started by two different forms of the ligand, the soluble and the membrane forms, which differentially activate the two cognate receptors TNR1A and TNR1B. In my *in vitro* model I employed sTNFα as a strong inducer of epithelial barrier dysfunction initially in combination with IFNγ, trying to resemble better the real pathophysiological conditions taking place in IBD, and successively alone, in order initiate the "clear" characterization of the sole TNFα signalling. Focusing now on this second purpose, the application of sTNFα in my model represented (given the nature of the ligand) a pharmacological modulation towards the (almost) selective agonism of TNR1A. Taking this into consideration, sTNFα, which determined a statistically significant barrier function impairment at all levels (experiment IIIc), became my first tool for the characterization of the specific role of TNR1A in intestinal epithelial barrier function.

In order to validate the model (as done for IFNγ with Emapalumab) and to establish a control of maximal (indirect) antagonism of TNR1A with regards to barrier function, I decided to establish the full neutralization of the ligand sTNFα in solution employing Adalimumab. The titration of

Adalimumab was performed in one biological replica, in normoxia, testing the concentrations 2.4, 4.8, 9.6, 19.2 and 24 µg/mL. A 12 hrs induction time was chosen, instead of 24 hrs, given the fact that it determined more drastic effects on the barrier function (experiment IIIc), and the pre-treatment with the different concentrations of Adalimumab for 12 hrs represented an equilibration of the media with the modulator. The results obtained for the titration of Adalimumab clearly showed that in all three analyses performed for assessing the overall epithelial barrier function, the application of Adalimumab (at all five chosen concentrations) determined a complete protection versus the shifts determined by the sTNFα applied for 12 hrs (compared to the "untreated" condition). I decided to continue working with the concentration 24 µg/mL as it did not determine any unwanted cytotoxic effect and it determined the highest protection (anyway comparable to the one observed for the other concentrations) at the level of the TEER.

The full neutralization of sTNFα at 24 µg/ml was initially replicated in a pilot experiment in which a pre-treatment for 6 hrs with the drug was followed by an induction and co-treatment with sTNFα for 24 hrs. In turn, the same experimental pipeline applied for the titration experiment was followed for the chosen concentration (at 24 µg/ml) in three biological replicas and all protective effects were found to be statistically significant. The full neutralization of sTNFα applied at 100 ng/mL with Adalimumab applied at 24 µg/mL, confirmed the validity of the model (so the possibility of completely nullifying the effects determined by the cytokine with regards to barrier function) and represented a control experiment of maximal (indirect) antagonism of TNR1A with regards to barrier function (being sTNFα the natural agonist of this receptor).

In order to infer the role of TNR1A with regards to intestinal epithelial barrier function I decided to nullify its function in my *in vitro* model following a pharmacological interference approach. Having the full neutralization of sTNFα with Adalimumab as a reference of full antagonism and maximal achievable barrier protection, I decided to perform a selective competitive orthosteric antagonism of TNR1A in the presence of its natural ligand, in the same way as I did for INGR1/INGR2. As for the previous modulations, the first step that I followed was the definition of the optimal working concentration of TROS for a maximal neutralization of the activity of TNR1A with regards to barrier function, in the presence of 100 ng/mL sTNFα. The titration of TROS consisted of three different experiments (of one biological replica each), in which the initial working concentrations defined in accordance to the literature, were gradually increased in order to achieve the optimal one. A pre-treatment with the different concentrations of TROS (2, 2.5, 3.5, 10, 15, 20 and 30 µM) was performed for 12 hrs, as an equilibration time of the media with the modulator. To this, followed a 12 hrs induction time (and co-treatment) with sTNFα, which was chosen as it determined more drastic effects on the barrier function than a 24 hrs one (experiment IIIc).

As a result of the first titration experiment (2, 2.5 and 3.5 µM), I found no relevant barrier protective effect at the TEER level determined by the aforementioned concentrations. A mild barrier protective effect at the level of the FD4 assay was observed but without following a dose-response fashion, and

a mild anti-necroptotic effect was observed for the two higher concentrations. As the LDH assay did not show any unwanted cytotoxicity, I decided to extend the titration range to much higher values in order to determine a detectable physiological effect in the whole 2D epithelial-like structure. It is known that in a tissue, or in an *in vitro* tissue-like structure, the effects determined by cytokines stay circumscribed to the single targeted cells and are not prone to be transferred from cell to cell via intercellular junctions. In order to overpass this "local" effect of sTNFα, appeared clear to me that, a part from working with a potent antagonist as TROS, was necessary to drastically increase its working concentration in my *in vitro* tissue model in order to optimize the neutralization of the highest possible number of receptors.

The second titration of TROS, in which the working concentration (15 µM) was increased more than four times with respect to the highest concentration of the first experiment, clearly defined the range of concentrations necessary to observe an effect of the modulation at the overall barrier function of the 2D epithelial-like structure. All three assays, TEER, FD4 permeability assay and LDH assay, demonstrated that the selective antagonism of TNR1A significantly protected the barrier dysfunction determined by sTNFα. Given the fact that no cytotoxicity was observed I decided to extend upwards the titration range in order to define the optimal working concentration of the drug (closer to the maximal non-toxic concentration). In the last experiment of titration, the three tested concentrations (10, 20 and 30 µM) determined a clear dose-dependent barrier protective effect assessed with all three aforementioned assays. As no unwanted cytotoxicity was determined, the experiment demonstrated the suitability of 30 µM as a working concentration, which was defined by me as the optimal one for a full antagonism of TNR1A in the presence of 100 ng/mL of its natural ligand sTNFα, in the specific cell culture conditions.

The replication (n=4) of the full antagonism of TNR1A with TROS at 30 µM confirmed that this receptor mediates most of the barrier function impairing effects (affecting all three the pore, leak and unrestricted permeability pathways) determined by sTNFα. This is a novel result that clearly contradicts Wang *et al.*, 2006[56], to my knowledge, the only work of full characterization of the TNFα signalling *in vitro*. The barrier function protective effects determined by the selective pharmacological modulation with TROS and assessed by measuring the TEER and with the FD4 and LDH assays reached statistical significance. On the other side, this experiment complemented the control experiment of antagonism of INGR1 in the presence of IFNγ clearly showing that is possible to fully protect the barrier function impairment induced by a pro-inflammatory cytokine by pharmacological targeting of membrane receptors, in this specific model. The outcome of this experiment also demonstrated the validity of the sTNFα working concentration 100 ng/mL (no side-effects determined through other pathways).

5.6. RNAseq: transcriptome expression profiling of the induction with sTNFα, of the full neutralization of the sTNFα signalling and of the full competitive orthosteric antagonism of TNR1A

By analyzing the transcriptome (the sum of all the RNA transcripts) of a cell line of interest in a specific experimental condition, a detailed and comprehensive image of the cellular pathways differentially regulated (with respect to a control condition) can be obtained. In order to start investigating the regulatory mechanisms involved in the barrier dysfunction determined by the sole activation of TNR1A, a whole-transcriptome expression analysis (of only mRNAs) was performed by RNAseq on all the conditions of the experiment of full neutralization of sTNFα in solution (Adalimumab at 24 µg/mL) and of the experiment of full competitive antagonism of only TNR1A (TROS at 30 µM).

Even though in the future I will analyze in detail the relevant functional gene clusters related to the cellular processes that account for the establishment of the barrier function (regulation of TJs and AJs and of the apoptotic, necroptotic and cell proliferation pathways), in this part of my work I just reported all significantly differentially expressed genes (absolute Log2FoldChange of the normalized mean hit counts ≥ 2) within all possible comparisons of the different experimental conditions, for each of the two experiments (n=3 for each). As expected, considering that TNFα is well known for its pleiotropic roles in the inflammatory immune response, I found several genes (126/127) significantly deregulated by the cytokine applied alone. Whereas the co-treatment with Adalimumab completely normalized the expression of all of them, the co-treatment with TROS restored the expression of around 56 genes. The differential outcome of the two treatments, at the transcriptomic level, could have been determined by: **i)** the higher efficiency of the antagonism fulfilled by the neutralization of the ligand in solution with respect to the targeting of a membrane receptor, **ii)** the capacity of Adalimumab of silencing the whole sTNFα signalling by avoiding not only the full agonism of TNR1A, but also the marginal agonism of TRN1B. The fact that both modulations led to highly comparable outcomes at the barrier function level (TEER, FD4 and LDH assays), but a discrepancy was observed with the RNAseq, confirms the high sensitivity of the transcriptional regulation with regards to subtle changes in the experimental conditions (full antagonism of the ligand versus full antagonism of the receptor that mediates most of the cellular physiological effects determined by the ligand).

Important to mention is that among the genes that presented the higher Log2FoldChanges upon induction with sTNFα, I found: *CCL20* (C-C Motif Chemokine Ligand 20), *DRGX* (Dorsal Root Ganglia Homeobox), *IL34* (Interleukin 34), *NOD2* (Nucleotide Binding Oligomerization Domain Containing 2), *LTB* (Lymphotoxin Beta), *PI3* (Peptidase Inhibitor 3), *TNF* (Tumor Necrosis Factor), *OR2I1P* (Olfactory Receptor Family 2 Subfamily I Member 1), *IL4I1* (Interleukin 4 Induced 1), *UBD* (Ubiquitin D), *NFKB2* (Nuclear Factor Kappa B Subunit 2), *NFKBIA* (NFKB Inhibitor Alpha)

and *NFKBIE* (NFKB Inhibitor Epsilon). Many of these genes are known to be generally upregulated in chronic inflammatory conditions, and the last three are involved in the regulation of the NF-κB signalling. Interestingly, *TNF* was also found highly upregulated, indicating a positive feedback loop of the signalling.

In order to disentangle the specific contribution of the single cytokines in the differential expression observed for *TNFRSF1A*, *TNFRSF1B*, *IFNGR1* and *IFNGR2* upon induction with the cocktail sTNFα/INFγ by RT-qPCR (Figure 75), the expression of these genes upon induction with only sTNFα was analyzed from the RNAseq data (Figure 116). Important to consider was that, even though the working concentrations were the same for both experiments (100 ng/mL), the induction time applied in the first one was 24 hrs and the one applied in the second one was 12 hrs. Regarding all the other parameters, both experiments were performed exactly in the same way. Unlike the upregulation of both *TNFRSF1A* and *TNFRSF1B* observed upon the co-treatment with sTNFα/INFγ (and determined by IFNγ, as described by Wang *et al.* 2006[56]), a slight downregulation of *TNFRSF1A* and a moderate upregulation of *TNFRSF1B* were observed upon induction with the sole sTNFα. Interestingly, the same upregulation observed by RT-qPCR for both *IFNGR1* and *IFNGR2* upon the co-treatment with both sTNFα and INFγ (Log2FoldChanges of 1.55 and 0.89, respectively), was observed by RNAseq for the sole induction with sTNFα (Log2FoldChanges of 1.5 and 1.14, respectively). This result contributes new data on the elucidation of the mechanisms underneath the synergism in between the two cytokines. As the co-treatments with either Adalimumab 24 μg/mL and TROS 30 μM determined a complete restoration of the expression levels of both *IFNGR1* and *IFNGR2* of the untreated condition, was evident that the sole activation of TNR1A induced the expression of the receptors mediating the IFNγ signalling.

A possible explanation for the slight down regulation of *TNFRSF1A* and the slight upregulation of *TNFRSF1B* determined by the induction with the sole sTNFα, could be a compensatory negative feedback loop of the pro-inflammatory, barrier-disruptive effects determined by sTNFa at the concentration employed. So, a downregulation of the receptor that mediated clear pro-inflammatory and barrier disruptive effects, and an upregulation of the one that might (I hypothesize) determine barrier protective effects.

Finally, I analyzed the expression of a series of genes with a functional relevance in the context of intestinal epithelial barrier function, upon induction with only sTNFα and upon co-treatment with the two antagonists directed towards different levels of the TNFα signalling (Table 8 and Figure 117). In this preliminary analysis of functional gene clusters, I mainly chose genes exerting a proven or a possible direct impact on the regulation of the three paracellular permeability pathways, and also genes that affect them by regulating upstream processes. I analyzed the expression of: **i)** genes codifying for intercellular and scaffolding TJPs involved in the regulation of both the pore and the leak permeability pathways, **ii)** the master regulator of the leak pathway *MYLK*, **iii)** genes codifying for markers of cell proliferation, **iv)** genes codifying for proteins involved in the activation of both

the extrinsic (activated by sTNFα) and the intrinsic apoptotic pathways, **v)** genes codifying for the main players in the activation of the necroptotic process. Genes related to cell proliferation, Apoptosis and Necroptosis were chosen as these processes directly affect the unrestricted permeability pathway. Is important to clarify that: **i)** intercellular and scaffolding TJPs regulate the paracellular permeability not only by being appropriately expressed but also, and very importantly, by reaching the functional latero-apical sub-cellular localization (a phenotype that can be only assessed by IF stainings), **ii)** the only apoptotic pathway expected to take place upon induction with sTNFα (and activation of the death receptor TNR1A) is the extrinsic one, so markers of the intrinsic pathway were included in order to analyze an eventual cross-talk in between them, **iii)** the most appropriate assays for assessing Apoptosis and Necroptosis are the ones that can detect the final cellular effects of the consummated processes (gDNA degradation for Apoptosis, plasma membrane lysis for Necroptosis, increase of paracellular permeability with regards to FD70 for both) or the ones that can detect the activation of the proteins that mediate them (cleavage of Caspases for Apoptosis and phosphorylation of the key players that mediate Necroptosis) and not gene expression analyses, **iv)** none of the analyzed genes reached the arbitrary threshold of significance (absolute Log2FoldChange≥2).

All Claudin genes expressed by T84 in the three conditions (untreated, cytokine only and co-treatment with the antagonist) of the two experiments with ADALIMUMAB 24 µg/mL and TROS 30 µM, were included in the analysis. Among them, is worth to mention an upregulation of *CLDN1* and *CLDN11* determined by sTNFα applied alone and counteracted by the co-treatments with ADALIMUMAB or TROS. Both of them are "sealing" Claudins which I would have expected to be downregulated by the cytokine induction. As already explained, their functional subcellular localization could have been eventually impaired by the induction and so their function at the TJs nullified, but I could not evaluate this by IF stainings. *CLDN2* is a "pore-forming" Claudin which, in line with the literature (see Section 1.5), I found upregulated by sTNFα applied alone. Interestingly, both co-treatments normalized its expression level, but TROS 30 µM was more efficient than ADALIMUMAB 24 µg/mL in determining that effect. *CLDN9* has an unknown function, but I found it downregulated by sTNFα applied alone in both experiments, and this phenomenon was counteracted by both co-treatments. *OCLN*, crucial for the regulation of the leak pathway, was found downregulated by sTNFα applied alone, as expected, and its expression normalized by both co-treatments, but more efficiently by TROS 30 µM. Another TJP crucial for the regulation of the leak pathway, *TJP1*, was found upregulated by sTNFα applied alone and its expression normalized by both co-treatments. Again, its delocalization should play a crucial role in this context.

The most important finding in this analysis of functional gene clusters concerned the master regulator of the leak permeability pathway *MYLK*, which determines the delocalization of Occludin and ZO-1 out of the TJ density. The induction with the sole sTNFα determined a differential expression of

MYLK with regards to the untreated condition, slightly below the arbitrary threshold of significance. In both experiments, sTNFα determined a downregulation of *MYLK* (Log2FoldChanges of -1.04 and -1.35). The co-treatments with either Adalimumab 24 µg/mL (complete neutralization of the sTNFα signalling) and TROS 30 µM (selective antagonism of TNR1A) determined a complete restoration of the expression levels of *MYLK*. Unlike what already described by others on CACO-2[53], on T84 the induction with only sTNFα (and so, the sole or main activation of TNR1A) determined a transcriptional downregulation of *MYLK*. My results do not give any information about the role of TNR1B in this regard which, in accordance to Wang *et al.,* 2006[56], mediates the upregulation of *MYLK* that affects the leak permeability pathway.

Concerning the genes related with the regulation of the unrestricted permeability pathway, the proliferation marker *MKI67* was found slightly downregulated by the induction with sTNFα and the opposite was observed for *PCNA* (even though I did not expect an increase in the proliferative capacities of T84 in any of the experimental conditions). *FADD*, which codifies for a protein involved in the activation of the extrinsic apoptotic pathway, appeared highly upregulated by the sole induction with sTNFα and its expression was normalized by the co-treatments with both modulators. Interestingly, the induction with only sTNFα had an effect on genes that codify for mediators of the intrinsic apoptotic pathway, evidencing a cross-talk in between both pathways (even though the activation of TNR1A by sTNFα initiates only the extrinsic apoptotic pathway). In line with a pro-apoptotic condition, the pro-apoptotic gene *TP53* was found upregulated by sTNFα and its expression was normalized by both co-treatments, and the anti-apoptotic gene *BLC2* was found downregulated by sTNFα and its expression was also normalized by both co-treatments. Finally, within the necroptotic gene cluster, is worth to mention *MLKL* which codifies for a protein that, when phosphorylated, executes the key necroptotic phenotype of the plasma membrane lysis. It was found moderately upregulated by the induction with only sTNFα, and its expression was partially restored by both co-treatments.

6. CONCLUSIONS

6.1. Differentiation of intestinal epithelial cells as 2D epithelial-like structures

As a first step towards the establishment of an *in vitro* model of the intestinal epithelium, I defined the optimal conditions for the differentiation of colorectal carcinoma epithelial cells as two-dimensional epithelial-like structures. Transformed cells usually represent the first choice for the establishment of an *in vitro* model, with associated functional assays, given their robustness in culture and given the possibility of pushing their differentiation without sophisticated protocols. With these cells is also possible to run a preliminary investigation of the biological phenomenon of interest, before the necessary replication of the findings in more physiologically relevant conditions (so implementing a normal cell line in the model and eventually also *in vivo*). The complete differentiation of T84 and CACO-2 was achieved by growing them over polycarbonate semipermeable supports for several days post-confluency (7-10 for T84 and 15-20 for CACO-2), in normoxic conditions, standard cell culture media and a simple coating with Collagen I at relatively low concentrations. The optimal seeding density was set at around 360 x 10^3 cells/cm^2, a suitable one for allowing an homogenous distribution of the cells over the membrane without delaying too much the attainment of cell confluency. The differentiation of the two cell lines, so the acquisition of cell polarity and the establishment of barrier function (at the multicellular level), was monitored with two functional assays that allow the assessment of the paracellular permeability towards ions and small molecules and by IF staining and subcellular localization of ZO-1. As a result of these experiments I found T84 as the optimal cell line to continue working with, because it differentiated faster, it reached higher TEER values, it tended to differentiate in a synchronized manner among technical replicas and it did not manifest excessively high proliferating capacities as CACO-2. A disadvantage of differentiating both cell lines in normoxia was that three-dimensional rather than two-dimensional structures were obtained, given the uncontrolled proliferating capacities of transformed cells. This phenomenon not only deviated the model from a two-dimensional physiologically relevant condition, but it also impaired the outcome of the IF, of the FD70 permeability assays and of the LDH assay, and introduced a (non-physiologically relevant) bias in the assessment of the barrier function. A solution for this issue came out from a pilot experiment in which T84 was differentiated over semipermeable supports, employing the same initial protocol with some improvements: the atmospheric O_2 was kept at 1% instead of 20%, mimicking the conditions observed *in vivo* at the distal portions of the villi, the porosity of the membrane was reduced to avoid the eventual formation of a double monolayer, and the coating was performed with Matrigel in order to mimic properly the basement membrane of the intestinal epithelium. The new protocol determined a relatively faster cell differentiation, the acquisition of relatively higher final TEER values and, importantly, the establishment of real monolayer in 2D (evidenced by confocal microscopy).

As a first candidate of normal intestinal epithelial cell line, I started the characterization of FHC that consists on an heterogenous cell population of mainly fibroblasts and colonic epithelial stem cells. In order to enrich for the second cellular population, I tested the simple technique of the differential plating, which proved not to be effective. With the series of conventional RT-PCRs that I employed for assessing the cellular composition of the two fractions of the differential plating, I could also confirm the expression of key intestinal epithelial stem cell markers *PROM1*, *LGR5* and *LRIG1*, so the presence of the cells of interest. A first attempt to differentiate these cells over TW inserts, in normoxic conditions, in standard cell culture media and without previously removing the excess of the fibroblasts, did not prove successful.

In summary, I could successfully differentiate a colorectal carcinoma cell line (T84) as a two-dimensional epithelial-like structure, in a support (the TW insert) which allows the application of key functional assays for assessing the paracellular permeability (TEER, FD4 and FD70) apart from cell viability and standard biochemical and molecular biological assays. This aspect, together with the full access to both apical and basolateral sides, represent in my opinion the great advantages of this model with respect to 3D models as organoids (or mini guts).

6.2. Expression of 5-HT3Rs genes in T84 and CACO-2 and identification of a putative novel *HTR3E* transcript variant

Out of the five members of the 5-HT_3Rs gene family (*HTR3A/B/C/D/E* genes), CACO-2 expressed *HTR3A/B/E* and T84 expressed all of them. Even though gene expression at the transcriptional level does not necessarily mean that the expression at the translational level will take place in the cell line of interest at the specific experimental conditions, these results are a good starting point for the initiation of the characterization of the role of 5-HT3Rs in intestinal epithelial barrier function employing the *in vitro* model presented in this thesis.

The conventional RT-PCR for *HTR3E*, in both cell lines, gave rise to an amplicon that was larger than the expected one. As a contamination with gDNA could be excluded (the RNA isolation included a treatment with DNAaseI), a putative novel splicing variant of this gene (that retained the last intron) was found to be expressed by these cell lines. A 3'RACE PCR showed that the 3' end of the transcript carried a sequence conserved in all the annotated *HTR3E* splicing variants. Unfortunately, the 5'RACE PCR gave rise to a band of 700-750 bp that could not be successfully cloned and sequenced, but that very probably contained the novel combination of exons of a new putative *HTR3E* splicing variant.

6.3. Establishment of the optimal pro-inflammatory input for determining the loss of barrier function and validation of the model for endpoint pharmacological interference analyses

An *in vitro* inflammatory model of the intestinal epithelium, suitable for the study of genes/proteins implicated in the intestinal epithelial barrier dysfunction that characterizes IBD, has been established in my PhD work. The model, with all its associated functional and molecular biological assays, constitutes a platform for the complete characterization of a candidate gene/protein of interest with regards to the key molecular mechanisms that regulate the paracellular permeability at the intestinal epithelium. As mentioned before, an abnormally increased level of paracellular permeability (barrier dysfunction) is at the basis of both the initiation and the chronic manifestation of IBD, making the model very useful for both the study of the pathomechanisms underlying this condition and for the identification of novel potential pharmacological strategies in this regard.

The establishment of the inflammatory model initially aimed to resemble *in vitro* the barrier dysfunction determined by a cocktail of pro-inflammatory cytokines, in a (patho-)physiologically relevant condition. Out of the two cytokines combinations tested, sTNFα/IL-1β and sTNFα/IFNγ, only the second one (hallmark of CD) determined a significant barrier dysfunction of fully differentiated T84 monolayers. Applying the concentration 100 ng/mL for each cytokine, and an induction time of 24 hrs, a significant barrier function impairment could be properly assessed with all TEER, FD4 and LDH assays. Considering this, and the fact that no unwanted cytotoxicity was determined, I defined that combination as the optimal one for establishing the inflammatory model. Other reasons consented me to justify the employment of that relatively high concentration for each cytokine: **i)** it can be found in the literature, for both cytokines, applied in similar experimental conditions, **ii)** slightly supraphysiological concentrations are necessary in order to determine the expected effect of a certain treatment *in vitro* (as cells in these conditions are in general more resilient to different experimental treatments, than cells in the *in vivo* condition), **iii)** transformed cell lines are more robust in culture and, as a consequence, are also less prone to respond to different experimental treatments.

In order to go into the details of the barrier dysfunction determined by the cocktail sTNFα/IFNγ, and initiate the characterization of the cellular signallings mediated by each of them, I decided to apply the single cytokines alone in the same working experimental conditions. The overall results of that series of experiments showed that the single cytokines sTNFα and IFNγ applied alone determined a milder effect than in combination. sTNFα determined an overall stronger barrier-disruptive effect than IFNγ, but milder than the one determined by their combination. This clearly showed that both are linked in an additive or in a synergistic interaction, as already described in the literature. The reasons behind the additive or the synergistic interaction are: **i)** a positive regulatory loop exerted by IFNγ with respect to *TNFRSF1A* and *TNFRSF1B*, at the transcriptional level (described in the

literature and confirmed in my PhD work by RT-qPCR), **ii)** a positive regulatory loop exerted by sTNFα with respect to *IFNGR1* and *IFNGR2* (described in my PhD work by RNAseq). Another interesting conclusion regarding the induction of barrier dysfunction with the single cytokines was that, especially for sTNFα, an incubation time of 12 hrs determined more drastic effects than an incubation time of 24 hrs. The reason for this could be an impairment of the bioactivity of the cytokines over time, in the culture media.

The induction with the sole IFNγ showed a very interesting result at the level of the LDH assay. A statistically significant decrease of the level of LDH in the apical media was observed upon induction with the cytokine with respect to the uninduced condition, indicating a probable anti-necroptotic effect in this context (described in the literature for other cell types). It must still be defined whether the difference of LDH in between both conditions corresponds to a real anti-necroptotic effect or if another phenomenon is taking place and both correspond to baseline levels of LDH (see section 6.3). Is worth to underline that even the putative anti-necroptotic effect of IFNγ applied alone, transmuted into a pro-necroptotic in the presence of sTNFα, which was more prominent than the one determined by the latter applied alone. This clearly evidences the synergistic interaction in between both cytokines.

A pilot experiment of titration of sTNFα on monolayers fully differentiated in hypoxia gave two important results. On one side, it demonstrated that, by acquiring a real 2D configuration, the monolayers were more responsive to the cytokine's induction, as the concentration 10 ng/mL applied in hypoxia determined a more drastic effect (at the levels of the TEER and the FD4 assays) than the concentration 100 ng/mL applied in normoxia. On the other side, a clear improvement of the FD70 assay (at least in one biological replica) could be observed and demonstrated that the multiple-layer configuration, acquired by T84 grown in normoxic conditions, was the reason for the complete absence of an increase of permeability towards this molecular species even upon induction with sTNFα 100 ng/mL. The implementation of this functional assay in hypoxic conditions, is of great importance as it allows the assessment of changes in the paracellular permeability determined by the modulation of the unrestricted pathway, and so, to indirectly assess the rate of Apoptosis and Necroptosis.

The possibility of inducing a significant barrier disruption at fully differentiated stages with single cytokines, gave me the idea of defining a standard procedure for performing any kind of experiment necessary for the characterization of the role of a certain gene/protein with regards to barrier function. Instead of applying a certain experimental treatment in a time-resolved manner (starting from sub-differentiating stages), I decided to apply them on fully differentiated monolayers and assess the effects with regards to barrier function (with all the established assays), in an endpoint approach. Working always at fully differentiated stages I was not only able to keep physiologically relevant conditions, but I was also able reduce the intrinsic variance (with regards to cell confluency and barrier function) in between the different monolayers of the same and of different experiments,

making them comparable. In my PhD work, I successfully validated the model for endpoint pharmacological interference experiments with Adalimumab and Emapalumab, that demonstrated the possibility of fully protecting the induced barrier disruption by neutralizing the cytokines in solution, and with TROS and αINGR1, that demonstrated the possibility of achieving comparable results by neutralizing the cognate receptors at the cells surfaces. Selectivity and potency of the drugs were considered and essential pre-requisite to avoid off-targets by default (selectivity) and to avoid off-targets by increasing the working concentration (potency). The targeting of the cognate receptors with TROS and αINGR1 demonstrated that high neutralizing doses (far higher than the ones defined by adapting to the model the EC_{50} values obtained from the literature) are necessary to overcome the cytokines-effects over tissue-like structures, as these kind of signallings are not easily transferred from cell to cell (meaning, the highest possible number of receptors in different cells has to be targeted in order to determine the expected effect with regards to barrier function). In any way, the absence of unwanted effects (Necrosis) for both cytokines and drugs treatments validated the working concentrations.

In summary, the presented model constitutes a platform for the characterization of the role of a specific gene/protein with regards to the key mechanism that define the level of paracellular permeability in a 2D epithelial structure, and goes beyond the context of chronic inflammation. The pharmacological interference approach combined with the key functional assays for assessing the three paracellular permeability pathways, allow the characterization of the role of any candidate protein with a putative role in barrier function, at the phenotypical level. Protein expression, functional subcellular localization, formation of complete Tight and Adherens junctional complexes, and paracellular permeability across the three described pathways, are the key phenotypes that can be assessed with the model and that are relevant with regards to the pathomechanisms of IBD. The assessment of the role of a certain protein by activating or nullifying its function pharmacologically, can be validated with interference approaches at both genetic and transcriptional levels also in this model (section 6.4). Is worth to consider that working at both the genetic and transcriptional levels may introduce a certain level of complexity in the interpretation of the results at the phenotypic level (the probability of introducing unwanted effects, for example by off-targets, increases drastically). That is why the selective and potent pharmacological interference approach remains the most powerful and informative one.

The last point to mention is that the complexity of the GI mucosa, especially in inflammatory conditions, supports the employment if such an *in vitro* model for the specific and clear characterization of the role a certain candidate gene/protein with regards to GI epithelial barrier function. The dense and intricated interconnection of endocrine and paracrine signallings that takes place *in vivo* at the GI wall, introduces a high level complexity to the interpretation of any experimental result with regards to barrier function in this context. Even though the *in vivo* level must inevitably be approached for a comprehensive understanding of the pathomechanisms of a

certain disease, and is the most relevant in terms of a potential translational application, is for sure not the best for the sole characterization of the specific role of a certain gene/protein candidate with regards to only GI epithelial barrier function.

6.4. Characterization of the TNFα/TNR1A/TNR1B signalling axis in intestinal epithelial barrier function

In my PhD work, I aimed to investigate the specific roles of TNR1A (*TNFRSF1A*) and TNR1B (*TNFRSF1B*) with regards to the key mechanisms regulating the intestinal epithelial barrier function, employing the pharmacological interference approach summarized in the previous section. As previously explained, the TNFα signalling cascade is initiated by mTNFα, which fully activates both TNR1A and TNR1B, and by sTNFα, which fully activates TNR1A and marginally activates TNR1B. The differential behavior of the two forms of the ligand TNFα allowed me to employ sTNFα as a full and almost selective agonist of TNR1A, a part from as a barrier function disruptive stimulus. In my PhD work, I have performed the complete characterization of TNR1A in this context employing the cytokine sTNFα, for its selective activation, the nanobody TROS, for its competitive and selective antagonism, and the antibody ADALIMUMAB, for its indirect competitive antagonism (by neutralization of sTNFα). The missing and crucial characterization of TNR1B could not be performed for unexplainable bureaucratical reasons, that did not depend on my person in any way, and that derived into critical logistical problems during my last year of Ph.D. The missing experiments were defined by me already on my third TAC meeting and will require the mTNFα-mimetic ARTOS, as a full, selective agonist of TNR1B, and the cytokine sTNFα, as an inducer of barrier disruption (see section 6.4). Unfortunately, during my last year of Ph.D. I could not have any access to the ARTOS (even though a collaboration established by me, in due time, should have provided it) and I could not have a full and regular access to an hypoxia incubator (necessary for the improvement of the *in vitro* model and for the application of all the assays that would have allowed me to perform the detailed characterization of all paracellular permeability pathways).

The nullification of all the barrier disruptive effects determined by sTNFα, applied at 100 ng/mL and for 12 hrs in my *in vitro* model, was achieved by a pre-treatment with Adalimumab at 24 µg/mL. The barrier-protective effects determined by the pre-treatment with Adalimumab reached statistical significance with all TEER, FD4 and LDH assays necessary for the assessment of the three paracellular permeability pathways. These results represented a reference experiment of maximal (indirect) antagonism of TNR1A with regards to barrier function (being sTNFα the natural agonist of this receptor). The nullification of the effects determined by sTNFα was also observed at the transcriptional level with the RNAseq experiment, considering that the pre-treatment with Adalimumab completely normalized the expression of all the genes significantly differentially expressed upon the cytokine-induction. In my PhD work I did not go into the details of the biological

function of the genes that were significantly differentially regulated by sTNFα, but a preliminary analysis showed that the majority of them are common mediators of the inflammatory responses.

Even though the biological nature of the ligand sTNFα indicated *a priori* an overall barrier impairing effect determined by the activation of TNR1A, the definitive characterization of this receptor in my *in vitro* model was realized by its selective competitive orthosteric antagonism, in the presence of its natural ligand. A pre-treatment with TROS at 30 µM determined a protection towards the barrier impairing effects determined by sTNFα, applied at 100 ng/mL and for 12 hrs in my *in vitro* model, comparable to the one determined by Adalimumab at 24 µg/mL. The barrier function protective effects covered all three the pore, leak and unrestricted permeability pathways, as they were assessed by measuring the TEER and with the FD4 and LDH assays. In all cases they reached statistical significance.

The results obtained with TROS and Adalimumab are novel because they clearly show that the pro-inflammatory effects of sTNFα, underlying the drastic barrier function impairment in T84, are mediated to a large extent by the activation of TNR1A. This clearly contradicts Wang *et al.*, 2006[56] that, to my knowledge, is the only work of complete characterization of the TNFα signalling *in vitro* (on CACO-2). The group first showed that the reason behind the synergism in between sTNFα and IFNγ is that the second one primes the expression of both *TNFRSF1A* and *TNFRSF1B* at a similar extent (as confirmed in my work by RT-qPCR). Then, with a pharmacological interference approach they showed that only TNR1B, but not TNR1A, is apparently required for the sTNFα-induced barrier dysfunction. The conceptual and methodological work of Wang *et al.*, 2006 presents different weak points as ignoring that sTNFα is the natural agonist of TNR1A (and fails to activate TNR1B, or only marginally does it), working at sub-differentiating stages (at TEER values of less than 250 Ω x cm^2) at which is very difficult to drive conclusions about barrier function, and employing commercial antibodies for the pharmacological interference experiments (which might not be highly selective and potent to determine the expected neutralizing effect).

Interestingly, the transcriptomic analysis by RNAseq showed that the co-treatment with TROS completely restored the expression of around half of the genes significantly differentially expressed upon induction with sTNFα. This important difference in the behavior of the modulations with TROS and Adalimumab, could have been determined by two reasons that very probably acted together: **i)** the higher efficiency of the antagonism fulfilled by the neutralization of the ligand in solution with respect to the targeting of a membrane receptor, and **ii)** the capacity of Adalimumab of silencing the whole sTNFα signalling (including also the marginal agonism of TRN1B). The fact that both modulations led to highly comparable outcomes at the functional level (TEER, FD4 and LDH assays, which assess the final and most relevant phenotypes of the 2D epithelial-like structures), but a discrepancy was observed at the transcriptomic level, confirms the high sensitivity of the transcriptional regulation with regards to subtle changes in the experimental conditions (full

antagonism of the ligand versus full antagonism of the receptor that mediates most of the cellular physiological effects determined by the ligand).

An important result that I obtained by analyzing the RNAseq expression profiles of functionally relevant genes in the context of intestinal epithelial barrier function was the observation of a downregulation of *MYLK* determined by sTNFα. In two different experiments (n=3 for each) performed on T84, I found that the induction with only sTNFα (and so, the sole or main activation of TNR1A) determined a transcriptional downregulation of *MYLK*, which others observed to be upregulated by both sTNFα and IFNγ in CACO-2[53,56]. My results do not give any information about the role of TNR1B in this regard, which should mediate the upregulation of *MYLK* that affects the leak permeability pathway[56].

7. OUTLOOK

7.1. Differentiation of intestinal epithelial cells in a 2D model and optimization of techniques

With a series of improvements, I will be able to obtain highly physiologically relevant 2D models (with both transformed and normal cell lines), in which not only full differentiation will be attained, but also maximal practicality in the application of all the necessary assays for investigating the key phenotypes of an intestinal epithelial structure, meaning cell polarization and barrier function.

An optimization of the differentiation protocol of T84 was already run by me reducing the concentration of O_2 to 1% atm., reducing the pore size of the semipermeable membrane to 0.4 μm and implementing the best possible coating ECM for mimicking the basement membrane (Matrigel or GelTrex). The result of the pilot experiment showed that an optimal coating with Matrigel should be defined employing a total protein concentration in between 150 μg/mL and 1 mg/mL, and allowing for a complete evaporation of the solvent overnight at 37°C in order to obtain the thinnest possible ECM layer with a reasonable protein concentration. The differentiation protocol could be further optimized by applying some kind of orbital motion during the culture in order to mimic the transit at the GI lumen, as physiological shear stress on epithelial cells is known to promote their differentiation[95,96]. Of course, the frequency and speed of the motion should be empirically defined as strong shear stress negatively affects fully differentiated monolayers that display high TEERs.

Once defined in detail the optimal protocol for a differentiation of T84 as a real monolayer, I will proceed with the optimization of key techniques. The pilot experiment ran in hypoxia (experiment IV), in which sTNFα was applied at three different concentrations for 24 hrs, already showed that a significant improvement of the FD70 assay can be achieved in these conditions. I will repeat that experiment with an induction time of 12 hrs, being this more effective for determining a barrier dysfunction than the 24 hrs one. The TUNEL and the BrdU assays will be run in the hypoxia model to see if the monolayer configuration determines an improvement of their outcome. If the outcome

of the TUNEL assay cannot be improved (proper staining of chromatin digested with DNAaseI) I will incorporate the Caspase-Glo® 3/7 Assay from Promega (a chemiluminescent assay for the assessment of the activation of Caspases 3 and 7, a convergent point of both extrinsic and intrinsic apoptotic pathways). If the outcome of the BrdU assay cannot be improved I will try to implement a scratch assay employing "ibidi chambers" on the TW inserts (hoping that, while removing the "ibidi chamber", the strongly associated epithelial cells will not be pulled off together). In the monolayer configuration, the IF staining protocol will be optimized in order to properly detect the different TJPs at the Tight Junctional density. The permeabilization step with 0.5 % TX-100 will be kept, Saponin 0.5 % will be included in both blocking and incubation buffers, and the fixation protocol will be changed in order to improve the antigen (and the specific epitope) retrieval. Following the information retrieved in the literature[97], a 10-20 min. fixation time at -20°C will be performed with Ice-cold Methanol 100 % or with a solution 1:1 Methanol:Acetone for a series of key TJP markers, in order to define the optimal protocol for each specific combination antigen-antibody. The TJP markers that I will initially consider will be: Claudin-1 ("sealing", intercellular TJP that regulates the pore permeability pathway) with the antibody "Thermo Fisher - 51-9000 #403", Claudin-2 ("pore forming", intercellular TJP that regulates the pore permeability pathway) with the antibody "Thermo Fisher - 51-6100 #404", Occludin (intercellular TJP that regulates the leak permeability pathway) with the antibody "Thermo Fisher - 71-1500 #381" and ZO-1 (scaffolding TJP that regulates the leak permeability pathway and that serves as a co-localization marker for TJ assembly) with the antibody "Thermo Fisher - ZO1-1A12 #387".

In order to complete the model, the differentiation of a normal intestinal epithelial cell line will have to be established in the TW insert format. My characterization of the FHC line showed that intestinal epithelial stem cells are present in the heterogeneous population, but under-represented with respect to fibroblasts. In order to differentiate the FHC intestinal epithelial stem cells over a semi-permeable membrane, I envision a series of key steps.

i) Modification the FHC medium in accordance to the media SCM-6F8 developed by Xia Wang *et al.*, 2015[98] and the information presented by Chopra *et al.*, 2010[99]. Will be included Epinephrin, R-spondin 1, Jagged-1, Noggin, Rock-inhibitor, SB431542 and Nicotinamide, and the levels of FBS will be kept at ± 2.5 %. By accordingly regulating the TGF-β/BMP (transforming growth factor-β/bone morphogenetic protein), Wnt/β-catenin, EGF (epidermal growth factor), IGF (insulin-like growth factor) and Notch pathways, the intestinal stem cells will be maintained in a highly clonogenic, ground state form.

ii) Implementation of an efficient method for getting rid of the fibroblasts and for enriching the heterogeneous cell population with the intestinal epithelial stem cells, immediately before starting the differentiation process.

iii) Testing of different seeding densities over semipermeable membranes pre-coated with Matrigel (optimal coating strategy).

iv) After letting the cells reach confluency in pro-stemness media added to both apical and basolateral sides, definition of the optimal differentiation protocol by testing: presence or absence (ALI culture implemented by Xia Wang *et al.*, 2015[98]) of media at the apical side, and maintenance of the pro-stemness media versus the change with a differentiation media (concentration of FBS higher than 2.5 %, suppression of Notch and Wnt signallings, etc.).

7.2. Complete characterization of the 5-HTRs system in intestinal epithelial barrier function

In order to identify the full-length sequence of the putative novel *HTR3E* splicing variant, the 5'RACE PCR should be repeated with new reagents and new enzymes for the preparation of the whole cell cDNA library with known 5'-end sequences. In the step of cDNA synthesis, the internal reverse primer can be employed instead of the GeneRacer™ Oligo dT Primer, as I already did, in order to obtain full length 5' fragments.

The elucidation of the eventual role/s of the 5-HTRs in intestinal epithelial barrier function could open the way to the development of new effective, non-highly immunosuppressive, pharmacological strategies directed towards the restoration of the epithelial barrier dysfunction that takes place in IBD. As happens for many cytokines receptors, 5-HTRs are expressed in both intestinal epithelial cells and immune cells located at the lamina propria, rendering more complicated this task. Another source of complexity is the well-known contradictory and opposed contribution of the single 5-HTRs with regards to a certain phenotype in a certain type of cell and tissue. That is why my plan for the initiation of this study will be to first of all check the expression of all the 5-HTRs known to be expressed by intestinal epithelial cells ($5\text{-HT}_{1,2,3,4,7}$Rs) at both mRNA and protein levels. Secondly, I will proceed with the dissection of the 5-HT signalling with regards to all the mechanisms involved in barrier function (in my *in vitro* model of the sole intestinal epithelium) by a systematic pharmacological characterization of each of the aforementioned 5-HTRs expressed by these cells. Taking into consideration the known pleiotropic roles of 5-HT and the multiplicity of receptors involved in the signalling (which often constitutes the basis for a diversification of an initial physiological role, during the evolutionary process), I will evaluate the effects of the selective pharmacological modulation of each of the receptors of interest in both directions. So, I will perform the full selective agonism and the full selective antagonism (in the presence of the selective agonist) for each of them, following the same methodological approach presented in this thesis: **i)** titration of the modulator, **ii)** definition of its optimal concentration, expected to be close to the m.n.t.c., **iii)** and repetition of the modulation with the optimal concentration, applying all relevant assays for assessing the mechanisms affecting the paracellular permeability.

Considering the intrinsic complexity of the signalling and of the pathomechanisms of IBD taking place at the GI mucosa, the translational aim of proposing a new potential therapeutical strategy of

barrier protection by targeting the 5-HT signalling, should be left aside momentously. A certain selective pharmacological modulation of these receptors performed in my *in vitro* model could not lead to the same outcome (with regards to barrier function) *in vivo*, where the receptors located at the plasma membranes of the immune cells of the lamina propria would be also targeted.

7.3. Inflammatory model and characterization of the synergism in between sTNFα and IFNγ

With the same procedure followed for sTNFα and IFNγ applied alone, different pro-inflammatory cytokines can be studied in this *in vitro* model with regards to intestinal epithelial barrier function. Cytokines that bind to different cognate receptors, as is the case of TNFα, are interesting candidates for investigating possible differential receptor-specific effects that could potentially lead to an improvement of the actual therapeutical strategies in IBD (with regards to the protection of the epithelial barrier dysfunction).

A barrier-disruption test should be performed with IL1β applied alone at different concentrations (monitoring the cytotoxicity) in order to understand if T84, expressing *IL1R1* at very low levels, is responsive to it or not.

The mechanisms underneath the synergism in between sTNFα and IFNγ were clearly elucidated with two transcriptional analyses that on side confirmed the information present in the literature (positive regulation of *TNFRSF1A* and *TNFRSF1B* exerted by IFNγ), and on the other brought to novel results. The positive regulation of *IFNGR1* and *IFNGR2* exerted by the sole sTNFα, observed by RNAseq, is a novel result that must be confirmed. I will repeat the expression analyses for the induction with the sole sTNFα for 12 hrs by RT-qPCR, and on the other side I will run the same analyses for the single induction with IFNγ. Doing so, I will confirm the positive regulation exerted on *TNFRSF1A* and *TNFRSF1B*, and evaluate the eventual effects on *IFNGR1* and *IFNGR2*, in order have the complete image of the cross-regulatory feedback in between the two cytokines and their respective cognate receptors.

In order to confirm the novel anti-necroptotic effects of IFNγ in intestinal epithelial cells, I will apply an inducer of Necroptosis different than sTNFα (that is engaged in a synergistic interaction with IFNγ), as for example HS-173 (an inducer of RIP3-dependent Necroptosis[100]), and I will then co-treat some cells with IFNγ 100 ng/mL and other cells with both IFNγ 100 ng/mL and Emapalulab 4 µg/mL. With the LDH assay, I should observe a clear pro-necroptotic effect determined by HS-173 (higher levels of LDH than the untreated condition), and anti-necroptotic effect (normalization of the increase of LDH determined by HS-173) on the cells co-treated with HS-173 and IFNγ, and finally a reversal of the anti-necroptotic effects determined by the co-treatment with HS-173, IFNγ and Emapalumab.

7.4. Complete characterization of the TNFα/TNR1A/TNR1B signalling axis in intestinal epithelial barrier function

Having conclusively defined the role of TNR1A in intestinal epithelial barrier function (in the transformed cell line T84), my first immediate objective is the precise characterization of the role of TNR1B in the same context, in exactly the same experimental conditions.

I will carry out the full and selective agonism of TNR1B with the (TNR1B-selective) mTNFα-mimetic ARTOS[101] applied alone and in the presence of sTNFα at 100 ng/mL, to understand if the activation of this receptor impairs or eventually protects the intestinal epithelial barrier function. The titration of ARTOS, for the definition of its optimal working concentration in my model, will be performed monitoring the dose-dependent response by assessing the expression of *IL10* (at the transcriptional level by RT-qPCR, or at the translational level with an ELISA assay). IL10 is an anti-inflammatory and barrier-protective cytokine known to be produced by T84[102]. As EHD2-scTNFR2, prototype of ATROS, significantly induces the expression of IL10[103], this positive regulatory loop will be employed to define the working concentration of ARTOS close to the m.n.t.c. (controlling always the cytotoxicity with the LDH assay). Once defined the working concentration, the two key experiments of sole application of ARTOS (as done for sTNFα applied alone) as well as the one of co-treatment with sTNFα (as done for TROS) will be run including the functional assays TEER, FD4 and LDH, and performing a transcriptomic analysis by RNAseq. In an additional experiment, I will nullify the effects of ARTOS (applied alone) with Adalimumab; given its capacity of binding mTNFα, I expect it to also neutralize ARTOS.

The completion of the work by the selective agonism of TNR1B may lead to further novel results, with a high translational impact on the actual anti-TNFα therapeutical strategies for IBD. The experiment of the application of ATROS in the presence of sTNFα could eventually show a barrier-protective effect determined by the activation of TNFR2. If that would be the case, the idea of modifying the actual anti-TNFα therapies, characterized by a global antagonism of both sTNFα and mTNFα signallings, would have a clear and concrete basis, at least concerning the intestinal epithelial barrier function. A single antagonism of TNFR1 (as clearly demonstrated in my PhD work), without any action or eventually with a parallel agonism of TNFR2, would decisively improve the actual global anti-TNFα therapies, characterized by drastic immuno-suppressive side-effects. Is very important to consider that the activation of the PI3K-PKB/Akt and of the non-canonical NF-kB pathways should mediate the cell survival and the pro-proliferative effects observed (at least in other cellular/tissue contexts, but very probably also in the intestinal epithelium) upon the selective agonism of TNR1B. Leaving aside the effects that the activation of TNR1B might determine on the TJs and AJs, with high probability the cell survival and the pro-proliferative aforementioned effects might, at least partially, counteract the pro-apoptotic and pro-necroptotic effects of the activation of TNR1A (and so, at least partially counteract the barrier impairment

determined by sTNFα). Is critical to consider that Gitter *et al.* 2000 concluded that 56% of the sTNFα-induced increase in epithelial permeability in HT-29/B6 monolayers could be accounted by the increase in Apoptosis[104]. Another very important aspect that is crucial to consider is that the complete characterization of the signalling pathway in my *in vitro* model will allow me to define the specific role of each receptor with regards to intestinal epithelial barrier function in the correct and most clear way. The characterization of the signalling pathway in *in vivo* models (for which there are already publications with contradictory results regarding the two receptors) automatically adds another level of complexity to the problem, since it increases drastically the difficulty to distinguish between the contributions of the TNFα signalling taking place in immune cells of the lamina propria (that, when modulated at different levels of the TNFα signalling, will directly affect the intestinal epithelial barrier in different ways by producing s/mTNFα and many other different cytokines) from the specific TNFα signalling taking place only in the intestinal epithelial cells. For that reason, the results obtained by me in my *in vitro* model can be considered independent and not directly comparable to the ones already obtained by others in *in vivo* models. So, as mentioned before, the only (to my knowledge) work of characterization of the whole signalling pathway *in vitro* was done by Wang *et al.*, 2006 in CACO-2, and my data already contradict their results.

In order to complete, in an exhaustive and detailed manner, the characterization of the TNFα/TNR1A/TNR1B signalling axis in intestinal epithelial barrier function, I will include all the envisioned functional assays and protein expression and localization analyses in the fully optimized hypoxia model (see section 6.1). I will proceed as follows.

i) I will re-do the titration of sTNFα and then of TROS (in the presence of the optimal sTNFα concentration) on the hypoxia model applying all the established functional assays. In the same way, I will run the three biological replicas of the full antagonism of TNR1A in hypoxia.

ii) I will re-do the titration of ARTOS on the hypoxia model applying all the established functional assays. In the same way, I will run the three biological replicas of the sole full agonism of TNR1B and of the full agonism of the receptor in the presence of sTNFα, in hypoxia. In these experiments I will analyze the effects of the agonism with regards to the expression of the cytokines receptors genes *TNFRSF1A*, *TNFRSF1B*, *IFNGR1* and *IFNGR2* and with regards to the expression of relevant genes related with barrier function (starting by *MYLK* and by relevant genes of the NFκB and PI3K/PKB/Akt pathways).

iii) I will carry out a validation of the selective antagonism of TNR1A by establishing a conditional KO cell line for *TNFRSF1A* in order to apply a selective genetic ablation in an endpoint analysis on fully differentiated monolayers induced with sTNFα. In the same kind of end-point experiment, I will employ a conditional KO cell line for *TNFRSF1B* and, by applying ARTOS, I will do an analogous validation for the selective agonism of TNR1B.

iv) I will analyze in detail the effects of the modulations that significantly protect the impairment (or that significantly amplify the impairment without inducing unwanted cytotoxic effects) of

the T84 monolayer by a whole-transcriptome expression analysis complemented by protein expression analysis of selected targets (SDS-PAGE-immunodetection and IF staining) in order to identify the signalling pathways differentially modulated. I will focus on the TJs ZO-1, Occludin, Claudin-1/2 expression and localization (IF followed by confocal microscopy imaging), on the regulation of the apoptotic and necroptotic pathways (expression of FAS and activation of Caspase 3/7) and on cell proliferation pathways (complemented by an IF BrdU assay or a scratch assay with cells grown on ibidi® chambers).

v) I will elucidate the potential underlying mechanisms by putting the data into biological context performing an Ingenuity® Pathway Analysis over all the expression data.

vi) I will validate all the findings on CACO-2 (cell line employed by Wang *et al.*, 2006) and on a normal epithelial cell line as FHC differentiated as 2D epithelial-like structures, and organoids (with the assays that can be applied in that configuration).

vii) I will complexify the 2D model by establishing a co-culture with innate immune cells in the basal compartment to modulate also the TNR1A/B expressed by these cells. This model will resemble better the *in vivo* condition observed at the GI mucosa, and will allow me to evaluate the effects of the pro-inflammatory cytokines released by the innate immune cells (resembling the ones of the lamina propria) over the epithelial-like monolayer.

The completion of the study of the TNFα/TNR1A/TNR1B signalling will represent a standard approach to follow for other candidate signalling pathways as the 5-HT one. More than 200 genes are involved in the development and in the progression of IBD and my *in vitro* platform represents a valuable tool for characterizing their roles with both genetic and pharmacological interference approaches. In the long term, this will allow to not only gain knowledge about the predisposition to develop the disease but also to develop novel therapeutical strategies aiming to improve the druggability not only of the immune cells at lamina propria, but also of the GI epithelial cells that play a crucial role in the pathomechanisms of this complex disease.

SUPPLEMENTARY MATERIAL

PRIMERS DESIGN

Conventional RT-PCR

All the annotated splicing variants for each gene of interest were identified on the ENSEMBL genome browser, UCSC Genome Browser and NCBI RefSeq. The information obtained from the three different databases was compared. All primers were designed either with Primer3 (v. 0.4.0) or with the Universal ProbeLibrary Assay Design Center (Roche) tools (in accordance to the requirements stated in the section 3.2.2.4.) aiming to amplify all possible annotated protein-coding splicing variants for each gene of interest (except for the *HTR3E* primers designed to amplify only specific variants). The amplifications of the resulting primers were analyzed with the UCSC *in-silico* PCR tool setting as a template the whole human genome (Dec. 2013 (GRCh38/hg38)) for both the coding and the genomic assemblies. The physico-chemical properties of each designed primer were analyzed with the OligoAnalyzer 3.1 tool.

Table S1: Splicing variants amplified by conventional RT-PCR primers.

Primer name	Ensembl transcripts accession numbers (protein-coding and non-coding)
*ARF1*_for	ENST00000478336.5; ENST00000477451.5; ENST00000473949.5; ENST00000482962.5; ENST00000540651.5; ENST00000470558.5; ENST00000272102.10; NST00000470670.5; ENST00000478424.5; ENST00000469235.5; ENST00000541182.1; ENST00000497165.5
*ARF1*_rev	
*SDHA*_for	ENST00000504309.5; ENST00000651543.1; ENST00000514233.1; ENST00000510361.5; ENST00000504824.5; ENST00000264932.11; ENST00000505555.5; ENST00000514027.5
*SDHA*_rev	
*TJP1*_for	ENST00000346128.10; ENST00000631203.1; ENST00000612628.3; ENST00000495972.6; ENST00000621049.4; ENST00000400011.6; ENST00000613680.4; ENST00000356107.10; ENST00000545208.6; ENST00000614355.4
*TJP1*_rev	
*HTR3A*_for	ENST00000506841.6; ENST00000299961.5; ENST00000504030.6; ENST00000355556.6; ENST00000510849.5; ENST00000375498.6
*HTR3A*_rev	
*HTR3B*_for	
*HTR3B*_rev	ENST00000537778.5; ENST00000260191.7
*HTR3C*_for	
*HTR3C*_rev	ENST00000318351.2
*HTR3D*_for	

*HTR3D*_rev	ENST00000382489.3; ENST00000428798.7; ENST00000334128.6
*HTR3E*_for	ENST00000436361.6; ENST00000425359.6; ENST00000440596.2; ENST00000335304.6; ENST00000415389.6
*HTR3E*_rev	
*HTR3E/5-HT3C1*_for	ENST00000436361.6; ENST00000440596.2; ENST00000335304.6
*HTR3E/5-HT3C1*_rev	
*HTR3Ea/HTR3Eb/HTR3EV3*_for	ENST00000425359.6; ENST00000415389.6
*HTR3Ea/HTR3Eb/HTR3EV3*_rev	
*VIL1*_for	ENST00000248444.10; ENST00000392114.6
*VIL1*_rev	
*KRT20*_for	ENST00000576098.2; ENST00000167588.4
*KRT20*_rev	
*ACTA2*_for	ENST00000480297.5; ENST00000224784.10
*ACTA2*_rev	
*PROM1*_for	ENST00000505450.5; ENST00000540805.5; ENST00000513946.1; ENST00000510224.5; ENST00000503884.5; ENST00000508167.5; ENST00000447510.6; ENST00000513448.5; ENST00000539194.5
*PROM1*_rev	
*LGR5*_for	ENST00000550851.5; ENST00000536515.5; ENST00000266674.10; ENST00000540815.2
*LGR5*_rev	
*LRIG1*_for	ENST00000383703.3; ENST00000475366.5; ENST00000273261.7; ENST00000498287.5
*LRIG1*_rev	
*OLFM4*_for	ENST00000219022.3
*OLFM4*_rev	

Note: *ARF1*_for/rev, *HTR3A*_for/rev, *HTR3B*_for/rev, *HTR3C*_for/rev, *HTR3D*_for/rev, *HTR3E*_for/rev, *HTR3E/5-HT3C1*_for/rev, *HTR3Ea/HTR3Eb/HTR3EV3*_for/rev, *VIL1*_for/rev; *KRT20*_for/rev, *ACTA2*_for/rev were previously designed in the laboratory of Prof. Dr. Beate Niesler.

RT-qPCR

RT-qPCR primers were designed (in accordance to the requirements stated in the section 3.2.2.5.) in the same way as conventional RT-PCR ones but employing preferentially the Universal ProbeLibrary Assay Design Center (Roche).

Table S2: Splicing variants amplified by RT-qPCR primers.

Primer name	**Ensembl transcripts accession numbers**

	(protein-coding and non-coding)
*HPRT1_* RT-qPCR_for	ENST00000475720.1; ENST00000462974.5; ENST00000298556.8
*HPRT1_* RT-qPCR_rev	
*SDHA_* RT-qPCR_for	ENST00000515815.5; ENST00000503674.5; ENST00000507522.1; ENST00000504309.5; ENST00000515752.5; ENST00000509564.1; ENST00000651543.1; ENST00000510361.5; ENST00000617470.4; ENST00000264932.11; ENST00000514027.5; ENST00000511810.5
*SDHA_* RT-qPCR_rev	
*ARF1_* RT-qPCR_for	ENST00000478336.5; ENST00000540651.5; ENST00000470558.5; ENST00000272102.10; ENST00000470670.5; ENST00000478424.5; ENST00000469235.5; ENST00000541182.1; ENST00000497165.5
*ARF1_* RT-qPCR_rev	
*TNFRSF1A_* RT-qPCR_for	ENST00000536194.1; ENST00000162749.6; ENST00000366159.8; ENST00000535958.1; ENST00000543995.5; ENST00000539372.5; ENST00000538363.1; ENST00000543048.5; ENST00000540022.5; ENST00000440083.6
*TNFRSF1A_* RT-qPCR_rev	
*TNFRSF1B_* RT-qPCR_for	ENST00000536782.2; ENST00000376259.7
*TNFRSF1B_* RT-qPCR_rev	
*IFNGR1_* RT-qPCR_for	ENST00000646036.1; ENST00000644894.1; ENST00000642390.1; ENST00000414770.5; ENST00000367739.8; ENST00000647124.1; ENST00000458076.5; ENST00000643119.1; ENST00000645753.1; ENST00000645045.1; ENST00000646898.1
*IFNGR1_* RT-qPCR_rev	
*IFNGR2_* RT-qPCR_for	ENST00000572016.5; ENST00000405436.5; ENST00000545369.2; ENST00000381995.5; ENST00000573079.5; ENST00000573887.2; ENST00000571550.5; ENST00000439213.5; ENST00000576463.5; ENST00000290219.10
*IFNGR2_* RT-qPCR_rev	
*IL1R1_* RT-qPCR_for	ENST00000452403.5; ENST00000413623.5; ENST00000410023.6; ENST00000409288.5; ENST00000424272.5; ENST00000409329.5; ENST00000409929.5; ENST00000430171.1; ENST00000450319.5; ENST00000409589.5; ENST00000442590.5
*IL1R1_* RT-qPCR_rev	

Note: *HPRT1_* RT-qPCR_for/rev were previously designed in the laboratory of Prof. Dr. Beate Niesler.

RT-qPCR PRIMERS STANDARD CURVES FOR EFFICIENCY EVALUATION AND RELATIVE QUANTIFICATION

The different pair of primers designed for RT-qPCR analyses were evaluated from standard curves obtained by amplifying a template with known expression of the gene of interest and then plotting

the $\log_{10}$ of 1:3 serial dilutions (quantities) together with the mean Ct values in a linear regression curve. The templates for the different genes of interest were selected in accordance to the information obtained from the mRNA expression data of the Human Protein Atlas. The selected standard curves (figures S1 to S8) were employed for the relative quantifications described in the section 3.2.2.5.

HPRT1

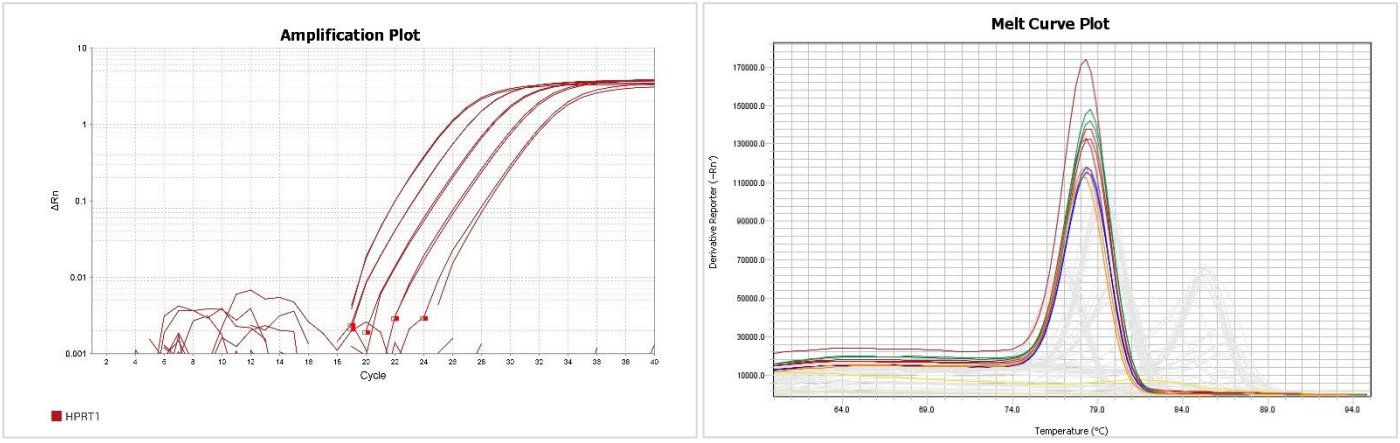

Template	Y-intercept	r^2	Slope	Efficiency
T84 differentiated +10 days	23.893	0.997	-3.444	95.142

Figure S1: RT-qPCR amplification and melting curve plots and standard curve parameters for *HPRT1* for/rev primers.

SDHA

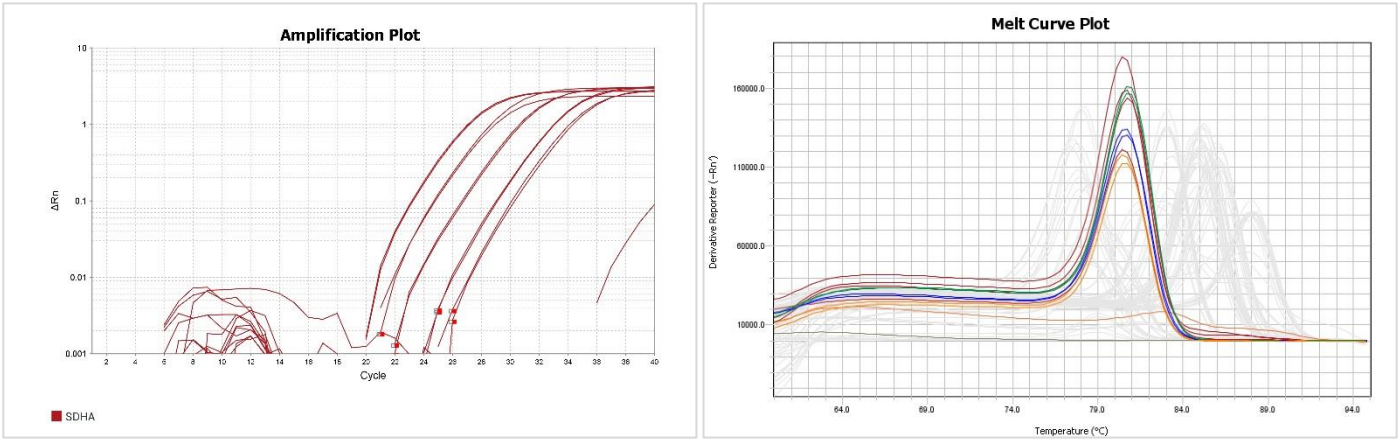

Template	Y-intercept	r^2	Slope	Efficiency
T84 differentiated +10 days	24.895	0.990	-3.892	80.691

Figure S2: RT-qPCR amplification and melting curve plots and standard curve parameters for *SDHA* for/rev primers.

ARF1

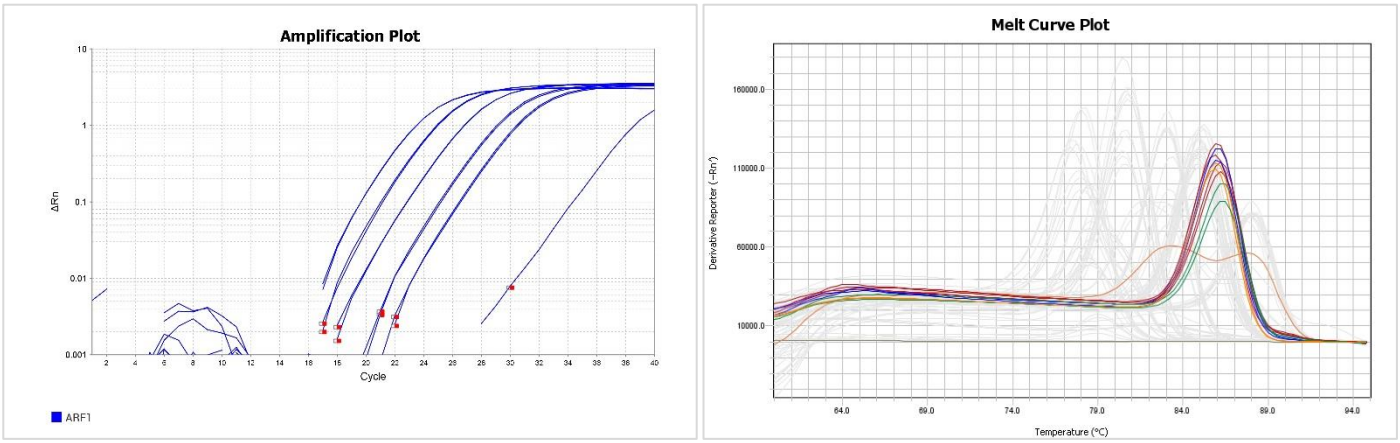

Template	Y-intercept	r^2	Slope	Efficiency
T84 differentiated +10 days	21.403	0.994	-3.816	82.842

Figure S3: RT-qPCR amplification and melting curve plots and standard curve parameters for *ARF1* for/rev primers.

TNFRSF1A

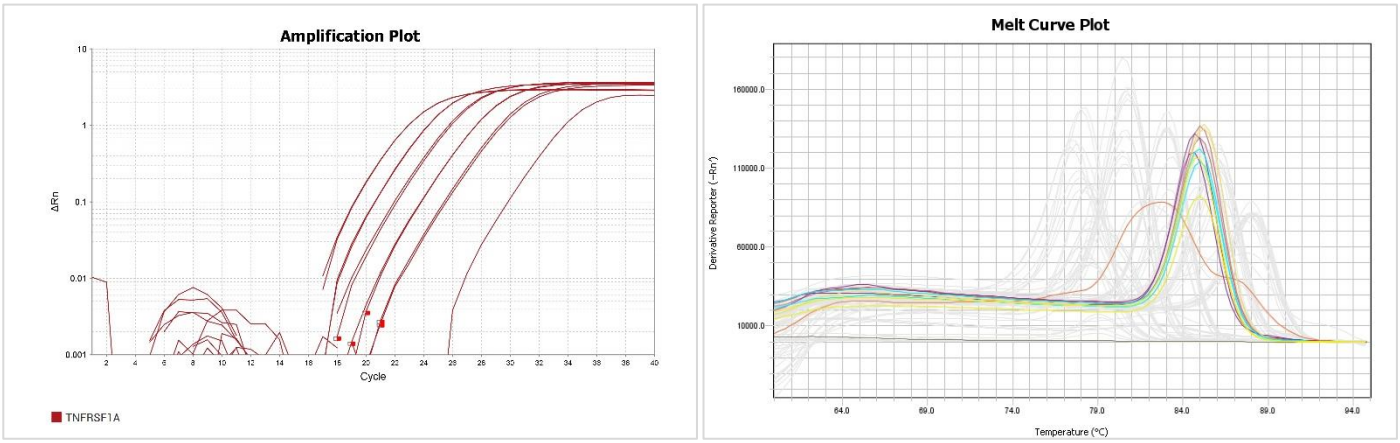

Template	Y-intercept	r^2	Slope	Efficiency
Polymorphonuclear leukocytes (RNA kindly provided by Dr. Guido Wabnitz, Institute of Immunology, University of Heidelberg)	20.820	0.997	-3.409	96.506

Figure S4: RT-qPCR amplification and melting curve plots and standard curve parameters for *TNFRSF1A* for/rev primers.

TNFRSF1B

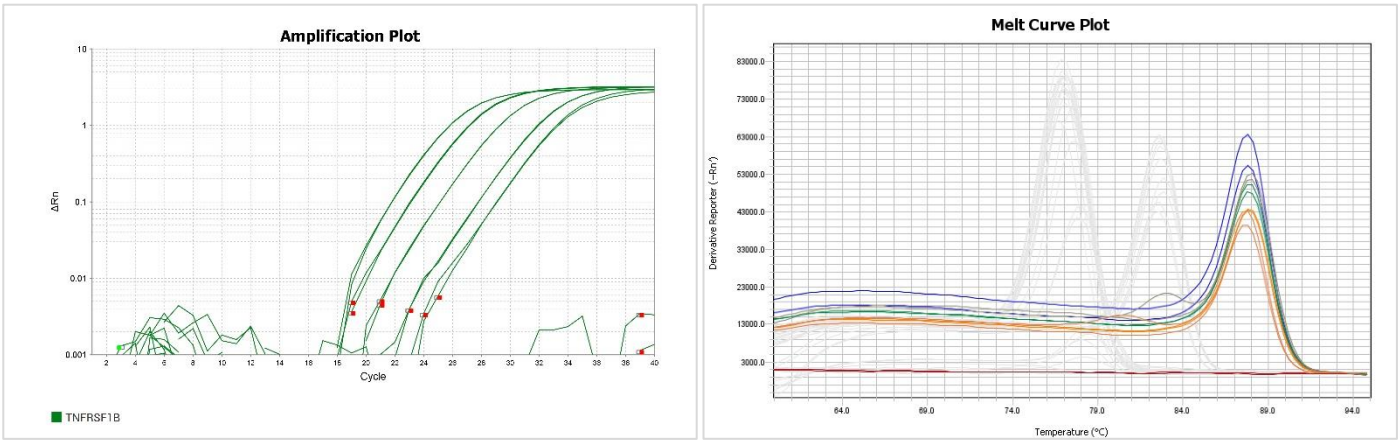

Template	Y-intercept	r^2	Slope	Efficiency
Monocytes (cells kindly provided by Antje Heidtmann, Institute of Immunology, University of Heidelberg)	23.591	0.987	-4.106	75.212

Figure S5: RT-qPCR amplification and melting curve plots and standard curve parameters for *TNFRSF1B* for/rev primers.

IFNGR1

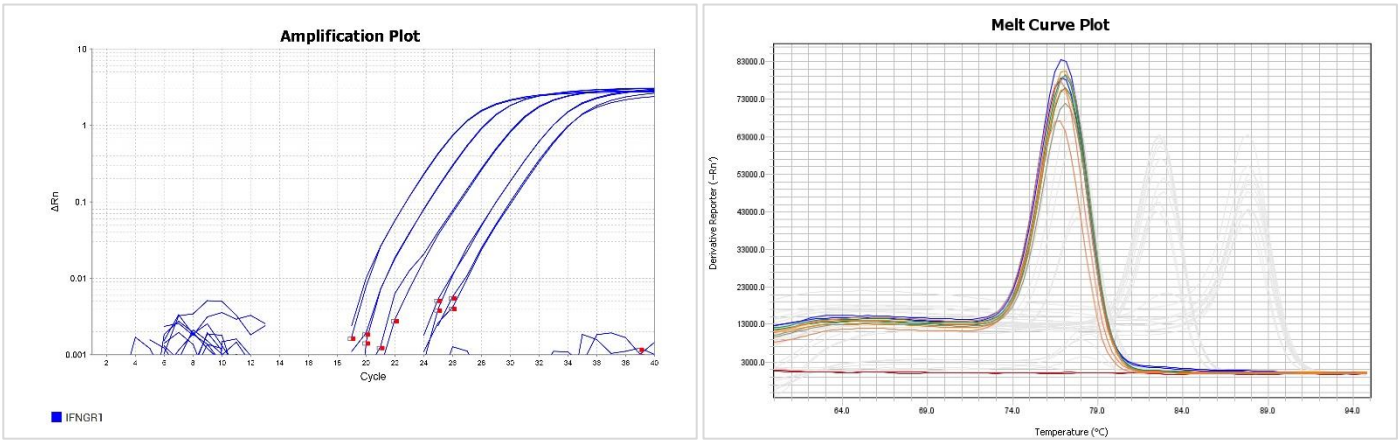

Template	Y-intercept	r^2	Slope	Efficiency
Monocytes (cells kindly provided by Antje Heidtmann, Institute of Immunology, University of Heidelberg)	24.269	0.986	-4.090	75.587

Figure S6: RT-qPCR amplification and melting curve plots and standard curve parameters for *IFNGR1* for/rev primers.

IFNGR2

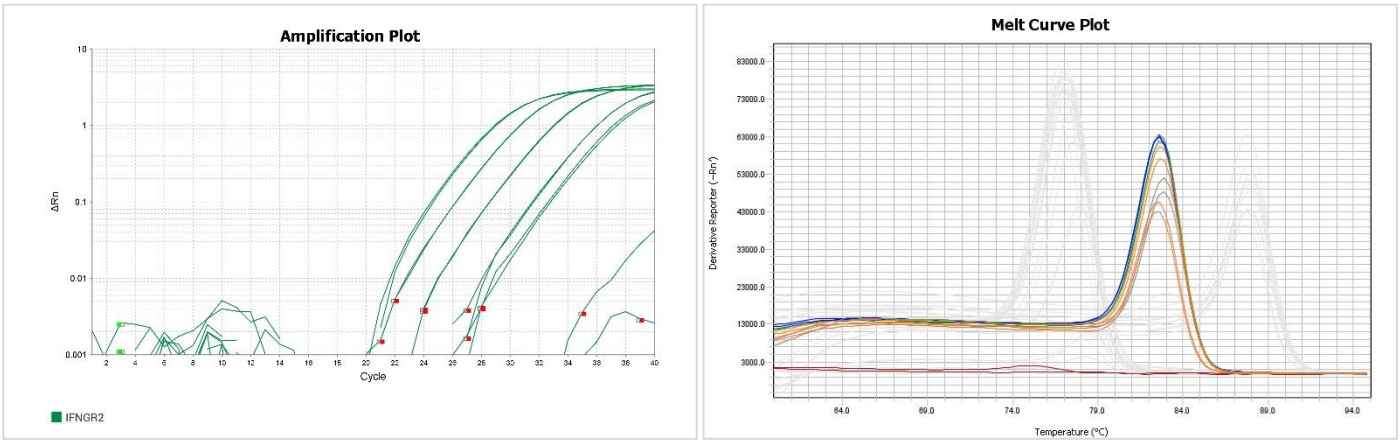

Template	Y-intercept	r^2	Slope	Efficiency
Monocytes (cells kindly provided by Antje Heidtmann, Institute of Immunology, University of Heidelberg)	26.798	0.985	-4.586	65.223

Figure S7: RT-qPCR amplification and melting curve plots and standard curve parameters for *IFNGR2* for/rev primers.

IL1R1

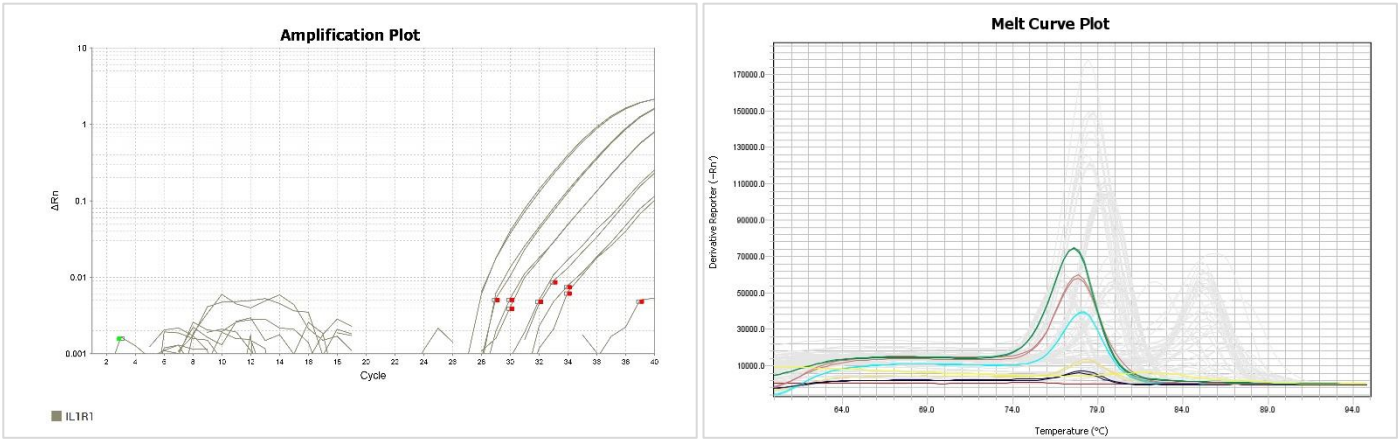

Template	Y-intercept	r^2	Slope	Efficiency
Monocytes (cells kindly provided by Antje Heidtmann, Institute of Immunology, University of Heidelberg)	29.957	0.993	-4.128	74.670

Figure S8: RT-qPCR amplification and melting curve plots and standard curve parameters for *IL1R1* for/rev primers.

SANGER SEQUENCING OF THE *HTR3E* INTERNAL AMPLICON OF 275 bp

Amplicon 275 bp (*HTR3E*_for/_rev on T84's cDNA) primer *HTR3E*_for

GGGCTTTTCCTGCGTCCAGTAAGGAAATAAGGGCCCGGGTCCTCACCCCCACCCACCT
GCCCGGTGTAGGGAAGTCACATTCCTCTTCCCCCACCTCCACTTCTCTGCTCCTGCCTC
CTTCCCTGTCTCCCTCCCTCCACAGGTGACATTTGCAGCCCATGGCTGAGTCTCTGTCT
TTCTGTAGGTGTGAAGGAGCCAGAGGTATCAGCAGGGCAGATGCCGGGCCCTGCGGA
GGCAAGCTGACAGGGAAGGAGGCAGGAGCAGAGAATTGGAGGTGGGGGAAGAGGAA
TGTGACTTCCCTCACCGCGCGATGTTTGGGGGTGAAACAGGCACTTATGTTCTTCTGCC
CGCAATGGGACGCAACTCCCCAGGAATTGCAATGTAGCAACTCCCCGCGGGTGGATG
GAGGTGAGACCGGCCATTATTTTTCTTCTACCGCGGATGTCAGGCCACTCCAAGGCTG
ATGCTAGGAGCAAAAA

Amplicon 275 bp (*HTR3E*_for/_rev on T84's cDNA) primer *HTR3E*_rev

GCGTACTGCTGCTGATCCTCCTGGCTCCTTACACCTACAGAAAGACAGAAGACTCAGC
CATGGGCTGCAAATGTCACCTGTGGAGGGAGGGAGACAGGGAAGGAGGCAGGAGCA
GAGAAGTGGAGGTGGGGGAAGAGGAATGTGACTTCCCTCACCGGGCAGGTGGGTGGG
GGTGAGACCCGGGCCCTTATTTTCCTTCTGGGGCGCAGTGGGACAGCATCTCCCCGGG
CTGTGCAGTGGAGCAACAGCCGGGGAGATGCTGTCCCGGCCGAAGGAAAATAAGGGC
CGGTCTACCCCCCTGCCGTGAGGGAAGTCAATTCTCTTCACTCCTTTCTGCTCGCTCTT
CTGTCTCTCCTCCAGTGACATTTGGCACAGGGCTGAATCTTGGTCTTTCTTTAAGTGTG
AAGGAGCAGAGGCTATCAGCAGGAAGATGCCCGGCCCTGCGAGGCGAGCTTAGGGGA

5'/3' RACE PCR INTERNAL PRIMERS DESIGN

The primers for the 5'/3' RACE PCRs of *HTR3E* were designed in accordance to the Invitrogen GeneRacer™ Kit user manual (Version L, 8 April 2004, 25-0355).

***HTR3E* EXON 7**

GTGTCTACTTCGCCCTGTGCCTGTCCCTGATGGTGGGCAGCCTGCTGGAGACCATCTTC
ATCACCCACCTGCTGCACGTGGCCACCACCCAGCCCCCACCCCTGCCTCGGTGGCTCC
ACTCCCTGCTGCTCCACTGCAACAGCCCGGGGAGATGCTGTCCCACTGCGCCCCAGAA
GGAAAATAAGGGCCCGGGTCTCACCCCCACCCACCTGCCCG

***HTR3E* EXON 8**

GTGTGAAGGAGCCAGAGGTATCAGCAGGGCAGATGCCGGGCCCTGCGGAGGCAGAGC
TGACAGGGGGCTCAGAATGGACAAGGGCCCAGCGGGAACACGAGGCCCAGAAGCAG
CACTCAGTGGAGCTGTGGTTGCAGTTCAGCCACGCGATGGACGCCATGCTCTTCCGCC
TCTACCTGCTCTTCATGGCCTCCTCTATCATCACCGTCATATGCCTCTGGAACACCTAG
GCAGGTGCTCACCTGCCAACTTCAGTCTGGAGCTTCTCTTGCCTCCAGGGACTGGCCA
GGTCTCCCCCCTTTCCTGAGTACCAACTATCATATCCCCAAAGATGACTGAGTCTCTGC
TGTATTCCATGTATCCCAATCCGGTCCTGCTGATCAATTCCAATCCCAGACATTTCTCC
CTGTTCCTGCATTTTGTTGGCTTCCTTCAGTCCTACCATATGGTTCTAGGTCCCTCTTAC
GTCATCTGCATAGCAGACTATACCTCTTCTGTCCGCTGACTTGCCCAATAAATAATTCT
GCAGAGA

*HTR3E*_for: 5´-TGCTCCACTGCAACAGCCCG-3´

*HTR3E*_rev: 5´-CCCTGTCAGCTCTGCCTCCG-3´

*HTR3E*_5' RACE_rev: 5´-TGCCTCCGCAGGGCCCGGCATCT-3´

*HTR3E*_5' RACE Nested_rev: 5´-CCGGCATCTGCCCTGCTGATACCT-3´

HTR3E_3' RACE_for: 5´-CCACTGCAACAGCCCGGGGAGAT-3´

HTR3E_3' RACE Nested_for: 5´-GGAAAATAAGGGCCCGGGTCTCA-3´

Figure S9: Primers for the 5'/3' RACE PCRs of *HTR3E*

5'/3' RACE CONTROL PCRs FOR ACTB (β-Actin)

Table S3: Programs of both Touchdown and Nested 5' and 3' control PCRs for *ACTB*.

Touchdown PCR	Nested PCR
13) 95°C for 15 minutes, 14) 94°C for 30 seconds, 15) 74°C for 2 minutes, 16) repeat steps 2) and 3) for 5 cycles, 17) 94°C for 30 seconds, 18) 72°C for 2 minutes, 19) repeat steps 5) and 6) for 5 cycles, 20) 94°C for 30 seconds, 21) 65°C for 30 seconds, 22) 72°C for 2 minutes, 23) repeat steps 8), 9) and 10) for 25 cycles, 24) 72°C for 10 minutes	1) 95°C for 15 minutes, 2) 94°C for 30 seconds, 3) 65°C for 30 seconds, 4) 72°C for 1 (5' RACE) or 2 (3' RACE) minutes, 5) repeat steps 2), 3) and 4) for 25 cycles.

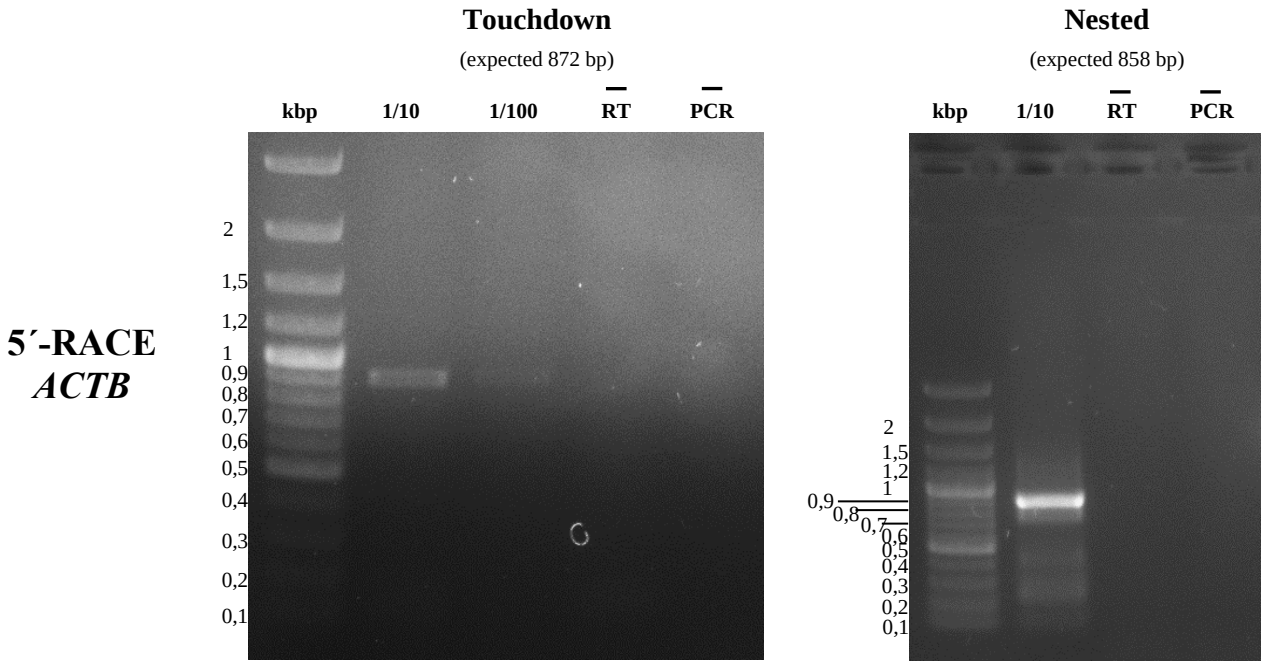

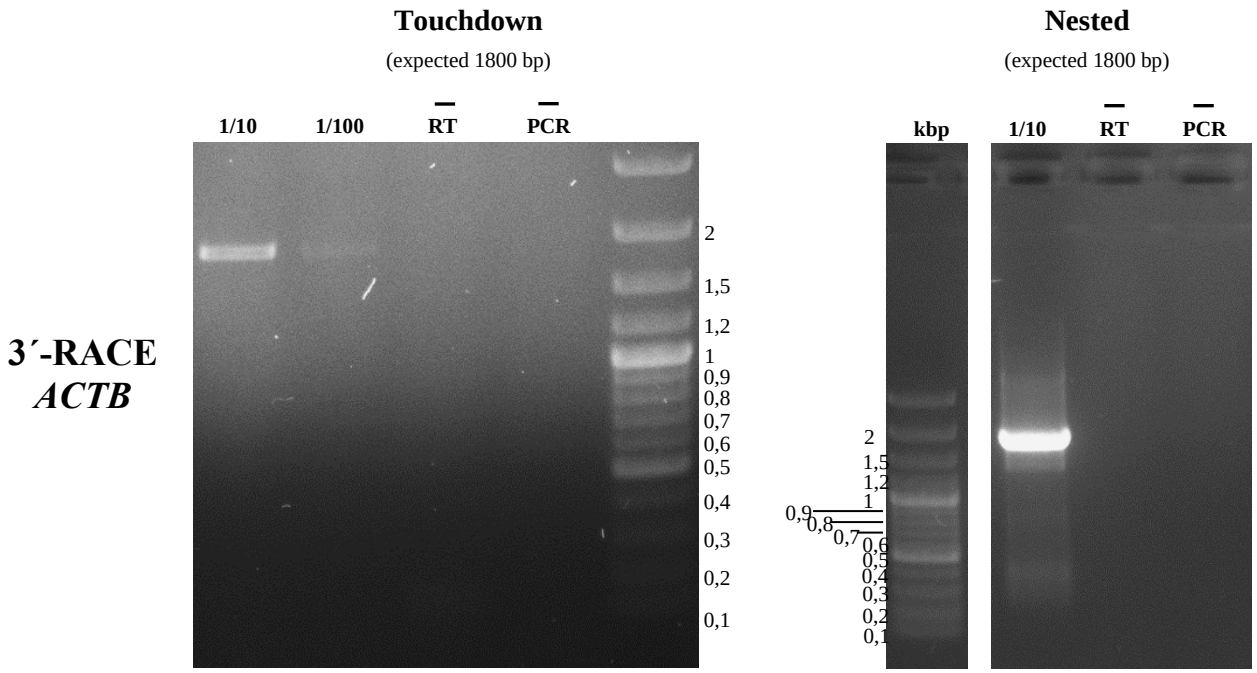

Figure S10: 5'/3' RACE PCRs (Touchdown and Nested) for *ACTB* from a RACE sscDNA library prepared from T84 passage 28 grown for 10 days over TW inserts. Two dilutions of the RACE sscDNA library were employed in order to define the optimal conditions for obtaining the best amplification out of the two consecutive PCR rounds.

SANGER SEQUENCING OF *HTR3E* 3' RACE AMPLICON AND ALIGNMENT

Sequencing results

pSTBlue1_*HTR3E* 3' RACE PCR fragment of 600 bp (primer T7_prom)

TGGGTGGGGTGGGGGACAGCATGCTGCAGACGCGTTACGTATCGGATCCAGAATTCG
TGATTGGAAAATAAGGGCCCGGGTCTCACCCCCACCCACCTGCCCGGTGTGAAGGAG
CCAGAGGTATCAGCAGGGCAGATGCCGGGCCCTGCGGAGGCAGAGCTGACAGGGGGC
TCAGAATGGACAAGGGCCCAGCGGGAACACGAGGCCCAGAAGCAGCACTCAGTGGA
GCTGTGGTTGCAGTTCAGCCACGCGATGGACGCCATGCTCTTCCGCCTCTACCTGCTCT
TCATGGCCTCCTCTATCATCACCGTCATATGCCTCTGGAACACCTAGGCAGGTGCTCAC
CTGCCAACTTCAGTCTGGAGCTTCTCTTGCCTCCAGGGACTGGCCAGGTCTCCCCCCTT
TCCTGAGTACCAACTATCATATCCCCAAAGATGACTGAGTCTCTGCTGTATTCCATGTA
TCCCAATCCGGTCCTGCTGATCAATTCCAATCCCAGACATTTCTCCCTGTTCCTGCATT
TTGTTGGCTTCCTTCAGTCCTACCATATGGTTCTAGGTCCCTCTTACGTCATCTGCATA
GCAGACTATACCTCTTCTGTCCGCTGACTTGCCCAATAAATAATTCTGCAGAAAAAAA
AAAAAAAAAAAAAAACACTGTCATGCCGTTACGTAGCGAATCTGAATTCGTCGACAA
GCTTCTCGAGCCTAGGCTAGCTCTAGACCACACGTGTGGGGGCCCGAGCTCGCGGCCG
CTGTATTCTATAGTGTCACCTAAATGGCCGCACAATTCACTGGCCGTCGTTTTACAACG
TCGTGACTGGGAAAACCCTGGCGTTACCCAACTTAATCGCCTTGCAGCACATCCCCCT
TTCGCCAGCTGGCGTAATAGCGAAGAGGCCCGCACCGATCGCCCTTTCCCAACAGTTG
CGCAGCTTGATGGCGAATGGAAATTGTAAGCGTATATTTTTGTAAATTCGCGTTAAAT
TTTTTGTTAAATCAGCTCATTTTTTACATAGCGAATCCGCTAATCCCTATATCAAGAAT
AGACGAATAGCGATGTTGTCAGTTGGACAGAGTTCATATAGACTGAACTCCACGTAGC

GTACGTCTATCAGGCGATGCATCGTACGTACCCTATACAGTTAGTCAGTCGTAGCTAT
CGTACCTAAGGATCCA

pSTBlue1_*HTR3E* 3‘ RACE PCR fragment of 600 bp (primer M13_fwd)

TCGCTGACTATAGATACAGCGGCCGCGAGCTCGGGCCCCCACACGTGTGGTCTAGAGC
TAGCCTAGGCTCGAGAAGCTTGTCGACGAATTCAGATTCGCTACGTAACGGCATGACA
GTGTTTTTTTTTTTTTTTTTTTTCTGCAGAATTATTTATTGGGCAAGTCAGCGGACAG
AAGAGGTATAGTCTGCTATGCAGATGACGTAAGAGGGACCTAGAACCATATGGTAGG
ACTGAAGGAAGCCAACAAAATGCAGGAACAGGGAGAAATGTCTGGGATTGGAATTGA
TCAGCAGGACCGGATTGGGATACATGGAATACAGCAGAGACTCAGTCATCTTTGGGG
ATATGATAGTTGGTACTCAGGAAAGGGGGGAGACCTGGCCAGTCCCTGGAGGCAAGA
GAAGCTCCAGACTGAAGTTGGCAGGTGAGCACCTGCCTAGGTGTTCCAGAGGCATAT
GACGGTGATGATAGAGGAGGCCATGAAGAGCAGGTAGAGGCGGAAGAGCATGGCGT
CCATCGCGTGGCTGAACTGCAACCACAGCTCCACTGAGTGCTGCTTCTGGGCCTCGTG
TTCCCGCTGGGCCCTTGTCCATTCTGAGCCCCCTGTCAGCTCTGCCTCCGCAGGGCCCG
GCATCTGCCCTGCTGATACCTCTGGCTCCTTCACACCGGGCAGGTGGGTGGGGGTGAG
ACCCGGGCCCTTATTTTCCAATCACGAATTCTGGATCCGATACGTAACGCGTCTGCAG
CATGCGTGGTACCGAGCTTTCCCTATAGTGAGTCGTATTAGAGCTTGGCGTAATCATG
GTCATAGCTGTTTCCTGTGTGAAATTGTTATCCGCTCACAATTCCACACAACATACGAG
CCGGAAGCATAAAGTGTAAAGCCTGGGTGCCTAATGAGTGAGCTAACTCACATTATTG
CGTTGCGCTCACTGCCCGCTTTCAGTCGGGAAACTGTCGTGCCAGCTGCATATGATCG
GCACGCGCGGGGAGAGCGATTGCGTATGGCGCTCTCGCTCTCGCTCACTGAACTCGCT
TGGCTCGGTCGTCGGCTGCCGCGAGCGTATCAGGCTCACTGATGCCGTAACCGTATCC
AGATCAGGGTATACGCAGTAGACTGTGAGCATGCCGAGACGACGTAGCCGATGCTGC
CTTTCAAGGTTCGATC

HTR3E 3´-RACE Nested_for	5´-GGAAAATAAGGGCCCGGGTCTCA-3´ 3´-TGAGACCCGGGCCCTTATTTTCC-5´
GeneRacer™ 3′ Nested Primer_rev	5´-CGCTACGTAACGGCATGACAGTG-3´ 3´-CACTGTCATGCCGTTACGTAGCG-5´

Alignment

I performed A BLAT search (http://genome.ucsc.edu/index.html) with the 3’RACE band sequence as the query and the whole Human genome as the subject.

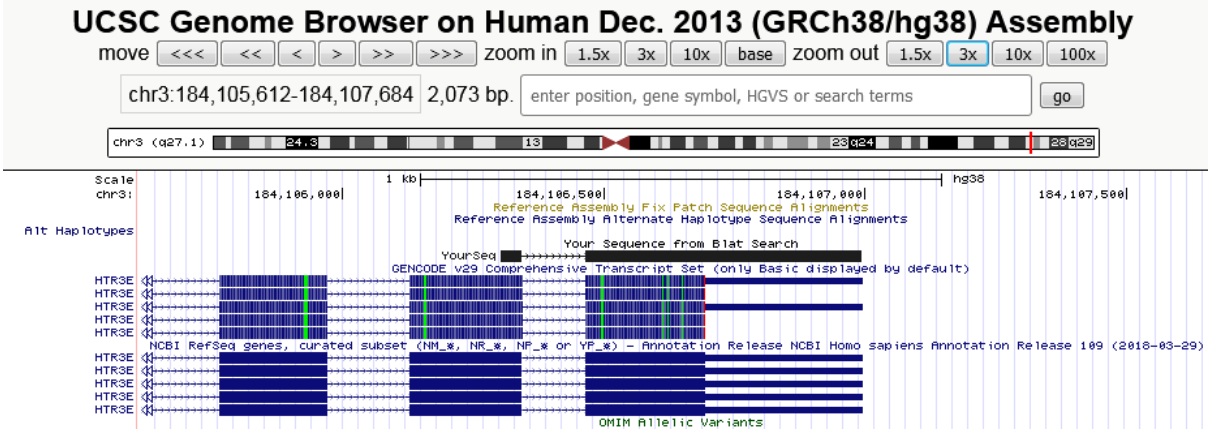

I confirmed the results by running Megablast alignments (https://blast.ncbi.nlm.nih.gov/Blast.cgi) with the 3'RACE band sequence as the query and the single *HTR3E* annotated transcripts as the subjects (data not shown).

NEGATIVE CONTROLS OF THE *IN SITU* IF STAININGS

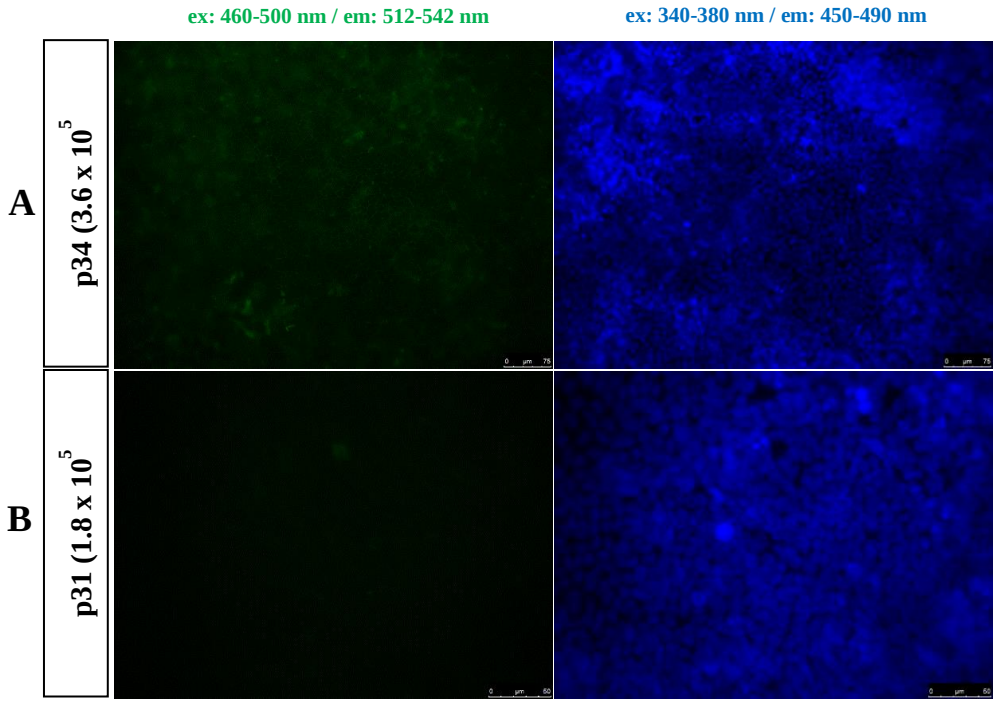

Figure S11: Negative controls of IF stainings of CACO-2 p31 (A) and p34 (B) after 20 days of growth over TW membranes. I followed the standard protocol but incubating the cells only with the secondary antibody Goat anti-mouse IgG (H+L) - Alexa Fluor 488 (blocking solution was employed instead of the primary antibody).

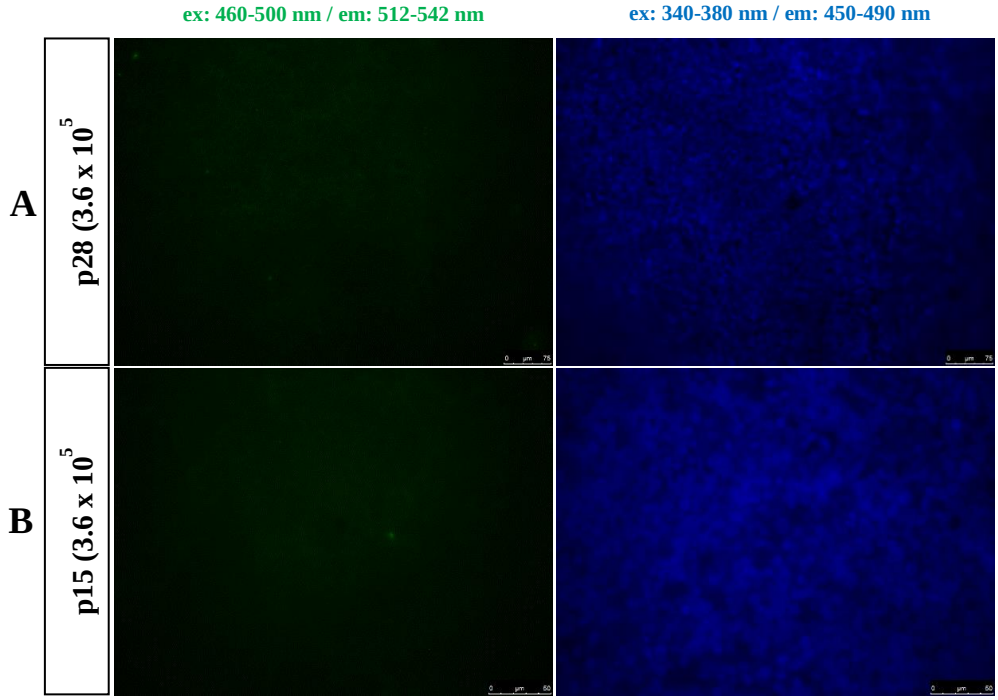

Figure S12: Negative controls of IF stainings of T84 p28 (A) and p15 (B) after 10 days of growth over TW membranes. I followed the standard protocol but incubating the cells only with the secondary antibody Goat anti-mouse IgG (H+L) - Alexa Fluor 488 (blocking solution was employed instead of the primary antibody).

NEGATIVE CONTROLS OF THE BrdU ASSAY

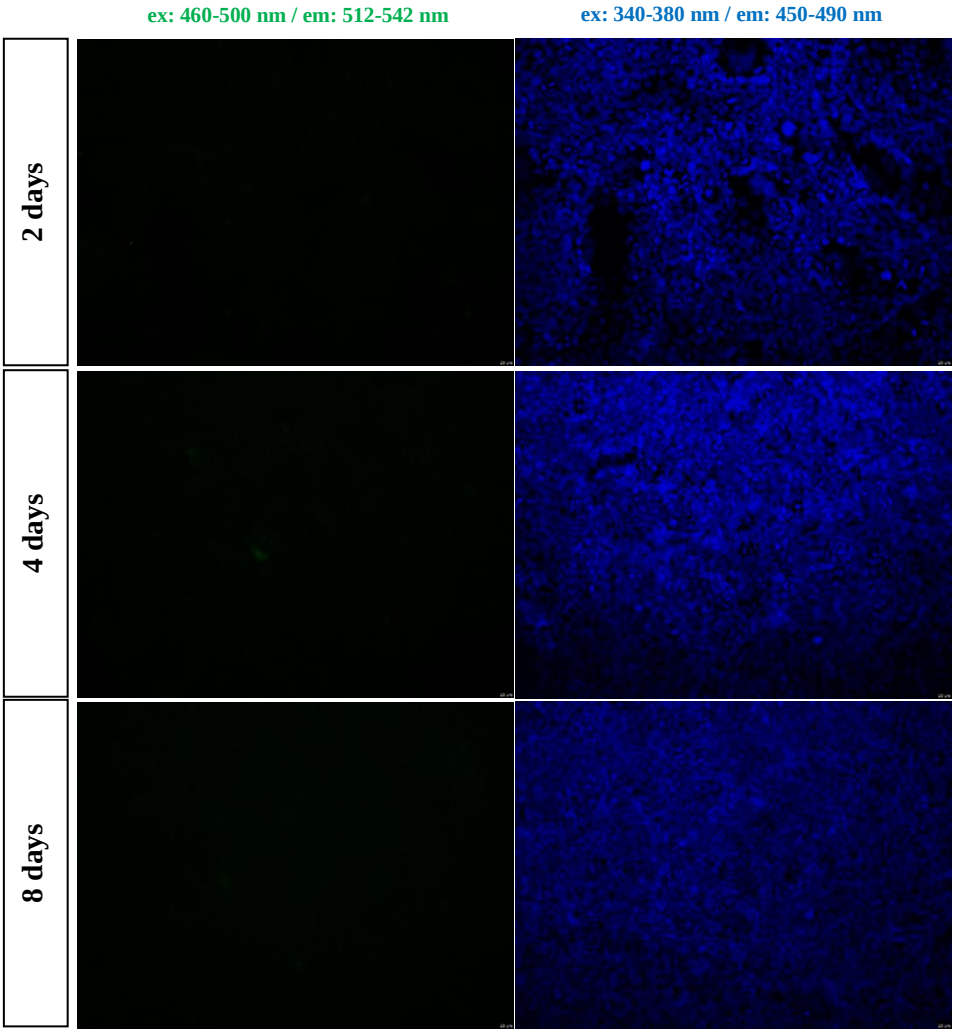

Figure S13: Negative controls of BrdU assay ran on T84 p26 after 2, 4 and 8 days of growth post-seeding over TW membranes. The IF stainings were carried out following the standard protocol but incubating the cells only in "incubation buffer" without α-BrdU and then proceeding with the incubation with goat anti-mouse IgG (H+L) labeled with Alexa Fluor 488.

RT-qPCR FOR *IL1R1*

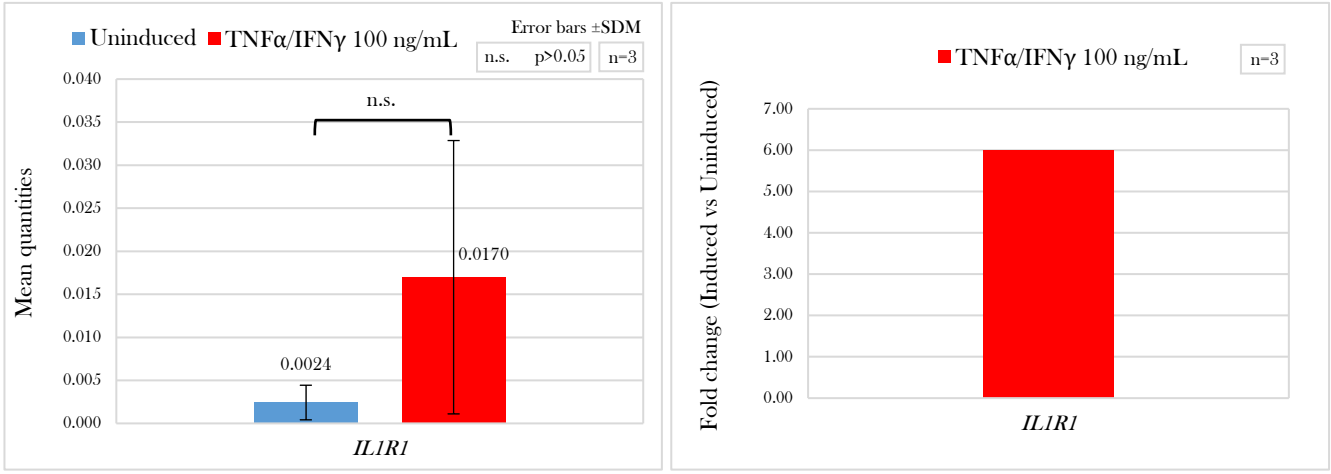

Figure S14: RT-qPCR for *IL1R1* performed on T84 cells grown for 10 days over TW membranes and treated basolaterally with TNFα and IFNγ at 100 ng/mL each for 24 hrs. The left graph shows the mean quantities normalized to *SDHA*, *HPRT1* and *ARF1*. Significance stated with a two-sided paired t-test, n=3 (error bars ±SD). The right graph shows the fold change (induced versus uninduced conditions).

THIRD TITRATION EXPERIMENT FOR α-INGR1/CD119

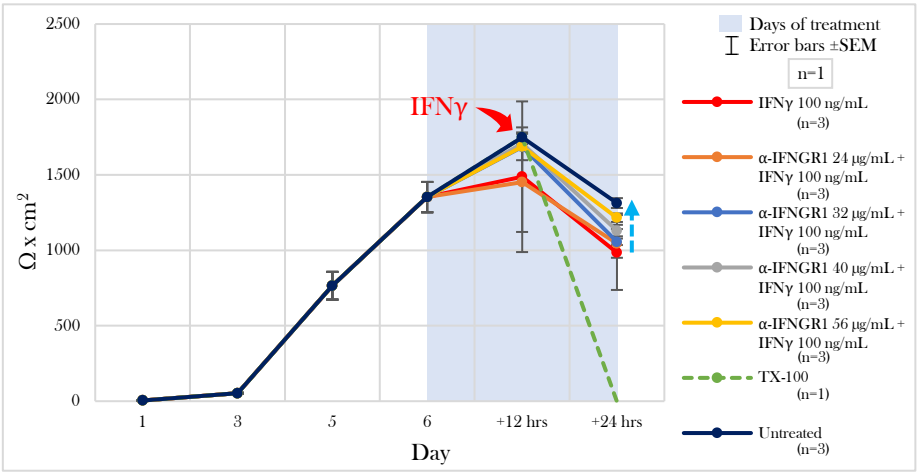

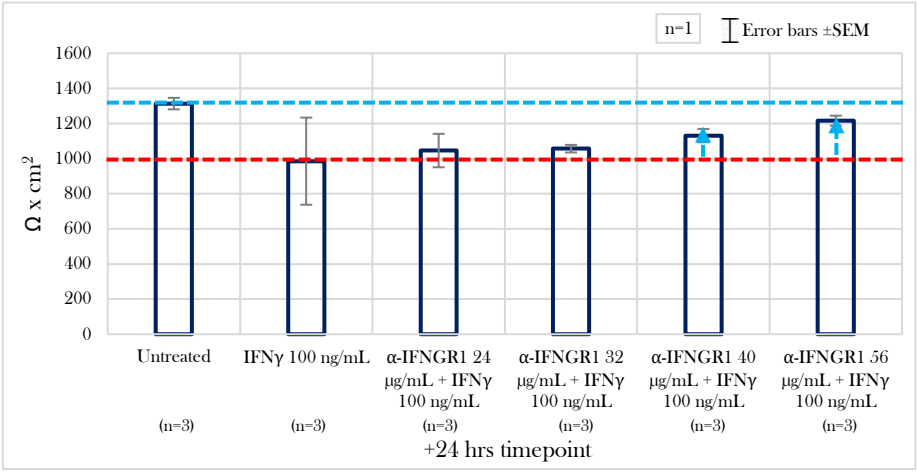

Figure S15: Third titration of α-INGR1/CD119: TEER measurements. Ω x cm^2 values over time from the single biological replica with three technical replicas per condition (upper graph). Average values for the five conditions ("untreated", "IFNγ alone", "co-treatment with α-INGR1/CD119 at 24, 32, 40 and 56 µg/mL") at 24 hrs post-induction induction for a single biological replica with three technical replicas per condition (lower graph). Error bars ±SEM.

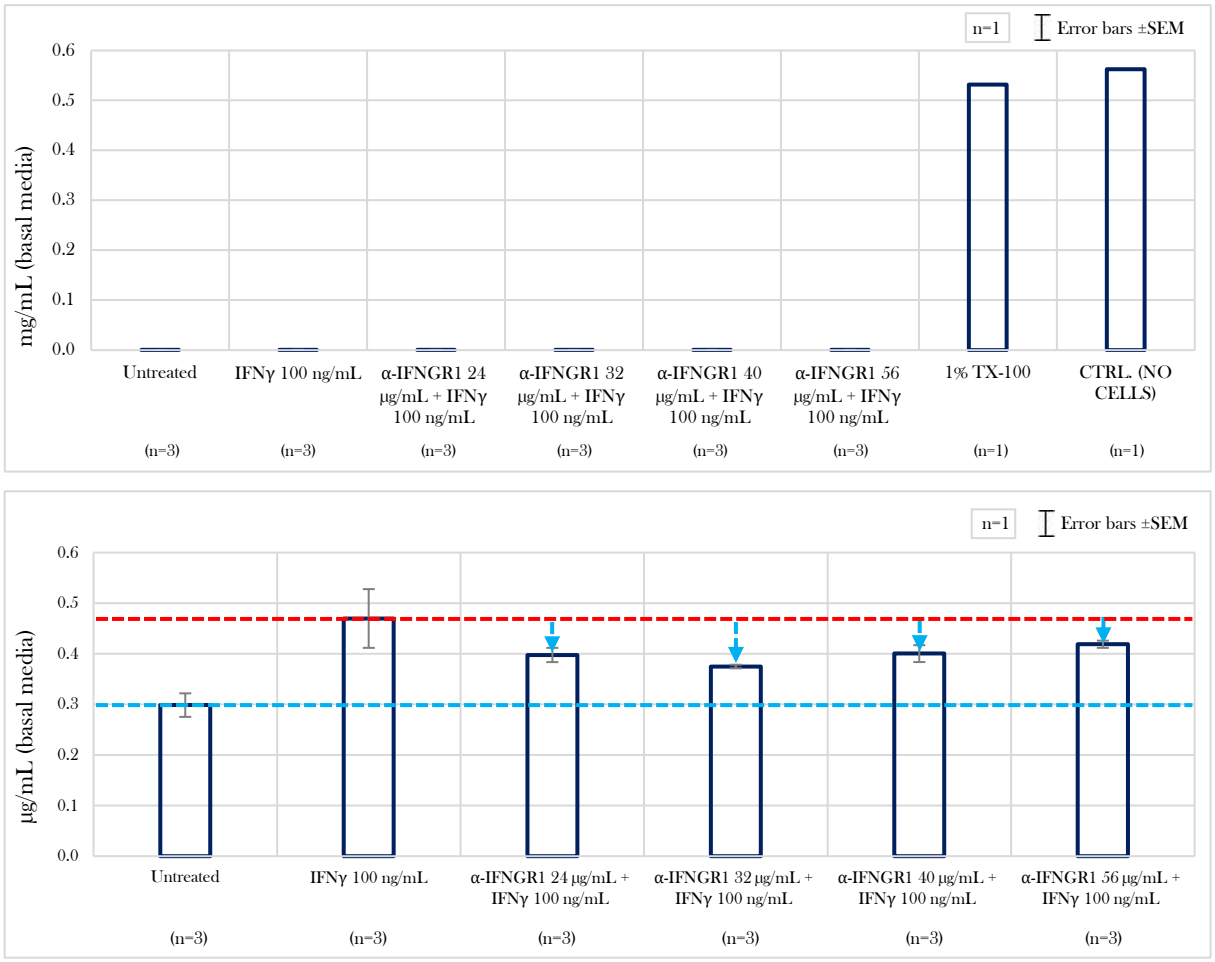

Figure S16: Third titration of α-INGR1/CD119: FD4 assay. Positive control of maximal permeability (TW with no cells and monolayers treated with 1% TX-100) in mg/mL (upper graph). Average values in µg/mL for the six conditions ("untreated", "IFNγ alone", "co-treatment with α-INGR1/CD119 at 24, 32, 40 and 56 µg/mL") at 24 hrs post-induction induction, for a single biological replica with three technical replicas per condition (lower graph). Error bars ±SEM.

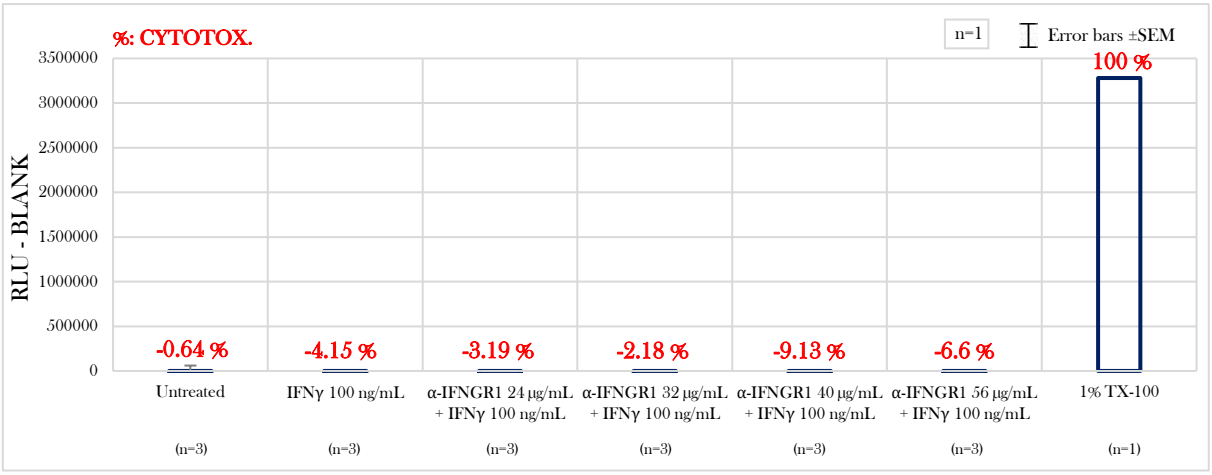

Figure S17: Third titration of α-INGR1/CD119: LDH assay. RLUs of the different conditions subtracted to the blank. In red the percentage of Necrosis/Necroptosis normalized to a control of maximal cell membrane lysis. One biological replica with three technical replicas per condition. Error bars ±SEM.

FULL NEUTRALIZATION OF sTNFα IN SOLUTION: 6 HRS OF PRE-TREATMENT PLUS 24 HRS OF CO-TREATMENT

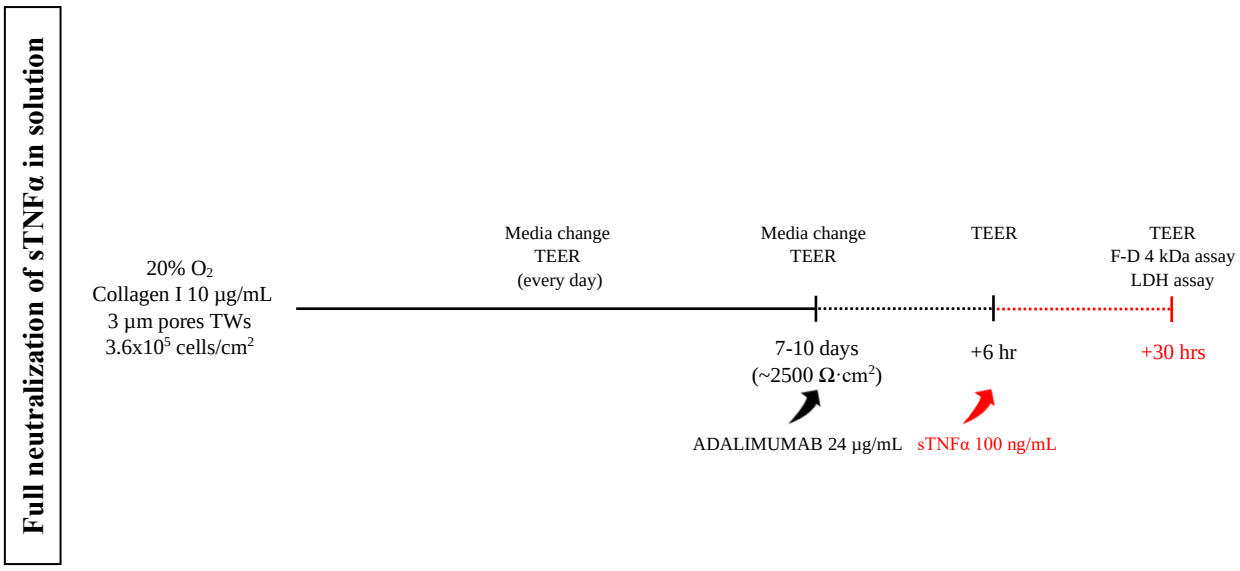

Figure S18: Schematic representation of a pilot experiment in which the optimal concentration of Adalimumab was pre-applied for 6 hrs on fully differentiated monolayers (~2500 Ω·cm^2), which were then induced with sTNFα 100 ng/mL for 24 hrs, in normoxia. In red are indicated the time frames during which the monolayers were stimulated with the cytokine from the basolateral side. Note: the different time frames depicted in the temporal axis are not in scale.

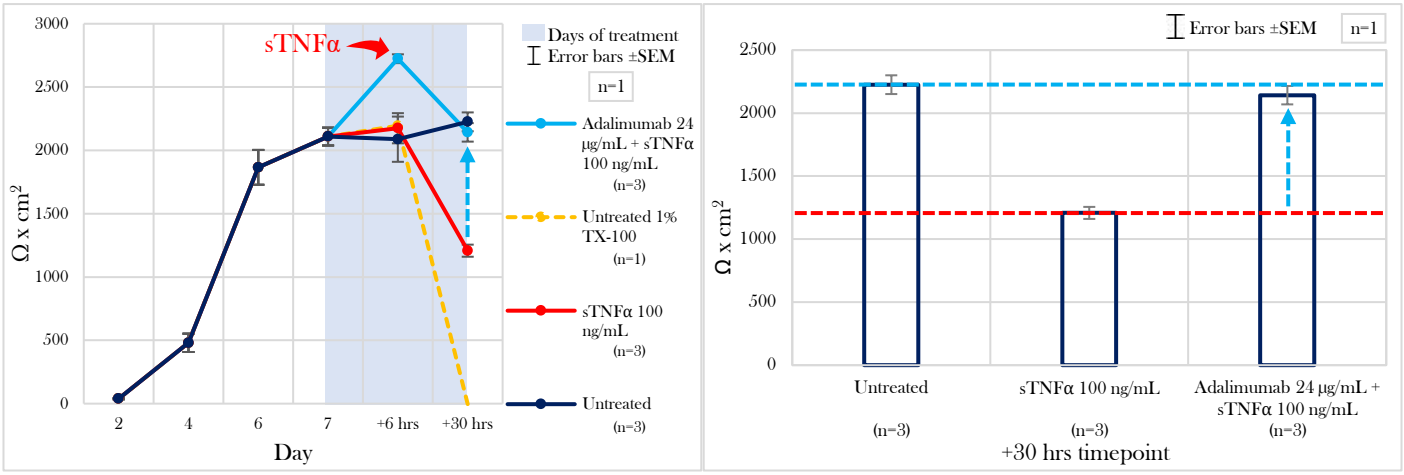

Figure S19: Full neutralization of sTNFα in solution: TEER measurements. Ω x cm² over time of the single representative biological replica with three technical replicas per condition (left graph). Average values for the three conditions ("untreated", "sTNFα alone" and "co-treatment with Adalimumab at 24 µg/mL") at 24 hrs post-induction induction (right graph). One biological replica with three technical replicas per condition. Error bars ±SEM.

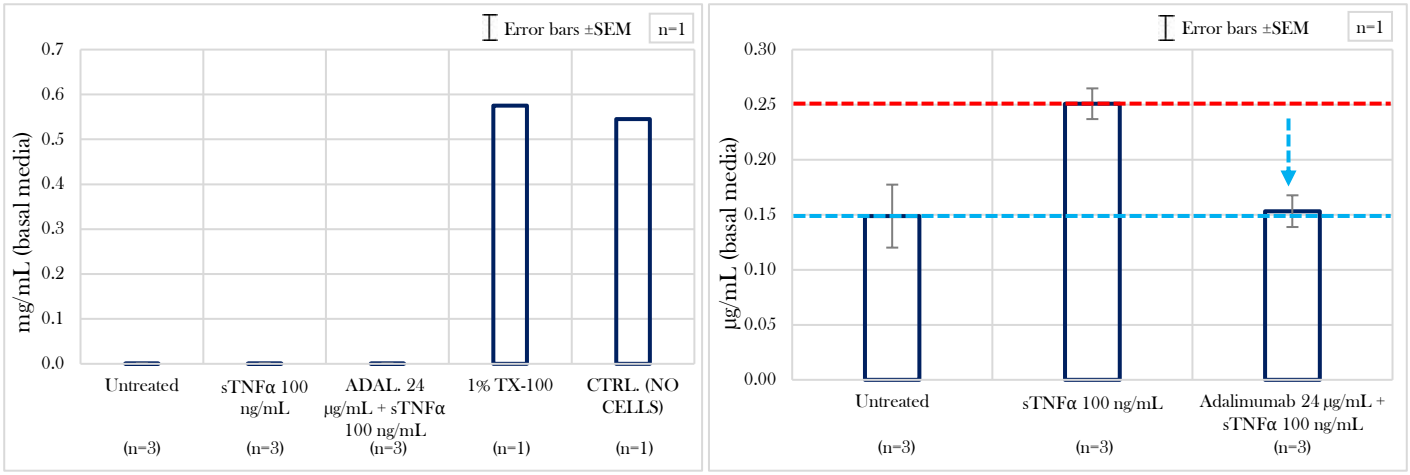

Figure S20: Full neutralization of sTNFα in solution: FD4 assay. Positive controls of maximal permeability (TW with no cells and monolayer treated with 1% TX-100) in mg/mL (left graph). Average values in µg/mL for the three conditions "untreated", "sTNFα alone" and "co-treatment with Adalimumab at 24 µg/mL" (right graph). One biological replica with three technical replicas per condition. Error bars ±SEM.

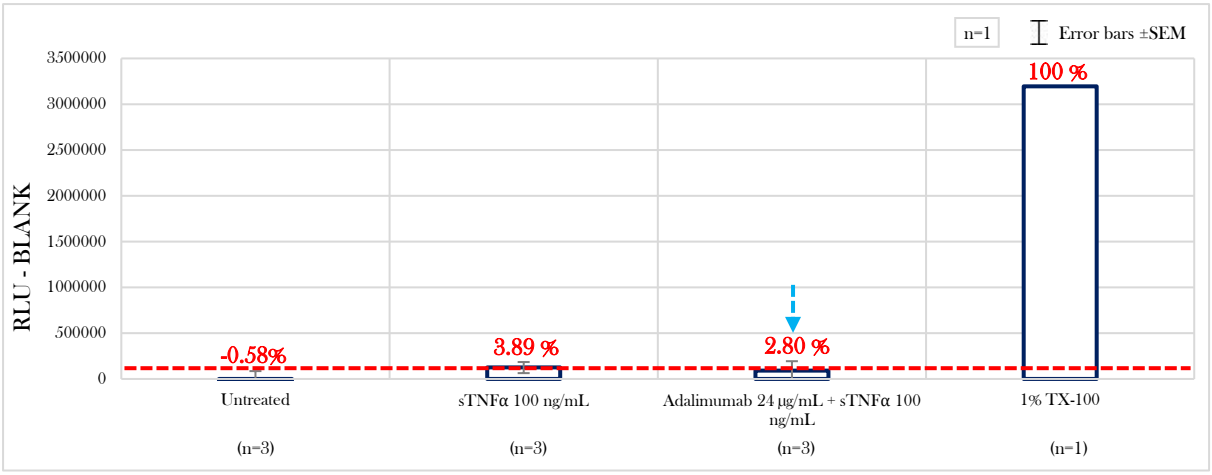

Figure S21: Full neutralization of sTNFα in solution: LDH assay. RLUs of the different conditions subtracted to the blank. In red the percentage of Necrosis/Necroptosis normalized to a control of maximal cell membrane lysis. One biological replica with three technical replicas per condition. Error bars ±SEM.

LITERATURE

1 Yoo, B. B. & Mazmanian, S. K. The Enteric Network: Interactions between the Immune and Nervous Systems of the Gut. *Immunity* **46**, 910-926, doi:10.1016/j.immuni.2017.05.011 (2017).

2 Gilbert, S. F. *Developmental Biology*. Tenth edn, (Andrew D. Sinauer, 2014).

3 Murphy, K. W., C. *Janeway's Immunobiology*. Ninth edn, (Garland Science, Taylor & Francis Group, 2017).

4 Quigley, E. M. M. Microbiota-Brain-Gut Axis and Neurodegenerative Diseases. *Curr Neurol Neurosci Rep* **17**, 94, doi:10.1007/s11910-017-0802-6 (2017).

5 Nishida, A. *et al.* Gut microbiota in the pathogenesis of inflammatory bowel disease. *Clin J Gastroenterol* **11**, 1-10, doi:10.1007/s12328-017-0813-5 (2018).

6 Ley, R. E., Peterson, D. A. & Gordon, J. I. Ecological and evolutionary forces shaping microbial diversity in the human intestine. *Cell* **124**, 837-848, doi:10.1016/j.cell.2006.02.017 (2006).

7 Qin, J. *et al.* A human gut microbial gene catalogue established by metagenomic sequencing. *Nature* **464**, 59-65, doi:10.1038/nature08821 (2010).

8 Belkaid, Y. & Harrison, O. J. Homeostatic Immunity and the Microbiota. *Immunity* **46**, 562-576, doi:10.1016/j.immuni.2017.04.008 (2017).

9 E., M. K. L. H. S. *Pathophysiology: the biologic basis for disease in adults and children*. Eight edn, (ELSEVIER, 2019).

10 Rhoades, R. A. B., D. R. *Medical Physiology, Principles for Clinical Medicine*. Fourth edn, (Lippincott Williams & Wilkins, 2013).

11 Reed, K. K. & Wickham, R. Review of the gastrointestinal tract: from macro to micro. *Semin Oncol Nurs* **25**, 3-14, doi:10.1016/j.soncn.2008.10.002 (2009).

12 Adak, A. & Khan, M. R. An insight into gut microbiota and its functionalities. *Cell Mol Life Sci* **76**, 473-493, doi:10.1007/s00018-018-2943-4 (2019).

13 Costa, M., Brookes, S. J. & Hennig, G. W. Anatomy and physiology of the enteric nervous system. *Gut* **47 Suppl 4**, iv15-19; discussion iv26, doi:10.1136/gut.47.suppl_4.iv15 (2000).

14 Uchida, K. & Kamikawa, Y. Muscularis mucosae - the forgotten sibling. *J Smooth Muscle Res* **43**, 157-177, doi:10.1540/jsmr.43.157 (2007).

15 Muenchau, S. *et al.* Hypoxic Environment Promotes Barrier Formation in Human Intestinal Epithelial Cells through Regulation of MicroRNA 320a Expression. *Mol Cell Biol* **39**, doi:10.1128/MCB.00553-18 (2019).

16 Said, H. M. G., Fayez K.; Kaunitz, Jonathan D.; Merchant, Juanita L. . *Physiology of the gastrointestinal tract*. Sixth edn, (Academic Press, 2018).

17 Noah, T. K., Donahue, B. & Shroyer, N. F. Intestinal development and differentiation. *Exp Cell Res* **317**, 2702-2710, doi:10.1016/j.yexcr.2011.09.006 (2011).

18 Shajib, M. S. & Khan, W. I. The role of serotonin and its receptors in activation of immune responses and inflammation. *Acta Physiol (Oxf)* **213**, 561-574, doi:10.1111/apha.12430 (2015).

19 Wu, H., Denna, T. H., Storkersen, J. N. & Gerriets, V. A. Beyond a neurotransmitter: The role of serotonin in inflammation and immunity. *Pharmacol Res* **140**, 100-114, doi:10.1016/j.phrs.2018.06.015 (2019).

20 Madara, J. L. & Carlson, S. L. Cup cells: further structural characterization of the brush border and the suggestion that they may serve as an attachment site for an unidentified bacillus in guinea pig ileum. *Gastroenterology* **89**, 1374-1386, doi:10.1016/0016-5085(85)90658-4 (1985).

21 Konjar, S., Pavsic, M. & Veldhoen, M. Regulation of Oxygen Homeostasis at the Intestinal Epithelial Barrier Site. *Int J Mol Sci* **22**, doi:10.3390/ijms22179170 (2021).

22 Patankar, J. V. & Becker, C. Cell death in the gut epithelium and implications for chronic inflammation. *Nat Rev Gastroenterol Hepatol* **17**, 543-556, doi:10.1038/s41575-020-0326-4 (2020).

23 Williams, J. M. *et al.* Epithelial cell shedding and barrier function: a matter of life and death at the small intestinal villus tip. *Vet Pathol* **52**, 445-455, doi:10.1177/0300985814559404 (2015).

24 Lee, J. L. & Streuli, C. H. Integrins and epithelial cell polarity. *J Cell Sci* **127**, 3217-3225, doi:10.1242/jcs.146142 (2014).
25 Li, A. C. & Thompson, R. P. Basement membrane components. *J Clin Pathol* **56**, 885-887, doi:10.1136/jcp.56.12.885 (2003).
26 Walko, G., Castanon, M. J. & Wiche, G. Molecular architecture and function of the hemidesmosome. *Cell Tissue Res* **360**, 363-378, doi:10.1007/s00441-014-2061-z (2015).
27 De Arcangelis, A. *et al.* Hemidesmosome integrity protects the colon against colitis and colorectal cancer. *Gut* **66**, 1748-1760, doi:10.1136/gutjnl-2015-310847 (2017).
28 Odenwald, M. A. *et al.* ZO-1 interactions with F-actin and occludin direct epithelial polarization and single lumen specification in 3D culture. *J Cell Sci* **130**, 243-259, doi:10.1242/jcs.188185 (2017).
29 Al-Ghadban, S., Kaissi, S., Homaidan, F. R., Naim, H. Y. & El-Sabban, M. E. Cross-talk between intestinal epithelial cells and immune cells in inflammatory bowel disease. *Sci Rep* **6**, 29783, doi:10.1038/srep29783 (2016).
30 Odenwald, M. A. & Turner, J. R. The intestinal epithelial barrier: a therapeutic target? *Nat Rev Gastroenterol Hepatol* **14**, 9-21, doi:10.1038/nrgastro.2016.169 (2017).
31 Hudson, L. E., Anderson, S. E., Corbett, A. H. & Lamb, T. J. Gleaning Insights from Fecal Microbiota Transplantation and Probiotic Studies for the Rational Design of Combination Microbial Therapies. *Clin Microbiol Rev* **30**, 191-231, doi:10.1128/CMR.00049-16 (2017).
32 Shen, L., Weber, C. R., Raleigh, D. R., Yu, D. & Turner, J. R. Tight junction pore and leak pathways: a dynamic duo. *Annu Rev Physiol* **73**, 283-309, doi:10.1146/annurev-physiol-012110-142150 (2011).
33 Zihni, C., Mills, C., Matter, K. & Balda, M. S. Tight junctions: from simple barriers to multifunctional molecular gates. *Nat Rev Mol Cell Biol* **17**, 564-580, doi:10.1038/nrm.2016.80 (2016).
34 Hartsock, A. & Nelson, W. J. Adherens and tight junctions: structure, function and connections to the actin cytoskeleton. *Biochim Biophys Acta* **1778**, 660-669, doi:10.1016/j.bbamem.2007.07.012 (2008).
35 Schoultz, I. & Keita, A. V. The Intestinal Barrier and Current Techniques for the Assessment of Gut Permeability. *Cells* **9**, doi:10.3390/cells9081909 (2020).
36 Zuo, L., Kuo, W.-T. & Turner, J. R. Tight Junctions as Targets and Effectors of Mucosal Immune Homeostasis. *Cellular and Molecular Gastroenterology and Hepatology* **10**, 327-340, doi:https://doi.org/10.1016/j.jcmgh.2020.04.001 (2020).
37 Overgaard, C. E., Daugherty, B. L., Mitchell, L. A. & Koval, M. Claudins: control of barrier function and regulation in response to oxidant stress. *Antioxid Redox Signal* **15**, 1179-1193, doi:10.1089/ars.2011.3893 (2011).
38 Chelakkot, C., Ghim, J. & Ryu, S. H. Mechanisms regulating intestinal barrier integrity and its pathological implications. *Exp Mol Med* **50**, 1-9, doi:10.1038/s12276-018-0126-x (2018).
39 Anderson, J. M. & Van Itallie, C. M. Physiology and function of the tight junction. *Cold Spring Harb Perspect Biol* **1**, a002584, doi:10.1101/cshperspect.a002584 (2009).
40 Abraham, C. & Cho, J. H. Inflammatory bowel disease. *N Engl J Med* **361**, 2066-2078, doi:10.1056/NEJMra0804647 (2009).
41 Zhang, Y. Z. & Li, Y. Y. Inflammatory bowel disease: pathogenesis. *World J Gastroenterol* **20**, 91-99, doi:10.3748/wjg.v20.i1.91 (2014).
42 Uniken Venema, W. T., Voskuil, M. D., Dijkstra, G., Weersma, R. K. & Festen, E. A. The genetic background of inflammatory bowel disease: from correlation to causality. *J Pathol* **241**, 146-158, doi:10.1002/path.4817 (2017).
43 Neurath, M. F. Cytokines in inflammatory bowel disease. *Nat Rev Immunol* **14**, 329-342, doi:10.1038/nri3661 (2014).
44 Steeland, S., Libert, C. & Vandenbroucke, R. E. A New Venue of TNF Targeting. *Int J Mol Sci* **19**, doi:10.3390/ijms19051442 (2018).
45 Orti-Casan, N. *et al.* Targeting TNFR2 as a Novel Therapeutic Strategy for Alzheimer's Disease. *Front Neurosci* **13**, 49, doi:10.3389/fnins.2019.00049 (2019).

46 Fischer, R., Kontermann, R. E. & Pfizenmaier, K. Selective Targeting of TNF Receptors as a Novel Therapeutic Approach. *Front Cell Dev Biol* **8**, 401, doi:10.3389/fcell.2020.00401 (2020).
47 Van Hauwermeiren, F., Vandenbroucke, R. E. & Libert, C. Treatment of TNF mediated diseases by selective inhibition of soluble TNF or TNFR1. *Cytokine Growth Factor Rev* **22**, 311-319, doi:10.1016/j.cytogfr.2011.09.004 (2011).
48 Wajant, H. & Siegmund, D. TNFR1 and TNFR2 in the Control of the Life and Death Balance of Macrophages. *Front Cell Dev Biol* **7**, 91, doi:10.3389/fcell.2019.00091 (2019).
49 Medler, J. & Wajant, H. Tumor necrosis factor receptor-2 (TNFR2): an overview of an emerging drug target. *Expert Opin Ther Targets* **23**, 295-307, doi:10.1080/14728222.2019.1586886 (2019).
50 Steeland, S. *et al.* Counteracting the effects of TNF receptor-1 has therapeutic potential in Alzheimer's disease. *EMBO Mol Med* **10**, doi:10.15252/emmm.201708300 (2018).
51 Williams, S. K. *et al.* Anti-TNFR1 targeting in humanized mice ameliorates disease in a model of multiple sclerosis. *Sci Rep* **8**, 13628, doi:10.1038/s41598-018-31957-7 (2018).
52 Yang, S. *et al.* Differential roles of TNFalpha-TNFR1 and TNFalpha-TNFR2 in the differentiation and function of CD4(+)Foxp3(+) induced Treg cells in vitro and in vivo periphery in autoimmune diseases. *Cell Death Dis* **10**, 27, doi:10.1038/s41419-018-1266-6 (2019).
53 Mankertz, J. & Schulzke, J. D. Altered permeability in inflammatory bowel disease: pathophysiology and clinical implications. *Curr Opin Gastroenterol* **23**, 379-383, doi:10.1097/MOG.0b013e32816aa392 (2007).
54 Buckley, A. & Turner, J. R. Cell Biology of Tight Junction Barrier Regulation and Mucosal Disease. *Cold Spring Harb Perspect Biol* **10**, doi:10.1101/cshperspect.a029314 (2018).
55 Al-Sadi, R., Boivin, M. & Ma, T. Mechanism of cytokine modulation of epithelial tight junction barrier. *Front Biosci (Landmark Ed)* **14**, 2765-2778, doi:10.2741/3413 (2009).
56 Wang, F. *et al.* IFN-gamma-induced TNFR2 expression is required for TNF-dependent intestinal epithelial barrier dysfunction. *Gastroenterology* **131**, 1153-1163, doi:10.1053/j.gastro.2006.08.022 (2006).
57 Coates, M. D., Tekin, I., Vrana, K. E. & Mawe, G. M. Review article: the many potential roles of intestinal serotonin (5-hydroxytryptamine, 5-HT) signalling in inflammatory bowel disease. *Aliment Pharmacol Ther* **46**, 569-580, doi:10.1111/apt.14226 (2017).
58 Kapeller, J. *et al.* Serotonin receptor diversity in the human colon: Expression of serotonin type 3 receptor subunits 5-HT3C, 5-HT3D, and 5-HT3E. *J Comp Neurol* **519**, 420-432, doi:10.1002/cne.22525 (2011).
59 Zuber, B., Rudstrom, K., Ehrnfelt, C. & Ahlborg, N. Epitope Mapping of Neutralizing Monoclonal Antibodies to Human Interferon-gamma Using Human-Bovine Interferon-gamma Chimeras. *J Interferon Cytokine Res* **36**, 542-551, doi:10.1089/jir.2016.0017 (2016).
60 Jespers, L. S., Roberts, A., Mahler, S. M., Winter, G. & Hoogenboom, H. R. Guiding the selection of human antibodies from phage display repertoires to a single epitope of an antigen. *Biotechnology (N Y)* **12**, 899-903, doi:10.1038/nbt0994-899 (1994).
61 Steeland, S. *et al.* Generation and characterization of small single domain antibodies inhibiting human tumor necrosis factor receptor 1. *J Biol Chem* **290**, 4022-4037, doi:10.1074/jbc.M114.617787 (2015).
62 Matter, K. & Balda, M. S. Functional analysis of tight junctions. *Methods* **30**, 228-234, doi:10.1016/s1046-2023(03)00029-x (2003).
63 Spring, K. R. Routes and mechanism of fluid transport by epithelia. *Annu Rev Physiol* **60**, 105-119, doi:10.1146/annurev.physiol.60.1.105 (1998).
64 Linnankoski, J. *et al.* Paracellular porosity and pore size of the human intestinal epithelium in tissue and cell culture models. *J Pharm Sci* **99**, 2166-2175, doi:10.1002/jps.21961 (2010).
65 Srinivasan, B. *et al.* TEER measurement techniques for in vitro barrier model systems. *J Lab Autom* **20**, 107-126, doi:10.1177/2211068214561025 (2015).
66 WPI. EVOM2 Epithelial Voltohmmeter INSTRUCTION MANUAL. **033116** (2009).

67 Pade, V. & Stavchansky, S. Estimation of the relative contribution of the transcellular and paracellular pathway to the transport of passively absorbed drugs in the Caco-2 cell culture model. *Pharm Res* **14**, 1210-1215, doi:10.1023/a:1012111008617 (1997).
68 Hoffmann, A. *et al.* High and Low Molecular Weight Fluorescein Isothiocyanate (FITC)-Dextrans to Assess Blood-Brain Barrier Disruption: Technical Considerations. *Transl Stroke Res* **2**, 106-111, doi:10.1007/s12975-010-0049-x (2011).
69 Zuo, L., Kuo, W. T. & Turner, J. R. Tight Junctions as Targets and Effectors of Mucosal Immune Homeostasis. *Cell Mol Gastroenterol Hepatol* **10**, 327-340, doi:10.1016/j.jcmgh.2020.04.001 (2020).
70 D'Arcy, M. S. Cell death: a review of the major forms of apoptosis, necrosis and autophagy. *Cell Biol Int* **43**, 582-592, doi:10.1002/cbin.11137 (2019).
71 ROCHE. *In Situ* Cell Death Detection Kit, Fluorescein. **11684795910** (2016).
72 ROCHE. 5-Bromo-2´-deoxy-uridine Labeling and Detection Kit I. **11296736001** (2016).
73 Bazzocco, S. *et al.* Highly Expressed Genes in Rapidly Proliferating Tumor Cells as New Targets for Colorectal Cancer Treatment. *Clin Cancer Res* **21**, 3695-3704, doi:10.1158/1078-0432.CCR-14-2457 (2015).
74 Madara, J. L., Stafford, J., Dharmsathaphorn, K. & Carlson, S. Structural analysis of a human intestinal epithelial cell line. *Gastroenterology* **92**, 1133-1145, doi:10.1016/s0016-5085(87)91069-9 (1987).
75 Natoli, M., Leoni, B. D., D'Agnano, I., Zucco, F. & Felsani, A. Good Caco-2 cell culture practices. *Toxicol In Vitro* **26**, 1243-1246, doi:10.1016/j.tiv.2012.03.009 (2012).
76 Kauffman, A. L. *et al.* Alternative functional in vitro models of human intestinal epithelia. *Front Pharmacol* **4**, 79, doi:10.3389/fphar.2013.00079 (2013).
77 Sambuy, Y. *et al.* The Caco-2 cell line as a model of the intestinal barrier: influence of cell and culture-related factors on Caco-2 cell functional characteristics. *Cell Biol Toxicol* **21**, 1-26, doi:10.1007/s10565-005-0085-6 (2005).
78 Stanifer, M. L. *et al.* Reovirus intermediate subviral particles constitute a strategy to infect intestinal epithelial cells by exploiting TGF-beta dependent pro-survival signaling. *Cell Microbiol* **18**, 1831-1845, doi:10.1111/cmi.12626 (2016).
79 van der Werf, C. S. *et al.* CLMP is essential for intestinal development, but does not play a key role in cellular processes involved in intestinal epithelial development. *PLoS One* **8**, e54649, doi:10.1371/journal.pone.0054649 (2013).
80 Niesler, B. 5-HT(3) receptors: potential of individual isoforms for personalised therapy. *Curr Opin Pharmacol* **11**, 81-86, doi:10.1016/j.coph.2011.01.011 (2011).
81 Kormanik, N. GAMIFANT(emapalumab) APPLICATION NUMBER: 761107Orig1s000. (CENTER FOR DRUG EVALUATION AND RESEARCH, 2018).
82 Clemens, M. J. M., A. G. *Lymphokines and Interferons: A Practical Approach (Practical Approach Series)*. (Oxford University Press, 1987).
83 Devriese, S. *et al.* T84 monolayers are superior to Caco-2 as a model system of colonocytes. *Histochem Cell Biol* **148**, 85-93, doi:10.1007/s00418-017-1539-7 (2017).
84 Beutel, O., Maraspini, R., Pombo-Garcia, K., Martin-Lemaitre, C. & Honigmann, A. Phase Separation of Zonula Occludens Proteins Drives Formation of Tight Junctions. *Cell* **179**, 923-936 e911, doi:10.1016/j.cell.2019.10.011 (2019).
85 Gross, E. R. *et al.* Neuronal serotonin regulates growth of the intestinal mucosa in mice. *Gastroenterology* **143**, 408-417 e402, doi:10.1053/j.gastro.2012.05.007 (2012).
86 Shajib, M. S., Baranov, A. & Khan, W. I. Diverse Effects of Gut-Derived Serotonin in Intestinal Inflammation. *ACS Chem Neurosci* **8**, 920-931, doi:10.1021/acschemneuro.6b00414 (2017).
87 Mawe, G. M. & Hoffman, J. M. Serotonin signalling in the gut--functions, dysfunctions and therapeutic targets. *Nat Rev Gastroenterol Hepatol* **10**, 473-486, doi:10.1038/nrgastro.2013.105 (2013).

88 Haub, S. *et al.* Serotonin receptor type 3 antagonists improve obesity-associated fatty liver disease in mice. *J Pharmacol Exp Ther* **339**, 790-798, doi:10.1124/jpet.111.181834 (2011).
89 Shajib, M. S. *et al.* Characterization of Serotonin Signaling Components in Patients with Inflammatory Bowel Disease. *J Can Assoc Gastroenterol* **2**, 132-140, doi:10.1093/jcag/gwy039 (2019).
90 Siddiqui, K. M. & Chopra, D. P. Primary and long term epithelial cell cultures from human fetal normal colonic mucosa. *In Vitro* **20**, 859-868, doi:10.1007/BF02619632 (1984).
91 Bruewer, M. *et al.* Proinflammatory cytokines disrupt epithelial barrier function by apoptosis-independent mechanisms. *J Immunol* **171**, 6164-6172, doi:10.4049/jimmunol.171.11.6164 (2003).
92 Schmitz, H. *et al.* Tumor necrosis factor-alpha (TNFalpha) regulates the epithelial barrier in the human intestinal cell line HT-29/B6. *J Cell Sci* **112 (Pt 1)**, 137-146 (1999).
93 Petecchia, L. *et al.* Cytokines induce tight junction disassembly in airway cells via an EGFR-dependent MAPK/ERK1/2-pathway. *Lab Invest* **92**, 1140-1148, doi:10.1038/labinvest.2012.67 (2012).
94 Lee, S. H., Kwon, J. Y., Kim, S. Y., Jung, K. & Cho, M. L. Interferon-gamma regulates inflammatory cell death by targeting necroptosis in experimental autoimmune arthritis. *Sci Rep* **7**, 10133, doi:10.1038/s41598-017-09767-0 (2017).
95 Trietsch, S. J. *et al.* Membrane-free culture and real-time barrier integrity assessment of perfused intestinal epithelium tubes. *Nat Commun* **8**, 262, doi:10.1038/s41467-017-00259-3 (2017).
96 Lindner, M., Laporte, A., Block, S., Elomaa, L. & Weinhart, M. Physiological Shear Stress Enhances Differentiation, Mucus-Formation and Structural 3D Organization of Intestinal Epithelial Cells In Vitro. *Cells* **10**, doi:10.3390/cells10082062 (2021).
97 Buckley, A. G. *et al.* Visualisation of Multiple Tight Junctional Complexes in Human Airway Epithelial Cells. *Biol Proced Online* **20**, 3, doi:10.1186/s12575-018-0070-0 (2018).
98 Wang, X. *et al.* Cloning and variation of ground state intestinal stem cells. *Nature* **522**, 173-178, doi:10.1038/nature14484 (2015).
99 Chopra, D. P., Dombkowski, A. A., Stemmer, P. M. & Parker, G. C. Intestinal epithelial cells in vitro. *Stem Cells Dev* **19**, 131-142, doi:10.1089/scd.2009.0109 (2010).
100 Park, J. H. *et al.* HS-173 as a novel inducer of RIP3-dependent necroptosis in lung cancer. *Cancer Lett* **444**, 94-104, doi:10.1016/j.canlet.2018.12.006 (2019).
101 Fischer, R. *et al.* A TNF receptor 2 selective agonist rescues human neurons from oxidative stress-induced cell death. *PLoS One* **6**, e27621, doi:10.1371/journal.pone.0027621 (2011).
102 Soriani, M., Bailey, L. & Hirst, T. R. Contribution of the ADP-ribosylating and receptor-binding properties of cholera-like enterotoxins in modulating cytokine secretion by human intestinal epithelial cells. *Microbiology (Reading)* **148**, 667-676, doi:10.1099/00221287-148-3-667 (2002).
103 Fischer, R. *et al.* Selective Activation of Tumor Necrosis Factor Receptor II Induces Antiinflammatory Responses and Alleviates Experimental Arthritis. *Arthritis Rheumatol* **70**, 722-735, doi:10.1002/art.40413 (2018).
104 Gitter, A. H., Bendfeldt, K., Schulzke, J. D. & Fromm, M. Leaks in the epithelial barrier caused by spontaneous and TNF-alpha-induced single-cell apoptosis. *FASEB J* **14**, 1749-1753, doi:10.1096/fj.99-0898com (2000).

DECLARATION OF ACADEMIC INTEGRITY

SWORN AFFIDAVIT ACCORDING TO §8 OF THE DOCTORAL DEGREE REGULATIONS OF THE COMBINED FACULTY OF NATURAL SCIENCES AND MATHEMATICS

I herewith declare that:

1. The thesis I have submitted entitled “Establishment of an *in vitro* platform for the characterization of proteins involved in the intestinal epithelial barrier dysfunction of Inflammatory Bowel Disease, with a focus on TNFα/TNR1A/TNR1B” is entirely my own work and derive from my own ideas. I have only used the sources indicated and have not made unauthorized use of services of a third party. Where the work of others has been quoted or reproduced, the source is always given.

2. I have not yet presented this thesis or parts thereof to a university as part of an examination or degree.

3. I am aware of the importance of a sworn affidavit and the criminal prosecution in case of a false or incomplete affidavit.

I affirm that the above is the absolute truth to the best of my knowledge and that I have not concealed anything.

_____ _____

Place and date Signature